THE UNIVERSITY *of* ADELAIDE

SUB CRUCE LUMEN

School of Biological Sciences
Department of Molecular and Cellular Biology

Investigating the Role of HIF-1 and HIF-2 Transcription Factors in Multiple Myeloma

Natalia Magdalena Martin

B.Sc. Biomedical (Hons)

A thesis submitted in fulfilment of the requirement
for the degree of

Doctor of Philosophy

April 2018

TABLE OF CONTENTS

ABSTRACT

Multiple myeloma (MM) is an incurable haematological malignancy of bone marrow plasma cells (PCs) that presents with symptoms such as increased bone marrow angiogenesis, osteolytic bone lesions, bone pain and hypercalcaemia. Once in the marrow, MM PCs localise to hypoxic niches and upregulate the Hypoxia Inducible Factors (HIF-1α and HIF-2α) to facilitate survival and disease pathogenesis. Whilst the HIFs have been shown to contribute to MM tumour growth, angiogenesis and osteolysis, the majority of data has focused on HIF-1α. As such, HIF-2α remains largely understudied and under-considered in current approaches to disease prognosis and treatment.

In this study, a lentiviral all-in-one Tet-inducible vector system was used to overexpress either HIF-1α or HIF-2α in murine 5TGM1 MM cells. Initial experiments *in vivo* using these cell lines in the established 5TGM1/C57BL/KaLwRij MM mouse model demonstrated comparable disease dissemination and tumour burden between uninduced stable 5TGM1 cells and control cells. Of particular interest, pilot experiments suggested there was a trend towards increased tumour burden in mice overexpressing HIF-1α or HIF-2α as detected by *in vivo* bioluminescence. Subsequent studies identified fundamental issues with transgene stability, showing a loss of expression over time in the stable cell lines, and demonstrated that they were unsuitable for use in the 4 week MM disease model.

An alternative strategy was developed to knock out either HIF-1α or HIF-2α in the 5TGM1 MM cells using CRISPR-Cas9 technology. With this strategy, MM cell lines lacking HIF-2α were successfully generated, characterised and used in *in vivo* experiments. C57BL/KaLwRij mice injected with 5TGM1 HIF-2α knockout cells showed a significant delay and overall reduction or, in some instances, a complete lack of tumour dissemination and disease development compared to wild type control 5TGM1 cells.

Together, the data presented in this dissertation demonstrate that HIF-2α is a critical contributing factor in MM disease progression *in vivo*, and suggest that HIF-2α has therapeutic potential in MM. This study has also generated valuable cell lines and methodologies for a more extensive comparative analysis of the specific roles of both HIF-1α and HIF-2α in MM.

DECLARATION

I certify that this work contains no material which has been accepted for the award of any other degree or diploma in my name, in any university or other tertiary institution and, to the best of my knowledge and belief, contains no material previously published or written by another person, except where due reference has been made in the text. In addition, I certify that no part of this work will, in the future, be used in a submission in my name, for any other degree or diploma in any university or other tertiary institution without the prior approval of the University of Adelaide and where applicable, any partner institution responsible for the join-award of this degree.

I give permission for the digital version of my thesis to be made available on the web, via the University's digital research repository, the Library Search and also through web search engines, unless permission has been granted by the University to restrict access for a period of time.

I acknowledge the support I have received for my research through the provision of an Australian Government Research Training Program Scholarship.

Natalia Magdalena Martin

18th of April 2018

ACKNOWLEDGEMENTS

To my friends who have shared the journey with me from afar or locally, thank you all from the bottom of my heart, you know who you are. A very special mention goes to one of my closest friends throughout my entire university education. Emma, thank you for being in my life and filling it with movie nights, late night chats that kept us up all night and endless wine-related escapades. Thank you also to Layla, for being the happy, intelligent, strong, driven and wonderful person that you are.

To my beautiful family, this thesis is for you and I hope you are as proud of it as I am. To my dear Abuela Teresa, for your endless belief in me and unconditional love, speaking with you always instills me with self-confidence and strength. To my little brother Brandon, thank you for everything. For the lunch catch ups, the coffee and bagels, the culinary adventures, the house parties, for the hour long chats about Eurovision and the honest fashion advice. You have grown into a sophisticated (dip dip dip dip dip), thoughtful and loving young man, and I love you dearly. I will miss our cooking experiments that always generated more food then we could eat, and were accompanied with a classy dry martini or festive mojito. To one of my biggest supporters, my mum. You would always answer my phone calls on the first ring and listen in earnest to my latest experimental update, even though you had no idea what I was working on half the time. You gave me strength, self-confidence, love and endless support any time I needed it. To my dad, you were the one who planted the seed of scientific curiosity, who inspired me to wonder 'why', and to explore the possibilities of where the future may take us. We often get lost in conversation over the latest scientific discoveries and you are always my most avid listener. I cannot wait to share and discuss my future adventures with you. Te quiero, Papa.

To my loving husband, Mark. The journey has been long and filled with ups and downs, but I could never have gotten through it without you by my side. We shared this experience together and are stronger for it. Thank you for listening to every presentation run-through and every thesis draft, for picking me up from the lab late at night and keeping me well fed. I love you and cannot wait to share the rest of this life together.

Lastly, and most importantly, to my partner in crime, Jacqueline. Man am I glad you moved my freezer and lab supplies into your bay! I will miss laughing at our own jokes for 20 minutes straight with tears running down our cheeks, and discussing every little detail of our experimental ~~disasters~~ achievements together over a Larry and Ladd

coffee. Over our PhDs, we have shared 3 conferences, 2 weddings, and an overseas honeymoon together... how could we not end up best friends? You are the strongest, hardest working person I know, and you taught me resilience against all the adversities that this PhD brought. More importantly, you always believed in me, and together we made it through. This PhD is yours as much as it is mine, and I will always cherish all the support you have given and continue to give me.

Pack 'er up boys….

Chapter 1
INTRODUCTION

1.1 Multiple Myeloma

1.1.1 General description

Multiple Myeloma (MM) is a haematological malignancy that accounts for approximately 1% of all cancers worldwide, and results in an estimated 80,000 deaths every year (Palumbo and Anderson 2011, Ferlay, Soerjomataram et al. 2015). Over the last 15 years, advancements in treatment have vastly improved management of the disease, providing patients with a range of therapeutic options to prolong and improve quality of life, however the disease remains incurable (Palumbo and Anderson 2011, Pulte, Gondos et al. 2011, Bianchi and Anderson 2014). MM is characterised by the clonal expansion of malignant plasma cells within the bone marrow (BM) following migration from secondary lymphoid organs (Mundy 1998, Kyle and Rajkumar 2004). These cancerous plasma cells arise from an accumulation of cytogenetic abnormalities that, in combination with microenvironmental changes, contribute to disease pathogenesis (Palumbo and Anderson 2011).

1.1.2 Pathogenesis and clinical manifestations

The development of malignant MM is preceded by two pre-malignant stages of disease; first monoclonal gammopathy of undetermined significance (MGUS), followed by smouldering multiple myeloma (SMM), both of which are asymptomatic and do not require treatment. As disease progresses, the gradual accumulation of neoplastic plasma cells (PCs) within the BM disrupts normal haematopoiesis. The presence of these abnormal PCs can be detected at all stages of disease through the excessive secretion of a clonal antibody, known as paraprotein (Palumbo and Anderson 2011).

Each of the three stages of disease can be identified and classified based on a defined set of clinical manifestations (Figure 1.1). In almost all instances, MM arises from MGUS, a benign condition primarily characterised by an excessive production of paraprotein with few additional features. Specifically, patients diagnosed with MGUS exhibit less than 3g/dL of paraprotein in their blood serum and less than 10% of their BM is comprised of PCs (Bianchi and Anderson 2014, Rajkumar, Dimopoulos et al.

2014). The incidence of MGUS is 3 - 4% in people over 50 years of age, where 0.5 – 1% of these will progress to MM per annum (Rajkumar, Dimopoulos et al. 2014).

The transition from MGUS to SMM is characterised by an increase in serum paraprotein, with patients exhibiting greater than 3g/dL and less than 60% of the BM consisting of PCs, but patients remain asymptomatic (Rajkumar, Dimopoulos et al. 2014). Patients with SMM have a 10% chance of developing MM in the first 5 years, and 70% by 15 years post diagnosis (Kyle, Remstein et al. 2007, Bianchi and Anderson 2014, Rajkumar, Dimopoulos et al. 2014). SMM broadly encompasses a range of patients, from those that display a very low rate of disease progression, to others that will rapidly develop malignant MM within 2 years of diagnosis, where the median age of diagnosis is 70 years of age (Palumbo and Anderson 2011, Rajkumar, Dimopoulos et al. 2014).

The clinical features required to diagnose malignant MM include clonal PCs comprising greater than 10% of the BM, detectable paraprotein (in the serum and blood), and the presentation of any of four key symptoms resulting in end-organ damage (Figure 1.1) (Campo, Swerdlow et al. 2011, Palumbo and Anderson 2011, Rajkumar, Dimopoulos et al. 2014). The four symptoms used to classify malignant MM are hypercalcaemia, renal insufficiency, anaemia and bone lesions (known by the acronym CRAB), all of which severely affect quality of life (Palumbo and Anderson 2011). MM patients will display varying combinations of the CRAB clinical features, requiring the confirmation of at least one of these for diagnosis of malignant MM (Campo, Swerdlow et al. 2011, Palumbo and Anderson 2011, Rajkumar, Dimopoulos et al. 2014).

The most common feature of MM is the bone lesions which are detected in more than 80% of newly diagnosed individuals (Kyle, Gertz et al. 2003, Palumbo and Anderson 2011). As the osteolytic bone damage progresses, patients can develop bone fractures, bone pain and spinal cord compression (Berenson 2005). Over time, the bone lesions can give rise to hypercalcaemia, although this is the least common of the CRAB symptoms amongst MM patients at diagnosis (Kyle, Gertz et al. 2003, Dimopoulos, Kastritis et al. 2008). At diagnosis of MM, 73% of cases present with

anaemia as a direct result of either MM PC expansion within the BM or renal impairment (Birgegard, Gascon et al. 2006). Comparatively, renal insufficiency is detected in 20-40% of newly diagnosed individuals' due to excessive circulating monoclonal light-chain. This light chain aggregates and deposits within kidney tubules causing obstruction and resulting in kidney damage (Eleutherakis-Papaiakovou, Bamias et al. 2007, Dimopoulos, Kastritis et al. 2008). This process is exacerbated by dehydration, hypercalcaemia and the medication used to treat other symptoms of renal failure. The degree of renal insufficiency changes based on the specific monoclonal light chain produced, where increased renal damage correlates with an increase in mortality rate (Eleutherakis-Papaiakovou, Bamias et al. 2007, Dimopoulos, Kastritis et al. 2008). Although treatment can be tailored based on the symptoms presented, the long term damaging effects of these clinical features inevitably result in death (Campo, Swerdlow et al. 2011, Rajkumar, Dimopoulos et al. 2014).
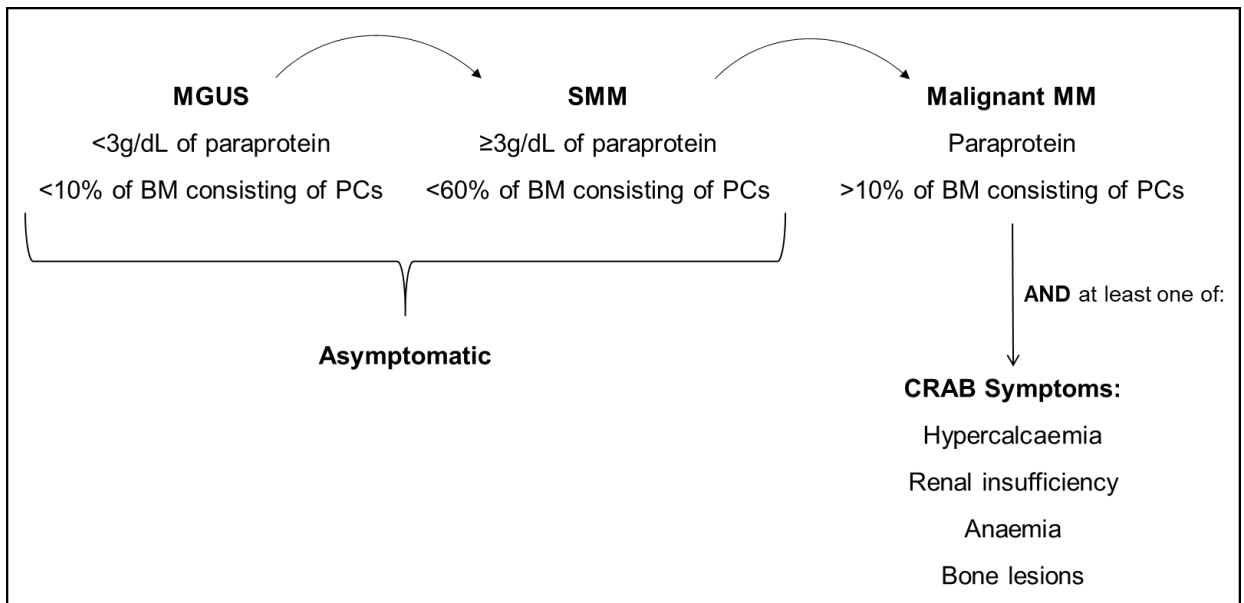
Figure 1.1: Flow chart of the development and clinical manifestation of MM. The three stages of MM; MGUS, SMM and malignant MM. MGUS and SMM are both asymptomatic and require no treatment. Both conditions can be clinically diagnosed in patients that present with specified parameters of paraprotein in the serum or urine and PC infiltration of the BM. Malignant MM is symptomatic, where patients can present with any combination of the CRAB symptoms, and requires treatment to extend and improve quality of life.

1.1.3 Genetic mutations in disease pathogenesis

The stages of MM disease are currently diagnosed based on the clinical features specified above, however, the development of MM is strongly driven by genetic mutations. Whilst cytogenetic criteria are not compulsory for diagnosis, they are required for MM patient classification in clinical trials and can be informative for staging diagnoses (Campo, Swerdlow et al. 2011). Although many genetic abnormalities have been identified, a number of the more prevalent mutations can be matched to MM progression and used as predictive hallmarks of disease stages (Morgan, Walker et al. 2012, Manier, Salem et al. 2016). These include both primary and secondary mutations acquired over the course of disease. Approximately 50% of MM patients present with genetic hyperdiploidy, most commonly trisomy of chromosomes, acquired early in disease (Chng, Kumar et al. 2007, Morgan, Walker et al. 2012, Pawlyn, Melchor et al. 2015, Manier, Salem et al. 2016). A broad range of secondary genetic abnormalities include further chromosomal translocations, insertions, deletions and epigenetic changes (Morgan, Walker et al. 2012, Manier, Salem et al. 2016). Importantly, these genetic abnormalities aid in disease pathogenesis by affecting pathways that control PC differentiation, cell cycle, DNA-damage repair and signalling pathways that contribute to specific disease symptoms.

1.1.4 Differentiation of PCs

Aberrant genetic expression in MM affects numerous pathways critical to MM cell formation and survival. Some of the earliest mutations that drive MM progression are acquired during the process of PC differentiation. Immature B cells are produced in the BM, becoming IgM-expressing naive B cells following genetic (VDJ) recombination (Shapiro-Shelef and Calame 2004). Upon entering the blood stream and reaching the periphery of secondary lymphoid organs, naive B cells that are exposed to antigen will differentiate into either short-lived PCs or memory B cells (LeBien and Tedder 2008). Antigen-stimulated cells that enter the germinal centre of secondary lymphoid organs undergo somatic hypermutation, resulting in isotype switching and affinity maturation (Arpin, Dechanet et al. 1995, Shapiro-Shelef and Calame 2004). These genetic changes produce the aforementioned memory B cells, and long-lived PCs that re-enter the peripheral blood and migrate back to the BM.

The cytogenetic mutations present in MM cells always include genes linked to somatic hypermutation, critical to the production of malignant differentiated PCs (Manier, Salem et al. 2016). These MM PCs then migrate from the germinal centres to the BM and proliferate (Zhan, Tian et al. 2003). Furthermore, analyses of the genetic pathways aberrantly affected in MM PCs show a great degree of overlap with those involved in non-malignant PC differentiation, proliferation and migration, emphasising the importance of these pathways for MM PC production and survival (Zhan, Tian et al. 2003, Shapiro-Shelef and Calame 2004).

1.1.5   Homing of PCs

The movement of B cells between various tissues and locations in the body is driven by chemical signals known as chemokines. Soluble chemokines are bound and recognized by chemokine receptors found on the surface of lymphocytes. Specific receptors found on B cells include CXCR4, CXCR5 and CCR7 (Cyster 2003). Different stromal and endothelial cells express the chemokines that interact with these receptors, allowing for compartmental recruitment of B cells to various tissue sites. As an example, stromal cells expressing CXCL13 will recruit CXCR5 expressing B cells to lymph follicles in the B cell zone of lymph nodes (Ansel, Harris et al. 2002). Similarly, stromal cells expressing CCL19 and endothelial cells expressing CCL21 will result in migration of CCR7 expressing cells (B cells, T cells and dendritic cells) to T cell zones of the lymph node during an immune response (Luther, Bidgol et al. 2002).

Newly differentiated long-lived PCs (both non-malignant PCs and MM PCs) emerge from germinal centres within the lymph follicle, and enter the peripheral blood to migrate to the BM. As observed in secondary lymphoid organs, the circulation of PCs to the BM and navigation of this microenvironment is mediated by chemokines and surface markers. Specifically, PCs express CXCR4 receptors which allow them to migrate towards the CXCL12 chemokine secreted into the environment by stromal cells. Directional migration towards the BM begins with a change in surface receptor expression, specifically higher levels of CXCR4 and comparatively lower levels of CXCR5 and CCR7 (Wehrli, Legler et al. 2001, Hauser, Debes et al. 2002). This lowers the response of PCs to environmental CXCL13, CCL19 and CCL21 chemokines in

secondary lymphoid organs, and results in movement out of the lymphoid tissues (Cyster 2003).

Cellular survival and proliferation in the BM requires the cooperation of a number of cell types such as stromal cells, immune cells, endothelial cells, adipocytes, extracellular matrix (ECM), osteoblasts and osteoclasts to maintain and control homeostasis (Podar, Richardson et al. 2007). Chemokine signalling is also crucial for these cellular interactions, by allowing PCs to locate and make cell-to-cell contact within the BM (Noll, Williams et al. 2012). Specifically, exposure to new sources of CXCL12 alongside additional chemo-attractants such as MCP-1, laminin-1 and IGF-1 promotes the migration of PCs to endothelial or stromal cell sites within the BM (Cyster 2003, Menu, Asosingh et al. 2004).

Following migration, cell-cell adhesion is mediated by a diverse array of cell surface receptors and signalling molecules such as VLA-4, VLA-5, ICAM-3, CD51, CD44, Syndecan-1 and CXCL12, which provide adhesive interactions between PCs, stromal cells and the ECM (Cyster 2003, Menu, Asosingh et al. 2004). These signalling molecules and receptors are crucial for supporting the growth of long-lived PC growth, as well as playing a crucial role in MM PC survival, proliferation and expansion (Noll, Williams et al. 2012). As such, the aberrant upregulation of specific factors by MM PCs, including CD44 and CXCL12, prolongs their survival in the BM (Zhan, Tian et al. 2003, Noll, Williams et al. 2012, Reijmers, Spaargaren et al. 2013).

Once adhered at specific sites, expression of matrix metalloproteinase by PCs such as MMP9, MMP2 and MMP7 aids in tissue invasion by breaking down ECM to reach the desired niche (Menu, Asosingh et al. 2004). Whilst in the BM, PC survival is further aided by the increased expression of additional cytokines including TNFα, APRIL, BAFF and IL-6 (Reijmers, Spaargaren et al. 2013). MM PCs that have infiltrated the BM aberrantly regulate the expression of a number of cytokines including TNFα, BAFF, APRIL, IL-6, VEGF, WNT, TGFβ and IGF-1 to promote cancer cell survival, proliferation, migration, blood vessel formation and bone destruction (Shapiro-Shelef and Calame 2004, Reijmers, Spaargaren et al. 2013).

1.1.6 MM disease in the bone marrow

The aberrant expression of cytokines and growth factors by MM PCs disrupts the normal BM microenvironment resulting in the aberrant elevation of specific biological processes, such as bone osteolysis and anaemia, which contribute to patient symptoms. Both *in vitro* and *in vivo* studies have linked the importance of secreted factors such as CXCL12 and MMP9 in MM PC homing and disease by directly correlating their expression with cell migration and tumour load (Menu, Asosingh et al. 2006). It is well understood that the bone osteolysis observed in MM patients arises from an increase in bone resorption and a decrease in bone formation driven by changes to osteoclast (cells that break down bone) and osteoblast (cells that create new bone) homeostasis. Elevated levels of CXCL12 have been detected in MM patient samples and its role characterised using MM cell lines in *in vitro* and *in vivo* studies (Zannettino, Farrugia et al. 2005, Diamond, Labrinidis et al. 2009). To this end, CXCL12 expression was shown to positively correlate with increased osteolytic bone damage through osteoclast recruitment and activation.

CXCL12 acts by inducing genes that activate osteoclasts such as RANKL, TRACP, carbonic anhydrase II and Cathespink (reviewed by (Edwards, Zhuang et al. 2008)). Osteoclasts express CXCR4 receptors that promote recruitment to sites of elevated expression of CXCL12, such as BM niches that contain proliferating MM PCs, advancing bone resorption (Zannettino, Farrugia et al. 2005). Osteoclasts also promote MM PC expansion through direct cell-to-cell contact which not only propagates bone destruction, but also contributes to a process known as angiogenesis (Ria, Catacchio et al. 2014).

Angiogenesis is the production of new blood vessels from the existing vasculature in response to the upregulation of external stimuli such as vascular endothelial growth factors (VEGFs) (Shweiki, Itin et al. 1992, Liao, Corle et al. 2007). Angiogenesis is also commonly stimulated as a response to low oxygen (hypoxia) that subsequently increases vascularisation and provides a renewed supply of oxygen to the effected tissue. This process is critical to many cancers including MM, where BM aberrant

angiogenesis is a feature associated with disease progression (Vacca, Ribatti et al. 1994). Notably, the BM contains hypoxic niches that are critical for processes such as haematopoiesis (Eliasson and Jonsson 2010). The naturally hypoxic microenvironments within the BM appear to also support the establishment of MM PCs, as shown in a murine model of MM (Asosingh, De Raeve et al. 2005). An independent study detected an increase in angiogenesis within MM infiltrated tissues compared to healthy BM (Asosingh, De Raeve et al. 2004). Importantly, this supported the expansion of CD45- murine MM PCs, a subpopulation that represents the majority of MM cells present at advanced stages of disease (Asosingh, De Raeve et al. 2003, Asosingh, De Raeve et al. 2004). The subsequent vascularisation of the BM promoted MM PC growth and expansion, resulting in the disruption of normal BM homeostasis (Asosingh, De Raeve et al. 2004). These studies have identified the pathways that control oxygen status in the BM as critical components to MM pathogenesis. The critical role of hypoxia in MM PC establishment and angiogenesis, has led to the investigation of hypoxic signalling pathways in MM disease progression.

1.2 Hypoxia and the Hypoxia Inducible Factors

1.2.1 Hypoxia: General description

A cell's ability to maintain oxygen homeostasis is crucial for its survival. As oxygen supplies to cells are often variable, cells utilise oxygen sensors and regulatory processes to rapidly respond to changes in oxygen levels, specifically hypoxia when the supply of oxygen is too low to meet cellular demand (Aragones, Fraisl et al. 2009, Semenza 2011).

States of hypoxia are found in many physiological and pathological situations, such as embryonic development, inflammation, ischemic stress and cancer pathogenesis (reviewed by (Semenza 2014)). The prolonged presence of hypoxia has detrimental effects, for example the hypoxia caused by a lack of blood supply (ischaemia) to the brain, if left unchecked, can result in stroke (Semenza 2003). In solid cancers, continued tumour growth results in the formation of highly dense and poorly vascularised regions that have limited oxygen supply, creating hypoxic regions and ultimately results in cell death. Cells in such poorly oxygenated microenvironments, including tumours, respond by upregulating factors to increase the oxygen supply, metabolically adapt, and prevent cellular apoptosis.

1.2.2 Hypoxia and Hypoxia Inducible Factors

The physiological and pathological changes that occur in response to hypoxia are controlled through the activation of a cascade of transcriptional programs. At the top of this cascade are a family of transcription factors known as the Hypoxia Inducible Factors (HIFs). Studies first discovered HIF as the factor that bound the enhancer element of erythropoietin, resulting in its transcriptional activation and the production of red blood cells in hypoxia (Semenza and Wang 1992, Wang and Semenza 1993).

HIF is a member of the basic helix-loop-helix/PER-ARNT-Sim (bHLH/PAS) family of transcription factors, and exists as a heterodimer (Wang, Jiang et al. 1995, Wang and Semenza 1995). HIF is made up of a regulated HIFα subunit that dimerises with the

HIFβ subunit, also known as the Aryl Hydrocarbon Nuclear Translocator (ARNT), to form a functional HIF transcription factor (Hoffman, Reyes et al. 1991, Jiang, Rue et al. 1996). The bHLH domain enables DNA binding and dimerisation, whilst the PAS-A and PAS-B domains provide both stability and specificity for heterdimerisation (Jiang, Rue et al. 1996).

There are three known HIFα isoforms; HIF-1α, HIF-2α and HIF-3α, all of which heterodimerise with HIFβ. HIF-1α and HIF-2α show a great degree of similarity in their conserved and functional domains, a feature that is not shared with HIF-3α (Figure 1.2) (Gu, Moran et al. 1998). HIF-1α and HIF-2α contain two transactivation domains, the N-TAD (N terminal transactivation domain) and the C-TAD (C-terminal transactivation domain) that are responsible for HIF transcriptional activity (Jiang, Rue et al. 1996, Jiang, Zheng et al. 1997, Pugh, O'Rourke et al. 1997). HIF-1α and HIF-2α also have a central ODDD (oxygen-dependent degradative domain), which is crucial for the oxygen-dependent regulation of HIF protein levels (Huang, Gu et al. 1998). While not as well studied as HIF-1α and HIF-2α, HIF-3α appears to play a more subtle and still poorly defined role in hypoxic gene induction (Heikkila, Pasanen et al. 2011).
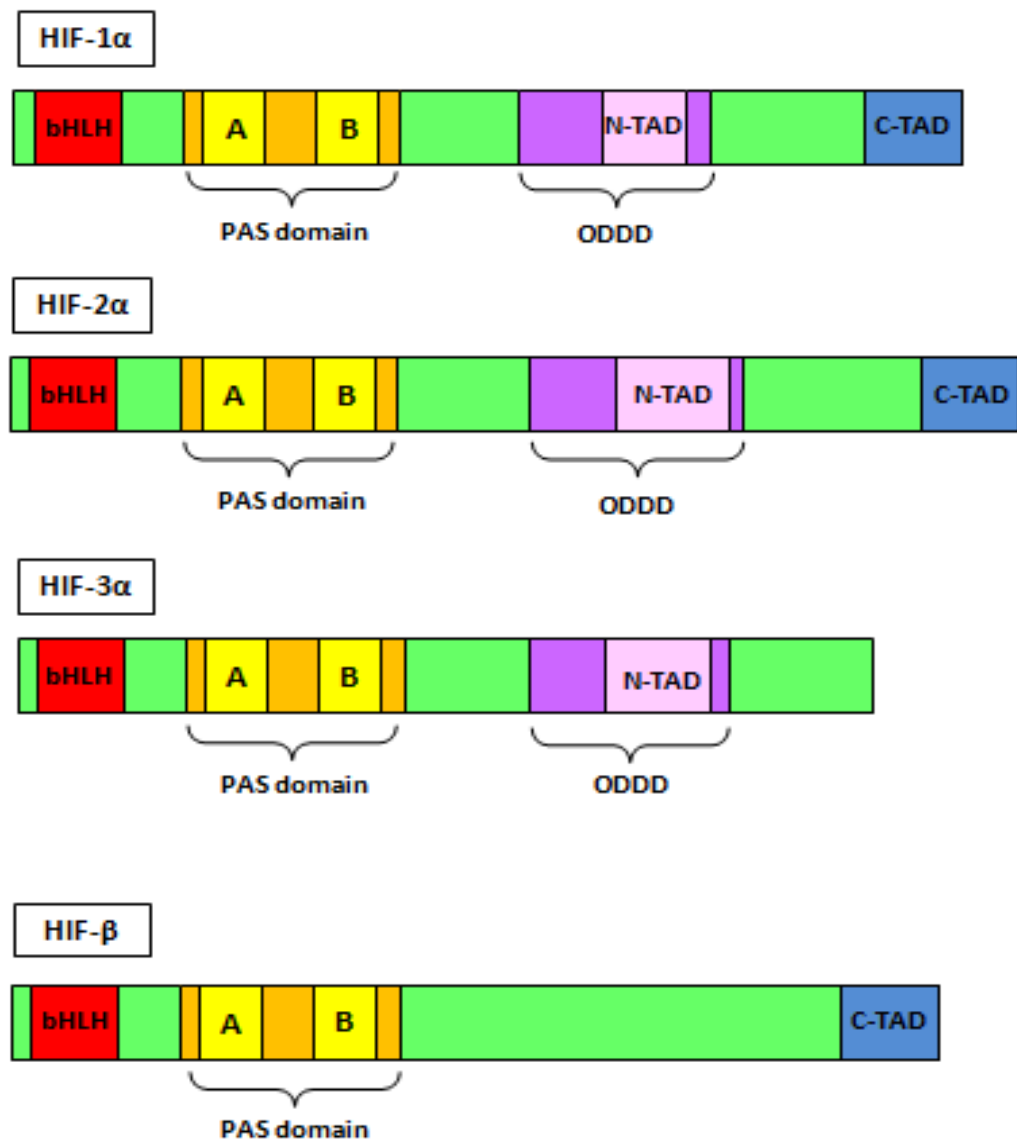
Figure 1.2: Schematic diagram showing the functional domains of the Hypoxia Inducible Factor subunits. Each of the α subunits can heterodimerise with a constitutively expressed partner HIF-β to form the active HIF transcription factor. The basic helix-loop-helix (bHLH) is the DNA-binding domain involved in dimerisation and binding to the DNA consensus sequence G/ACGTG. The PAS (Per, Arnt, Sim homology) domain also promotes heterodimerisation. All three HIFα subunits share an N-TAD (N-terminal activation domain) found within an oxygen dependent degradation domain (ODDD), but only HIF-1α and HIF-2α contain a C-TAD (C-terminal activation domain).

The HIFα protein is highly sensitive to changes in oxygen levels, where exposure to normoxic conditions results in its rapid degradation (Wang, Jiang et al. 1995, Huang, Gu et al. 1998). Three enzymes known as the prolyl hydroxylase domain-containing enzymes (PHDs) regulate HIFα through oxygen-dependent hydroxylation of the ODDD, resulting in rapid protein degradation (Epstein, Gleadle et al. 2001, Ivan, Kondo et al. 2001, Jaakkola, Mole et al. 2001). These hydroxylases require oxygen and 2-oxoglutarate as substrates along with iron and ascorbate as cofactors to function, resulting in the production of hydroxylated HIFα protein, succinate and carbon dioxide as products (Jaakkola, Mole et al. 2001). The PHD's dependence on oxygen for HIFα protein regulation, demonstrates their crucial role in cellular oxygen sensing.

In normoxia, the PHDs add hydroxyl groups to two proline residues located within the ODDD's of both HIF-1α (P564 and P402 in human HIF-1α) and HIF-2α protein (P530 and P405 in human HIF-2α) (Figure 1.3) (Huang, Arany et al. 1996, Huang, Gu et al. 1998, Bruick and McKnight 2001, Epstein, Gleadle et al. 2001). Proline hydroxylation provides sites of interaction for the von Hippel-Lindau proteins which form part of an E3 ubiquitin-protein ligase complex. This interaction results in polyubiquitination of the HIFα protein in the cytoplasm and its subsequent rapid degradation in the proteasome (Huang, Gu et al. 1998, Maxwell, Wiesener et al. 1999).

The three PHDs (PHD1-3) are known to hydroxylate the HIFα proteins in a non-redundant manner. Although the three isoforms functionally regulate the HIFs, this is dependent on their relative expression levels which can vary across different cell types, and inherent specificity for different HIFα proteins (Appelhoff, Tian et al. 2004, Takeda, Aguila et al. 2008). Knock down studies of all three hydroxylases identified PHD2 as the main isoform responsible for HIFα degradation (Berra, Benizri et al. 2003).

Whilst the PHDs play a key role in HIF degradation, they are not the only hydroxylases that regulate HIFα proteins. Factor Inhibiting HIF (FIH) is an asparaginyl hydroxylase whose oxygen-dependent modification of the HIFα C-TAD in normoxia ensures that any HIFα that has escaped degradation is not fully activated. This is achieved by the hydroxylation of a specific asparagine residue found within the C-TAD of HIF-1α (N803

in human HIF-1α) and HIF-2α (N851 in human HIF-2α), preventing recruitment of transcriptional co-activator CBP/p300 and formation of an active transcription complex (Hewitson, McNeill et al. 2002, Lando, Peet et al. 2002, Lando, Peet et al. 2002, Koivunen, Hirsila et al. 2004).

In hypoxia, the oxygen-dependent hydroxylases lose activity and HIFα protein is less efficiently hydroxylated, avoids proteolysis and translocates to the nucleus (Figure 1.3). The hydroxylases are so sensitive to cytoplasmic oxygen levels that stabilisation of HIFα occurs within minutes of exposure to hypoxia (Salceda and Caro 1997, Jewell, Kvietikova et al. 2001). Following translocation of HIFα to the nucleus, heterodimerisation occurs with its partner factor HIFβ to form a functional HIF transcription factor capable of interacting with the transcriptional co-activators. The HIFs bind to a specific consensus sequence (G/ACGTG) on the DNA known as the Hypoxic Response Element (HRE) to regulate specific target genes (Semenza and Wang 1992).
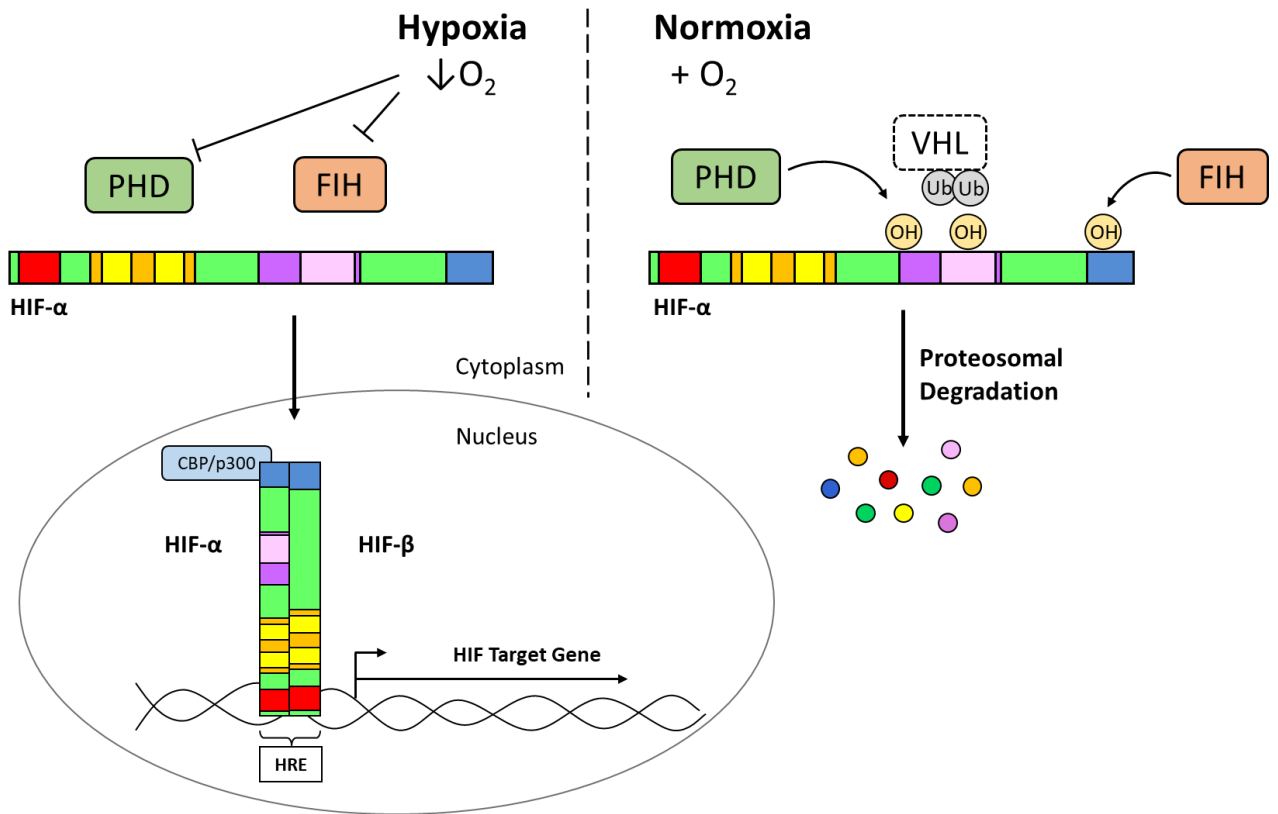
Figure 1.3: HIF post-translational hydroxylase regulation showing the interactions between HIF-α protein and hydroxylases (PHD and FIH) under normoxic conditions and between the HIF-α protein and HIF response element on target genes under hypoxic conditions. Normoxia detail includes the hydroxylated residues and resulting degradation of HIF-α protein. Hypoxia detail shows the absence of hydroxylated residues, stabilisation of HIF-α protein and subsequent translocation into the nucleus where the HIF-α subunits can heterodimerise with HIF-β.

Functional experiments, gene profiling and expression arrays in numerous cell types have shown that the HIFs are central to regulating hundreds of different target genes (Semenza and Wang 1992, Wenger, Stiehl et al. 2005, Elvidge, Glenny et al. 2006, Hu, Iyer et al. 2006, Benita, Kikuchi et al. 2009, Mole, Blancher et al. 2009, Xia, Lemieux et al. 2009). Gene activation is not limited to direct target genes but also indirectly through the regulation of other key biochemical pathways. This results in a complicated network of target genes with far-reaching consequences in response to hypoxic stress (Ortiz-Barahona, Villar et al. 2010, Schodel, Mole et al. 2013). Specific pathway examples include vascular remodelling, erythropoiesis, glycolysis, cell proliferation, angiogenesis and epithelial to mesenchymal transition (EMT) (Dengler, Galbraith et al. 2014, Lee and Simon 2015).

1.2.3 HIF-1 and HIF-2

Despite the similarities in structure and hydroxylation-dependent regulation of HIF-1α and HIF-2α, studies have shown differences in their roles in embryonic development, cell-dependent expression patterns and selected target gene regulation (reviewed by (Hu, Wang et al. 2003, Sowter, Raval et al. 2003)). HIF-1α knockout mice are embryonically lethal at day E10.5 and HIF-2α knockout mice from E16.5, confirming the importance of the HIFs in embryonic development, and importantly, demonstrating that the two factors are non-redundant during mouse development (Iyer, Kotch et al. 1998, Ryan, Lo et al. 1998, Tian, Hammer et al. 1998). Although both factors are essential for development, the morphological defects differed between HIF-1α and HIF-2α knockout mice and interestingly, differences were reported between three independently derived HIF-2α knockout mice (Tian, Hammer et al. 1998, Peng, Zhang et al. 2000, Compernolle, Brusselmans et al. 2002).

HIF-1α knockout mice presented with abnormal cardiovascular formation in addition to aberrant vascularisation in other parts of the embryo that was linked to the dysregulated expression of hypoxic target genes such as *Vegf-A* (Iyer, Kotch et al. 1998, Ryan, Lo et al. 1998). Comparatively, the first of three independent HIF-2α knockout studies showed the cause of death to be bradycardia as a result of a disruption in catecholamine homeostasis (Tian, Hammer et al. 1998). Interestingly,

HIF-2α knockout mice that could survive to adulthood were created by backcrossing heterozygous HIF-2α knockout mice from the original 129S6/SvEvTac strain generated by Tian *et al* with heterozygous C57BL/6J HIF-2α knockout mice, to create 129S6/SvEvTac:C57BL6J HIF-2α knockout mice (Tian, Hammer et al. 1998, Scortegagna, Morris et al. 2003). These mice showed a number of physiological and molecular phenotypes including retinopathy, cardiac hypertrophy, skeletal myopathy, metabolic abnormalities, impaired homeostasis of reactive oxygen species, and pancytopenia as a result of deficient haematopoietic development (Scortegagna, Ding et al. 2003, Scortegagna, Ding et al. 2005). Importantly, these results support a role for HIF-2α in haematopoiesis, with important implications for a potential role in MM.

A second independently derived HIF-2α null mouse study resulted in embryonic death between days E9.5 and E12.5 from haemorrhagic and severe vascular remodelling defects (Peng, Zhang et al. 2000). Lastly, a third study produced HIF-2α knockout mice that presented with a fault in lung surfactant production alongside the previously observed vascular remodelling which ultimately lead to heart failure, lung collapse and respiratory failure at E13.5 (Compernolle, Brusselmans et al. 2002) Whilst the different physiological deficiencies observed between the HIF-2α knockout experiments was likely attributed to variations in mouse genetic backgrounds, comparisons between the HIF-1α and HIF-2α knockout models demonstrate distinct phenotypes. These are not fully explained by their relative expression patterns (see below), and are likely to reflect inherent differences in function mediated by distinct target gene repertoires.

In normal cells and tissues, HIF-1α mRNA is considered to be ubiquitously expressed whilst HIF-2α mRNA expression is specifically expressed in endothelial, epithelial, fibroblast, macrophage and neural cells as well as in the lung and carotid body (Tian, Hammer et al. 1998, Talks, Turley et al. 2000, Wiesener, Jurgensen et al. 2003). Conditional HIF-1α knockout studies identified a range of distinct roles for HIF-1α that was consistent with its ubiquitous expression, and supported the knockout experiment performed by Iyer *et al* and Ryan *et al* (Iyer, Kotch et al. 1998, Ryan, Lo et al. 1998). These functions included adaptation of the skin to hypoxia (Boutin, Weidemann et al. 2008), metabolic control in skeletal muscle (Mason, Howlett et al. 2004), bactericidal activity of macrophages (Peyssonnaux, Datta et al. 2005), acute inflammatory

responses (Cramer, Yamanishi et al. 2003), brain development (Tomita, Ueno et al. 2003, Milosevic, Maisel et al. 2007), and normal heart function (Huang, Hickey et al. 2004). HIF-2α conditional knockout studies unveiled specialised functions, some of which overlapped with the complete knockout animal data discussed above. Specifically, mice containing endothelial cells with deficient HIF-2α expression displayed altered vessel permeability consistent with the vascular deficiencies observed by Peng *et al* (Peng, Zhang et al. 2000, Skuli, Liu et al. 2009). Other physiological effects of conditional HIF-2α knockout included anaemia (Gruber, Hu et al. 2007), iron deficiency (Mastrogiannaki, Matak et al. 2009) and erythropoietin dysregulation in both hepatocytes and astrocytes (Rankin, Biju et al. 2007, Weidemann, Kerdiles et al. 2009). These data reveal a highly context-dependent role for HIF-2α, consistent with its tissue specific expression and function.

Comparative assessment of HIF expression in a cancer context showed that HIF-1α, HIF-2α or both factors could be upregulated (Zhong, De Marzo et al. 1999, Talks, Turley et al. 2000). HIF-1 and HIF-2 have been shown to share many of the same target genes, such as the angiogenic activator *Vegf-A*, and regulate some common pathways. These findings were not surprising given the similarity in sequence and structure between the two factors, and that both recognise and bind the same consensus HRE sequence for target gene regulation. Despite this, not all target genes are regulated by both HIFs, for example *Bnip3* and *Epo* have been found to be HIF-1 or HIF-2 preferential targets, respectively, in a context specific manner (Raval, Lau et al. 2005, Lee and Simon 2015). Hence the differential expression patterns of HIF-1α and HIF-2α in normal tissue only partially explain why the two factors regulate different target genes, and in cases where both HIFα proteins are expressed in the same cells, they clearly demonstrate target gene specificity.

1.2.4 HIF-1 and HIF-2 in cancer

Extensive research of the HIFαs in cancer survival has shown that their expression patterns can be just as critical to cancer survival as they are to non-malignant cells and tissues. Many human cancers have been shown to aberrantly upregulate both HIF-1α and HIF-2α from early stages of disease, an observation that correlated with more

aggressive disease and higher mortality rates (Talks, Turley et al. 2000, Semenza 2014). Despite the differential expression patterns of HIF-1α and HIF-2α in normal tissues, the upregulation of both HIFs similarly promote a more aggressive phenotype in a broad range of cancers including lung, stomach, breast, brain, ovarian, skin, colorectal, bladder and bone malignancies (Talks, Turley et al. 2000). Whilst this this has been shown for the majority of cancers, there is evidence for the differential roles of HIF-1α compared to HIF-2α in specific cancers.

Direct disruption of either HIFα isoform identified HIF-1α, but not HIF-2α, as a critical hypoxic regulator in breast cancers cells, whilst the same study identified HIF-2α as the critical factor driving the hypoxic response in renal carcinoma cells (Sowter, Raval et al. 2003). Subsequent studies in these cancer contexts showed that HIF-1α and HIF-2α had differential roles in target gene regulation, and ultimately in tumour growth (Raval, Lau et al. 2005). Specifically, HIF-1α but not HIF-2α targeted *Bnip3* regulation, whilst HIF-2α primarily regulated *cyclinD1*, *Tnfα* and *Vegf-A*. Multiple studies have also shown that the two HIFs can have opposing roles. For example HIF-2α increases renal cell carcinoma (RCC) tumour growth, whilst HIF-1α reduces growth through the differential regulation of glycolytic and metabolic pathways (Raval, Lau et al. 2005, Biswas, Troy et al. 2010). In many cases, HIF-2α is associated with more aggressive disease and poorer patient prognosis (Lofstedt, Fredlund et al. 2007). From these data, it is evident that differential expression of HIF-1α and HIF-2α can result in significantly different disease outcomes.

The differential expression patterns and roles of HIF-1α and HIF-2α allude to a difference in their regulation. A study by Bracken *et al.* compared the expression of HIF-1α and HIF-2α protein under various oxygen conditions and found a delayed induction of HIF-2α compared to HIF-1α in PC12 and HeLa cells under various oxygen conditions, but not in HEK293T, Cos-1, CACO2 and HepG2 cells (Bracken, Fedele et al. 2006). Interestingly, whilst HIF-1α protein was stabilised in PC12 and HeLa cells following treatment with the hypoxia mimetic 2,2-dipyridyl (DP), which inactivates the PHDs by chelating iron, HIF-2α protein expression was not affected, further supporting a differential mode of regulation between the two factors. Further evidence using a neuroblastoma cell line (SK-N-BE(2)C), showed similar delayed induction of HIF-2α

protein compared to HIF-1α (Holmquist-Mengelbier, Fredlund et al. 2006). A more recent study also using neuroblastoma cells found the same differential expression pattern and identified an upregulation in *Hif2α* mRNA to be responsible for the delayed hypoxic protein expression (Lin, Cong et al. 2011).

These data identify an acute versus chronic induction of HIF-1α and HIF-2α protein, respectively, in some cancer cell types that could have significant implications on their roles in cancer progression, tumour growth and disease prognosis *in vivo*. Furthermore, the differential regulation together with differential expression and target gene selectivity, support distinct roles for the HIFα proteins in cancer.

1.3 Understanding the role of HIF-1 and HIF-2 in MM

1.3.1 The use of animal models to study MM

Animal models are very good tools to study the molecular and cellular mechanisms driving disease in an *in vivo* context and are often required as a prerequisite to clinical studies. Currently, a number of different mouse model systems are available to study MM, including the use of pristane injected BALB/c mice, SCID xenograft mice, SCID-hu models and 5T murine models (5TMM) (Libouban 2015).

The earliest model was created by injecting BALB/c mice with the mineral oil pristine into the peritoneum (Potter 1986). This treatment resulted in the formation of numerous plasmacytomas within the peritoneal cavity that could be retransplanted into pristine-prepared mice. Whilst the cancerous plasma cells in this model closely resembled MM cells, these tumours differed significantly in that they were located in the peritoneum, were not spontaneous and contained different oncogenic rearrangements to the human disease (Potter 1986, van den Akker, Radl et al. 1996, Gado, Silva et al. 2001).

Other models include the use of severe combined immunodeficiency (SCID) mice, specifically a SCID-xenograft model and a SCID-hu model. The SCID-xenograft mice were created from either the intravenous or intraperitoneal injection of cancer cells including primary human MM cells or MM cell lines (Asosingh, Radl et al. 2000, Libouban 2015). These mice displayed osteolysis, BM involvement and the presence of a paraprotein, symptoms like those observed in human MM. The SCID-hu mouse model involved taking human foetal bone fragments and engrafting these into mice (Urashima, Chen et al. 1997, Yaccoby, Barlogie et al. 1998). These mice were then injected with human MM cells, thus providing a microenvironment that better supported human MM cell homing and growth in the BM.

Ageing C57Bl/KalwRij mice spontaneously develop MM at a frequency of 0.5% in mice greater than 2 years old (Radl, De Glopper et al. 1979, Radl, Croese et al. 1988, Radl 1990). The cancerous cells were harvested from the BM of these mice and intravenously injected into young healthy mice, resulting in the development of MM.

The syngeneic cells isolated from these mice and then injected into healthy mice were referred to as the 5T series. Eight different cell lines were isolated from individual mice and tested using this model. (Vanderkerken, De Raeve et al. 1997, Radl 1999). Of these 8 characterised lines, the two most studied are the 5T2 and the 5T33 murine models. Tumour was first detected at 9 weeks using 5T2 murine model, with moderate tumour growth and bone lesions developing over 4 months. In contrast, the 5T33 murine model showed detectable tumour at 2 weeks, displayed evidence of bone lesions and developed terminal disease at 4-5 weeks, making this the more aggressive model of MM. Characterisation of both models showed that the MM cells home to the BM, where they secrete abundant paraprotein which can be detected in the peripheral blood, thus creating a murine model with comparable symptoms to those observed in the human disease (Garrett, Dallas et al. 1997, Vanderkerken, De Raeve et al. 1997).

Both the 5T2 and 5T33 murine models of MM represent excellent pre-clinical models, due to their successful use to both characterise the pathology of MM in mice, and test the efficacy of potential drug therapies such as bisphosphonates (Radl, Croese et al. 1985, Manning, Chamberlain et al. 1995, Dallas, Garrett et al. 1999). However, both require taking MM cells from aged mice, and injecting these directly into young mice (Degrassi, Hilbert et al. 1993, Vanderkerken, De Raeve et al. 1997). A newer MM cell line known as the 5TGM1 line overcomes this limitation as it can be propagated *in vitro* without the need for supplementation, stromal cell support or conditioned media. As with the aforementioned 5T2 and 5T33 models, the 5TGM1/C57BL/KaLwRij model has also been successfully used for pre-clinical drug analysis (Edwards, Edwards et al. 2008). The 5TGM1 cells are derived from the 5T33 cells, and as such, display a similar aggressive disease phenotype developing over 4 weeks (Dallas, Garrett et al. 1999). This model has been widely used in place of the 5T33 murine model to explore the molecular pathways and cellular interactions that drive disease from both an *in vitro* and an *in vivo* perspective.

1.3.2 Angiogenesis, bone osteolysis and MM

The rapid proliferation of cancer cells in solid tumours often compromises oxygen supply to the area and threatens cellular survival. In response, there is an increase in

angiogenic stimuli (such as hypoxia and expression of VEGFs) that subsequently upregulate angiogenesis to relieve hypoxic stress and support tumorigenesis (Maxwell, Dachs et al. 1997). In normal tissues, once the oxygen supply has been restored, the decreased expression of angiogenic factors and the increased expression of angiostatic factors halts angiogenesis (Klein, Roghani et al. 1997). In cancerous tissues however, an equilibrium between angiogenic and angiostatic factors is not reached and angiogenesis continues to be upregulated, thus sustaining tumour growth and expansion (Papetti and Herman 2002).

Angiogenesis is not only critical to solid tumour formation, but also for the progression of haematological diseases. The earliest study of angiogenesis in MM analysed the BM microvessel density (MVD) as a measurement of angiogenesis between MGUS and MM patients (Vacca, Ribatti et al. 1994). This study discovered significantly increased BM MVD in patients with active MM, and was the first to identify a correlation between angiogenesis and disease prognosis in MM (Vacca, Ribatti et al. 1994). As was briefly mentioned in section 1.1.6, investigations by Asosingh *et al* further explored the role of angiogenesis in MM disease progression *in vivo* (Asosingh, De Raeve et al. 2004). BM samples were isolated at weekly intervals from 5T2MM mice, and MVD analysed by staining for CD31 and counting the number of blood vessels present (Figure 1.4). BM MVD in the 5T2MM mouse model identified a pre-angiogenic stage with slow tumour growth that preceded an increase in MVD termed the 'angiogenic switch'. The increase in angiogenesis was immediately followed by progressive tumour expansion until the end stage of disease was reached, demonstrating a link between angiogenesis and disease progression. Furthermore, this was the first study to show a pre-clinical assessment of angiogenesis through to terminal disease, considering that clinically diagnosed patients already present with established angiogenesis.

In addition to the angiogenic response observed in the BM, the emergence of detectable bone lesions is commonly associated with progressive MM. Patients with symptomatic osteolysis display elevated levels of CXCL12 that act to increase osteoclast driven bone resorption (Zannettino, Farrugia et al. 2005). Further investigation using *in vitro* experimentation and patient samples showed that CXCL12 directly promotes both osteolysis and angiogenesis in MM (Martin, Dewar et al. 2006).

The link between bone resorption and neovascularisation shows that both symptoms correlate with a poor disease prognosis.
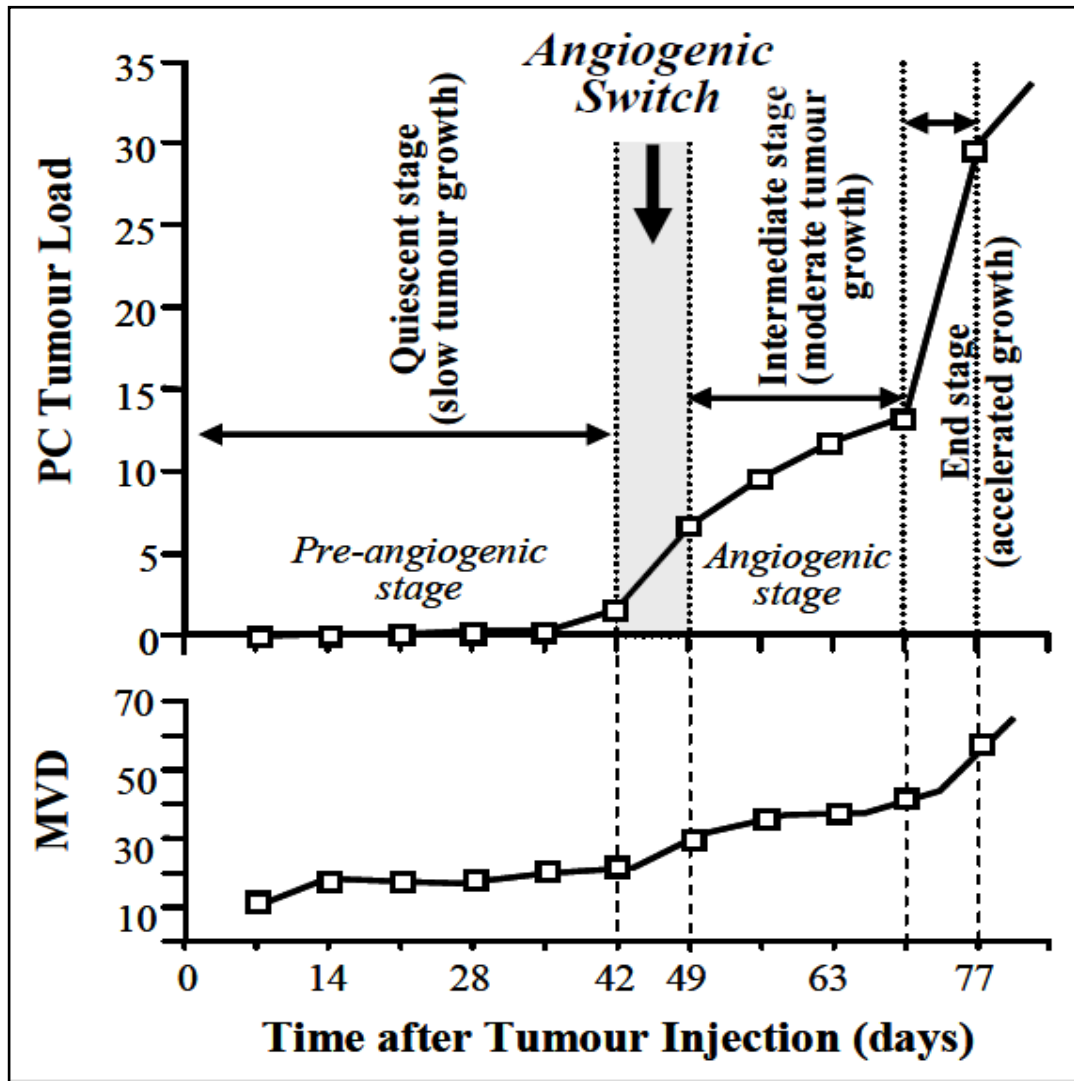
Figure 1.4: Schematic of the 5T2MM mouse model system demonstrating the quiescent, intermediate and end stages of multiple myeloma disease. The progression of disease following the slow growing quiescent stage is driven by an upregulation in angiogenesis labelled the "angiogenic switch". The upregulation of angiogenesis (MVD) correlates with an increase PC tumour load, accelerating until the end stage of disease. Figure adapted with permission (Asosingh, De Raeve et al. 2004).

1.3.3 Hypoxia, HIF and MM

In solid tumours, the resulting hypoxic microenvironment contributes to cancer cell survival and metastasis, through processes such as angiogenesis, to advance disease (Harris 2002, Subarsky and Hill 2003). Comparatively, far less is known about the role of hypoxia in haematological diseases. Early studies using the 5T2MM murine model and the hypoxyprobe pimonidazole and HIF-1α to measure BM hypoxia, demonstrated that the BM of both normal and diseased mice were hypoxic (Asosingh, De Raeve et al. 2005). Interestingly, the CD45+ 5T2MM cell subpopulation present at early stages of disease were more resistant to apoptosis in hypoxia (Asosingh, De Raeve et al. 2003, Asosingh, De Raeve et al. 2005). This resistance provided a critical advantage in the naturally hypoxic microenvironment of the BM, and was the first study to demonstrate that hypoxia is important for MM establishment in the BM.

The upregulation of HIF in hypoxia results in transcriptional changes to numerous pathways that are critical to non-malignant and malignant cellular survival. The use of HIF-1α as a measure of hypoxia in 5T2MM mice therefore suggested that HIFα could be directly contributing to MM cell survival and expansion in the hypoxic BM microenvironment. Immunohistochemical analyses of BM specimens from both SCID-hu and 5T33MM mice injected with MM cells, showed a correlation between tumour burden and HIF-1α expression (Azab, Hu et al. 2012). Hypoxia was also shown to influence MM cell homing by increasing the number of circulating cells *in vivo*. Furthermore, intravenous injection of mice with MM cells lacking HIF-1α expression (using siRNA knockdown) showed a loss of the hypoxia-dependent accelerated dissemination of cells to the BM, where the number of circulating cells was similar to normoxia experiments. Lastly, a decrease in adhesion of MM cells to BM stromal cells isolated from MM patients was observed in hypoxic conditions. This correlated with an increase in HIF-1α and HIF-2α expression and a decrease in E-cadherin expression, suggesting that hypoxia potentially influences migration of cells from the BM using the HIF pathway. The data from this study not only confirmed that HIF-1α plays a role in MM tumour growth in the BM, but suggested that HIF-1α is linked with MM cell homing and metastasis.

Investigations by Storti *etal* further explored the role of the HIF-1α, and the downstream pathways it regulates, on MM disease parameters *in vitro* and *in vivo* (Storti, Bolzoni et al. 2013). Short hairpin RNA knockdown of HIF-1α in human MM cells showed a loss of specific angiogenic target gene expression in hypoxia, including *Vegf-A* and *MMP9*. This directly linked the HIF-1α transcriptional pathway with MM angiogenesis. In addition, the expression of pro-osteoclastogenic target genes *MIP1A* and *IL-7* were significantly decreased in HIF-1α knockdown MM cells. This data was supported by *in vivo* experiments where the HIF-1α knockdown MM cells were injected subcutaneously into SCID-NOD mice, resulting in a HIF-1α-dependent decrease in tumour size and angiogenesis (via CD34 and VEGF immunostaining). Furthermore, intratibial injection of the HIF-1α knock down MM cells into mice demonstrated a decrease in BM angiogenesis and bone resorption. These data supported previous findings, highlighting a hypoxia-dependent role for HIF-1α in MM tumour growth. Importantly, this study directly linked HIF-1α with angiogenesis, a critical symptom for MM disease progression.

In recent times, HIF-1α has not only been associated with MM tumour growth, angiogenesis and metastasis, but also with cellular metabolism, BM-MM PC interactions, drug resistance, and MM relapse (Borsi, Perrone et al. 2014, Borsi, Perrone et al. 2014, Ria, Catacchio et al. 2014). Human MM cells treated with the HIF-1α antagonist EZN-2968 resulted in a decrease in adhesion and downstream expression of IL-6 and VEGF, showing that HIF-1α is important for MM and BMSC interactions and the molecular expression profile that follows (Borsi, Perrone et al. 2014). Furthermore, treatment of MM cells with EZN-2968 resulted in lowered cellular proliferation and significant changes to metabolism (Borsi, Perrone et al. 2014). This disruption to MM cell homeostasis highlighted the potential for HIF-1α as a therapeutic target. This was explored in MM patients, where HIF-1α was upregulated compared to MGUS, early MM and MM patients in remission (Ria, Catacchio et al. 2014). Inhibition of HIF-1α by siRNA or panobinostat treatment (an indirect HIF-1α inhibitor) in MM endothelial cells isolated from these patients, showed decreased angiogenesis and increased sensitivity to bortezomib and lenalidomide drug treatments.

These data link HIF-1α expression with MM establishment, metastasis and disease prognosis *in vitro* with the support of some *in vivo* experimentation, however they did not include an assessment of HIF-2α alongside HIF-1α in MM.

1.3.4 HIF-1 and HIF-2 in MM

To date, the majority of studies assessing the significance of HIF in MM have focused exclusively on HIF-1α, with a paucity of data on the contribution of HIF-2α. HIF-1α and HIF-2α are known to have differential roles in a cancer context, where HIF-2α has been shown to result in more aggressive disease and poorer disease prognosis in some cancers (Lofstedt, Fredlund et al. 2007). Whilst HIF-2α remains understudied, there are some key papers published prior to the commencement of this PhD and throughout my studies that have provided evidence of the importance of HIF-2α in MM.

A study by Giatromanolaki *et al* showed that both HIF-1α and HIF-2α are upregulated in BM samples from MM patients, and this correlated with an upregulation in MVD (using CD31) (Giatromanolaki, Bai et al. 2010). Furthermore, there was an observed correlation between HIFα expression and VEGF. Approximately 40% of patients showed an induction of the HIF-VEGF pathway that was associated with an increase in BM angiogenesis. This correlation between BM MVD, VEGF expression and HIF-1α and HIF-2α expression suggested that both factors contribute to MM angiogenesis in a patient context.

An extensive study by Martin *et al,* using both patient samples and cell lines, was the first to directly compare both HIFs and their contribution to MM disease (Martin, Diamond et al. 2009). Immunohistochemistry was used to stain for HIF-1α, HIF-2α and CXCL12 in patient BM biopsies and interestingly found that HIF-2α and CXCL12 were co-expressed in MM PCs. Further investigation showed that HIF-1α protein, HIF-2α protein and CXCL12 mRNA were upregulated in the LP-1 human MM cell line under hypoxic conditions. Given that CXCL12 is a key contributor to MM bone resorption (Diamond, Labrinidis et al. 2009) and that HIF-1α expression has also been linked to bone resorption (Storti, Bolzoni et al. 2013), the correlation between HIF-1α, HIF-2α

and CXCL12 expression supports a role for the HIFα pathway in supporting MM disease progression.

Analyses of HIF-2α protein expression in LP-1 cells under hypoxic conditions (Figure 1.5) showed a delayed response to hypoxia of approximately 6 hours when compared to HIF-1α, as has been observed in other cell lines (Bracken, Fedele et al. 2006, Holmquist-Mengelbier, Fredlund et al. 2006, Martin, Diamond et al. 2009). The delayed induction in HIF-2α protein correlated with the induction of CXCL12 mRNA observed following 24 hours of hypoxic treatment (Figure 1.5) (Martin, Diamond et al. 2009). The independent overexpression of HIF-1α and HIF-2α in LP-1 cells induced CXCL12 mRNA expression, whilst conversely, knockdown of HIF-1α and HIF-2α decreased CXCL12 mRNA expression. In both experiments, HIF-2α had a greater effect on CXCL12 expression levels when compared to HIF-1α, where CXCL12 mRNA upregulation in hypoxia was lost in HIF-2α knockdown cells (Martin, Diamond et al. 2009). Following these *in vitro* experiments, LP-1 cell lines overexpressing either HIF-1α, HIF-2α or CXCL12 were subcutaneously injected into BALB/c nude mice, where all three cell lines showed increased tumour size and angiogenesis. These data implicated both HIFα isoforms in MM disease progression and was the first study to directly compare HIF-1α and HIF-2α in MM using both *in vitro* and *in* vivo experimentation. Importantly, the differential expression of HIF-1α and HIF-2α was observed and HIF-2α found to affect angiogenesis through the HIF-CXCL12 pathway.

The CXCL12 chemokine not only influences angiogenesis and bone osteolysis in MM, but facilitates MM PC homing to, and retention within, the BM as discussed in section 1.1.5. Furthermore, BM hypoxia correlated positively with MM PC dissemination through the HIFα pathway (Azab, Hu et al. 2012). Based on these data, a recent study by Vandyke *et al* explored the mechanistic role of the HIF-2α-CXCL12 pathway in MM PC dissemination (Vandyke, Zeissig et al. 2017). HIF-2α overexpression in the RPMI-8226 human MM cell line resulted in decreased migration and adhesion to stromal cells whilst overcoming CXCL12 signalling from stromal cells, potentially allowing MM PCs to egress from the BM and recirculate. Further investigation found that HIF-2α may regulate MM PC dissemination through upregulation of the CCR1 chemokine receptor, where increased CCR1 expression was associated with MM PC circulation in the

peripheral blood of MM patients. Overall, the direct correlation of HIF-2α with increased angiogenesis and dissemination suggests a more prominent role for HIF-2α in MM disease severity and prognosis compared to HIF-1α.
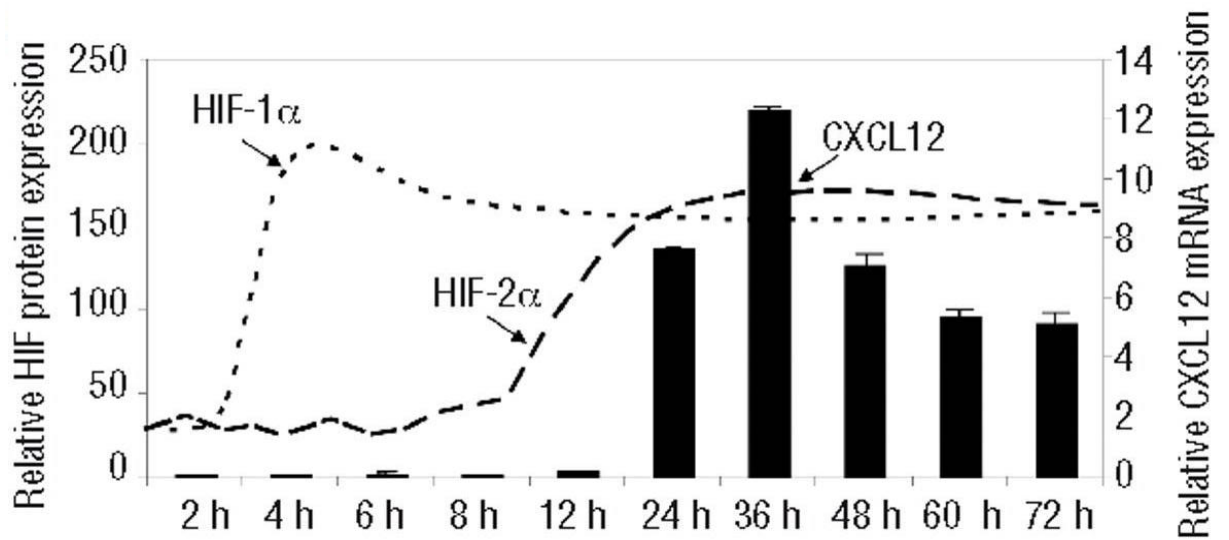
Figure 1.5: Graph showing the mRNA levels of chemokine CXCL12 measured via qPCR (solid bars) compared to the HIF-1α and HIF-2α protein levels (dotted lines) measured via quantitative western blot of protein extracts from LP-1 cells in hypoxia. Data reproduced with permission (Martin, Diamond et al. 2009).

In summary, whilst both HIF-1α and HIF-2α contribute to disease as evidenced by Giatromanolaki *et al* (Giatromanolaki, Bai et al. 2010) and Martin *et al* (Martin, Diamond et al. 2009), their differential expression patterns support significantly different roles for these two factors in MM pathogenesis. HIF-1α has been directly correlated with various clinical aspects of MM including angiogenesis, tumour burden, homing, dissemination, BM hypoxia and bone resorption. Despite this, to date, no study has analysed the direct effect of HIF-1α on complete disease progression from tumour establishment through to end-stage disease using a systemic *in vivo* model of murine MM.

Compared to HIF-1α, the contribution of HIF-2α to MM pathogenesis remains largely understudied and under-considered in current approaches to disease prognosis and treatment, despite recent findings. In addition to this paucity of data, no analysis of the direct role of HIF-2α on disease progression has been performed *in vivo* using murine models for MM. Furthermore, there has been no comparative analysis of both HIFα isoforms in MM disease progression and severity *in vivo.*

1.4 Project aims

Aim

Investigate the specific roles of HIF-2α compared to HIF-1α in multiple myeloma disease progression using the 5TGM1/C57BL/KaLwRij MM mouse model system.

Hypothesis

HIF-2α plays an important role in MM disease progression *in vivo* that is distinct from HIF-1α.

Approach

To investigate the direct role of HIF-1α and HIF-2α *in vivo*, the 5TGM1 cell line will be genetically modified to alter HIFα expression *in vitro*. The initial stratey will be to use the TetOn3G vector system to generate stable cell lines that inducibly overexpress HIFα following tetracycline treatment. This will provides temporal and reversible control of HIFα expression *in vivo,* allowing for the isolation of effects on disease progression from any confounding effects on cellular homing to the bone marrow.

The HIF-1α and HIF-2α modified 5TGM1 cells will subsequently be used for *in vivo* studies with the C57BL/KaLwRij mouse strain to assess the differential roles of the two factors in MM disease. Specific disease parameters that will be assessed include systemic tumour burden using *in vivo* bioluminescence, serum paraprotein using electrophoresis and tumour homing, growth and dissemination using Immunohistochemical analyses of the bone marrow and spleen.

Chapter 2
MATERIALS AND METHODS

2.1 Materials

2.1.1 Equipment

ABI 7500 StepOnePlus Realtime PCR	Applied Biosystems
Agarose Gel System	BioRad
Benchtop Centrifuge S415D	Beckman Coulter
Biophotometer	Eppendorf
ChemiDoc MP Imaging System	Biorad
DNA Engine Peltier Thermal cycler	Bio-Rad
Emax Precision Microplate Reader	Molecular Devices
Gallios	Beckman Coulter
Imaging System	BioDoc-it
IVIS Lumina XRMS^{TM}	Perkin Elmer
IVIS Spectrum^{TM}	Perkin Elmer
IVIS Xenogen^{TM}	Perkin Elmer
Leica EG1150 H Paraffin Dispenser	Leica Biosystems
MoFlo Astrios High Speed Cell Sorter with CyClone^{TM} (Using Summit Software Version 6.2)	Beckman Coulter
Nanodrop 2000	Thermo Fisher
NanoZoomer HT digital scanner	Hamamatsu
Nikon Eclipse TE300 (using NIS-Elements AR software)	Nikon
SDS-PAGE mini gel system	BioRad
Shandon Excelsior ES Tissue Processor	Thermo Fisher
TC10 Automated Cell Counter	Bio-Rad
UV Transilluminator	UVP
Wet Transfer System	BioRad

2.1.2 Consumables

12 x 75 mm Polystyrene tubes 35mm cell strainer cap	In vitro technologies
12 x 75 mm Polystyrene tubes	In vitro technologies
96-Well Reaction Plate (0.1mL) (MicroAmp Fast)	Applied Biosystems (Life Technologies)
AnaeroGen Hypoxia Sachet	Oxoid (Australia)
BD Falcon Tubes	BD Biosciences
Cell counting slides for TC10, Dual-Chamber	Bio-Rad
Cell Strainers (for Flow Cytometry)	Falcon
Corning 3603: 96 Well Assay Plate (Black sides, clear bottom)	Sigma Aldrich
Cuvettes	Eppendorf
EU Opti-seal	Bioplastics
FACS tubes	BD Biosciences
Microfuge Tubes	Eppendorf
Mini Collect Z Serum Seperator (gold cap)	Greiner Bio-One (Interpath)
Nitrocellulose Membrane	PALL life sciences
PAP Pen	Sigma-Aldrich
Tissue culture plasticware	Sigma Aldrich

2.1.3 General Chemicals and Reagents

1kb DNA Plus Ladder	Invitrogen
40% Bis-Acrylamide Solution	BioRad
Agarose (molecular biology grade)	Sigma-Aldrich
Amido Black Staining Solution	Sigma-Aldrich
Ampicillin	Sigma-Aldrich
Big Dye Terminator	Invitrogen
DAB 3.3 3,3'-Diaminobenzidine	Sigma
Dako Target Retrieval Solution	Agilent

Depex Mounting Medium	VMR
D-Luciferin Firefly, potassium salt	Biosynth
dNTPs	Finnzymes
Doxycycline Hyclate	Sigma-Aldrich
Glutamax	Invitrogen
HEPES	Invitrogen
HRP Substrate	Millipore
Kanamycin	Sigma-Aldrich
Lipofectamine 2000	Invitrogen
Oligo-dTs	Promega
Polybrene	Sigma-Aldrich
Polyfect	Qiagen
Ponceau Red	Sigma Aldrich
Precision Plus Dual Colour Standards	BioRad
Protein G-sepharose	Sigma-Aldrich
Puromycin	Sigma Aldrich
RNase Zap	Amersham
SYBR-Green Mastermix	Roche
TRI Reagent	Sigma-Aldrich
Tween 20	Sigma Aldrich

2.1.4 Commercial Kits

BCA Assay	Pierce
Big Dye Sequencing enzyme and buffer	Applied Biosystems
DNA Miniprep Kit (QIAprep Spin)	Qiagen
DNA Nucleobond Xtra Midi kit	Macherey-Nagel
DNase I treatment kit	Invitrogen
Gel Extraction Kit (QIAquick)	Qiagen
Hydragel Protein K20	Sebia
LR Clonase II	Invitrogen
pGEMTeasy TA cloning system	Promega

| RNeasy Mini Kit | Qiagen |
| Superscript III cDNA synthesis kit | Invitrogen |

2.1.5 Enzymes

DNase I	Invitrogen
Gibson's Isothermal Assembly Mix	New England Biolabs
(Ligase, Polymerase, Exonuclease)	
Klenow Fragment (DNA Polymerase)	New England Biolabs
Pfu turbo polymerase	Stratagene
Restriction Enzymes	New England Biolabs
Superscript III	Invitrogen
T4 DNA Ligase	New England Biolabs
Taq Polymerase	New England Biolabs

2.1.6 Antibodies

Primary – Western Blot & Immunoprecipitation

HIF-1α   Novus Biologicals (NB100-449): purified rabbit polyclonal antibody raised against C-terminus (aa775-826) of HIF-1α protein (1:1000 in 5% skim milk in TBS-T, overnight at 4°C)

HIF-2α   Novus Biologicals (NB100-122): purified rabbit polyclonal antibody raised against C-terminus of mouse/human HIF-2α protein (1:1000 in 5% skim milk in TBS-T, overnight at 4°C)

HIF-2α   Origene (TA801746): mouse monoclonal antibody raised against aa584-870 of HIF-2α

α-Tubulin   Novus Biologicals (NB600-506): purified rat monoclonal antibody (1:2000 in 5% skim milk in TBS-T, overnight at 4°C)

SUMO-1   Santa Cruz (sc-9060): rabbit polyclonal antibody
(FL-101)

Primary – Immunohistochemistry

GFP   Rockland Immunochemicals (A600-401-215): purified rabbit polyclonal antibody (1:1000 in 3% normal horse serum in PBS)

Secondary – Western Blot & Immunoprecipitation

anti-rabbit IgG   Pierce (31460): goat polyclonal, HRP conjugated (1:10000 in 5% milk in TBS-T, for 1 hour at 4°C)

anti-rat IgG   Abcam (ab6845): goat polyclonal, HRP conjugated (1:10000 in 5% milk in TBS-T, for 1 hour at 4°C)

Secondary – Immunohistochemistry

anti-biotinylated rabbit IgG   Vector Lab (H&L BA-1000): goat polyclonal, biotin-conjugated (1:250 in 3% normal horse serum in PBS)

Tertiary – Immunohistochemistry

SAV-HRP   Pierce (21130): Streptavidin Horseradish Peroxidase conjugate (1:100 in 3% normal horse serum in PBS)

2.1.7 Plasmids

2.1.7.1   Cloning plasmids

pGem-T Easy

A commercial plasmid (Promega) used to clone PCR amplified products.

pCMV-Sport6-HIF-1α and *pCMV-Sport6-HIF-2α*

pCMV-Sport6 is a Gateway mammalian expression vector. Two versions of the vector containing either HIF-1α or HIF-2α were provided by Prof Andrew Zannettino (A, Zannettino, University of Adelaide SAHMRI, Adelaide), who purchased the vectors commercially through Open Biosystems.

pENTR2B-IRESmCherry

The pENTR2B plasmid is a Gateway Entry Vector. The IRES-mCherry cassette was subcloned from a pLenti4/TO/mCherry plasmid (constructed from previously characterised vector (Barrett, Parham et al. 2011)) into the pENTR2B vector (Thermo Fisher) MCS using XhoI and EcoRV restriction digestion by Dr Duncan Hewett (D, Hewett, University of Adelaide SAHMRI, Adelaide).

pENTR2B-HIF-1α-IRESmCherry and *pENTR2B-HIF-2α-IRESmCherry*

Both *Hif1α* and *Hif2α* were PCR amplified from the pCMV-Sport6 vectors with primers containing a KpnI site in the sense primer, and a NotI site in the antisense primer. The PCR product was then purified, A-tailed, ligated into pGem-T Easy and the sequence identity confirmed via Sanger sequencing (section 2.2.1). The *Hifαs* were then each digested from pGem-T Easy using KpnI and NotI. The pENTR2B-IRESmCherry vector was linearised using complete digestion with NotI and partial digestion with KpnI, as the IRES contained a KpnI site. The digested *Hif1α* and *Hif2α* cDNAs were then individually ligated into the linearised pENTR2B-IRESmCherry vector. Restriction digestion and Sanger sequencing confirmed that the IRESmCherry cassette was intact and located immediately downstream of HIFα in both vectors.

pENTR2B-HIF-1α and *pENTR2B-HIF-2α*

The IRESmCherry cassette of pENTR2B-HIFα-IRESmCherry was removed by digesting with EcoRV and XhoI. The XhoI 5' overhang was removed using the 3'-5' exonuclease activity of the DNA polymerase I Klenow fragment, producing a linearised plasmid with blunt ends. These ends were ligated and the resulting pENTR2B-HIFα plasmid confirmed using restriction digestion and Sanger sequencing.

pENTR1A-dTomato

A Gateway Entry vector with the dTomato sequence cloned into the MCS. This plasmid was provided by Dr David Bersten (University of Adelaide) (Bersten, Sullivan et al. 2015).

2.1.7.2 Lentivirus packaging plasmids

All vectors detailed below were obtained via commercial sources and were provided by Prof Murray Whitelaw (M, Whitelaw, University of Adelaide).

pMD2.G

A Vesicular Stomatitis Virus glycoprotein (VSV-G) expressing lentiviral plasmid compatible with second and third generation packaging lentiviral systems. The VSV-G creates an envelope that facilitates lentiviral entry into cells.

pRSV-Rev

A third generation packaging lentiviral plasmid expressing Human Immunodeficiency Virus (HIV-1) Rev cDNA from the RSV U3 promoter. The Rev regulatory gene is essential for lentiviral replication *in vivo*.

pCMV-dR8.2 dvpr

A lentiviral packaging vector used in combination with the pMD2.G envelope plasmid when producing the lentiviral particles for *in vivo* transduction.

2.1.7.3 Mammalian expression plasmids

pLV410 (empty) and pLV410-dsRed

The lentiviral, Gateway compatible mammalian expression vectors were provided by Dr David Bersten (University of Adelaide) (Bersten, Sullivan et al. 2015), but were originally supplied by Prof Simon Barry (S, Barry, Robinson Research Institute, Adelaide).

pLV410-HIF-1α and *pLV410-HIF-2α*

Both *Hif1α* and *Hif2α* were subcloned from the pENTR2B-HIFα vector into the pLV410 vector using Gateway cloning.

pLV410-TetOn3G

A lentiviral vector constitutively expressing the TetOn3G transactivator protein (Bersten, Sullivan et al. 2015). This plasmid is co-transfected with a second plasmid containing a TRE3G promoter located upstream of a transgene. Upon cellular treatment with doxycycline, the TetOn3G transactivator protein will bind to the TRE3G promoter to drive expression of the transgene.

pLV-TRE3G-PGK-TetOn3G-IRES-GFP (LVTPTG)

A modified all-in-one TetOn3G vector system provided by Dr David Bersten (Bersten, Sullivan et al. 2015). This is a lentiviral vector expressing the TRE3G promoter that drives inducible expression of a transgene that can be cloned in using Gateway technology. Immediately 3' of the TRE3G promoter is the TetOn3G transactivator and GFP under the control of a constitutive PGK promoter. Treatment with doxycycline will activate the TetOn3G to inducibly drive transgene expression from the TRE3G promoter.

pLV-TRE3G-PGK-TetOn3G-IRES-puromycin (LVTPTP)

A lentiviral vector identical to LVTPTP, but with a puromycin selection cassette replacing GFP (Bersten, Sullivan et al. 2015).

pLVT-HIF-1α-PTP, pLVT-HIF-2α-PTP, pLVT-HIF-1α-PTG and pLVT-HIF-2α-PTG

Hif1α and *Hif2α* were each subcloned from the pENTR2B-HIFα plasmids into the pLVTPTP (Figure 2.1) and pLVTPTG vectors using Gateway cloning, and functionally tested to confirm inducible expression of *Hif1α* or *Hif2α* mRNA.
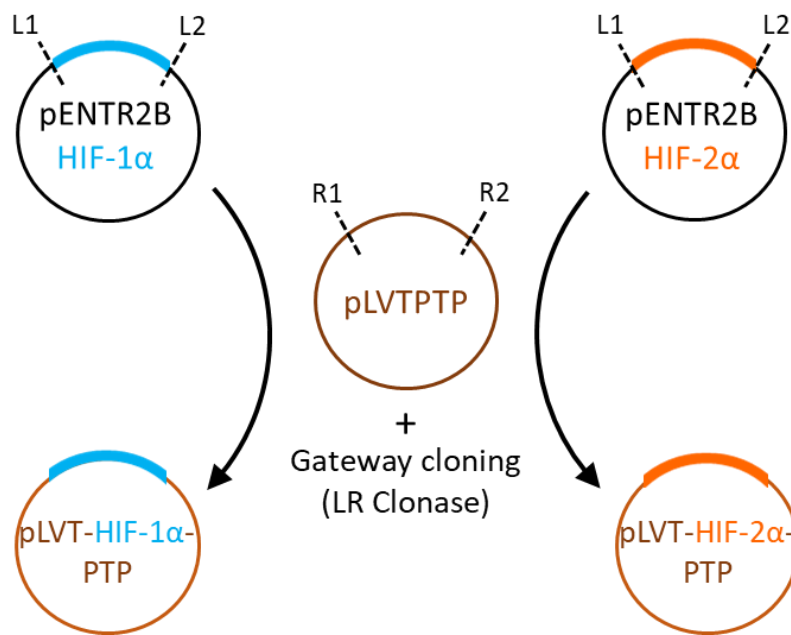
Figure 2.1: Schematic of the Gateway cloning strategy used to create the LVT-HIF-1α-PTP and LVT-HIF-2α-PTP mammalian expression vectors. The pENTR2B vectors contain either *Hif1α* or *Hif2α* flanked by L1 and L2 sites. An LR reaction was performed using LR Clonase to recombine the L-flanked *Hif1α* or *Hif2α* with the R1 and R2 sites found on the pLVTPTP destination vector, to create the LVT-HIF-1α-PTP abd LVT-HIF-2α-PTP mammalian expression vectors.

pLV-TRE3G- EF1-TetOn3G-P2A-dTomato (LVTETPT)

The Gibson's isothermal assembly cloning strategy was used to create the LVTETPT vector (Gibson, Young et al. 2009). The pLVPTG vector was digested with MluI and NheI to remove the PGK-TetOn3G-IRESGFP sequences of the plasmid. Two sets of primers were designed to produce PCR products that overlap with the linearised pLVT backbone to introduce the desired sequences (Figure 2.2). The first primer set specifically amplified the EF1α-TetOn3G cassette from the pLV410TetOn3G vector with the P2A cleavage peptide encoded into the reverse primer. The second primer set amplified the dTomato sequence from the pENTR1A-dTomato vector. The primer design included ends that sequentially complemented the digested ends of the pLVT backbone and the neighbouring PCR product. As a result, both PCR products contained overhangs that were complementary to each other and the digested backbone, ensuring efficient ligation using Gibson's isothermal assembly. Successful assembly was confirmed by restriction digest and Sanger sequencing prior to functional testing.
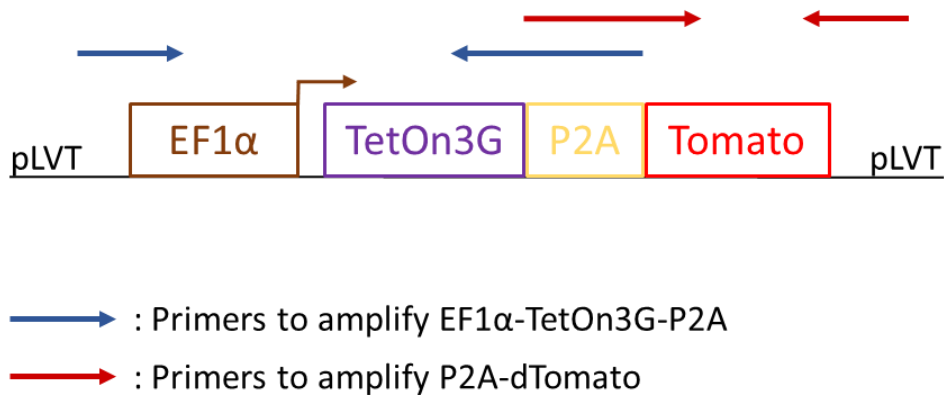
Figure 2.2: Schematic of the primer design used to create the LVTETPT mammalian expression vector. The blue primers produce a PCR product that contains a 5' 40 bp overhang whose sequence is complementary to the digested pLVT backbone. The 3' end of this PCR product is complementary to the PCR product resulting from amplification with the primers shown in red. This second PCR product (red primers) also shares 40 bp of complementary sequence with the opposing end of the linearised pLVT vector. These design specifications allow for the assembly of the pLVT backbone, EF1α-TetOn3G-P2A product and P2A-dTomato product to produce a functional plasmid.

pLVT-HIF-1α-ETPT and *pLVT-HIF-2α-ETPT*

Hif1α and *Hif2α* were each subcloned from the pENTR2B-HIFα plasmids into the pLVTETPT vector using Gateway technology (Figure 2.3)
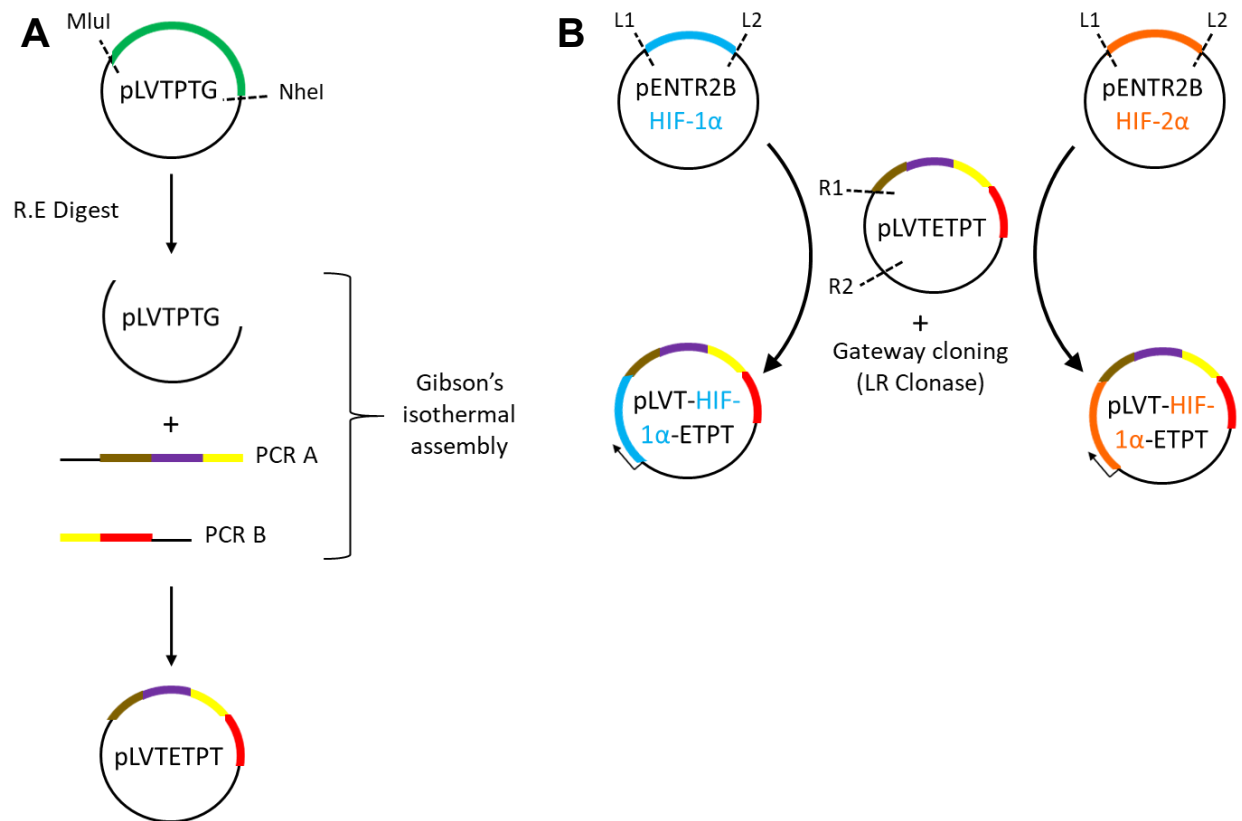
Figure 2.3: Schematic of the cloning strategy used to create the LVT-HIF-1α-ETPT and LVT-HIF-2α-ETPT mammalian expression vectors. A) The pLVTPTG vector was digest with Restriction Enzymes (R.E) MluI and NheI. This pLVTPTG backbone was then combined with the EF1α-TetOn3G-P2A product (PCR A) and the P2A-dTomato product (PCR B) as described in Figure 2.1, using Gibson's isothermal assembly to create the pLVTETPT vector B) Gateways cloning using the pENTR2B-HIF-1α or the pENTR2B-HIF-2α entry vectors and the pLVTETPT vector to create the pLVT-HIF-1α-ETPT and pLVT-HIF-2α-ETPT mammalian expression vectors.

2.1.7.4   CRISPR-Cas9 plasmids

pSpCas9(BB)-2A-GFP (PX458)

Encodes the Cas9 endonuclease from *S.pyogenes* followed by a 2A-GFP resulting in the production of both Cas9 and GFP (Ran, Hsu et al. 2013). This vector contains a BbsI restriction enzyme site that enables the directional insertion of the single guide RNA (sgRNA) sequence of interest, resulting in targeted cleavage of genomic DNA (gDNA) using CRISPR-Cas9 Technology.

pSpCas9-HIFα-2A-GFP

Two sets of sgRNAs targeting different sequences were designed for both HIF-1α and HIF-2α using the Benchling CRISPR Design Tools (https://benchling.com/editor) by Yinan Ma as depicted in Figure 4.1. The two sgRNAs designed for HIF-1α and HIF-2α cut either side of exon 2, resulting in the complete loss of this exon to generate a knockout cell line. Two sets of each of these (A and B) were designed for both HIF-1 and HIF-2 to generate two independent cell lines to mitigate against the possibility of "off target" effects of the sgRNAs. The sense and antisense sgRNA sequences were annealed and cloned into the BbsI-digested PX458 vector by Yinan Ma, generating the pSpCas9-HIF-1α-2A-GFP and pSpCas9-HIF-2α-2A-GFP plasmids, specifically the plasmids made were:

Plasmid	Position
pSpCas9-HIF-1α sgRNA Intron 1A-GFP	Chr12: 73925922 - 73925941
pSpCas9-HIF-1α sgRNA Intron 2A-GFP	Chr12: 73927054 - 73927073
pSpCas9-HIF-1α sgRNA Intron 1B-GFP	Chr12: 73925936 - 73925955
pSpCas9-HIF-1α sgRNA Intron 2B-GFP	Chr12: 73927055 - 73927074
pSpCas9-HIF-2α sgRNA Intron 1A-GFP	Chr17: 86796475 - 86796494
pSpCas9-HIF-2α sgRNA Intron 2A-GFP	Chr17: 86797774 - 86797793
pSpCas9-HIF-2α sgRNA Intron 1B-GFP	Chr17: 86796479 - 86796498
pSpCas9-HIF-2α sgRNA Intron 2B-GFP	Chr17: 86797766 - 86797785

2.1.8 Oligonucleotides

2.1.8.1   Cloning and Screening Primers

General

 T7 Terminator sequencing primer   GGTTCTGGTTCTGGCCATT

HIF primers to amplify from pCMV-Sport6 and sequence from pGEMT-easy

mHIF-1α Primer 1: Sense	GGTACCCACCGATTCGCCATGGAGGGC (KpnI – *mHIF-1α*)
mHIF-1α Primer 1: Antisense	GCGGCCGCTCAGTTAACTTGATCCAAAGCT CTGAG (NotI - *mHIF-1α*)
mHIF-1α Primer 2: Sense	ATGGGTTATGAGCCGGAAG
mHIF-1α Primer 2: Antisense	GGGTAGAAGATGGAGATGC
mHIF-2α Primer 1: Sense	GGTACCCACGGCCACGGCGACAATGAC (KpnI – *mHIF-2α*)
mHIF-2α Primer 1: Antisense	GCGGCCGCTCAGGTGGCCTGGTCCAGAGC (NotI - *mHIF-2α*)
mHIF-2α Primer 2: Sense	CGAGGAGCTACTTGGACGCTC
mHIF-2α Primer 2: Antisense	GGCCAGTGCTCAGACTCTGTC

Sequencing primers of 3'*Hifa* and IRES-mCherry from pENTR2B-IRESmCherry

pENTR2B: Antisense	GTAACATCAGAGATTTTGAGACAC
3' *mHIF-1α* Seq: Sense	CCACAGCTGACCAGTTACG
3' *mHIF-2α* Seq: Sense	GACTGTGAGGTGAACGTGC

Isothermal Assembly primers to create LVT-HIFα-EPTP vector

LVTPT-EF1αTet: Sense	TCGTTCAGCTTTCTTGTACAAAGTGGTTGATATC ACGCGTACCGTCGACCTCGACGGATC
EF1αTet-P2A: Antisense	AGGCCCGGGGTTTTCTTCAACATCTCCTGCTTG CTTCGTGGCCCCGGGGAGCATGTCAAGGT
P2A-dnucTom: Sense	CACGAAGCAAGCAGGAGATGTTGAAGAAACCC CGGGCCTATGGTGAGCAAGGGCGAGGAG

dnucTom-LVTPT: Antisense   GGAAAGCCCTACGAACCACTGAACAAATGGCAC
TAGGCTAGCCGCTTAGCCGTGTACCTTTCTCTT
CTT

TRE3G-*Hifα*-EF1α cassette primers for sequence confirmation from LVT-HIFα-EPTP vector

3' TRE3G: Sense	ACTTCCTACCCTCGTAAAGTC
5' EF1α Promoter: Antisense	TCTTTGCAAAGCTCGGTC
mHIF-1α 315aa: Sense	CTGGGTTGAAACTCAAGC
mHIF-1α 12aa: Antisense	CGACGTTCAGAACTCATC
mHIF-2α 316aa: Sense	CGGAGGATATGTGTGGCTG
mHIF-2α 14aa: Antisense	CTCCTTCCTCAGCTCTGAG

2.1.8.2   CRISPR Primers

Hifα CRISPR sgRNA oligonucleotides

mHIF-1α – Intron 1A: Sense	CACCGATCCGCAGGTGGGCTAGTAA
mHIF-1α – Intron 1A: Antisense	AAACTTACTAGCCCACCTGCGGATC
mHIF-1α – Intron 2A: Sense	CACCGTTTTTAAAGAGCGGCGTTAT
mHIF-1α – Intron 2A: Antisense	AAACATAACGCCGCTCTTTAAAAAC
mHIF-2α – Intron 1A: Sense	CACCGACCCGTGTTAGTACGTGATA
mHIF-2α – Intron 1A: Antisense	AAACTATCACGTACTAACACGGGTC
mHIF-2α – Intron 2A: Sense	CACCGTGGAGCGGGACTCTCGCCAG
mHIF-2α – Intron 2A: Antisense	AAACCTGGCGAGAGTCCCGCTCCAC
mHIF-1α – Intron 1B: Sense	CACCGGAGTCAGAGTGCTGATCCGC
mHIF-1α – Intron 1B: Antisense	AAACGCGGATCAGCACTCTGACTCC
mHIF-1α – Intron 2B: Sense	CACCGTTTTTAAAGAGCGGCGTTA
mHIF-1α – Intron 2B: Antisense	AAACTAACGCCGCTCTTTAAAAAC
mHIF-2α – Intron 1B: Sense	CACCGTCCATATCACGTACTAACAC
mHIF-2α – Intron 1B: Antisense	AAACGTGTTAGTACGTGATATGGAC
mHIF-2α – Intron 2B: Sense	CACCGGACTCTCGCCAGAGGTCCAG
mHIF-2α – Intron 2B: Antisense	AAACCTGGACCTCTGGCGAGAGTCC

*Hif*α screening of CRISPR knockout cell lines

mHIF-1α – Screening 1: Sense	AGGAGGCTCAGCAAAGGAAGAC
mHIF-1α – Screening 1: Antisense	TGATCTTTCCGAGGACCTGGATTC
mHIF-2α – Screening 1: Sense	GATTGCCCTCTGTTGCGGATAG
mHIF-2α – Screening 1: Antisense	AAAGAAGAACGCATCGGCTGAG
mHIF-2α – Screening 2: Sense	GACCATCCATGTTATGTG
mHIF-2α – Screening 2: Antisense	CTTTCTGCCTGTCTTTG
mHIF-2α – Screening 3: Sense	CGAGCTCCCTAACTAAC
mHIF-2α – Screening 3: Antisense	TCAGCTACTCTTTCAGAC
mHIF-2α – Screening 4: Sense	CAGTCTTGTCAGACTTATC
mHIF-2α – Screening 4: Antisense	GTCTTTCCCATATATCCTTC
mHIF-2α – Screening 5: Sense	GCTAAGGACTTGTAAAGC
mHIF-2α – Screening 5: Antisense	CTTCACTTGGACATTGG

2.1.8.3   qPCR Primers

mHIF-1α: Sense:	CGGCGAGAACGAGAAGAA
mHIF-1α: Antisense:	GAAGTGGCAACTGATGAGCA
mHIF-2α: Sense:	CATAAGCTCCTGTCCTCAGTCTGC
mHIF-2α: Antisense:	GCTGTGTCCTGTTAGTTCTACCTG
mVegf: Sense:	ATCCGCATGATCTGCATGG
mVegf: Antisense:	AGTCCCATGAAGTGATCAAGTTCA
mBnip3: Sense:	GTAGAACTGCACTTCAGCAATGG
mBnip3: Antisense:	GGGCTGTCACAGTGAGAACTC
mGlut1: Sense:	GGGCATGTGCTTCCAGTATGT
mGlut1: Antisense:	ACGAGGAGCACCGTGAAGA
mPolr2a: Sense:	GCACCATCAAGAGAGTGCAG
mPolr2a: Antisense:	GGGTATTTGATACCACCCTCTG
mHprt: Sense:	AGTCCCAGCGTCGTGATTAGC
mHprt: Antisense:	CCAAATCCTCGGCATAATG
GFP: Sense:	AGAAGAACGGCATCAAGGTG
GFP: Antisense:	GAACTCCAGCAGGACCATGT
mCherry: Sense:	CCCAGACCGCCAAGC

mCherry: Antisense:	GTCACGGTCACCACGC
Tomato: Sense:	TCCCCGATTACAAGAAGCTG
Tomato: Antisense:	CCCATGGTCTTCTTCTGCAT

2.1.9 Buffers and Solutions

4x SDS Load Buffer:	0.5 M Tris pH 6.8, β-Mercaptoethanol, 0.05 M Bromophenol blue, 10% SDS, 10% Glycerol
6x DNA Load Buffer:	50% Glycerol, 0.01% Bromophenol blue, 0.01% Xylene cyanol, 0.01mM EDTA pH 8.0
Decalcification Solution:	744.4 g EDTA, 75 g NaOH in 1 L PBS
D-Luciferin Feed:	200 mg doxycycline hyclate, 10 g sucrose in 1 L Water
ECL:	100 mM Tris pH 8.5, 30%H_2O_2, 250 mM Luminol, 90 mM p-coumaric acid
General IP Buffer:	250 mM NaCl, 20 mM HEPES pH 8.0, 0.1% Igepal, 1 mM EDTA
gDNA Extraction Buffer:	100 mM NaCl, 20 mM Tris HCl pH 7.5, 0.5% SDS, 10 mM EDTA
SDS-PAGE Separating Gel:	187 mM Tris pH 8.8/0.1% SDS, 10% polyacrylamide, 10% APS, TEMED
SDS-PAGE Stacking Gel:	62.5 mM Tris pH 6.8/0.1% SDS, 5% polyacrylamide, 10% APS, TEMED
SDS-PAGE Running Buffer:	25 mM Tris-Glycine pH 8.3/0.1% SDS
Paraprotein Destain	10% Acetic Acid, 25% isoporanol

Phosphate Buffered Saline (PBS)	137 mM NaCl, 10 mM Phosphate, 2.7 mM KCl, pH 7.4
RBS Lysis Buffer:	0.5 M NH$_4$Cl in PBS
Tris Buffered Saline (TBS)	50 mM Tris-Cl, pH 7.6, 150 mM NaCl
TBS-T:	TBS/0.1% Tween 20
Wet Transfer Buffer:	30 mM Tris pH 7, 1.44% glycine, 20% MeOH
Whole Cell Extract Buffer (IP):	0.42 M NaCl, 20 mM HEPES pH 8.0, 0.5% Igepal, 25% Glycerol, 0.2 mM EDTA, 1.5 mM MgCl$_2$, 1 mM DTT (added immediately prior to use)
Whole Cell Extract Buffer (Western Blot):	0.5 M NaCl, 1 M Tris pH 7.9, 10% Igepal, 0.5 M EDTA in PBS

2.1.10 Bacterial Strains

DH5α cells:

An *E. coli* bacterial strain used for plasmid preparation and cloning experiments. Genotype: F⁻Φ80d*lac*ZΔM15, Δ(*lacZYA-argF*) U169, *deo*R, *rec*A1, *end*A1, *thi*-1, *gyr*A96, sup*E*44, *hsd*R17(r$_K$⁻m$_K$⁺), λ⁻.

DB3.1 cells:

An *E coli* strain for Gateway cloning specifically containing a gyrase mutant that allows for the replication of plasmids expressing the *ccd*B protein that normally inhibits growth of most other *E coli* strains. Genotype: F⁻, *gyr*A462, *end*A1, D(*sr*1-*rec*A), *mcr*B, *mrr*, *hsd*S20(r$_B$⁻, m$_B$⁻), *sup*E44, *ara*-14, *gal*K2, *lac*Y1, *pro*A2, *rps*L20(Sm^r), *xyl*-5, λ⁻, *leu*, *mtl*-1.

2.1.11 Eukaryotic Cell Lines

HEK293T cells:

Transformed human embryonic kidney cells cultured for transfection of mammalian expression plasmids. ATCC CRL-1573.

5TGM1 cells:

The murine 5TGM1 MM cell line is genetically modified to constitutively express the HSV1-tk/GFP/Luc (TGL) triple modality reporter gene used for non-invasive *in vivo* imaging and MM cell isolation (Noll, Hewett et al. 2014, Cheong, Chow et al. 2015). Integration of the TGL construct was achieved by transduction with SFG-NES-TGL retroviral particles, where the retroviral promoter present within the LTR (long terminal repeat) drives TGL expression (Mori, Shimizu et al. 2004, Ponomarev, Doubrovin et al. 2004, Oyajobi, Munoz et al. 2007, Labrinidis, Diamond et al. 2009). The HSV1-tk component is a Herpes Simplex Virus 1 – Thymidine Kinase reporter gene used to image cells *in vivo* via micro positron electron tomography, a feature that was not utilised in this dissertation. The GFP (green fluorescent protein) and Luc (firefly luciferase) components were used for both *in vitro* and *in vivo* experiments. The GFP was used to isolate 5TGM1 cells from the BM of diseased mice using flow cytometry. The firefly luciferase generates luminescence upon the addition of D-luciferin, and was used to detect progressive tumour development non-invasively using *in vivo* bioluminescence (Ponomarev, Doubrovin et al. 2004, Labrinidis, Diamond et al. 2009).

2.2 Methods

2.2.1 Molecular Techniques

PCR amplification from DNA

The majority of PCR reactions were performed using Taq polymerase. Pfu Ultra was used to amplify the complete *Hif-1α* and *Hif-2α* genes, as both genes are large and required high fidelity synthesis and Pfu Ultra has a lower error rate than Taq. Secondly, the Phusion DNA polymerase was used to amplify products for Gibson's isothermal assembly reaction. Some reactions also required 3% DMSO.

Taq:

A single reaction contained 0.25 µL of Taq polymerase, 2.5 µL of 10 Thermopol buffer, 1 µL of 10 mM dNTPs, 1 µL each of forward and reverse primer (10 µM), 100 ng template DNA and MQ water to a final volume of 25 µL. Cycling parameters: 95°C for 30 seconds, then [95°C for 20 seconds, 55-65°C depending on the primers for 30 seconds, 68°C for 60 seconds per kb amplified] repeated for 40 cycles, 68°C for 5 minutes and hold at 4°C.

Pfu Ultra:

A single reaction contained 0.5 µL of Pfu Ultra enzyme, 2.5 µL of 10x Pfu Ultra buffer, 1 µL of 10 mM dNTPs, 1 µL each of forward and reverse primer (10 µM), 100 ng template DNA and MQ water to a final volume of 25 µL. Cycling parameters: 95°C for 2 minutes, then [95°C for 30 seconds, 55-65°C depending on the primers for 30 seconds, 72°C for 60 seconds per kb amplified] repeated for 40 cycles, 72°C for 10 minutes and hold at 4°C.

Phusion:

A single reaction contained 0.5 µL of Phusion enzyme, 5 µL of 5x HF Phusion buffer, 1 µL of 10 mM dNTPs, 1 µL 50 mM $MgCl_2$, 1 µL each of forward and reverse primer (10 µM), 100 ng template DNA and MQ water to a final volume of 25 µL. Cycling parameters: 98°C for 30 seconds, then [98°C for 10 seconds, 60°C for 30 seconds, 72°C for 60 seconds] repeated for 35 cycles, 72°C for 5 minutes and hold at 4°C.

Plasmid transformation

Short transformations were performed by adding 0.5 µL of purified plasmid DNA to 50 µL of chemically competent DH5α *E. coli* cells. The sample was then placed on ice for 10 minutes, followed by a 90 seconds heat shock at 42°C before being placed on ice for a further 2 minutes. The DNA/bacterial cell mixture was then spread evenly onto LB/agar plates with the appropriate antibiotic selection and left at 37°C overnight.

Long transformation were performed by adding 5 µL of ligation and Gateway reactions to 50 µL of chemically competent DH5α *E. coli* cells. The samples were placed on ice for 20 minutes, heat shocked at 42°C for 90 seconds and left on ice for 2 minutes. 250 µL of SOC media was added and samples were gently agitated at 37°C for 1-2 hours. Samples were then centrifuged at 200 g to pellet cells and 250 µL of supernatant removed. The cell pellet was then gently resuspended and plated on LB/agar plates with the appropriate antibiotic selection and left at 37°C overnight.

Plasmid mini preparation

5 mL of LB cultures containing the appropriate antibiotic (100 µg/mL ampicillin and 50 µg/mL kanamycin) inoculated from a single colony were grown overnight at 37°C. Samples were then processed according to the manufacturer's instruction (MiniPrep, QIAPrep Spin Kit, Qiagen). 1 µL of purified sample was then quantified and assessed for quality with a Nanodrop spectrophotometer.

Plasmid midi preparation

100 mL of LB cultures containing the appropriate antibiotic (100 µg/mL ampicillin and 50 µg/mL kanamycin) inoculated from a single colony were grown overnight at 37°C. Samples were then processed according to the manufacturer's instruction (Nucleobond Xtra Midi, Macherey-Nagel). 1 µL of purified sample was then quantified and assessed for quality with a Nanodrop spectrophotometer.

Restriction enzyme digestion of DNA

Restriction digest reactions were performed at 37°C using 0.5 µL of the NEB enzyme, 1 µL of 10 x NEB buffer, 500 ng of DNA and MQ water to a final volume of 10 µL.

Agarose gels and gel extractions

DNA samples including PCR products, plasmids and restriction digests were analysed on agarose gels via gel electrophoresis. Depending on the expected size of the DNA sample, either 1% or 2% agarose gels were made using agarose powder dissolved in Tris-Borate-EDTA (TBE) buffer with ethidium bromide. Gels were run at 100-120 V for 40 minutes and analysed on a UV transilluminator. Bands were excised and DNA purified from the gel using the QIAquick (QIAGEN) gel extraction kit as per manufacturer's instructions and stored at -20°C.

Ligation

DNA ligation reactions were performed using 1 µL of T4 ligase (2 U/µL), 1 µL of 10x T4 ligase buffer, 1 µL of 10 mM ATP, a 3.5:1 molar ratio of insert DNA:vector DNA, and sterile water to a final volume of 10 µL. Reactions were left overnight at 16°C followed by a long transformation. Single colonies were selected for plasmid minipreps, DNA analysed by restriction digestion and gel electrophoresis.

Gateway Cloning

Gateway reactions were performed using 2 µL of LR Clonase II, 6 µL of TE, 1 µL of Entry vector (diluted to 300 ng/µL), 1 µL of Destination vector (diluted to 150 ng/µL). Reactions were incubated at room temperature for 1 hour before adding 2 µL of Proteinase K (2 µg/µL) and incubating at 37°C for 10 minutes. Samples were then used in a long transformation. Single colonies were selected for plasmid minipreps, and DNA analysed by restriction digestion and gel electrophoresis.

PCR product ligation into pGEM-Teasy

PCR amplified products were prepared for pGEM-Teasy insertion by first A-tailing the product in 1 µL of Taq (5 U/µL), 1.5 µL of 10x Thermopol buffer, 0.5 µL of 10 mM dATP, 0.5 µL of 50 mM $MgCl_2$, 5 µL of PCR product and 6.5 µL of MQ water. The reaction was left at 70°C for 30 minutes before being ligated with pGEM-Teasy in a reaction including 1 µL of T4 Ligase (2 U/µL), 7.5 µL 2x Ligation buffer, 1 µL pGEM-Teasy and 5.5 µL of A-tailed PCR product. This reaction was then left overnight at 16°C, followed by transformation in DH5α cells and plating on LB/Ampicillin agar spread with 20 µL of Xgal and 100 µL of 100 mM IPTG. Plates were incubated at 37°C overnight and only the white colonies were selected for plasmid minipreps.

Gibson's Isothermal Assembly

PCR and Gibson's isothermal assembly primer design were performed to the specifications outlined by Zhang *etal* (Gibson, Young et al. 2009).

Sanger Sequencing

A sequencing reaction was prepared by combining 1 µL of Big Dye Terminator, 3 µL of 5x commercial sequencing buffer, 0.5 µL of primer, 400 ng of DNA and MQ Water to a total of 15 µL. The sample then underwent the following cycling parameters: 95°C for 3 minutes, then [95°C for 30 seconds, 50°C for 15 seconds, 60°C for 4 minutes] repeated for 25 cycles, and hold at 4°C. The reaction was then placed into a microcentrifuge tube in addition to 80 µL of 75% isopropanol and 1 µL of glycogen. Following an incubation of 30 minutes at room temperature, the sample was centrifuged at 16,000 g for 20 minutes. The supernatant was removed, the pellet washed in 250 µL of 75% isopropanol and centrifuged again. Once the supernatant was removed, the pellet was air dried for 10 minutes at 42°C and the sample was sent to the Australian Genome Research Facility for analysis.

DNaseI treatment of RNA

1 µg of RNA was added to 1 µL of DNase I (2 U/µL), 1 µL of 10x DNase I reaction buffer, and MQ water to a volume of 10 µL. The reaction was left at room temperature for 15 minutes and then 1 µL of 25 mM EDTA was added and the sample incubated at 65°C for 10 minutes to inactivate the DNase I enzyme.

cDNA synthesis

DNase I treated or non-treated RNA samples were added to 1 µL of oligo DTs (500 ng/µL), 1 µL of 10 mM dNTPs and MQ water to a final volume of 13 µL. The RNA was incubated at 65°C for 5 minutes and placed on ice for 1 minute. A mixture including 0.5 µL of Superscript III (200 U/µL) reverse transcriptase (or water for noRT control), 4 µL 5x First Strand buffer, 1 µL of 0.1 M DTT and 1 µL of MQ water was incubated at 50°C for 60-90 minutes followed by a heat inactivation at 70°C for 15 minutes.

Quantitative PCR (qPCR)

Quantitative PCR was performed in triplicate for each cDNA sample and a water control sample. Each triplicate sample reaction was performed for the target gene of interest and an endogenous control gene. The endogenous control genes were chosen based on their stable expression under various experimental treatments, and used to normalise target gene expression. A single reaction contained 10 µL of SYBR Green mastermix, 0.4 µL each of forward and reverse primers (10 µM), 1 µL of cDNA (or no RT) and 8.2 µL of MQ water. Samples were then pipetted into 96-well trays, sealed and centrifuged at 200 g. The trays were then placed into the StepOnePlus realtime thermocycler (Applied Biosystems) and cycled under the following conditions: 95°C for 10 minutes, then [95°C for 10 seconds, 60°C for 30 seconds] repeated for 40 cycles. A melting curve was also performed on the products under the following conditions: 95°C for 15 seconds, 60°C for 1 minute and ramping rise in temperature up to 95°C, with readings made every 0.5°C. Raw data was obtained from the StepOne v2.1 software, exported and relative amounts of the targeted mRNA quantified using Q-Gene software (Muller, Janovjak et al. 2002).

2.2.2 Cell Culture Techniques

2.2.2.1 Maintenance of Cell Lines

All cell lines were maintained at 37°C with 5% CO_2 and humidified environmental conditions. Hypoxia treatment of cell cultures was achieved by placing cells within air-tight containers with an anaerobic sachet (Oxoid, Australia), creating an atmospheric environment of <1% O_2 as previously described (Vandyke, Zeissig et al. 2017). Where specified, some experiments were performed using a humidified hypoxia chamber with a controlled atmospheric environment of 1% O_2 at 37°C with 5% CO_2 as previously described (Vandyke, Zeissig et al. 2017). Cells were maintained in hypoxia for 16 – 72 hours as specified.

HEK293T cell line

HEK293T cells were cultured in Dulbecco's Modified Eagle's Medium (DMEM) (Life Technologies, Cat 12430062) supplemented with 10% FCS. Cells were passaged every 2-3 days using trypsin.

5TGM1 mouse multiple myeloma cell line

The 5TGM1 murine myeloma cell line was kindly provided by Professor Andrew Zannettino (University of Adelaide, SAHMRI, Adelaide, Australia). These cells were maintained at a cellular density of $2 - 5 \times 10^5$ cells/mL cultured in Iscove's Modified Dulbecco's Medium (IMDM) (Sigma Aldrich, Cat I3390) supplemented with 20% FCS, 100 mM sodium pyruvate, 200 mM L-glutamine and 1M HEPES buffer.

Thawing cells

Frozen vials of cells were placed into a 37°C water bath until thawed. Immediately upon thawing, 9 mL of pre-warmed media was added and the cells centrifuged at 200 g for 5 minutes. The supernatant was aspirated and the cell pellet was then resuspended in 7 mL of fresh media and transferred to a 25 cm^2 flask.

Freezing cells

Cells were trypsinised (293T and P19 only) and centrifuged at 200 g for 5 minutes. Cell pellets were resuspended in media at a concentration of 1×10^7 cells/mL. An aliquot of 500 µL of cells was placed into cryotubes containing 400 µL of FCS and 100 µL of DMSO. Cells were stored immediately at -80°C for 1 week before being stored in the vapour phase of a liquid nitrogen tank for long term storage.

2.2.2.2   Cellular extraction methods and associated experiments

gDNA isolation

5TGM1 cells were grown in 24-well trays at a concentration of 5×10^5 cells/mL. A total of 500 µL of cells per sample was centrifuged at 200 g for 5 minutes, the supernatant removed and 250 µL of extraction buffer, freshly supplemented with 5 µL of Proteinase K (20 mg/ml) was added. This mixture was incubated at 37°C for 4 hours before transferring to a microcentrifuge tube and 125 µL of 6 M NaCl solution added. The sample was shaken vigorously, placed on ice and spun at 16,000 g for 10 minutes at 4°C. The supernatant was transferred to a new tube and 1 mL of 100% ethanol added. The sample was gently mixed and centrifuged again at 16,000 g for 2 minutes at room temperature. The supernatant was removed, the pellet washed with 500 µL of 75% ethanol and centrifuged at 16,000 g for 2 minutes. The supernatant was removed, the pellet left to air dry then resuspended in 80 µL of 1x TE. gDNA quantity was measure using a Nanodrop spectrophotometer.

RNA isolation

RNA extractions were performed on 5TGM1 or HEK293T in a 6 cm dish. 5TGM1 cells were plated at a concentration of 2×10^5 cells/mL and grown for 16-72 hours with and without treatment as specified (Chapter 3 &4). RNA was extracted from HEK293T cells when at a confluency of 80-90%. Media was removed either by centrifugation at 1000 g for 2 minutes and aspiration for 5TGM1 (non-adherent) cells, or by immediate aspiration for the HEK293T and P19 (adherent) cells. 500 µL of TRIzol reagent was added to the cells and homogenised using a pipette for 5TGM1 cells, or cells were

scraped then homogenised for HEK293T and P19 cells. The sample was transferred to a microcentrifuge tube, 200 µL of chloroform added and shaken vigorously for 15 seconds. Samples were then centrifuged at 11,000 g for 15 seconds at 4°C, 350 µL of the top aqueous phase was transferred to a microcentrifuge tube and 350 µL of 70% ethanol added. The sample is then added to an RNeasy mini column (Qiagen) and the wash and extraction steps followed according to the manufacturer's recommendations, with a final elution in 30 µL of RNA in RNase-free water. RNA quantity and purity was assessed using the Nanodrop spectrophotometer and gel electrophoresis.

Protein extraction

Protein extractions were performed on 5TGM1 or HEK293T cells grown in a 6 cm dish. 5TGM1 cells were plated at a concentration of $2x10^5$ cells/mL and grown for 16-72 hours with and without treatment as specified (Chapter 3). HEK293T or P19 cells were extracted at approximately 80-90% confluency. Media was removed by centrifugation at 1000 g for 1 minute followed by aspiration for 5TGM1 cells, or simply aspiration for the HEK293T cells. 5 mL of ice cold PBS was immediately added, gently swirled and aspirated for adherent cells, or gently mixed and then centrifuged at 1000 g for 1 minute for 5TGM1 cells. WCE buffer (WB) was added (100 µL per dish, with 1 µL of fresh Protease Inhibitor) and homogenised using a pipette for 5TGM1 cells, or cells were scraped then homogenised for HEK293T and P19 cells. Samples were left on ice for 20 minutes, centrifuged at 800 g for 5 minutes and the supernatant retained. Protein quantity was measured using a BCA protein assay (Pierce) as per the manufacturer's instructions.

Western blot

Protein samples were aliquoted, 4x SDS Load Buffer added and the samples heated at 95°C for 10 minutes. The samples were subsequently loaded onto a 10% SDS-PAGE gels and run in 1x GTS at 120 V for 80 minutes. Following separation, the proteins were transferred onto nitrocellulose in Wet Transfer Buffer at 0.35 mA at 4°C for 1 hour. The membrane was placed in Ponceau Red to visualise protein transfer and to facilitate cutting of the membrane in preparation for antibody incubation. The

membrane was then blocked in 10% skim milk diluted in TBS-T for 1 hour and then washed 3 x 5 minutes in TBS-T. Primary antibody (including target and control) diluted in 5% skim milk was applied and left rotating at 4°C overnight. Membrane washes were performed (3 x 5 minutes with TBS-T) prior to the application of an appropriate secondary antibody diluted in 5% skim milk. This was left for 1 hour before the membrane was washed (3 x 5 minutes with TBS-T). ECL was applied for 1 minute before visualising protein bands using the ChemiDoc (Bio-Rad).

Immunoprecipitation

Immunoprecipitation was performed on protein samples extracted from 5TGM1 cells using the method described above with WCE buffer (IP). 500 µg of protein was added to IP buffer to a final volume of 300 µL. The samples were incubated with 1 µg of primary antibody (including target and control), rocking overnight at 4°C. 500 µL of Protein G Sepharose (PGS) was diluted in 500 µL of IP buffer, centrifuged at 225 g for 2 minutes at 4°C and the supernatant removed. The PGS was then blocked in 500 µl of 0.05 µg/µl BSA in IP buffer and incubated for 1 hour at 4°C and the wash step repeated. An aliquot of 40 µl of blocked PGS (per sample) was then added to the protein sample and incubate at 4°C, rocking for 1 hour. This was then centrifuged at 225 g for 2 minutes at 4°C and the supernatant retained and stored at -20°C (unbound control). The pellet was then resuspended in 1 mL of IP buffer and rocked at 4°C for 5 minutes. The sample was then washed 3 times and the supernatant removed. An aliquot of 10 µl of 4x SDS Load Buffer was added to the pellet and heated at 95°C for 5 minutes and centrifuged at 800 g to pellet the resin. The supernatant was then loaded on an SDS-PAGE gel and a western blot analysis performed.

2.2.2.3 Cellular modifications and analyses

Transient transfections

Transient transfections were performed on HEK293T cells using Lipofectamine 2000 at 3:1 Lipofectamine 2000:Plasmid DNA as per the manufacturer's instructions. Cells were plated in 6 cm dishes at 40-60% confluency, with cells not exceeding 95%

confluency at the end of the experiment. At 6 hours post transfection, fresh media was applied in addition to treatment such as hypoxia (sachet for 16-72 hours) or doxycycline hyclate (2 µg/mL for 16 hours).

Lentivirus production

A 75 cm^2 flask was seeded with 3x10^6 HEK293T cells in 10 mL of media. After 24 hours, 12.5 µg of the lentiviral plasmid of choice, 7.5 µg of pCMV-dvrp 8.2, 6.25 µg of pRSV-Rev and 3.75 µg of pMD2.G was added to 1 mL of media combined with 70 µL of Lipofectamine 2000. This mixture was incubated for 20 minutes and added to the HEK293T cells. After a 24 hours, the media was removed and 10 mL of fresh media applied to the flask. After a further 48 hours, the media was harvested, centrifuged at 360 g for 10 minutes and filtered through a 0.45 µm filter. The virus was either stored at -80°C or immediately used for cellular transduction.

Lentivirus transduction

Lentiviral transduction of 5TGM1 cells was performed in a 24-well tray by adding 1 mL of lentivirus with 1µL of polybrene (8 µg/mL) to 500 µL of cells at 2x10^5 cells/mL. After 24 hours, the media was replaced with fresh IMDM. After a further 24 hours the cells were either treated with puromycin to select for infected cells, or assessed for fluorescence using an inverted microscope. For cells infected with lentiviral vectors expressing fluorophores, successful integrants were isolated using fluorescence-activated cell sorting (FACS) (see section 2.2.2.4).

Microscopy

Cells expressing a fluorophore via transient transfection or lentiviral transduction were analysed using an inverted microscope (Nikon Eclipse TE300). GFP fluorescence was visualised using a FITC filter whilst dsRed, mCherry and dTomato fluorescence was visualised using a TxRed filter. Fluorescent cells were imaged at 10x and 20x magnification and at an exposure time of 1 milliseconds.

FACS

All cell analyses and sorting using flow cytometry was performed at the Detmold facility (SA Pathology, Adelaide). Cell sorting was performed by Detmold staff using the Astrios (Beckman Coulter), with the addition of the CyClone™ unit for experiments requiring single cell sorting into 96-well plates. Cell analyses for fluorescence were performed on the Gallios flow cytometer (Beckman Coulter).

5TGM1 cells were sorted at a maximal concentration of 2×10^7 cells/mL. Immediately prior to FACS analysis, cells were centrifuged for 5 minutes at 200 g, resuspended in 500 µL of IMDM supplemented with 2% FCS at the specified concentration and passed through a 30 µm filter. Sorted cells were collected into polystyrene tubes containing 2 mL of IMDM + 2% FCS, spun for 5 minutes at 200 g and placed into fresh IMDM supplemented with 20% FCS, 100 mM sodium pyruvate, 200 mM L-glutamine and 1 M HEPES buffer. For single cell sorting into 96-well plates, wells were pre-filled with 100 µL of regular 5TGM1 growth media. Samples were prepared in the same manner for fluorescence analysis.

2.2.2.4   CRISPR Cas9 knockout experiment

All CRISPR Cas9 knockout experiments for the HIF-2α knockout 5TGM1 lines used in Chapter 4 were performed by Yinan Ma. These experiments were repeated by myself when attempting to generate more clone HIF-2α clones and create HIF-1α knockout cell lines.

Transient transfection of 5TGM1 cells

The pSpCas9-HIFα-2A-GFP vectors were created as described in section 2.1.7.4. 5TGM1 cells were plated in 6-well plates in 4 mL of media at a concentration of 2×10^5 cells/mL. These cells were transiently transfected with a combination of plasmids to create 4 different knockout cells lines as below:

 HIF-1α knockout A   pSpCas9-HIF-1α sgRNA Intron 1A-GFP and

pSpCas9-HIF-1α sgRNA Intron 2A-GFP

HIF-1α knockout B   pSpCas9-HIF-1α sgRNA Intron 1B-GFP and

pSpCas9-HIF-1α sgRNA Intron 2B-GFP

HIF-2α knockout A   pSpCas9-HIF-2α sgRNA Intron 1A-GFP and

pSpCas9-HIF-2α sgRNA Intron 2A-GFP

HIF-2α knockout B   pSpCas9-HIF-2α sgRNA Intron 1B-GFP and

pSpCas9-HIF-2α sgRNA Intron 2B-GFP

All wells were also co-transfected with the pLV410-dsRed vector, allowing for selection of successfully transfected cells. Each transient transfection reaction was performed with a total of 4 µg of DNA (SpCas9-IntA, SpCas9-IntB and dsRed containing plasmids) and 20 µL of polyfect as per the manufacturer's instructions.

Identification and isolation of successfully transfected 5TGM1 cells

At 24 hours post-transfection, cells were assessed for dsRed fluorescence using microscopy. FACS was performed (section 2.2.2.3) at 48 hours post initial transfection on 5TGM1 cells expressing both GFP and dsRed, to isolate successfully transfected cells (Detmold facility, SA pathology, Adelaide). The GFP and dsRed double positive cells underwent single cell sorting into 96-well trays and were cultured for 2-3 weeks to allow for cellular recovery and expansion. Once confluent, surviving clones were moved into a 24 well tray and expanded for 3 days. Following expansion, 80% of each well was taken to make gDNA (section 2.2.2.2).

PCR screening and confirmation of 5TGM1 HIFα knockout cells

PCR reactions were performed with Taq polymerase and Phusion enzyme as previously described (section 2.2.1). The gDNA extracted from the potential 5TGM1 HIFα knockout clones, was used in a series of PCR reactions using CRISPR HIFα screening primers that flank exon 2, with the desired loss of exon 2 evident by a smaller PCR product in agarose gel electrophoresis. PCR products corresponding to

successful knockouts were subject to gel extraction, A-tailing, ligation into pGEM-Teasy and analysis via Sanger sequencing.

2.2.2.5   5TGM1 knockout cell line characterisation

Luciferase Assay

Prior to *in vivo* use, the luciferase activities of all newly modified 5TGM1 cell lines were analysed. 5TGM1 cells were aliquoted in triplicate in 96-well plates (black sides, clear bottom) at 1×10^6, 2×10^5, 4×10^4, 8×10^3 and 1.6×10^3 cells/well in a final volume of 100 µL media per well, and incubated at 37ºC for 1 hour. D-Luciferin substrate at a stock concentration of 30 mg/mL was diluted 1/100 with PBS, 100 µL added to each well and the plate incubated at 37ºC for 20 minutes on the pre-warmed IVIS Xenogen^{TM} platform. Luminescence intensity was then detected using the IVIS Xenogen^{TM} system at 1 minute and 10 minute exposure intervals with the specific settings of small binning and field of view B (15cm). Analyses were performed for each well using the Living Image 2.50.1 software.

Proliferation Assay

Cell proliferation rates of monoclonal 5TGM1 HIF-2α CRISPR knockout cell lines were determined using luciferase expression as an indirect measure of cell number. 5TGM1 cell lines were plated into 96-well plates (black sides, clear bottom) in triplicate at a concentration of 5×10^3 cells per well in a final volume of 100 µL and grown in hypoxic or normoxic conditions and analysed after both 3 days and 5 days. On the fifth day, a series of standards were plated for each cell line at concentrations of 5×10^5, 2×10^5, 1×10^5, 5×10^4, 2×10^4, 1×10^4, 5×10^3 and 2×10^3 cells/well in a final volume of 100 µL media. D-Luciferin (30 mg/mL) was then diluted 1/100 with PBS, 100 µL added to each well and the plates incubated at 37ºC for 20 minutes on the pre-warmed IVIS Lumina XRMS^{TM} platform. Luminescence intensity was then detected using the IVIS Lumina XRMS^{TM} system using Auto Function, and analysed as described above.

2.2.3 *In Vivo* and *Ex Vivo* Techniques

2.2.3.1   *In vivo* mouse experiments

Mouse injections

5TGM1 cell lines were injected into C57Bl/KalwRij mice between 6 and 8 weeks of age. 5TGM1 cell lines were thawed and cultured for approximately 3 days prior to injection. Where specified, LVTETPT cell lines were resorted immediately prior to injection. Cells were diluted to a concentration of 5×10^6 cells/mL in ice cold PBS, kept on ice and 100 µL of cells was injected into mice via tail vein injection (performed by Dr Jacqueline Noll).

Mouse treatment

Mice were routinely assessed and weighed 3 times weekly and monitored daily to assess their general health. The duration of the animal experiment was 4 weeks, unless stated otherwise. For mice injected with the LVTETPT cell lines, mice were fed with doxycycline hyclate supplemented water (1 mg/mL + 5% sucrose) and feed (600 mg/kg) twice weekly.

Monitoring disease progression

Tumour growth was monitored in the 2nd, 3rd and 4th weeks post injection by intraperitoneal administration of 150 mg/kg of luciferin in sterile PBS. Mice were anaesthetised (3% constant isofluorane inhalation) and after 10 minutes, *in vivo* bioluminescence was measured using either the IVIS Xenogen™ (Chapter 3) or the IVIS Spectrum™ (Chapter 4). When using the IVIS Xenogen™, mice were imaged at varying exposure times of 30 seconds, 1 minute and 5 minutes, where the highest bioluminescence reading for each mouse was selected for quantification purposes. When using the IVIS Spectrum™, mice were imaged using the Bioluminescence function in the Imaging Wizard of the Living Image software, resulting in auto detection of tumour. As previous, the Living Image software was used to measure bioluminescence.

2.2.3.2   *Ex vivo* sample collection and processing

Cardiac bleed

At the end of the study, mice were anaesthetised with 2% isoflurane gas and cardiac bleeds (approximately 1 mL) performed and collected in Mini Collect Z Serum Seperator tubes and stored on ice. Cervical dislocation of mice was performed immediately after blood collection as per ethics approved protocols (University of Adelaide Ethics Approval M-2012-227)). Blood samples were centrifuged at 1200 g for 10 minutes and the serum transferred into microcentrifuge tubes.

Paraprotein analysis

Mouse serum was analysed for presence of paraprotein, an indicator of disease burden, using the Hydragel Protein(E) K20 system (Sebia) as per the manufacturer's instructions. The dried gel was immersed in Amido Black Staining Solution for 4 minutes and destained three consecutive baths of paraprotein destain (section 2.1.9). The gel was then imaged using the ChemiDoc (Bio-Rad) and bands quantified using Image Lab software (Bio-Rad).

Mouse dissection and processing

Various cell and tissue samples were isolated from mice *post mortem*. The spleen and hind legs were dissected and immediately submerged in 10% formalin. Alternatively, BM cells were isolated from the hind legs (refer to Chapters 3 and 4 for when which procedure was used) by flushing the femur and tibia with 6 mL of ice-cold 10% FCS in PBS. The flushed cells were centrifuged at 110 g for 5 minutes, supernatant removed and the pellet resuspended in 500 µL of IMDM + 2% FCS. To these samples, 2 mL of RBC lysis buffer was added and left for 10 minutes before repeating the centrifugation step and resuspending again in 500 µL of IMDM + 2% FCS. These samples were analysed using FACS and the tumour cells isolated (section 2.2.2.3). mRNA was extracted from the 5TGM1 cells and qPCR analysis performed (section 2.2.2.2).

The hind legs that were placed in the fixative were stored at 4°C for 1 week. Legs were then placed in decalcification solution and rocked for approximately 2 weeks with fresh solution applied three times weekly. Complete decalcification was confirmed by x-ray using the IVIS Lumina XRMS™ before the legs were sliced in half longitudinally. The spleens and legs were then placed in the Shandon Excelsior ES Tissue Processor overnight through sequential changes of ethanol, xylene and paraffin. The tissue samples were then embedded in paraffin (Histology Services at SA Pathology), and 5µm sections were cut and mounted on glass slides for microscopic analyses.

H&E staining

Tissue slides were submerged for 2 x 1 minute in xylene to remove wax. Then 3 x 30 second ethanol washes were performed to remove xylene. Slides were rinsed in running water followed by distilled water for 10 second. This was followed by a 5 minute submersion in Mayer's haematoxylin solution and rinse in running tap water. The slides were placed in bicarbonate solution for 10 seconds and the wash step repeated. Samples were then differentiated in 0.3% acid-alcohol for 5 seconds and immediately washed. Slides were then submerged in bicarbonate again for 10 seconds and washed. A final stain was applied by submerging slides in eosin for 2 minutes followed by 3 x 30 second ethanol incubations and a final two changes of xylene for 30 second each. Slides were then individually mount in Depex, dried and imaged using the Nanozoomer (SA Pathology, Adelaide).

Immunohistochemistry staining

Tissue slides were de-waxed in a consecutive series of baths in xylene (3 x 2 minutes) followed by ethanol (3 x 2 minutes). Subsequently, slides were washed in RO water (3 x 5 minutes) and PBS (1 x 5 minute). Endogenous peroxidase activity was quenched by incubating slides in freshly made 30% H_2O_2 in methanol for 30 minutes at room temperature in the dark. Slides were washed (3 x 5 minutes in PBS) and circles drawn around the tissue using a PAP pen. Slides were blocked in 3% normal horse serum (in PBS) for 2 hours at room temperature. The blocking solution was then removed and

the tissue incubated in primary antibody overnight at 4°C. The primary antibody was removed and 3 x 5 PBS washes performed. Secondary antibody was applied to the tissue and incubated at room temperature for 30 minutes. This antibody was removed, tissue samples washed (3 x 5 minutes PBS) and tertiary antibody applied for 1 hour. During this time the DAB solution was made by first combining 13.6 mL 0.2M HCl, 12.4 mL 0.2M Tris and 24 mL water and adjusting pH to 7.7 with NaOH. To this, 50 μL of 30% H_2O_2 and 300 μL of DAB was added. The tertiary antibody rinsed with distilled water and DAB solution applied until a colour change was observed on the tissue (7-10 minutes). The DAB solution was carefully removed and 3 x 5 minute PBS followed by 3 x 5 distilled water washes applied. The slides were then counterstained in Mayer's haematoxylin for 1 minute, rinsed in RO water, submerged in 0.3% acid alcohol for 2 seconds, rinsed in RO water, submerged in bicarbonate solution for 10 seconds, rinsed and dehydrated in ethanol (3 x 2 minutes) and xylene (2 x 2 minutes). Slides were then individually mount in Depex, dried and imaged using the Nanozoomer (SA Pathology, Adelaide).

2.2.4 Statistical Analysis

Data was presented as mean ± standard error of the mean (SEM). Significant differences between treatment groups were determined by either t-tests or ANOVA (Analysis of Variance) as appropriate. Paired student t-test was performed using Microsoft Excel where a null hypothesis was rejected when a significance of $p \leq 0.05$ was reached. Either one-way ANOVA with Dunnett's post-test or two-way ANOVA with Sidak's post-test was performed, as appropriate, using GraphPad Prism Version 7.

Chapter 3
THE DESIGN, GENERATION AND CHARACTERISATION OF AN INDUCIBLE HIFα EXPRESSION SYSTEM IN MULTIPLE MYELOMA CELLS

3.1 Introduction

Aberrant upregulation of both HIF-1α and HIF-2α have been implicated in MM disease progression (Giatromanolaki, Bai et al. 2010). Importantly, HIF-1α and HIF-2α display differential expression patterns in MM, suggesting that each factor could play critically different roles in disease (Martin, Diamond et al. 2009). Despite this, there is a paucity of data in relation to the specific contributions made by HIF-1α and HIF-2α in the pathogenesis of MM.

Genetic manipulation, both *in vitro* and *in vivo*, is routinely used to explore the complex roles of the products of specific genes in biology. Commonly used techniques include constitutive and inducible systems that enable the upregulation, downregulation or silencing of gene expression. As summarised in Chapter 1, the HIFs regulate hundreds of target genes and influence numerous pathways involved in processes such as cellular migration, adhesion and proliferation. With this in mind, the inducible TetOn3G vector system was chosen to modulate HIFα expression in mouse MM cells, for subsequent use in an animal model of disease. TetOn3G modified cells upregulate gene expression in the presence of doxycycline, making the system both inducible and reversible in cells. As such, the doxycycline-dependent activation of HIF-1α and HIF-2α following disease establishment in mouse experiments would allow for the direct assessment of the role of each HIFα in disease progression, eliminating confounding effects on initial BM homing that may arise with constitutive expression.

The use of mouse models to assess disease overcomes the need to infer pathophysiological contexts from *in vitro* experiments. The 5TGM1 mouse MM cell line can be easily propagated *in vitro*, and develops aggressive MM over 4 weeks when injected into C57BL/KaLwRij mice (Dallas, Garrett et al. 1999), making it an excellent model for manipulating HIFα expression and assessing the significance of these molecular pathways *in vivo*. The work in this chapter aimed to generate and characterise 5TGM1 cells engineered to inducibly overexpress either HIF-1α or HIF-

2α for use in the 5TGM1/C57BL/KaLwRij MM mouse model of disease, and characterise the specific roles of each HIF on MM disease progression *in vivo*.

3.2 Results

### 3.2.1 Profiling of 5TGM1 cells: assessment of expression of *Hif1α*, *Hif2α* and their target genes under hypoxic conditions.

The expression profiles of *Hif1α*, *Hif2α* and their target genes in 5TGM1 cells is not known. As such, prior to genetically modifying HIFα in the 5TGM1 cells, the expression of endogenous *Hif1α*, *Hif2α* and a selection of target genes in normoxic and hypoxic culture conditions was characterised using quantitative PCR (qPCR). Previous studies have shown that the expression of a number of controls or "housekeeping" genes commonly used as normalisation controls for qPCR, such as *β-actin* and *Gapdh*, are affected by hypoxic treatment (Bakhashab, Lary et al. 2014). With this in mind, before the HIFs and downstream target genes could be analysed by qPCR, a suitable "housekeeping" gene was selected for normalisation. Initial experiments compared the effect of hypoxia (<1% O_2) on the expression of commonly used control genes in 5TGM1 cells, and found that *hypoxanthine-guanine phosphoribosyltransferase (Hprt)* and *RNA polymerase II subunit A (Polr2a)* showed no significant variation with hypoxic treatment (data not shown). As such, *Hprt* and *Polr2a* were used for normalisation in all subsequent qPCR experiments.

To examine the expression of *Hif1α*, *Hif2α* and their target genes in hypoxia, 5TGM1 cells were cultured under hypoxic (<1% O_2) conditions for 16, 24, 48, and 72 hours, or in normoxia as a negative control (Figure 3.1). The relative *Hif1α* mRNA levels in 5TGM1 cells showed no hypoxia induced changes in expression (Figure 3.1A). In contrast, *Hif2α* exhibited elevated expression in all hypoxic samples when compared to the normoxic control, with a peak of more than three times the control after 48 hours of hypoxic treatment (Figure 3.1B). Although hypoxic induction of *Hif2α* expression was consistently observed, with a peak at 48 hours of hypoxic treatment across all three independent experiments, when these data were averaged, statistical significance was not reached using a paired student t-test, most likely due to variation between the datasets (Data from representative single experiments are presented in Figure 3.1, and data for all three independent experiments presented in Appendices 1-4).

Three well characterised HIF-inducible target genes were chosen to assess HIF activity in the 5TGM1 cells under hypoxic conditions, specifically *VegfA*, *Bnip3* and *Glut1* (Figure 3.1C-E) (Choi, Oh et al. 2008, Benita, Kikuchi et al. 2009, Ria, Todoerti et al. 2009). A hypoxia-dependent upregulation of *VegfA, Bnip3 and Glut1* mRNA was confirmed in 5TGM1 cells by qPCR. Specifically, mRNA induction was detected after 16 hours of hypoxic treatment and remained elevated until 72 hours, with *Bnip3* showing the greatest fold induction as reported in other cell types (Choi, Oh et al. 2008). These data are consistent with a HIF-dependent induction of typical target genes in hypoxia and thus are consistent with hypoxia-dependent HIF activity in 5TGM1 cells.

As the oxygen-dependent regulation of HIF-1α and HIF-2α is predominantly post-translational, numerous attempts were made to detect the expression of endogenous HIFα proteins by western blotting. However, while the expression of these proteins could be detected in numerous human MM cell lines, they could not be consistently detected in the 5TGM1 cells, most likely due to the species-selectivity of the primary antibodies and expression levels in the 5TGM1 cells.

A

B

C

D

Bnip3

E

Glut1
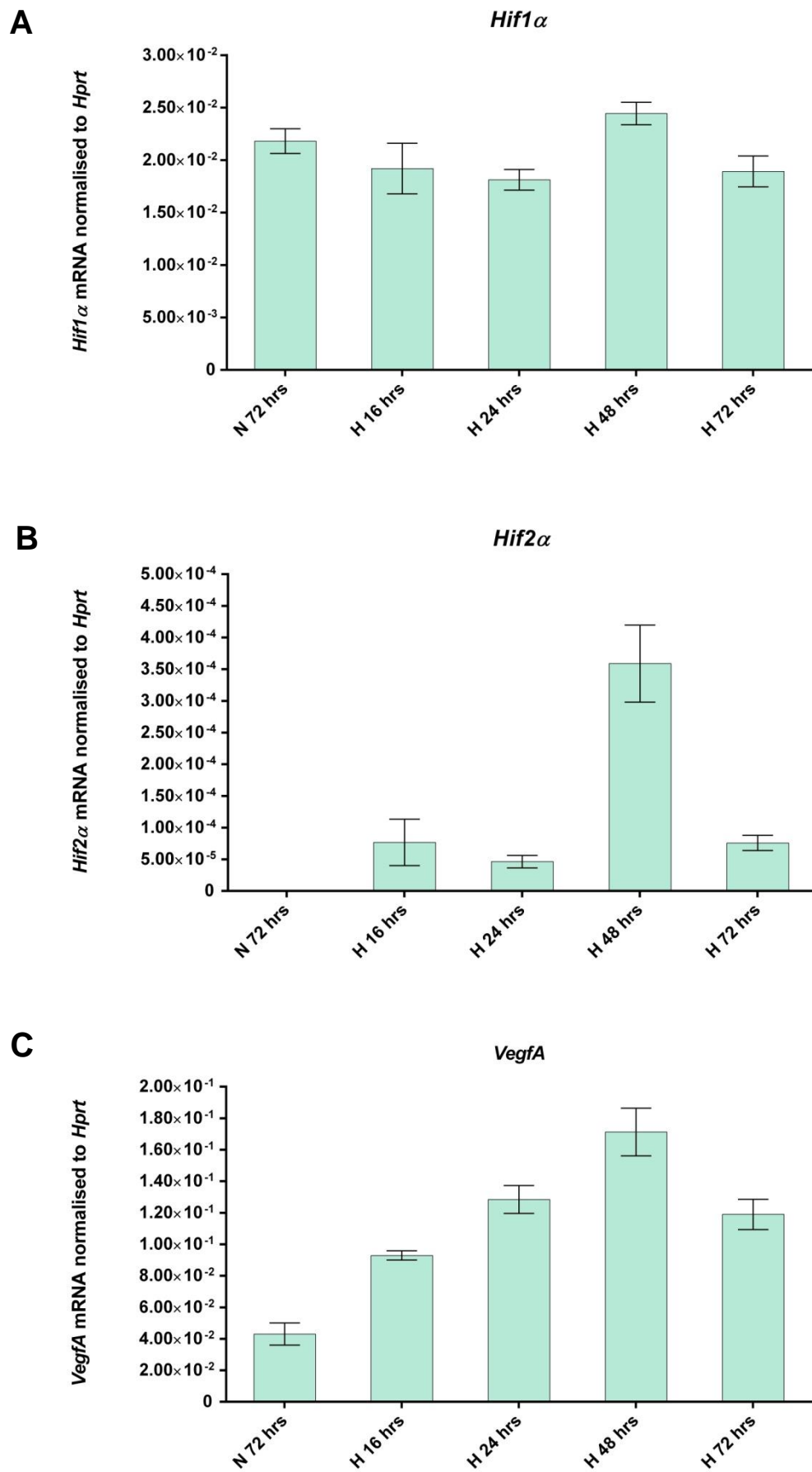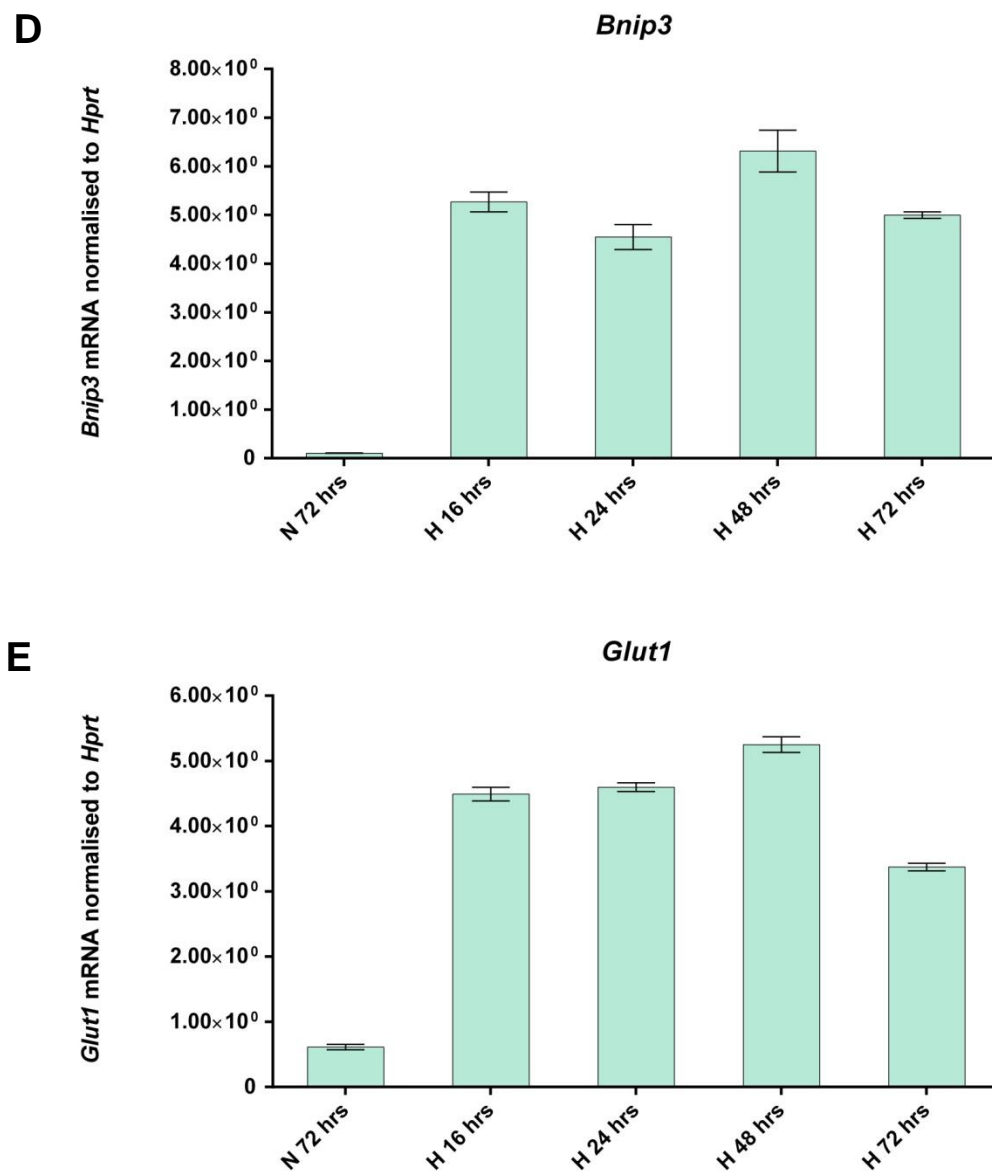
Figure 3.1: Characterisation of *Hifα* and target gene expression in response to hypoxia in 5TGM1 cells. 5TGM1 cells were cultured in normoxia (N) for 72 hours or hypoxia (H) for 16, 24, 48 and 72 hours. RNA was extracted and equivalent amounts were reverse transcribed and used for quantitative PCR analysis performed using primers targeting *Hif1α* (A)*, Hif2α* (B), *Vegf-A* (C)*, Bnip3* (D) and *Glut1* (E). Relative expression of each gene was normalised to the housekeeping gene *Hprt*. Data are graphed as the mean of triplicate samples +/- standard error of the mean from a single experiment, and are a representative of 3 independent experiments.

3.2.2 Creation and characterisation of puromycin selectable Tet-inducible all-in-one HIF overexpressing stable cells.

To investigate the specific roles of HIF-1α and HIF-2α in MM, the lentiviral TRE3G-PGK-TetOn3G-IRES-puromycin (or LVTPTP) all-in-one inducible vector system was chosen to inducibly overexpress each murine HIFα in 5TGM1 cells. One major advantage of the LVTPTP vector is its reported lack of background gene expression in the absence of doxycycline *in vitro* and *in vivo* (Bersten, Sullivan et al. 2015), making the system more robust than the original dual TetOn3G plasmid system. This lentiviral based system provides improved transduction efficiencies over traditional transfection methods. Additionally, both the constitutively expressed Tet-activator protein and doxycycline-inducible target gene are expressed by separate promoters from a single plasmid (LVTPTP) which further improves transfection efficiency (Figure 3.2). The LVTPTP all-in-one vector also constitutively expresses a puromycin resistance gene, enabling antibiotic selection of transduced cells.

3.2.2.1   Subcloning and Transient transfections

Hif1α and *Hif2α* were subcloned from a pENTR2B vector into both the LVTPT-Puromycin (LVTPTP) and LVTPT-GFP (LVTPTG) plasmids (provided by Dr David Bersten (Bersten, Sullivan et al. 2015)) , as described in section 2.1.7, and sequence integrity was verified by Sanger sequencing. The GFP expressing version was used to determine transfection efficiency in HEK293T cells. To assess expression of the HIFα proteins from the LVT-HIF-1α-PTG and LVT-HIF-2α-PTP plasmids, both were transiently transfected into HEK293T cells and treated with doxycycline as described in section 2.2.2.3. Analysis of the LVTPTG and LVT-HIFα-PTG transfected cells by fluorescence microscopy showed high transfection efficiencies of 70-80%. Inducible overexpression of HIF-1α and HIF-2α protein was assessed by western blot following transient transfection of the LVT-HIFα-PTP vector.

Untransfected cells (U) with and without doxycycline treatment (DOX) showed no detectable HIF-1α protein, as expected (Figure 3.3 A). A band corresponding to

endogenous human HIF-1α of approximately 110 kDa was observed in samples treated with the hypoxia mimetic 2,2-dipyridyl (DP). LVT-HIF-1α-PTP transfected samples also displayed high HIF-1α protein expression upon treatment with doxycycline. This HIF1-α protein induction was comparable to constitutively expressed mouse HIF-1α protein from the LV410-HIF-1α vector positive control (Figure 3.3 A, HIF1 Ctrl).

As expected, the untransfected cells (U) with and without doxycycline treatment (DOX) also showed no detectable HIF-2α protein (Figure 3.3 B). In LVT-HIF-2α-PTP transfected cells, the HIF-2α protein detected in the absence of doxycycline was greatly enhanced following the addition of doxycycline, to levels comparable to the constitutively expressed control (Figure 3.3 B). Importantly, these data confirmed the doxycycline inducible expression of both of the HIFα proteins from the LVT-HIF-PTP vectors, and their suitability for the generation of stable cell lines.
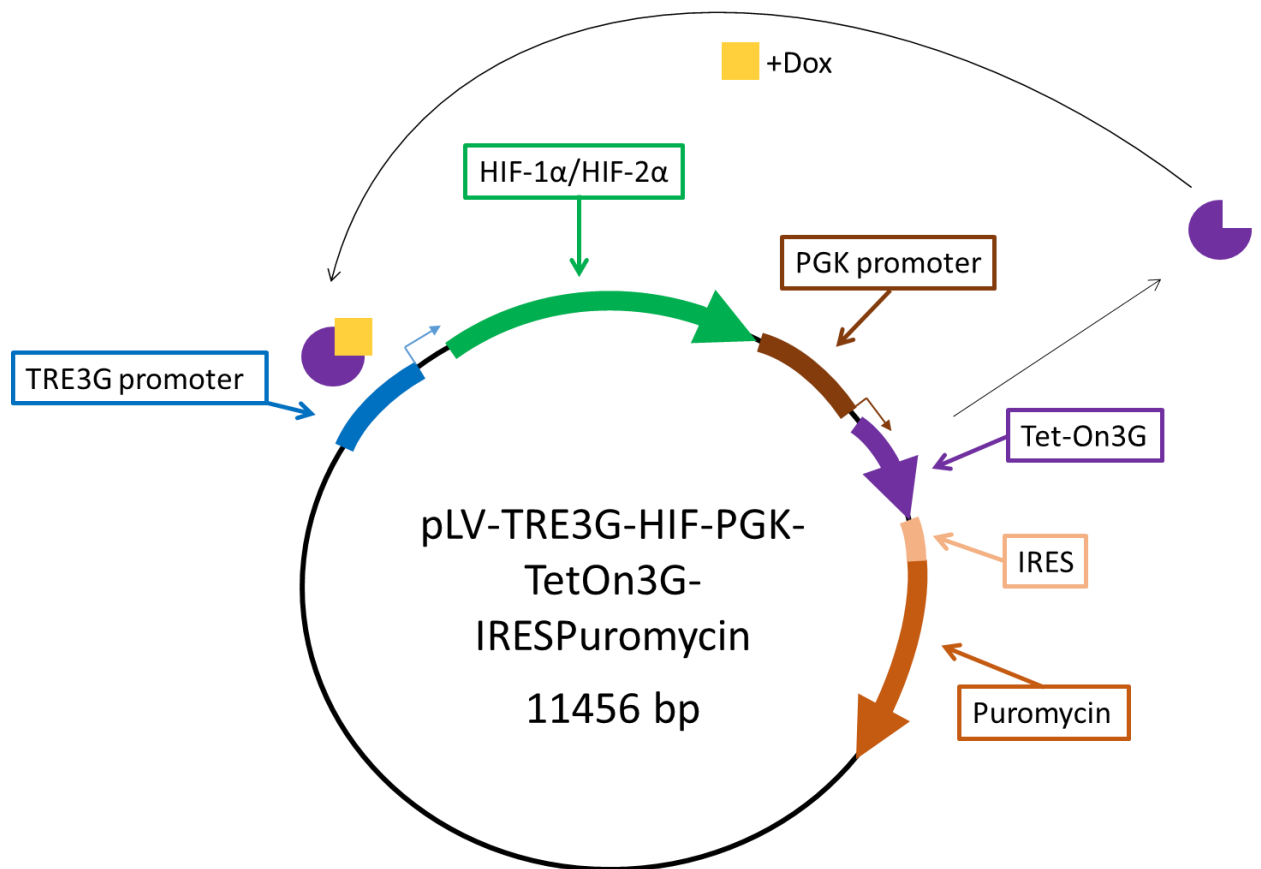
Figure 3.2: Schematic of the LVT-HIFα-PTP mammalian expression vector. The lentiviral plasmid is an all-in-one vector system based on the Tet-On3G® system, combining the constitutive Tet-activator vector with the doxycycline inducible vector that drives expression of our gene of interest. Expression of the target gene, in this case *Hif1α* or *Hif2α,* is controlled by a TRE3G promoter that is dependent on the presence of the constitutively expressed Tet-activator, and doxycycline treatment. The all-in-one vector constitutively expresses the Tet-Activator and a puromycin selection cassette from a PGK promoter. An IRES element allows for the independent translation of both the Tet-activator and the downstream puromycin selection cassette from a single transcript. The constitutive expression of the puromycin from the PGK promoter allows for specific selection of mammalian cells virally infected with the LVT-HIFα-PTP plasmid using puromycin.

A

B

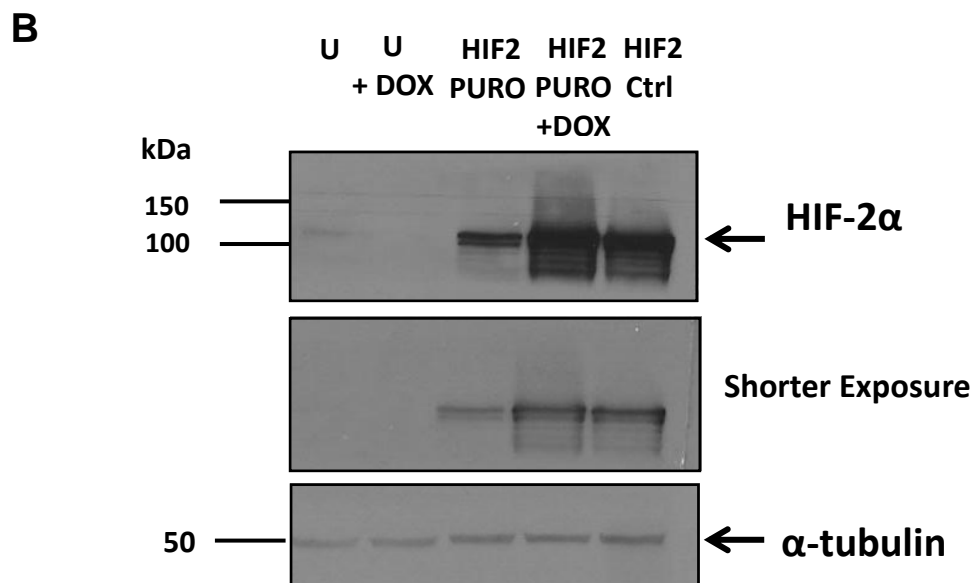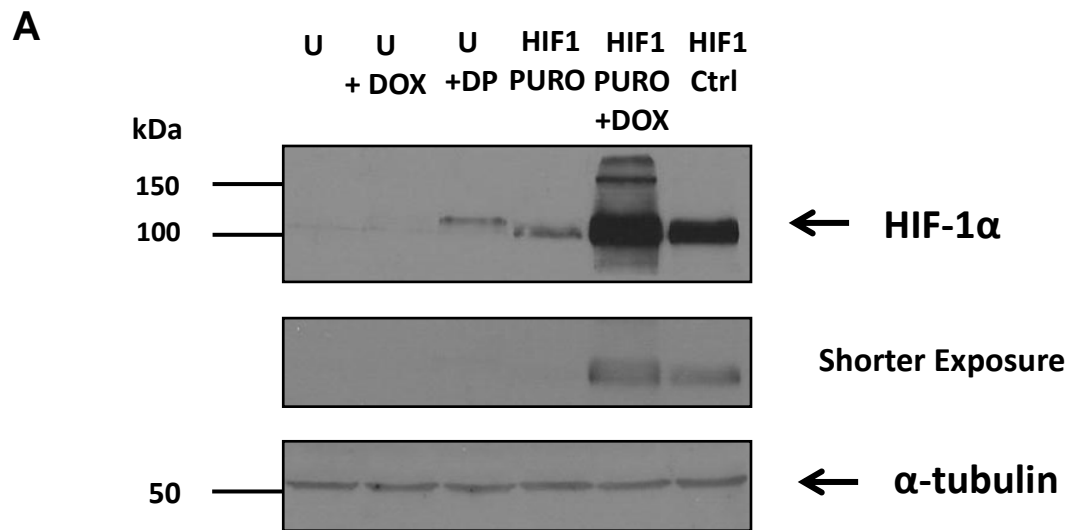**Figure 3.3: Assessment of HIF-1α and HIF-2α protein induction from the LVT-HIFα-PTP vector in transiently transfected HEK293T cells.** HEK293T cells were transiently transfected with either the LVT-HIF-1α-PTP vector (A) or the LVT-HIF-2α-PTP vector (B). Following transfection, cells were cultured for 16 hours in the presence of 2 µg/mL final concentration of doxycycline. Whole cell lysates were collected, denatured, run on a 10% SDS gel and HIFα protein levels detected via western blot. A) Western blot incubated with polyclonal HIF-1 specific antibody. Control samples include untransfected negative controls with and without doxycycline treatment (U and U+DOX), positive controls treated with hypoxia mimetic 2,2'-dipyridyl (U+DP) to detect endogenous HIF-1 protein, and HEK293T cells transiently transfected with pLV410-HIF-1α that constitutively overexpresses HIF-1α (HIF1 Ctrl). The two experimental samples were the HEK293T cells transiently transfected with the LVT-HIF-1α-PTP vector and treated with or without doxycycline (HIF1 PURO and HIF1 PURO+DOX). An antibody specific to α-tubulin was used as a loading control. B) Western blot incubated with polyclonal HIF-2α specific antibody. Control samples include two untransfected negative controls (U and U+DOX) and a positive control from HEK293T cells transiently transfected with pLV410-HIF-2α that constitutively overexpresses HIF-2α (HIF2 Ctrl). The two experimental samples include the HEK293T cells transiently transfected with the LVT-HIF-2α-PTP vector and treated with or without doxycycline (HIF2 PURO and HIF2 PURO+DOX). α-tubulin was used as a loading control. Data are representative of three independent experiments.

3.2.2.2   Puromycin kill curves and lentiviral titration

To generate stable cell lines, two key components of the LVTPTP plasmids were required. The puromycin cassette was required for antibiotic selection whilst the long terminal repeats (LTR) allowed high efficiency lentiviral-mediated infection of the target cells and stable integration into the host genome.

To assess puromycin sensitivity, uninfected 5TGM1 cells were cultured in the presence of 1, 2, 4 and 6 µg/mL of puromycin. Cell survival was measured daily by staining with Trypan blue and counting viable cells using a haemocytometer. The cells continued to proliferate with 1 µg/mL of puromycin, but 4 µg/mL and 2 µg/mL killed all 5TGM1 cells by days 4 and 8, respectively, and were used for subsequent selection experiments (Figure 3.4).

To generate lentivirus, HEK293T cells were transiently co-transfected with the lentiviral packaging and envelope expressing vectors in combination with either LVTPTP empty control, LVT-HIF-1α-PTP, LVT-HIF-2α-PTP or LVT-dsRed-PTP vectors. The LVT-dsRed-PTP lentivirus was included as a control to measure cellular transduction using the inducibly expressed fluorescent dsRed protein. Following viral production, the LVT-dsRed-PTP lentivirus was titrated and tested on the 5TGM1 cells to assess the transduction efficiency of these cells. The titration data were used to identify the optimal volume of lentivirus that maximised transduction frequency in these cells. As such, the lentiviral volume that resulted in the best dsRed expression was selected for subsequent stable cell line production Three days following infection, 2 µg/mL doxycycline was added to the cells, incubated overnight and dsRed expression assessed for each titration point using a haemocytometer and fluorescence microscopy. The resulting transduction frequencies (i.e the number of dsRed positive cells/total number of GFP positive 5TGM1 cells) showed that the optimal volume of virus was 1 mL with a transduction rate of 20.4% (Table 3.1).
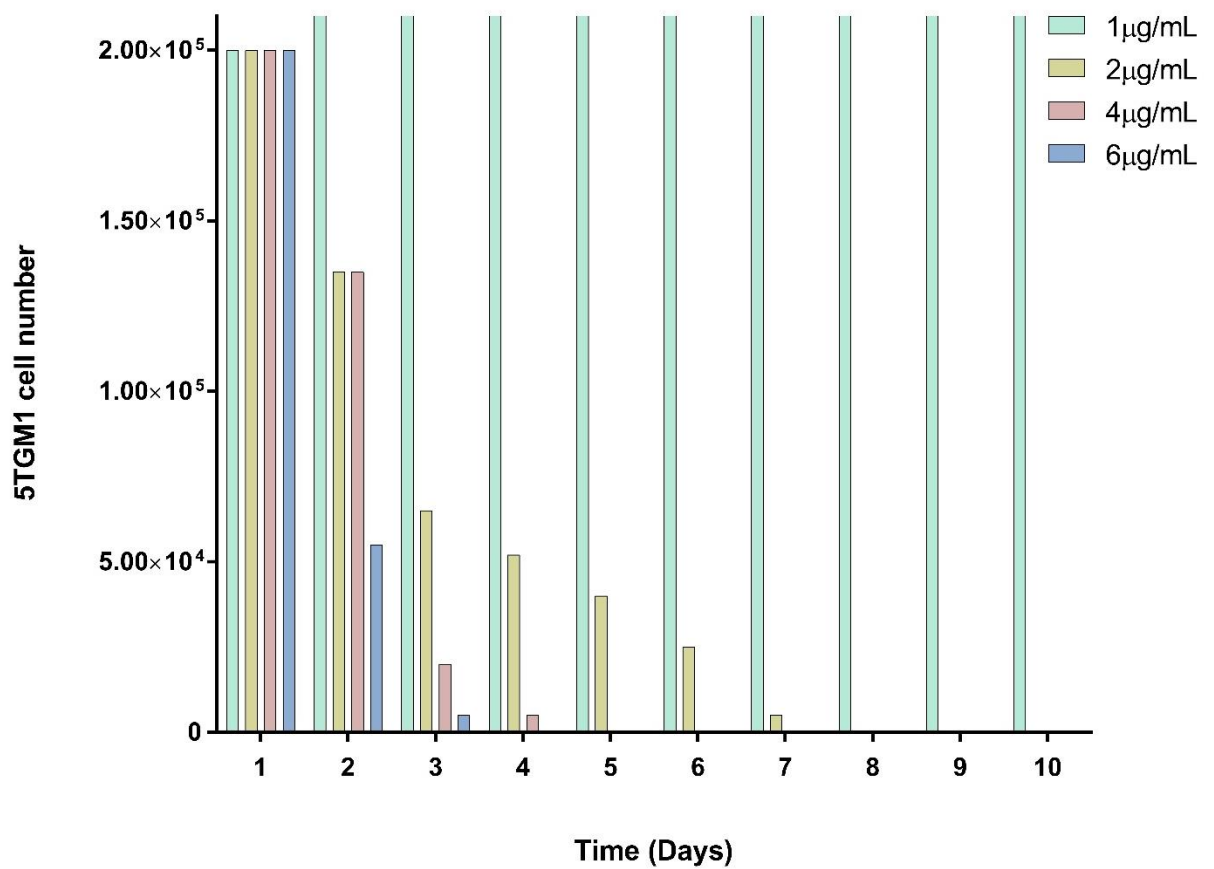
Figure 3.4: Puromycin kill-curve of 5TGM1 cells. A) 5TGM1 cells were treated with 1 μg/mL, 2 μg/mL, 4 μg/mL or 6 μg/mL of puromycin. Cell survival was monitored daily by Trypan Blue staining and live cell number recorded for 10 days.

Table 3.1: Lentivirus titration to optimise transduction rate in 5TGM1 cells.

	1 mL Lentivirus	0.5 mL Lentivirus	0.25 mL Lentivirus	0.1 mL Lentivirus
GFP Positive (Number of cells)	162	104	155	121
dsRed Positive (Number of cells)	33	12	6	0
Transduction % (dsRed/GFP)	20.4%	11.5%	3.9%	0%

5TGM1 cells were infected with lentivirus containing the LVT-dsRed-PTP vector.

3.2.2.3   Virus optimisation to create a stable cell line

To create stable cell lines, 5TGM1 cells were infected with 1 mL of LVTPTP, LVT-HIF-1α-PTP, LVT-HIF-2α-PTP or LVT-dsRed-PTP containing lentivirus and treated with either 4 µg/mL or 2 µg/mL of puromycin. Cells treated with 4 µg/mL of puromycin in combination with viral infection did not survive, with no viable cells detected with trypan blue staining after 6 days of selection. Cells treated with 2 µg/mL of puromycin resulted in increasing cellular stress and death over time, where the low number of surviving cells expressed dsRed by fluorescent microscopy, but displayed slowed growth rates and abnormal morphology.

Attempts were made to improve cell survival and morphology, including lowering puromycin concentrations to 1 µg/mL, the intermittent removal of puromycin for 1 week when increased cellular death was observed, and the addition of conditioned media from untreated 5TGM1 cells. Removal of puromycin increased cell survival, however, the percentage of dsRed positive cells in the culture rapidly decreased. Reduced puromycin concentrations in combination with the addition of conditioned media also increased cell survival, but the surviving cells grew slowly, never returned to a logarithmic growth phase, showed persistent irregular morphology and displayed unstable dsRed expression. Despite numerous attempts the cells did not recover a normal cellular growth rate or morphology and stable dsRed expressing cell lines could not be generated. These results indicated that the 5TGM1 cells are sensitive to puromycin at the concentrations required for selection. Hence, an alternative strategy for selection of transduced cells was required to generate 5TGM1 cell overexpressing HIF-1α and HIF-2α.

3.2.3 Designing and creating a modified lentiviral Tet-inducible all-in-one vector for overexpression of HIF-1α and HIF-2α

3.2.3.1   Design, creation and testing of modified LVTETPT vector system

To address the puromycin-associated cellular stress, a new TetOn3G vector system was designed based on the LVTPTG vector. In place of puromycin selection, the dTomato fluorophore was used to enable selection of successfully transduced 5TGM1 cells using FACS. An advantage of this method was that FACS had successfully been used previously to create stable cell lines in 5TGM1 cells (Noll, Hewett et al. 2014, Cheong, Chow et al. 2015).

The IRES element of the pLVTPTG vector was also replaced with a P2A (porcine teschovirus-1) self-cleaving peptide sequence. Previous studies have shown that the gene that follows an IRES sequence is frequently expressed at different levels to the preceding gene. The virally derived 2A small "self-cleaving" peptides enable the production of multiple proteins from a multicistronic cassette with minimal variation in protein expression from adjacent genes (Szymczak, Workman et al. 2004, Kim, Lee et al. 2011). These 2A peptides are 18-22 nucleotides long, function through ribosomal skipping, and have been used successfully in both cultured cell lines and whole animal experiments (Kim, Lee et al. 2011). The replacement of the IRES with the P2A sequence enables efficient constitutive expression of both the Tet-On3G transactivator and dTomato proteins from a single promoter.

In addition to these changes, the PGK promoter driving constitutive expression of the Tet-On3G transactivator was replaced with the EF1α promoter which shows comparatively stronger promoter activity across multiple different mammalian cell types transduced with lentiviral vectors (Qin, Zhang et al. 2010).

Once the new Lentiviral-TRE3G-EF1α-TetOn3G-P2A-dTomato (LVTETPT) plasmid was generated and verified by Sanger sequencing, HIF-1α and HIF-2α were subcloned into the vector and also verified by sequencing.
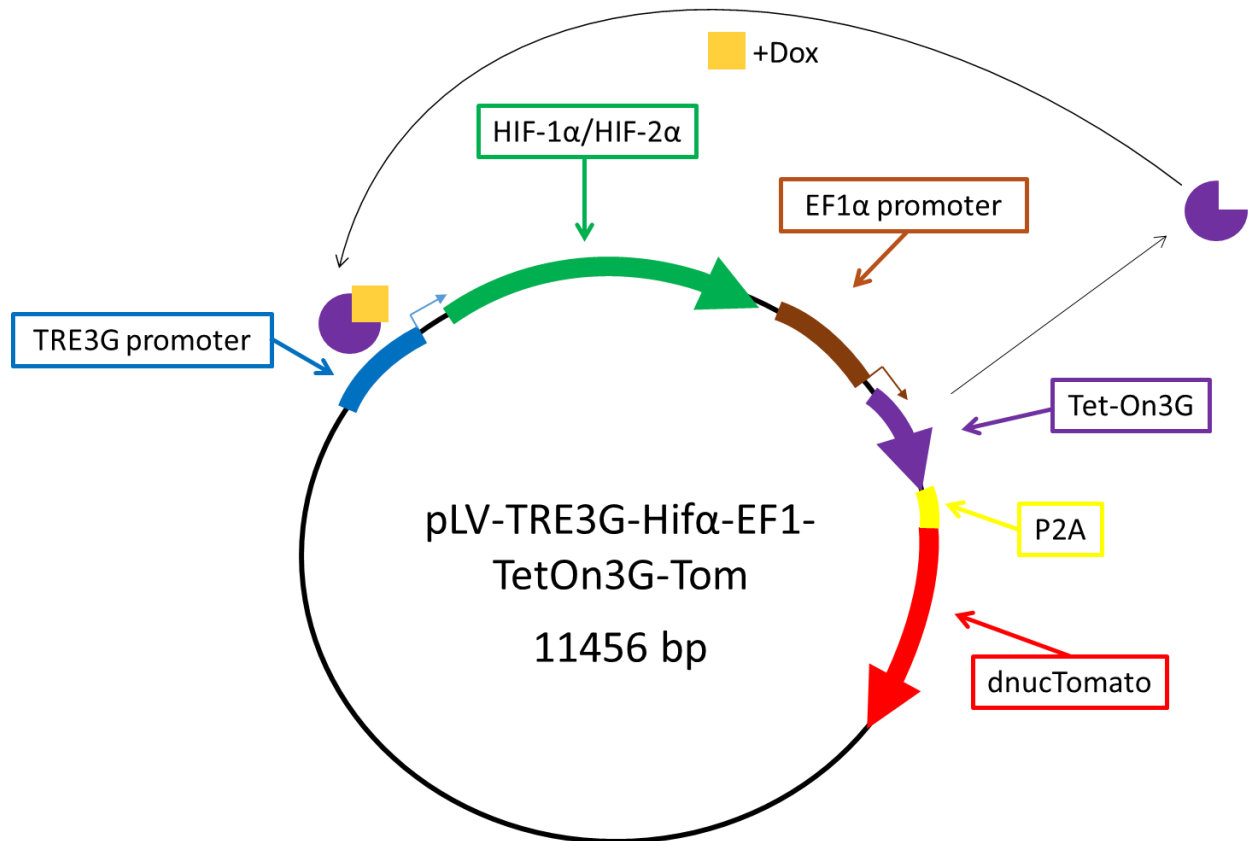
Figure 3.5: Schematic of the LVT-HIFα-ETPT mammalian expression vector. This lentiviral plasmid is a modified version of the all-in-one TetOn3G vector system (LVTPTG). The Tet transactivator (TetOn3G) is constitutively expressed from the EF1α promoter, allowing for its continual expression in mammalian cells. The TetOn3G gene is immediately followed by a self-cleavage P2A peptide sequence and the gene encoding dTomato. The P2A component allows for the production of two separate proteins from a single mRNA transcript. The fluorescent dTomato protein produced is used for selection of infected cells and localises to the nucleus of the cell allowing for easy microscopic identification. The TRE3G promoter allows for the controllable expression of either HIF-1α or HIF-2α upon the treatment of cells with doxycycline.

3.2.3.2   Functional testing of the LVTETPT plasmid in cells

The functionality of the LVTETPT, LVT-HIF-1α-ETPT and LVT-HIF-2α-ETPT plasmids were assessed using transient transfection of HEK293T cells. Fluorescence microscopy of the transfected HEK293T cells confirmed constitutive expression of dTomato and functionality of the P2A sequence from all three plasmids (Figure 3.6). The dTomato also appeared to be predominantly nuclear, which was expected given that this dTomato contained a nuclear localisation signal. The inducible expression of murine HIF-1α and HIF-2α protein was also assessed in HEK293T cells transiently transfected with 2 different preparations of either LVT-HIF-1α-ETPT or LVT-HIF-2α-ETPT plasmids followed by western blot analysis (Figure 3.7).

Untransfected HEK293T cells with and without doxycycline treatment showed no detectable HIF-1α protein (Figure 3.7 A). Comparatively, cells transfected with the LV410-HIF-1α constitutive expressing positive control showed clear expression of mouse HIF-1α protein. Cells transfected with the LVT-HIF-1α-ETPT vector showed no detectable HIF-1α protein without doxycycline treatment as expected, however, no HIF-1α protein was induced in response to doxycycline treatment despite high transfection efficiencies of approximately 75% (Figure 3.6).

Untransfected HEK293T cells also showed no detectable HIF-2α protein, with or without doxycycline treatment, as expected (Figure 3.7 B). In contrast to HIF-1α, a band corresponding to mouse HIF-2α protein was detected from LVT-HIF-2α-ETPT transfected samples following doxycycline treatment, with levels comparable to the constitutively expressing LV410-HIF-2α control (Figure 3.7 B). This confirmed the doxycycline-dependent induction of HIF-2α protein from LVT-HIF-2α-ETPT transfected cells.

The lack of HIF-1α protein observed with doxycycline treatment suggested that the induced HIF-1α protein may have been degraded by prolyl hydroxylation-mediated ubiquitylation. To address this, hypoxic treatment was included. Specifically, treatment

of cells with hypoxia should result in the inactivation of the PHDs and thus stop the degradation of HIF-1α protein. If the HIF-1α proteins were being over expressed in response to doxycycline, then the levels of induced HIF-1α expression should be considerably greater than the levels of endogenous HIF-1α protein observed in the absence of doxycycline treatment.

Untransfected and LVT-HIF-1α-ETPT transfected HEK293T cells treated with and without doxycycline produced no detectable HIF-1α protein (Figure 3.8) as seen previously. Under hypoxia, endogenous human HIF-1α protein induction was observed in untransfected cells, as expected (U+H). Endogenous HIF1α protein was also observed in cells transfected with LVT-HIF-1α-ETPT and cultured under hypoxic conditions without doxycycline treatment (HIF1+H). Importantly, a further induction in HIF-1α protein was observed in the LVT-HIF-1α-ETPT sample treated with both doxycycline and hypoxia (HIF1+DOX+H) when compared to LVT-HIF-1α-ETPT cells without doxycycline (HIF1+H). As had been previously shown in Figure 3.3 A, the induced sample (HIF1+DOX+H) displayed a doublet of HIF-1α protein consistent with the band pattern observed in the constitutively expressed mouse HIF-1α positive control (Hif1 Ctrl) (Figure 3.8). From these data, the doxycycline-inducible overexpression of HIF-1α from the LVT-HIF-1α-ETPT vector was confirmed when treated with a combination of doxycycline and hypoxia. Importantly the doxycycline-dependent induction of both HIF-1α and HIF-2α protein from LVTETPT transfected cells confirmed that the new vectors were both functional. Furthermore, these data showed that the P2A sequence was efficiently producing both the Tet Activator and dTomato proteins from a single transcript

Bright Field   TxRed

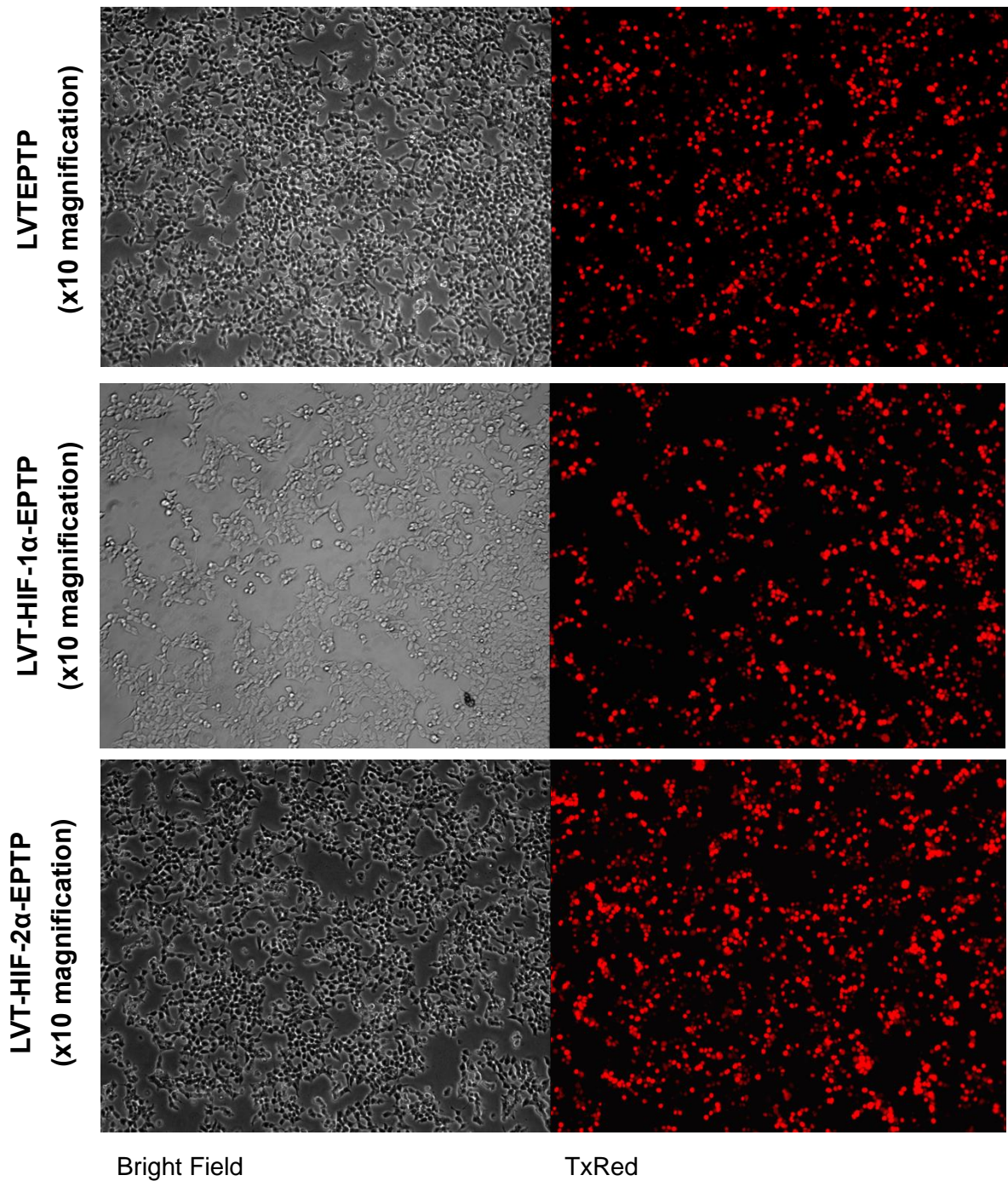**Figure 3.6: Constitutive dTomato expression from LVT-HIF-1α-ETPT.** HEK293T cells were transiently transfected with the LVT-HIF-1α-ETPT vector. After 24 hours, the cells were observed using microscopy and images taken at 10x magnification. The image on the left is a bright field view of the cells at a 1 ms (milli second) exposure, whilst the image on the right uses the TxRed filter at 100 ms exposure.

Figure 3.7: Assessment of HIF-1α and HIF-2α protein induction from the LVT-HIFα-ETPT vector in transiently transfected HEK293T cells. HEK293T cells were transiently transfected with either the LVT-HIF-1α-ETPT (A) vector or the LVT-HIF-2α-ETPT vector (B). Following transfection, cells were cultured overnight in the presence of 2 μg/mL of doxycycline. Whole cell lysates were separated by a 10% SDS gel and HIFα protein levels detected via western blot. Experimental control samples consisted of untransfected samples with and without doxycycline treatment (U and U+DOX), and pLV410-HIF-1α (HIF1 Ctrl) or pLV410-HIF-2α (HIF2 Ctrl) constitutively overexpressing vectors. Experimental samples were cells transfected with two different plasmid preparations of HIF-1α or HIF-2α inducible vectors (HIF1 P1, HIF1 P2, HIF2 P1, and HIF2 P2) with and without 16 hours doxycycline treatment (HIF1 P1+DOX, HIF1 P2+DOX, HIF2 P1+DOX, HIF2 P2+DOX). Endogenous α-Tubulin protein was used as a loading control. Data are representative of three independent experiments.
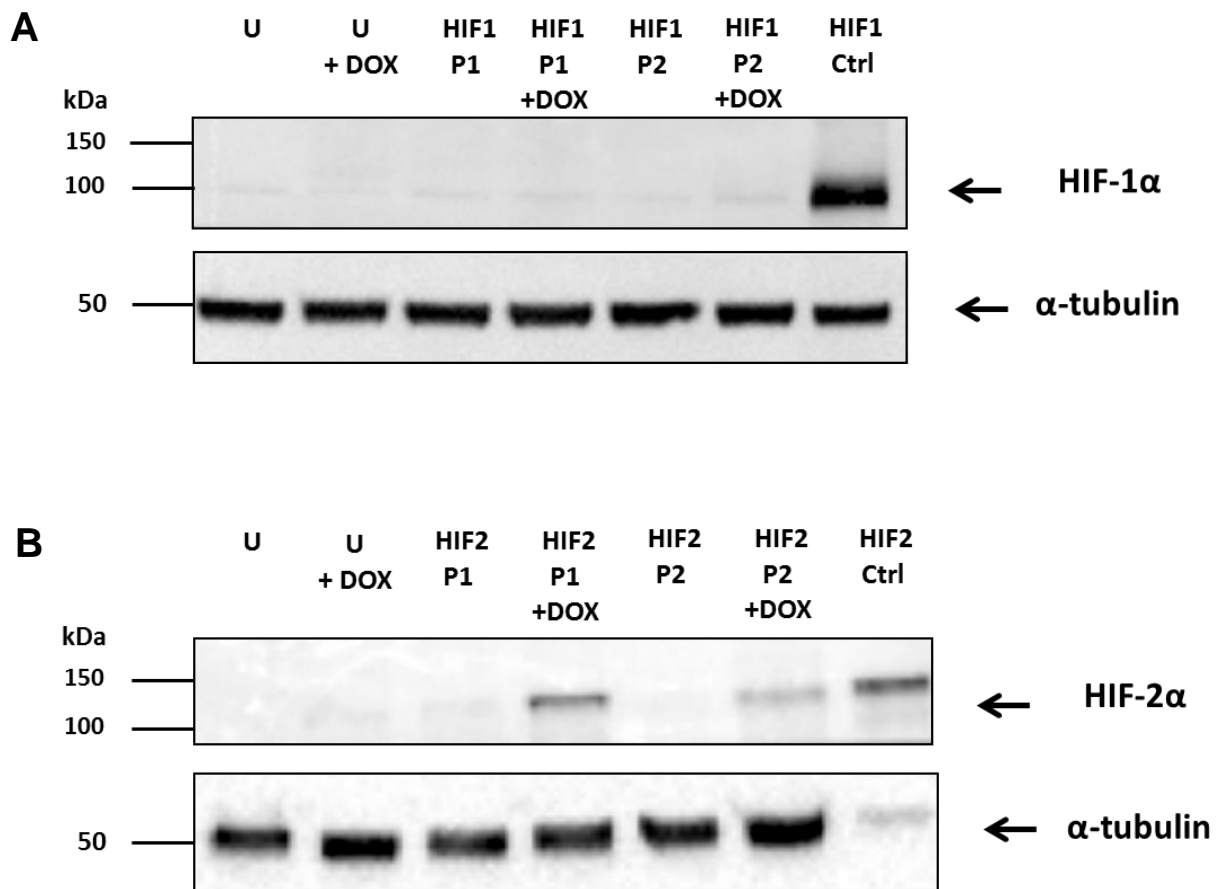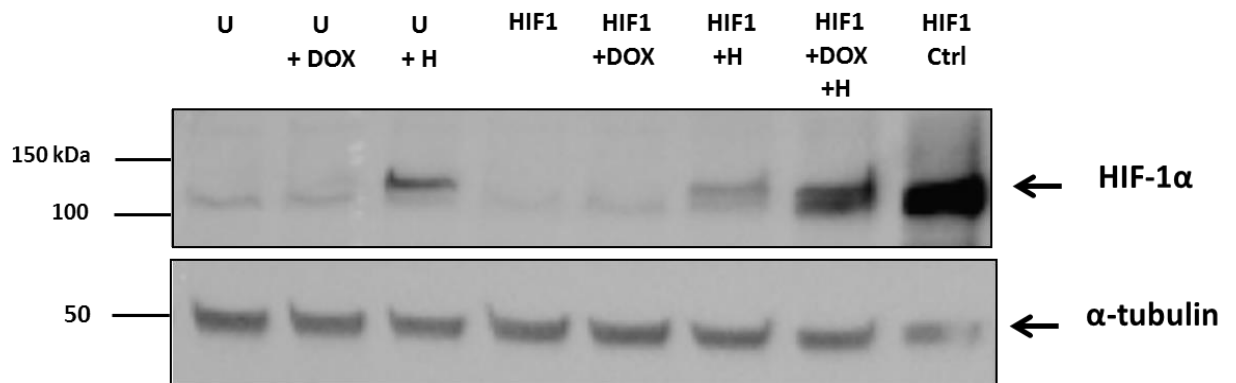
Figure 3.8: Western blot of HIF-1α protein induction from the LVT-HIFα-ETPT vector in transiently transfected HEK293T cells. HEK293T cells were transiently transfected with the LVT-HIF-1α-ETPT vector and, where specified, cultured for 16 hours in either hypoxia (+H), with doxycycline at a final concentration of 2 µg/mL (+DOX) or both (+DOX+H). Whole cell lysates were collected, denatured, run on a 10% SDS gel and HIFα protein levels detected via western blot. Experimental control samples consisted of untransfected samples (U) in various treatments and a pLV410-HIF-1α constitutively overexpressing control (HIF1 Ctrl). Endogenous α-Tubulin protein was used as a loading control. Data representative of three independent experiments.

### 3.2.4 Creation and characterisation of 5TGM1 LVTETPT stable cells *in vitro*

Lentivirus was made containing the LVTETPT (empty control), LVT-HIF-1α-ETPT or LVT-HIF-2α-ETPT constructs. Based on the previous experiment (see section 3.2.3.2), a volume of 1 mL of viral particle-containing conditioned media was used to infect 5TGM1 cells and create the three stable cell lines. Cells expressing both GFP and dTomato were sorted 2 days after infection using FACS to isolate pools of cells in which the LVTETPT, LVT-HIF-1α-ETPT or LVT-HIF-2α-ETPT plasmids were stably integrated (Figure 3.9). In this initial sort, 6.0%, 7.5% and 3.7% of cells were transduced with the LVTETPT, LVT-HIF-1α-ETPT and LVT-HIF-2α-ETPT plasmid, respectively. Each stable pool of cells underwent a second round of sorting to obtain a pure population of GFP and dTomato expressing cells. The newly created LVTETPT stable cell lines were then assessed for the doxycycline-specific induction of each HIFα.

3.2.4.1   Characterisation of HIF expression in 5TGM1 stable cell lines by qPCR

The HIF-1α inducible (LVT-HIF-1α-EPTP), HIF-2α inducible (LVT-HIF-2α-EPTP) and empty vector control (LVTETPT) 5TGM1 cell lines were treated for 16 hours with 2 µg/mL of doxycycline, hypoxia or a combination of hypoxia and doxycycline. Quantitative PCR analysis of *Hif1α* or *Hif2α* mRNA expression showed no hypoxia or doxycycline-dependent upregulation of either *Hifα* in the empty vector control cells (Figure 3.10 A & B). LVT-HIF-1α-EPTP and LVT-HIF-2α-EPTP infected 5TGM1 cells showed background levels of expression compared to the empty vector control, with a 1.7 fold and 8.5 fold increase in *Hif1α* and *Hif2α* mRNA expression, respectively. Neither *Hif1α* nor *Hif2α* mRNA was induced following hypoxia treatment in the HIF-1α inducible or HIF-2α inducible cell lines. Importantly, following treatment with doxycycline, *Hif1α* mRNA levels were induced in the HIF-1α inducible line by 12 fold (Figure 3.10 A), and *Hif2α* mRNA levels were induced in the HIF-2α line greater than 100-fold (Figure 3.10 B), both in the presence and absence of hypoxia. An increase in *Hif1α* and *Hif2α* mRNA expression following either doxycycline or the combined doxycycline and hypoxia treatment was consistently observed across all three

independent experiments (Figure 3.10 and Appendix 5-6). Despite this, when averaging the mean of all three experiments, statistical significance was not reached using a paired student t-test due to variation between datasets, therefore data from a representative replicate is included in this chapter (Figure 3.10).

Overall, these data confirmed that the LVT-HIF-1α-EPTP and LVT-HIF-2α-EPTP 5TGM1 stable cell lines overexpress HIF-1α and HIF-2α respectively in a doxycycline dependent manner, and could be used to assess the comparative roles of HIF-1α and HIF-2α in MM.

A

	LVTETPT % (dTom/GFP)	LVT-HIF-1α-ETPT % (dTom/GFP)	LVT-HIF-2α-ETPT % (dTom/GFP)
First Sort	6.0	7.5	3.7
Second Sort	86.1	74.0	81.3
Purity Test (post second sort)	99.7	99.3	99.2

Purity Test: flow cytometry analysis of 5TGM1 cell lines expressing both GFP and dTomato following the second round of FACS, to confirm the creation of pure cell lines.

B
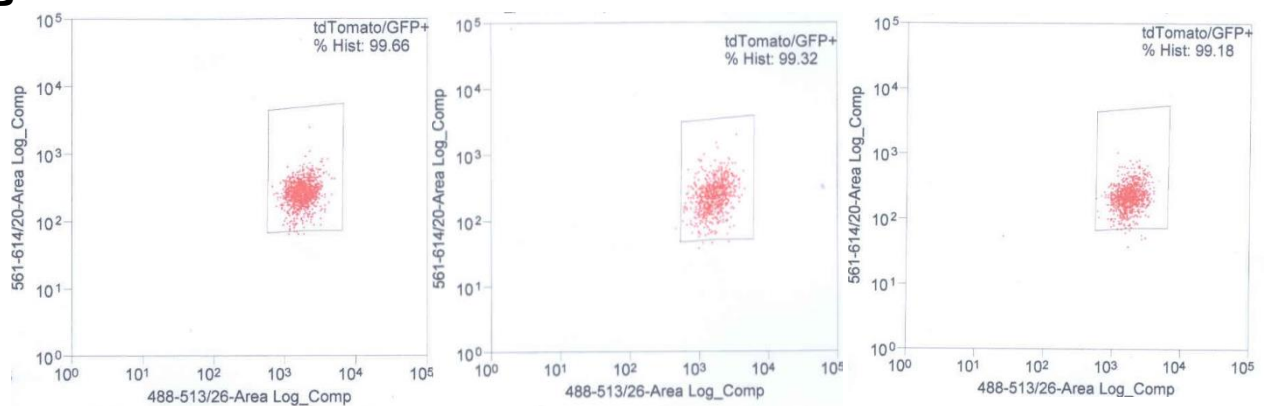
Figure 3.9: FACS of 5TGM1 cells lentivirally infected with LVTETPT, LVT-HIF-1α-ETPT or LVT-HIF-2α-ETPT constructs. 5TGM1 cells at a concentration of $2x10^5$ cells/mL were infected with LVTETPT, LVT-HIF-1α-ETPT or LVT-HIF-2α-ETPT containing lentivirus. Cells displaying both GFP and dTomato fluorescence were sorted by FACS. A) Table showing the percentage of infected cells sorted to create each stable cell line using FACS. Each pooled sample underwent two rounds of sorting followed by a purity test for double positive fluorescent cells in each newly made cell line. B) The percentage of cells expressing both dTomato and GFP from the total population of LVTETPT, LVT-HIF-1α-ETPT and LVT-HIF-2α-ETPT infected cells following the second round of FACS.

A

B
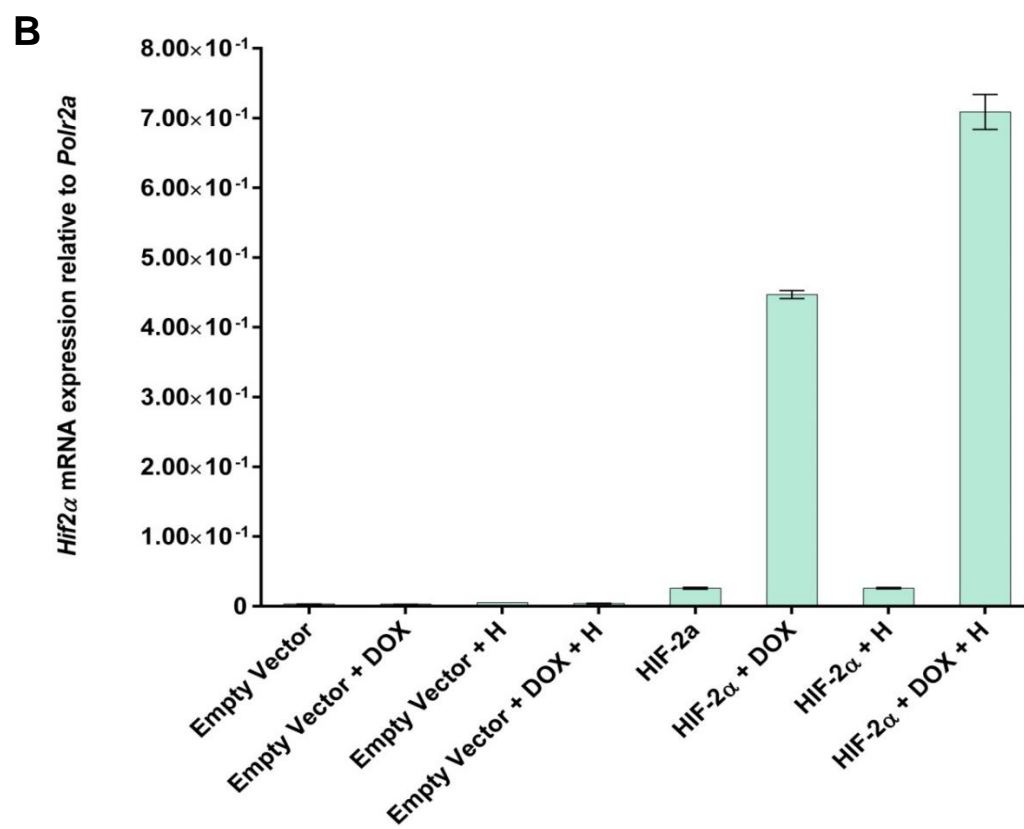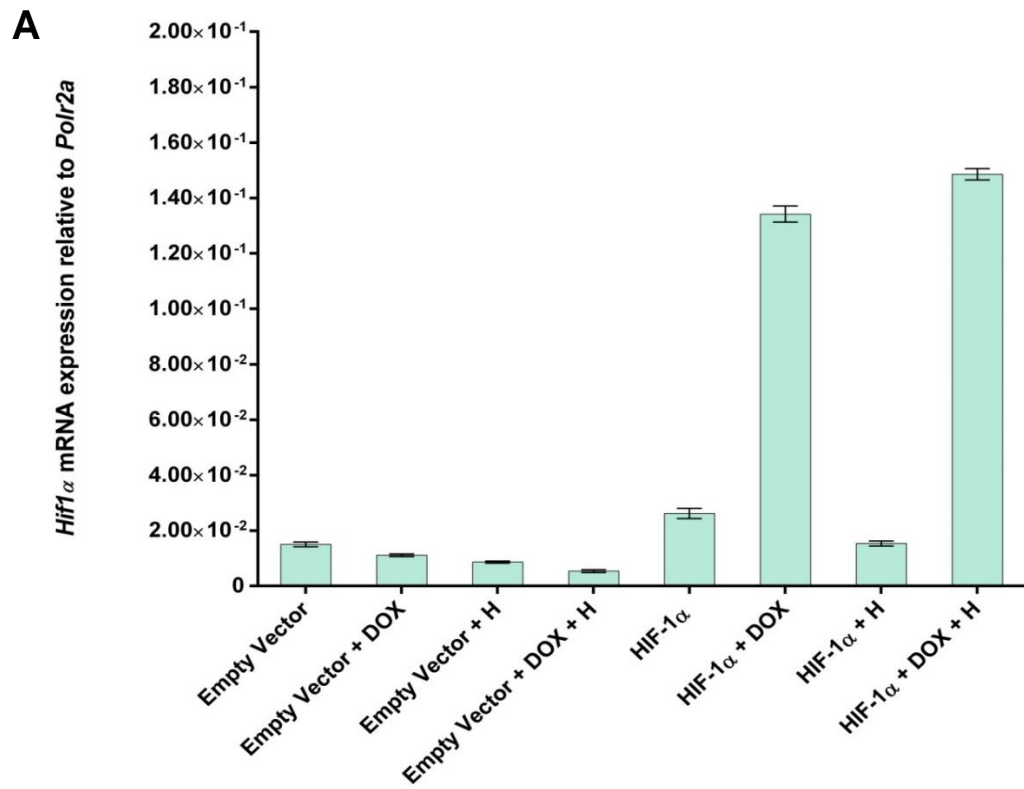
Figure 3.10: Assessment of *Hif1α* and *Hif2α* mRNA induction in 5TGM1 cells integrated with the LVT-HIFα-ETPT vector. 5TGM1 cell lines were transduced with lentivirus particles containing either the LVTETPT, LVT-HIF-1α-EPTP, or LVT-HIF-2α-EPTP vectors and where specified, cultured for 16 hours with no treatment, in hypoxia (+H), with doxycycline at a final concentration of 2 µg/mL (+DOX) or both (+DOX+H). Cellular mRNA was extracted and cDNA produced for quantitative PCR analysis. Samples were then assessed for either *Hif1α* (A) or *Hif2α* (B) mRNA expression normalised to the housekeeping gene *Polr2a*. Data are representative of three independent experiments.

3.2.5   Characterisation of 5TGM1 LVTETPT stable cell lines for an *in vivo* mouse model of MM

3.2.5.1   Luciferase expression in 5TGM1 LVTETPT stable cell lines

The 5TGM1 cell line is used in conjunction with the C57Bl/KaLwRij mouse strain as a pre-clinical model of MM (Dallas, Garrett et al. 1999). To directly compare the role HIF-1α and HIF-2α play in MM disease development and progression, the LVT-HIFα-ETPT stable cell lines were characterised prior to evaluation in the C57BL/KaLwRij mouse model. A crucial component of this model was the luciferase gene stably integrated within the 5TGM1 cells, which allowed for assessment of tumour burden using *in vivo* bioluminescence. It was important to determine whether the luciferase activity across each cell line was comparable, thus ensuring that any changes in tumour burden observed *in vivo* were attributed to changes in HIFα expression, not differences in luciferase expression. D-luciferin was added to each cell line and cellular luminescence quantified in photons/sec using the Xenogen IVIS imaging system, allowing for a comparative assessment of luciferase activity across all three cell lines.

The LVTETPT, LVT-HIF-1α-ETPT and LVT-HIF-2α-ETPT stable lines were plated at concentrations of $1x10^6$, $2x10^5$, $4x10^4$, $8x10^3$ and $1.6x10^3$ cells per well, D-luciferin added and luminescence measured. The LVTETPT empty vector control showed approximately half of the luciferase activity (photons/second) when compared to both the HIF-1α (p=0.0012) and HIF-2α (p=0.0109) overexpressing lines, which showed comparable levels of luciferase activity to each other (p=0.094) (Figure 3.11). Consequently, mice injected with the LVT-HIF-1α-ETPT and LVT-HIF-2α-ETPT cell lines could be directly comparable *in vivo*, whilst mice injected with LVTETPT control cells would expectedly show an underestimate amount of tumour burden.
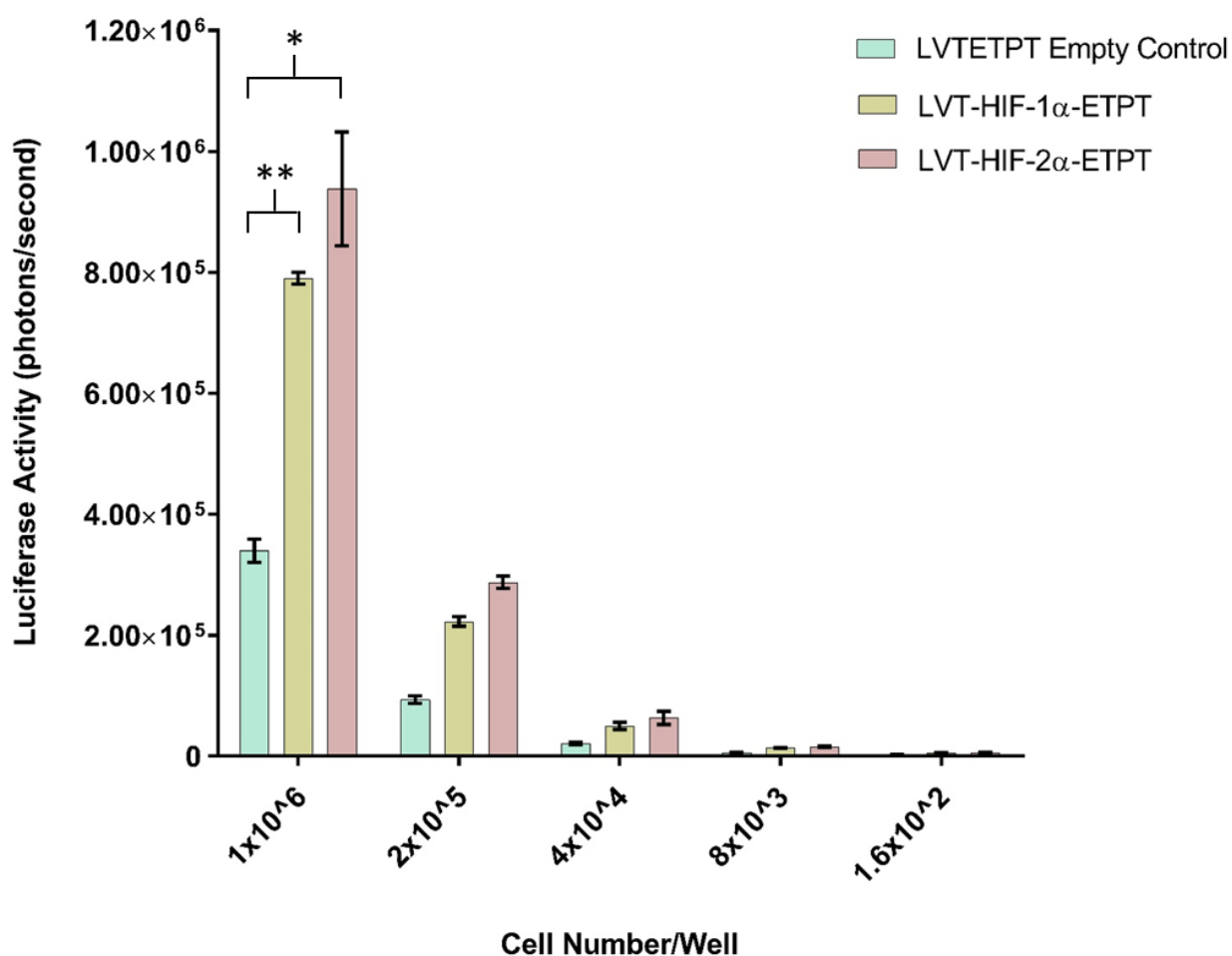
Figure 3.11: Comparative analysis of luciferase activity between 5TGM1 LVTETPT empty control, LVT-HIF-1α-ETPT and LVT-HIF-2α-ETPT stable cell lines. 5TGM1 LVTETPT empty control cells, LVT-HIF-1α-ETPT and LVT-HIF-2α-ETPT stable cells were plated at 1/5 serial dilutions from 1×10^6 to 320 cells/well in triplicate in a 96-well tray. D-luciferin stock of 30 mg/mL diluted 1/100 was added to each well and left to incubate at 37^0C for 30 minutes. All cell lines constitutively express luciferase from a triple modality gene which cleaves the D-luciferin to produce light measured in photons/sec. Images were taken at an exposure time of 10 minutes, and light emission measured using the IVIS Xenogen^{TM}. Data are mean values +/- standard error of the mean of 3 independent experiments, each with triplicate samples, where significance was determined using paired student t-test (*p-value <0.05, ** p-value <0.01).

3.2.5.2   Homing and dissemination of stables cells in the 5TGM1/C57BL/
KaLwRij MM mouse model

The LVTETPT stable cell lines were next tested in a small scale experiment within the 5TGM1/C57BL/KaLwRij mouse model system to assess their ability to home to the BM and disseminate in mice over 4 weeks. Mice were injected with 5×10^5 cells in 100 μL of PBS, or an equivalent volume of PBS alone for control mice, via the tail vein. Mouse injection and treatment groups included PBS, Empty Vector (LVTETPT), HIF-1α (LVT-HIF-1α-ETPT), HIF-1α+DOX (LVT-HIF-1α-ETPT plus doxycycline), HIF-2α (LVT-HIF-2α-ETPT) and HIF-2α+DOX (LVT-HIF-2α-ETPT plus doxycycline) with 3 mice in each group (Figure 3.12). Mice were administered weekly with D-luciferin via intraperitoneal injection and tumour growth was assessed using *in vivo* bioluminescence. Specifically, greyscale images overlayed with pseudo-coloured images of mice were taken and used to quantifiably measure luminescence from injected tumour cells, where the intensity and size of the signal was proportional to tumour cell number (Figure 3.12).

The spread of intramedullary tumours at multiple sites throughout the mice was minimal at 3 weeks post injection. Assessment of mice at 4 weeks post injection showed dissemination of tumour to multiple skeletal sites throughout the animal, most notably the hind leg long bones, in all three cell lines (EV, HIF-1α and HIF-2α) (Figure 3.12 A & B). This BM localisation and dissemination was consistent with other studies using the parental 5TGM1 cell line (Garrett, Dallas et al. 1997, Alici, Konstantinidis et al. 2004, Libouban 2015). Quantification of tumour burden in each mouse group showed that the empty vector control cells produced comparatively less bioluminescence (Figure 3.12 C). This was consistent with findings from luciferase analyses of each cell line *in vitro* prior to injection (section 3.2.6.1). Importantly, tumour burden was established in most mice at 4 weeks confirming that all three 5TGM1 LVTETPT cell lines were capable of homing to the BM. Interestingly, graphed data showed a trend towards a doxycycline-dependent increase in tumour burden in mice injected with both the LVT-HIF-1α-ETPT and LVT-HIF-2α-ETPT expressing 5TGM1 cells (Figure 3.12 C), although these differences were not statistically significant,

possibly due to the low number of mice used in this preliminary experiment and the lowered luciferase expression from the empty vector control line.

Front View

Back View

C
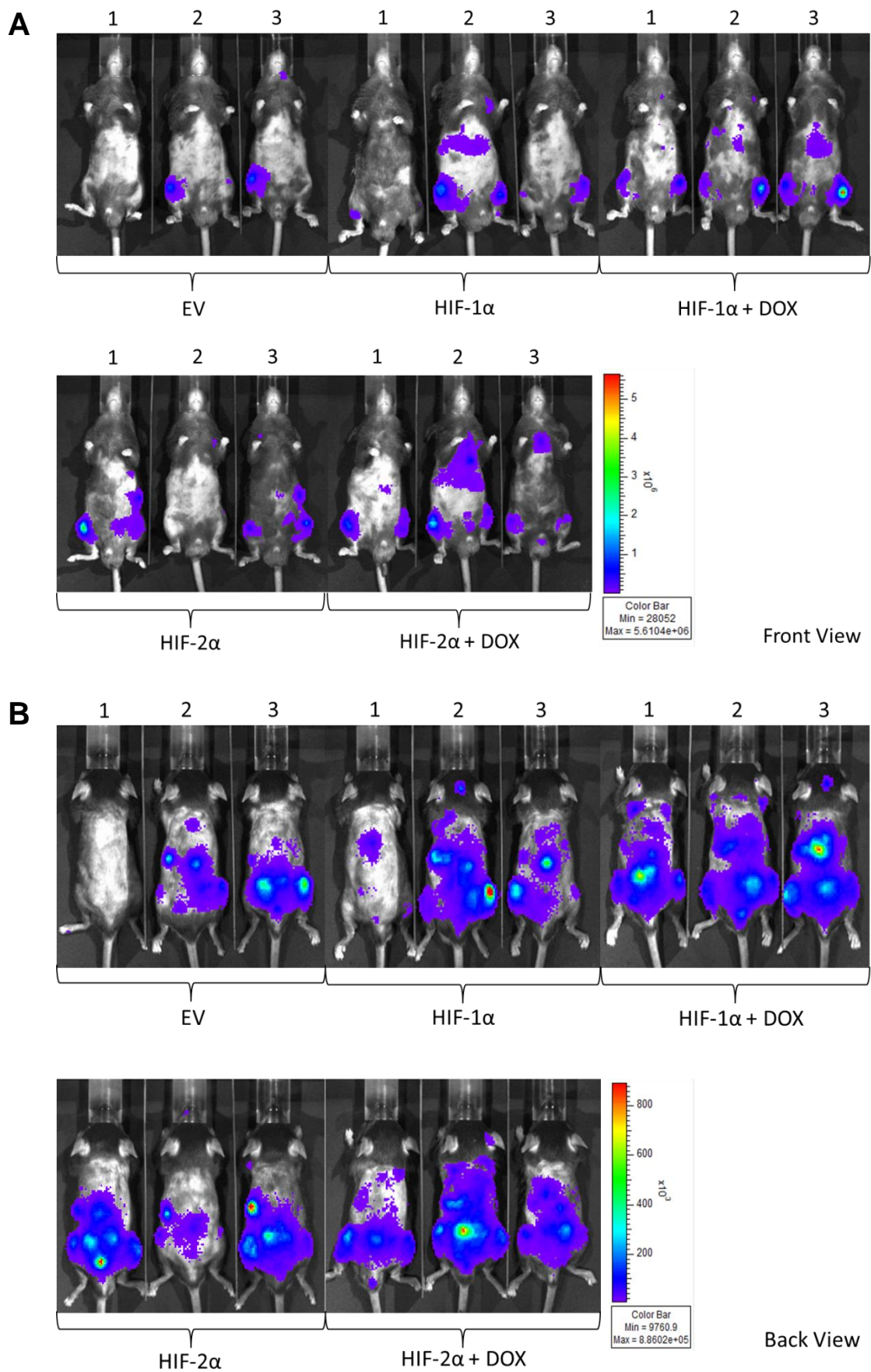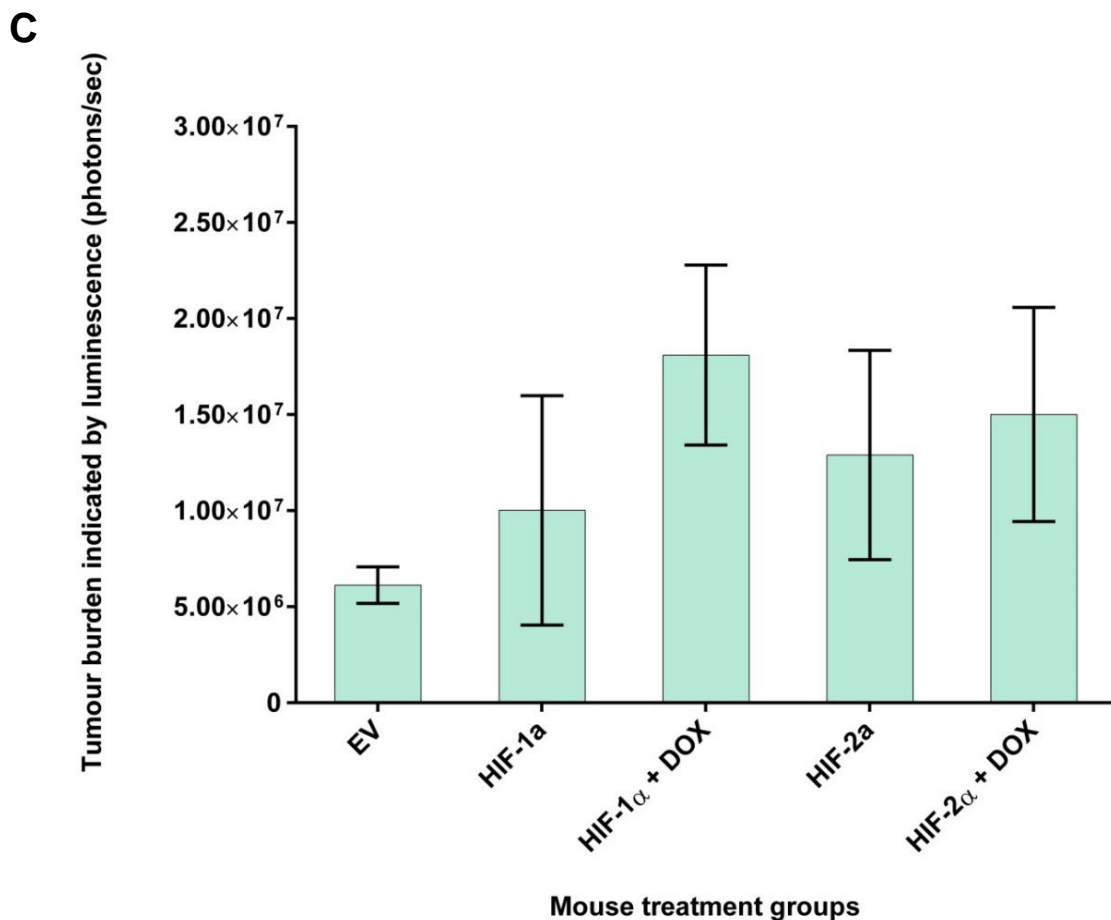
Figure 3.12: LVTETPT, LVT-HIF-1α-ETPT and LVT-HIF-2α-ETPT cells home to the bone marrow and disseminate in a 4 week multiple myeloma mouse model as shown by *in vivo* bioluminescence. Tail vein injections of 5TGM1 LVTETPT, LVT-HIF-1α-ETPT and LVT-HIF-2α-ETPT stable cell lines were performed on C57Bl/KaLwRij mice in a preliminary MM mouse experiment. Five mouse treatment groups were set up, specifically EV (LVTETPT empty control), HIF-1α (LVT-HIF-1α-ETPT), HIFα plus doxycycline treatment (+ DOX), HIF-2α (LVT-HIF-2α-ETPT) and HIF-2α + DOX. A & B) The mice were analysed through intraperitoneal injection of D-luciferin and imaging using *in vivo* bioluminescence four weeks following tail vein injection. C) The combined luciferase activity in each mouse group was quantified and graphed as a measure of tumour burden between the control and sample groups. Tumour was quantified in photons/second using the IVIS Xenogen™. Data for each mouse group (n=3) shown as mean +/- standard error of the mean, where significance was analysed using one-way ANOVA with Dunnett's post-test.

3.2.5.3   Assessment of 5TGM1 LVTETPT stable cells *in vivo*

The 5TGM1 cell line expresses GFP, allowing for the isolation of the MM cells from mice *ex vivo*. The expression of dTomato from the LVTETPT construct allows for the specific selection of 5TGM1 LVTETPT expressing cells. Given the exciting trend towards elevated levels of tumour burden in LVT-HIFα-ETPT mice (Figure 3.12), the isolation of these cells could be used to examine the doxycycline-dependent upregulation of HIFα proteins and target genes from 5TGM1 LVT-HIFα-ETPT injected mice *ex vivo*.

Following identification of cellular homing to mouse hind legs four weeks post injection, the mice were euthanised and the BM flushed from the femora. The mixed population of flushed BM cells were then treated to lyse red blood cells (RBCs) and FACS used to isolate the dual fluorescent GFP-dTomato expressing 5TGM1 LVTETPT cells. Unexpectedly, FACS analysis revealed that none of the cells displayed detectable dTomato expression. Furthermore, the proportion of BM cells that were expressing detectable GFP was very low, between 0-1.75%, whereas this was typically between 20-40% in other similar experiments using 5TGM1 cells (A, Zannettino, personal communication). Due to this very low proportion of fluorescent cells, the 5TGM1 cells were not able to be effectively isolated and analysed by FACS. Instead, mRNA was extracted from the total population of BM cells for each mouse sample and GFP, *Hif1α* and *Hif2α* levels quantified by qPCR (Figure 3.13). These data confirmed the low levels of GFP expressed in the femoral BM population of all of the mice when compared to a 5TGM1 GFP-expressing positive cell line grown *in vitro*. Consistent with these data, no HIFα induction was detected in mouse groups that were fed doxycycline compared to those that were not (data not shown).
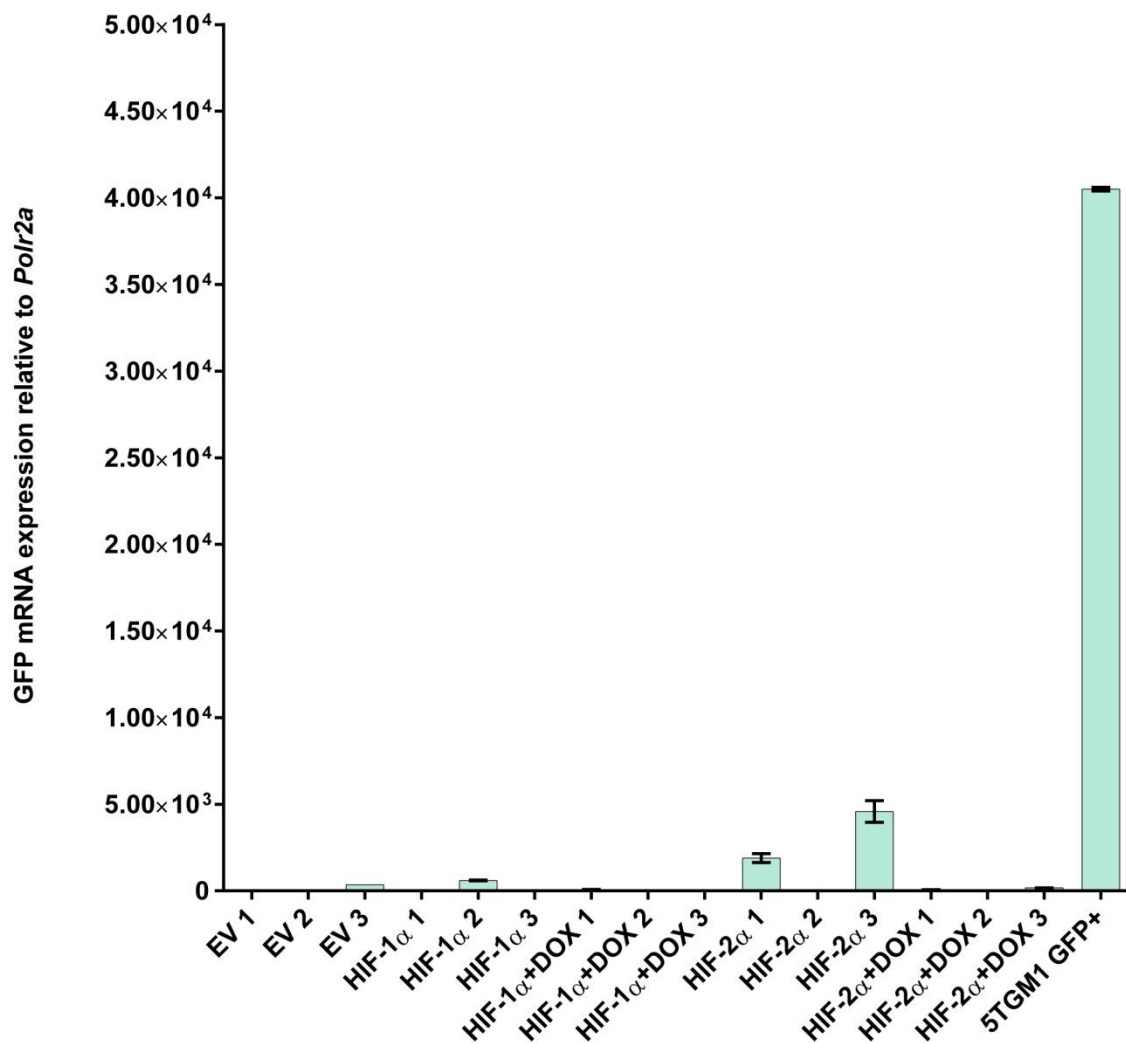
Figure 3.13: Quantification of GFP mRNA expression in BM cell lysates isolated
***ex vivo* from individual mice.** 5TGM1 cells were isolated from the femoral BM of each
mouse 4 weeks following injection of the tumour cells. Following red blood cell lysis,
mRNA was extracted and used to make cDNA for qPCR analysis of GFP expression
levels in each mouse. Relative GFP expression was assessed by normalising to the
housekeeping gene *Polr2a*. GFP expression levels of a pure population of 5TGM1 cells
is included as a control. Data are mean values +/- standard error of the mean for
triplicate samples from one independent experiment.

3.2.6 Characterisation and optimisation of 5TGM1 LVTETPT *in vivo* mouse experiments

3.2.6.1   Optimisation of the 5TGM1-LVTETPT/C57BL/KaLwRij animal model

Given the promising trends of HIF-α doxycycline-dependent changes in tumour burden observed in the first *in vivo* experiment with a small number of mice, a second experiment was performed (Figure 3.14). However, due to the immediate availability of only 10 age-matched mice, this experiment was reduced to include the analysis of only one of the LVT-HIFα-ETPT lines with and without doxycycline treatment with 5 mice in each group. As HIF-2α had been less studied than HIF-1α in MM but implicated as a major contributor to MM disease progression (Martin, Diamond et al. 2009), it was chosen as the cell line to assess in this next experiment.

Due to the lack of dTomato expression in BM cells analysed by FACS from the first mouse experiment, it was postulated that HIF-2α overexpression may influence homing to the BM and dissemination, resulting in less tumour and therefore low numbers of 5TGM1 cells and dTomato expression. Therefore, a modified protocol was employed where doxycycline was administered only once MM disease had been established as assessed by *in vivo* bioluminescence.

Ten mice were injected with 5TGM1 LVT-HIF-2α-ETPT cells and *in vivo* bioluminescence used to monitor disease progression weekly. Cellular dissemination and homing to the marrow was observed at three weeks post-injection by bioluminescence. At this time point, 5 mice were fed doxycycline-supplemented food and water from the third week for the remainder of the study. Four weeks post-injection, quantitative bioluminescence showed there was no significant change in tumour burden between the no doxycycline and doxycycline treated groups as determined by paired student t-test (Figure 3.14 B). The trend towards an increase in tumour burden with doxycycline treatment observed in Figure 3.11 was not seen in this experiment.

This may reflect either the use of the modified doxycycline treatment regime, or that the trend observed in the smaller experiment was not reproducible.

A

B
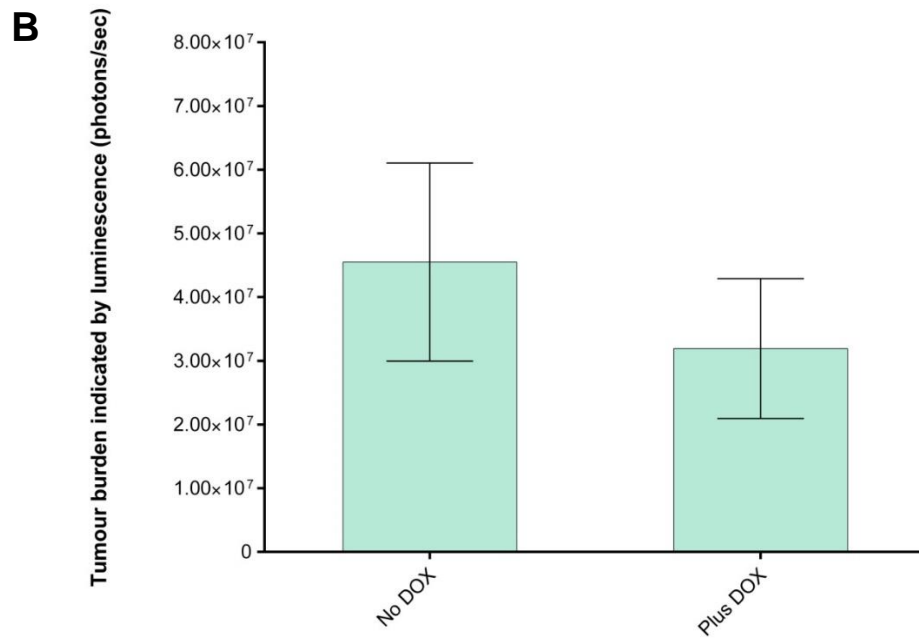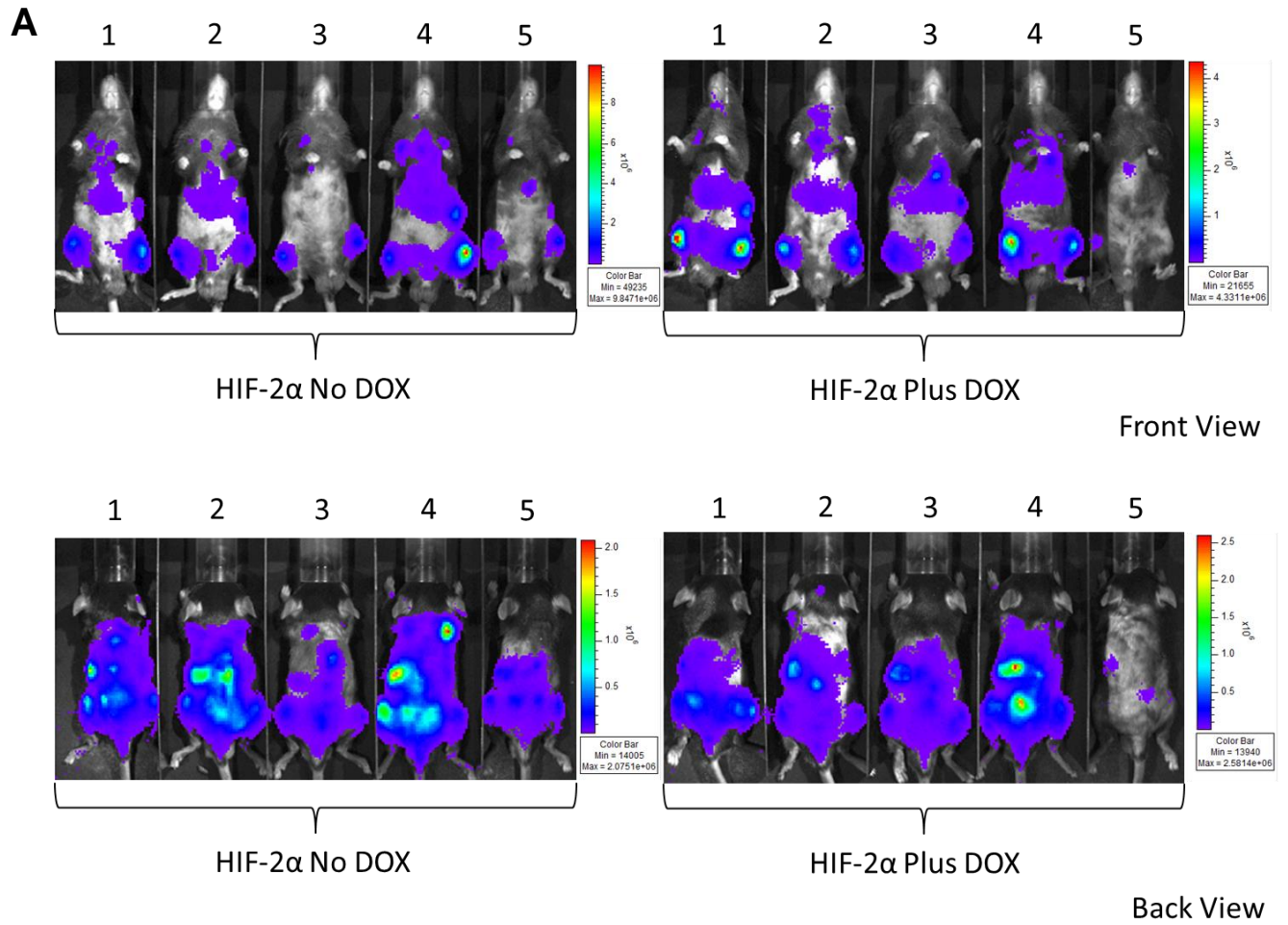
Figure 3.14: Second LVT-HIF-2α-TPT 5TGM1 MM mouse experiment. Ten C57Bl/KaLwRij mice were injected with 5TGM1 stably expressing LVT-HIF-2α-ETPT and divided into two treatment groups, no doxycycline (DOX) or plus DOX. Disease establishment within the BM was confirmed using *in vivo* bioluminescence prior to DOX treatment. A) Tumour burden images using *in vivo* bioluminescence following intraperitoneal injection of D-luciferin in mice four weeks post injection and after one week of DOX treatment. B) The combined luciferase activity in each mouse group was quantified and graphed as a measure of tumour burden between the no DOX and plus DOX groups. Data for each mouse group (n=5) shown as mean +/- standard error of the mean, where significance was analysed using paired student t-test.

To ascertain whether the modified doxycycline treatment protocol had improved the proportion of GFP and dTomato positive cells detected by flow cytometry, the femora of mouse 1 and mouse 4 in both treatment groups were flushed and BM cells analysed, as these showed the highest tumour burden by bioluminescence (Figure 3.14). The proportion of GFP positive cells in all mice, as shown by FACS, was between 2.4 and 20%. However, the relative proportion of GFP cells that were dTomato positive was extremely low, between 0.06 and 0.12%, demonstrating that less than 1% of the GFP positive cells were dTomato positive (Figure 3.15 A). As a result, cells could only be sorted based on GFP expression alone and were subsequently analysed by qPCR. These results showed very low levels of *dTomato* mRNA compared to GFP, which was consistent with the FACS data (Figure 3.15 B). Furthermore, only very low levels of *Hif2α* mRNA could be detected via qPCR in the GFP sorted cells, with no difference between the doxycycline treated or untreated samples, consistent with the very low dTomato expression levels.

The low levels of detectable *dTomato* expression in the FACS isolated 5TGM1 cells, raised concerns that dTomato and HIFα expression were being lost in the LVTETPT 5TGM1 cell lines over time (ie. between thawing cells for injection and the analysis 4 weeks later *ex vivo*). To investigate the stability of the dTomato and HIFα expression in the cell lines *in vitro*, some of the same cells that were thawed and used for mouse injection had been continually cultured and were analysed by flow cytometry 6 and 8 weeks after thawing. After the final sort of these cells before the initial freezing, more than 99% of each line was comprised of GFP and dTomato positive cells. In contrast, after culturing for 6 weeks, between 26 and 50% were double positive and only 15 – 44% after culturing for a further 2 weeks (Table 3.2). This showed that whilst most cells were GFP positive, the proportion of GFP cells that were also expressing dTomato decreased following prolonged growth *in vitro*. This revealed an issue with dTomato stability prior to mouse injection and confirmed the hypothesised instability of the LVTETPT cell lines *in vitro*. Furthermore, these data highlighted the importance of dTomato proportions in the 5TGM1 LVTETPT cell lines post thaw, and the value of a re-sort to maximise dTomato expression prior to animal injection.

A

	GFP (% of total)	GFP + dTomato (% of total)
Mouse 1 no DOX	20	0.06
Mouse 4 no DOX	8.8	0.05
Mouse 1 + DOX	2.4	0.02
Mouse 4 + DOX	8.9	0.12

B
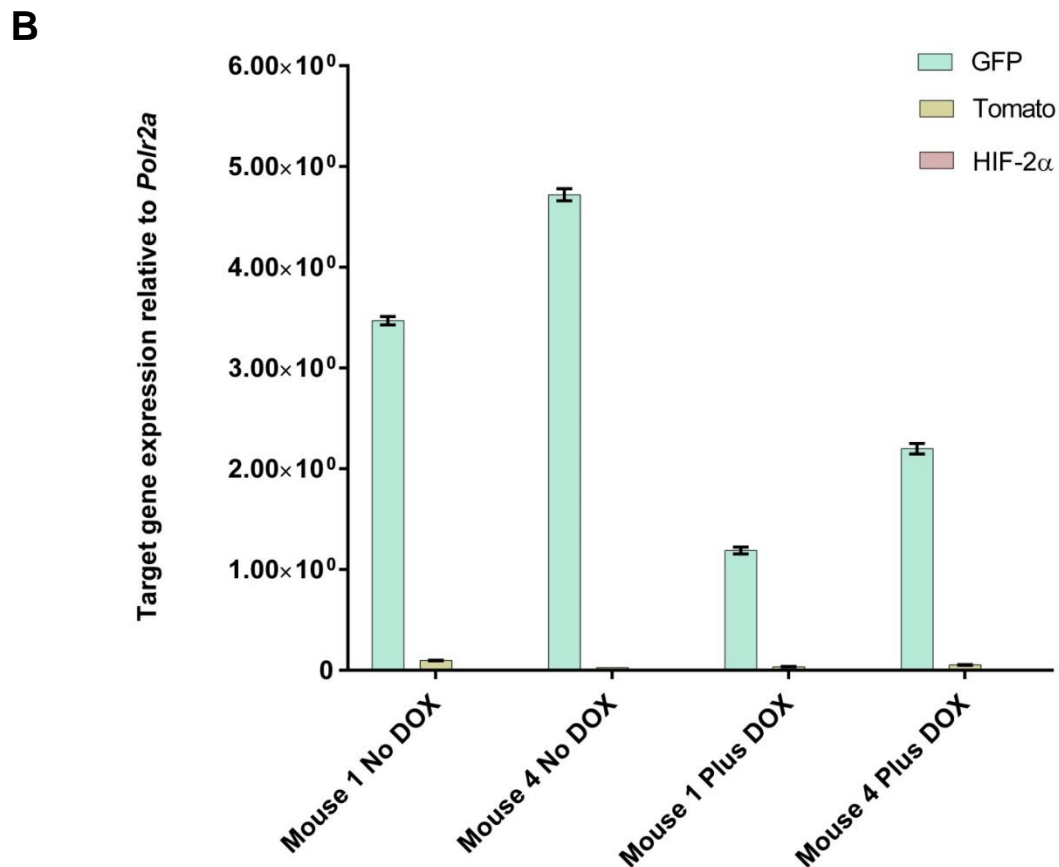
Figure 3.15: Detection of GFP and dTomato from 5TGM1 cells isolated *ex vivo* reveals low dTomato expression. FACS was used to assess GFP and dTomato expression in cells flushed from the BM of mice displaying the highest femoral and tibial tumour burden in Figure 3.14, specifically Mouse 1 and Mouse 4 from both the no DOX and plus DOX mouse groups. A) The percentage of cells expressing GFP and dTomato from the BM population in each mouse was assessed by FACS analysis (shown as a percentage of the total BM population). B) Analysis of *GFP*, *dTomato* and *Hif2α* mRNA by qPCR in GFP sorted mouse samples *ex vivo*. Data are mean values +/- standard error of the mean for triplicate samples.

Table 3.2: Percentage of GFP and dTomato positive cells in cultured LVTETPT 5TGM1 cells lines

	6 Weeks			8 Weeks		
	EV	HIF1	HIF2	EV	HIF1	HIF2
%GFP+dTomato	38.2	26.2	50.2	18.2	15.1	44.2

The 5TGM1 LVTETPT, LVT-HIF-1α-ETPT and LVT-HIF-2αETPT stable cell lines were grown for 6 and 8 weeks *in vitro*, and the proportion of GFP and dTomato positive cells determined using flow cytometry.

3.2.7 Assessment and optimisation of 5TGM1 LVTETPT stability *in vitro* and *in vivo*

3.2.7.1   Characterisation of dTomato stability in 5TGM1 LVTETPT cell lines

To further examine the stability of dTomato in the 5TGM1 LVTETPT cell lines, two independent vials of each of the 5TGM1 LVTETPT, 5TGM1 LVT-HIF-1α-ETPT and 5TGM1 LVT-HIF-2α-ETPT cell lines were thawed and assessed using flow cytometry. Analysis of two frozen stocks after recovery post-thaw (4 days) showed a low proportion (4-18%) of surviving cells expressing dTomato for all three LVTETPT cell lines, with significant differences in absolute percentages between the two independent vials which may have contributed to the low percentage of dTomato cells detected *ex vivo*. (Table 3.3).

Each of the thawed cell lines were sorted for GFP and dTomato expression using FACS to isolate a pure population of dTomato expressing cells (approximately 98%, Table 3.3). The newly sorted cell lines were cultured *in vitro* and flow cytometry used to assess the percentage of dTomato positive cells weekly for four weeks. The purpose of assessing cells over four weeks was to match duration of the *in vivo* MM experiments. All of the cell lines displayed a gradual decrease in the proportion of dTomato positive expression over the course of the 4 weeks, with the LVT-HIF-1α-ETPT showing the greatest decrease (Table 3.4). Specifically, the majority of the LVTETPT and LVT-HIF-2α-ETPT stable cells remained dTomato positive, but less than half of the LVT-HIF-1α-ETPT cells were positive for dTomato after 4 weeks. These data confirmed an inherent instability in dTomato expression in cells when cultured in vitro, and an explanation for the low level of dTomato positive cells isolated *ex vivo*.

While these data showed the expression of dTomato in these cells was unstable, the loss of dTomato expression was gradual and the proportion of dTomato positive 5TGM1 cells following 4 weeks of growth *in vitro* were greater than the approximate 1% seen *ex vivo* (Figure 3.15 A). The low proportion of dTomato positive cells post-thaw identified the requirement for cells to be re-sorted prior to injection into mice. As

such, a third animal experiment was performed to ascertain if the re-sorted cells remain stable enough to sort for GFP and dTomato *ex vivo*, and to compare the proportional loss of dTomato between *in vitro* culturing and the *in vivo* MM mouse model.

Table 3.3: Proportion of 5TGM1 LVTETPT stable cell lines expressing dTomato post thaw using FACS.

dTomato percentages post-thaw

Days Post Thaw	Aliquot 1 dTomato (% of total)			Aliquot 2 dTomato (% of total)		
	EV	HIF1	HIF2	EV	HIF1	HIF2
D4	14.1	15.2	17.8	3.6	4.5	3.6
S0	~98.0	~98.0	~98.0	~98.0	~98.0	~98.0

FACS analysis of two different aliquots of newly thawed LVTETPT, LVT-HIF-1α-ETPT and LVT-HIF-2α-ETPT cell lines in two different frozen aliquots of each stable cell line 4 days post thaw. Cells were then re-sorted using FACS to obtain a pure population of dTomato positive cells (S0).

Table 3.4: Proportion of 5TGM1 LVTETPT stable cell lines expressing dTomato post sort using FACS.

dTomato percentages post-sort

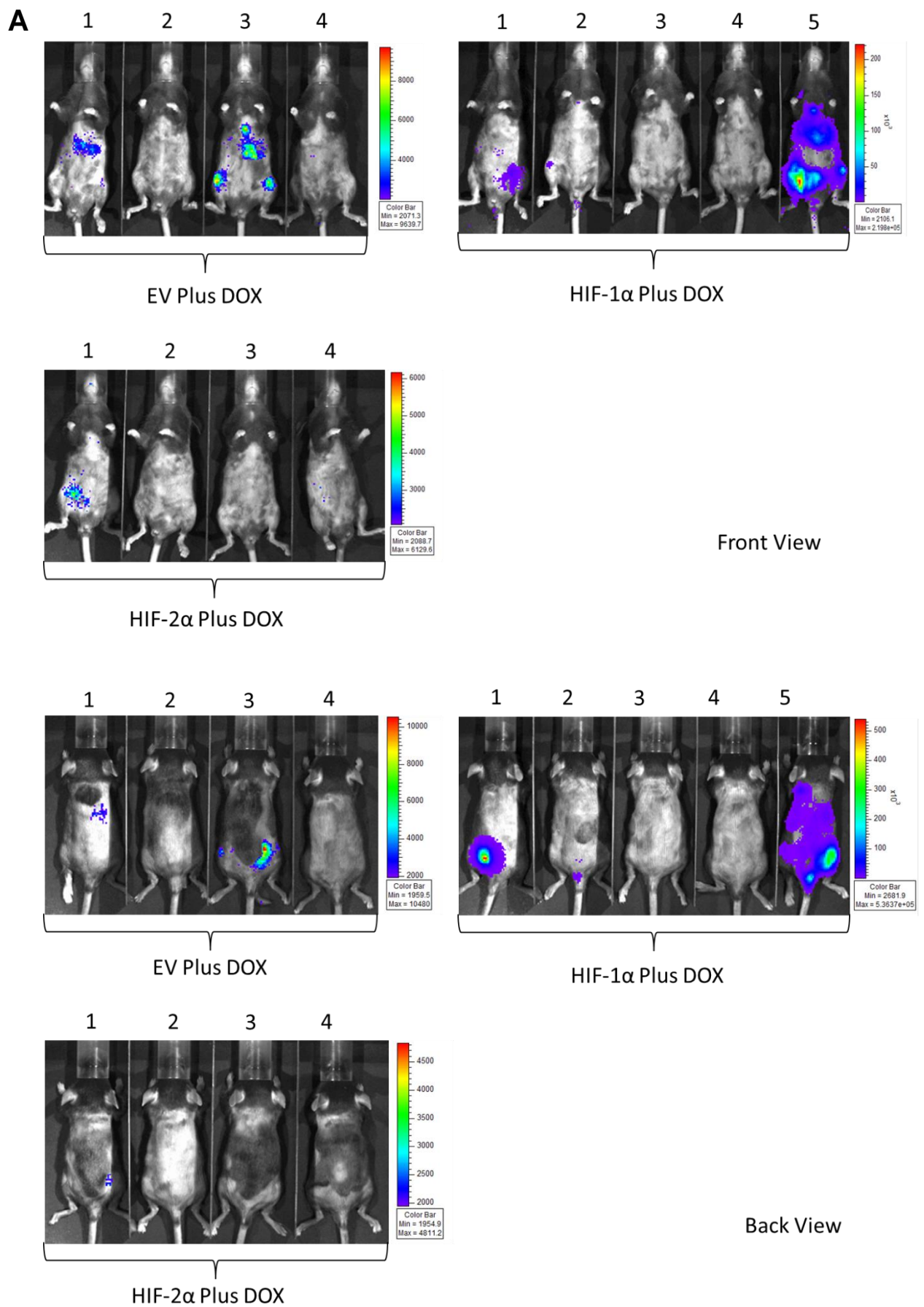| Days Post Sort	Aliquot 1 dTomato (% of total)			Aliquot 2 dTomato (% of total)		
	EV	HIF1	HIF2	EV	HIF1	HIF2
S7	94.1	79.0	90.3	89.2	84.1	93.5
S14	88.4	53.0	88.6	83.7	68.3	85.0
S21	91.9	34.0	89.0	80.6	56.8	85.4
S28	92.5	18.3	68.2	88.8	49.3	84.9

Assessment of dTomato stability in the newly sorted cell lines was assessed every week for 4 weeks using Flow Cytometry.

3.2.7.2   Investigating the stability of 5TGM1 LVTETPT cells *in vivo*

The third animal experiment was performed using cell lines that had been thawed and then sorted by FACS 3 days prior to injection to ensure the highest proportion of dTomato positive cells. Mice were injected with LVTETPT empty vector control (4 mice), LVT-HIF-1α-ETPT (5 mice) and LVT-HIF-2α-ETPT (4 mice) cell lines and fed doxycycline 3 weeks post injection. Surprisingly, *in vivo* bioluminescence showed significantly lower levels of tumour burden than previously observed at four weeks post injection, including for the LVTETPT control line (data not shown). Consequently, the study was extended to five weeks to allow disease to develop to levels more comparable to the 4-week end point of the previous experiments (Figure 3.16).

After 5 weeks the BM cells were flushed for analysis. Given that the exact location of tumour within the hind legs was hard to discern, both the femora and tibiae of mice with the most detectable tumour were flushed. Five samples were taken in total and analysed for GFP and dTomato expression, specifically two from the empty vector control (mouse 3), two from the HIF-1α inducible mouse group (mouse 1 and mouse 5) and one from the HIF-2α inducible mouse group (mouse 1) (Figure 3.16 A). Out of the five BM samples, only one had detectable GFP fluorescence by microscopy and FACS, the sample from mouse 5 from the HIF-1α inducible group. FACS showed that 6.7% of cells within this sample were GFP positive (Figure 3.16 B), which was slightly higher than the 0.02 - 0.12% observed that seen in the previous animal experiment (Figure 3.15 A). None of the samples had any detectable dTomato expression, demonstrating that re-purifying the cells immediately prior to injection did not improve the percentage of GFP and dTomato expressing cells in mouse tumour sites after the development of MM.

The continued low proportion dTomato expressing 5TGM1 LVTETPT cells, both *in vitro* and *in vivo*, identified a fundamental issue with the stability of expression over time with the LVTETPT cell system. Therefore, a new expression system was required to assess the comparative roles of HIF-1α and HIF-2α in MM.

A

B

Bone marrow cells from HIF1 Mouse 5 *ex vivo* (20x magnification)

Bright Field   FITC   Merged

C

HIF1 Mouse 5_Right Leg (G1: Cells)

Tomato GFP+
% Hist: 6.71
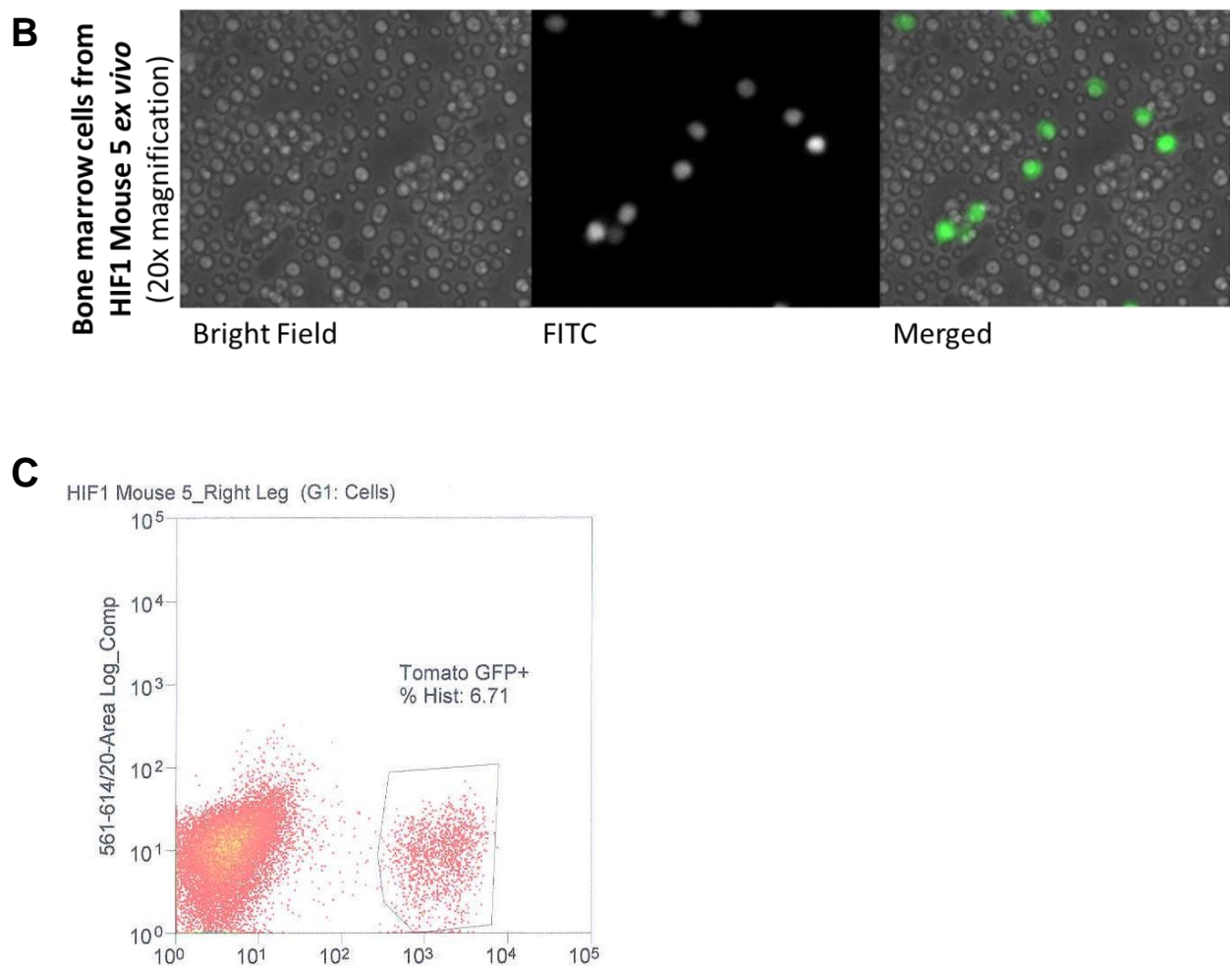
Figure 3.16: Third mouse experiment incorporating optimised conditions from *in vitro* (FACS) experiments on dTomato stabilisation. C57Bl/KaLwRij mice were injected with 5TGM1 cells stably expressing LVTETPT, LVT-HIF-1α-ETPT and LVT-HIF-2α-ETPT inducible constructs that were re-sorted using FACS 3 days prior to tail vein injection. Mice were fed doxycycline 3 weeks post injection and disease establishment shown at 5 weeks. A) Tumour burden images using *in vivo* bioluminescence following intraperitoneal injection of D-luciferin in mice five weeks post stable cell injection. B) Microscopic analysis of cells *ex vivo* assessing GFP expression compared to bright field images in a mixed cell sample isolated from the BM of HIF-1α Mouse 5. Images were taken at 20x magnification with exposures of 1ms for bright field view and 1000ms for FITC (GFP wavelength) view. C) FACS analysis was performed on the BM extract and showing the percentage of GFP positive cells within the population.

3.3 Discussion

The 5TGM1/C57BL/KaLwRij MM animal model was chosen to assess the roles of HIF-1α and HIF-2α on MM disease progression *in vivo*. 5TGM1 cells were shown to induce a typical hypoxia-dependent expression of genes (Figure 3.1), where specifically, the induction in *Hif2α* mRNA but not *Hif1α* mRNA observed in hypoxia, was consistent with studies using human multiple myeloma and neuroblastoma cells (Martin 2008, Lin, Cong et al. 2011).

A modified TRE3G-PGK-TetOn3G-Puromycin (LVTPTP) 'all-in-one' vector was chosen to create the 5TGM1 stable cell lines that inducibly over-express HIF1-α and HIF-2α, thereby generating a tool for analysing the direct consequence of HIF-1α and HIF-2α modification *in vivo*. This LVTPTP vector had been used previously with great success to create stable lines using a number of different mammalian cell lines (Zhang, Wang et al. 2007, Bersten, Sullivan et al. 2015). An induction of both HIF-1α and HIF-2α protein following doxycycline treatment of the transiently transfected plasmid was observed in the new LVT-HIFα-PTP system, confirming that the HIFα genes subcloned from the TRE3G-HIFα vector were functional (Figure 3.3). Whilst the expression levels of doxycycline-induced HIF-2α protein were similar to the constitutively expressed control (LV410-HIF-2α), low levels of HIF-2α protein were observed in LVT-HIF-2α-PTP transfected cells without doxycycline. Research by David Bersten and others have documented protein expression from the TRE3G system in the absence of doxycycline treatment in cells that have been transiently transfected with the vector (Bersten, Sullivan et al. 2015). Importantly, this background expression was not observed in stable cells lines generated using the same vectors. As such, it would be expected that less HIF-2α protein would be detected in the LVT-HIF-2α-PTP stable 5TGM1 cells without doxycycline treatment. Comparatively, there was no 'leaky' expression of HIF-1α protein from HEK293T cells transiently transfected with LVT-HIF-1α-PTP vector in the absence of doxycycline treatment. This may be attributed to a more efficient turnover of HIF-1α through post-translational regulation, which is consistent with the mRNA data (Figure 3.1) and previous studies (Martin 2008, Lin, Cong et al. 2011).

The generation of LVTPTP-expressing 5TGM1 stable cell lines was performed using the LVT-HIFα-PTP vectors alongside a LVT-dsRed-PTP control. *In vitro* analyses identified unstable dsRed expression from cells virally infected with the LVT-dsRed-PTP vector and treated with puromycin. Furthermore, poor cellular survival under puromycin selection was observed in LVT-HIFα-PTP and LVT-dsRed-PTP infected 5TGM1 cells, therefore stable cell lines could not be generated. Whilst it was possible to replace the puromycin resistance gene with a different antibiotic resistance gene, an alternate strategy using fluorescent selection to rapidly and efficiently sort cells using FACS was chosen based on the previously successful use of this strategy on MM cell lines, including 5TGM1 cells (Noll, Hewett et al. 2014, Cheong, Chow et al. 2015). Importantly, FACS does not adversely affect cellular viability *in vitro* or in the *in vivo* animal model system. Taking into account these data, the new LVTETPT vector was made with a dTomato fluorophore for stable cell line selection (Figure 3.5).

Functional analyses of the LVT-HIF-1α-ETPT vector showed the expected doxycycline-dependent upregulation of HIF-2α protein in transfected HEK293T cells, however, no inducible HIF-1α protein was detected in normoxia compared to a constitutively expressing positive control (Figure 3.7). This was likely due to the rapid degradation of HIF-1α protein via hydroxylation as previously discussed, resulting in levels of protein that were not easily detectable by western blot. This had been observed previously and hypoxia treatment successfully used to stabilise overexpressed HIF-1α protein (V. Bhakti, personal communication). Consistent with these data, the combined hypoxia and doxycycline treatment on LVT-HIF-1α-ETPT transfected cells produced detectable levels of HIF-1α protein above that observed in the hypoxia control samples, demonstrating that HIF-1α was inducibly overexpressed from the LVT-HIF-1α-ETPT vector (Figure 3.8).

Lentivirus was made from the LVTETPT, LVT- HIF-1α-ETPT and LVT- HIF-2α-ETPT vectors and subsequently used to make 5TGM1 stable cell lines using FACS with transduction rates of 6.0%, 7.5% and 3.7% (Figure 3.9). This was lower than the 20.4% previously observed in Table 3.1. The composition of a plasmid, and each individual

lentivirus preparation can alter transduction efficiency. Given the maximal volume of lentivirus was used, there were enough cells transduced to sort for LVTETPT expressing cells, and these transduction efficiencies fell between the range of 1 – 30% at which integration of multiple transgene copies are minimised (White, Renda et al. 1999, Sastry, Johnson et al. 2002), this discrepancy was not explored further.

Inducible expression of both *Hif1α* and *Hif2α* mRNA was confirmed in the 5TGM1 LVT-HIF-1α-ETPT and LVT-HIF-2α-ETPT sorted cell lines following treatment with either doxycycline alone, or a combination of doxycycline and hypoxia (Figure 3.10). This demonstrated that the combined hypoxia and doxycycline treatment was not required to induce *Hif1α* mRNA expression, despite being necessary for HIF-1α protein detection (Figure 3.8), as overexpressed mRNA would be unaffected by post-translational regulation. Also noted in Figure 3.10, basal levels of *Hif1α* mRNA, but not *Hif2α* mRNA, were detected in the empty vector cell line. This was consistent with the requirement for 48 hours of hypoxic treatment to observe a maximal induction of *Hif2α* mRNA in earlier experiments (Figure 3.1). Furthermore, the lack of detectable *Hif2α* mRNA observed in the empty vector cell line treated in hypoxia (Figure 3.10) was not unexpected, given the detection of some *Hif2α* mRNA at 16 hours of hypoxic treatment in Figure 3.1 was not reproducibly observed across all replicates (Appendix 1).

Attempts to confirm the doxycycline inducible expression of HIF-1α and HIF-2α protein failed from 5TGM1 LVT-HIF-1α-ETPT and LVT-HIF-2α-ETPT cells respectively, with neither endogenous nor overexpressed HIFα being detected by western blot. A lack of detectable endogenous murine HIFα protein expression by western blot has been observed previously for the 5TGM1 cell line, despite being able to detect protein in human MM cell lines such as LP-1 cells (Martin, Dewar et al. 2006). Given the low transduction efficiencies (approximately 3 - 8%) made it likely that the 5TGM1 stable cells contained single integrants of the transgenes, the lack of detectable protein from the stable cells compared to the transiently transfected cells (Figure 3.7) could have been due to hundreds of copies of the LVT-HIFα-ETPT plasmid producing higher detectable levels of protein. Despite this, both HIF-1α and HIF-2α were doxycycline

inducible from the LVTETPT vector by both transient transfection in HEK293T cells (protein expression) and in 5TGM1 LVTETPT cells at the mRNA level. As such, the LVT-HIF-1α-ETPT and LVT-HIF-2α-ETPT 5TGM1 cell lines were subsequently used in *in vivo* experiments to ascertain the importance of the HIFs in MM disease.

Preliminary experiments identified tumour burden in 13 of the 15 mice using *in vivo* bioluminescence to measure luciferase activity (Figure 3.12). Femoral BM cells isolated *ex vivo* showed very low levels of GFP (0-1.75%) and no detectable dTomato expression by flow cytometry and qPCR (Figure 3.13). These poor GFP expression levels did not reflect the detected luciferase activity that clearly demonstrated good expression of luciferase from the same triple modality gene. Furthermore, *in vitro* analyses of GFP from the LVT-HIFα-ETPT stable cell lines using microscopy and FACS prior to animal injection did not show any obvious decrease compared to the original cell line. These observations made it unlikely that expression from the GFP gene was adversely affected by selection or experimental conditions. Conversely, the dTomato gene is controlled by a different promoter to GFP, and would be integrated at a different genomic site to the triple-modality reporter gene, which may have contributed to the complete lack of detectable dTomato expression observed compared to GFP. Human error during the dissection and flushing techniques combined with the low resolution and level of tissue penetration obtained when analysing tumour burden using the IVIS Xenogen™, could have adversely affected the efficient isolation of 5TGM1 cells from the bone marrow and thus contributed to the low detectable levels of GFP.

In the second mouse experiment, a number of changes to the experimental protocol were made to improve the establishment and detection of tumour burden. Firstly, the 5TGM1 LVT-HIF-2α-ETPT cells were monitored for homing to the BM and detectable tumour established prior to the addition of doxycycline treatment. This was done to ensure that the induction of the HIF-2α prior to BM establishment did not adversely affect tumour burden. Secondly, both the femora and tibiae were flushed for BM

isolation given the insufficient resolution of the IVIS Xenogen™ to determine if tumour was located in the distal femur or the proximal tibia.

A large improvement in the proportion of GFP positive cells detected by FACS of 2 - 20% was observed, a result more comparable to the expected range of 20-40%, suggesting that the optimised protocol improved isolation of the 5TGM1 cells from the BM (Figure 3.15). However, this did not resolve the very low proportion of dTomato positive cells (0.02 – 0.12%) as measured by flow and qPCR. Despite efforts to maximise the proportion of dTomato positive cells prior to injection of the mice, no dTomato was detectable by FACS in cells isolated *ex vivo* from a third animal experiment (Figure 3.16). From these data, it is possible that there is an issue with survival of 5TGM1 cells containing the dTomato transgene *in vivo*, although this is not obvious with the cells grown in culture, or alternatively there is an issue with the continuous expression of dTomato stability in these stable lines. In conclusion, these data showed there was a fundamental issue with the stability of dTomato expression and as such, the LVTETPT system was not suitable as a tool for HIFα manipulation in the 5TGM1/C57BL/KaLwRij MM mouse model, and a new system would need to be employed for future experimentation.

The work performed within this chapter identified that there were fundamental issues with transgene expression from the 5TGM1 LVTETPT system, even before the cells were injected into mice. It is known that transgene silencing can occur following retroviral and lentiviral infection (Ellis and Yao 2005). Epigenetic modifications such as methylation have been identified as contributors to transgene instability, particularly when the loss of expression is high and immediate as is seen in stem cells and following cellular differentiation (Niwa, Yokota et al. 1983, Ellis 2005). Although these severe transgenic instabilities were identified in primary cells, they can still occur in stable cell lines made using retroviral or lentiviral techniques, just at lower frequencies. Interestingly, transgene expression can not only be lost immediately, but also temporally, or within a particular subset in a cellular population (Niwa, Yokota et al. 1983, Laker, Meyer et al. 1998, Vroemen, Weidner et al. 2005). Further

characterisation found that silencing of virally integrated genes can be complete, variegated or gradually lost over long-term growth in some instances (Yao, Sukonnik et al. 2004). Although epigenetic changes play a critical role, addressing these modifications does not completely alleviate these issues, further emphasising the complexity of transgene silencing in retroviral and lentiviral stable cell lines (Swindle and Klug 2002, Iba, Mizutani et al. 2003).

Undesirable integration sites have been shown to result in genetic instability and shutdown or deletion of the inserted gene, leading to heterogeneous expression (Bersten, Sullivan et al. 2015). Specifically, it has been found that transgenes located near DNA repeats such as centromeric satellite DNA or flanking methylation sites, results in silencing of transgene expression through restricted transcriptional activation as mentioned above (Talarico, Peverali et al. 1988, Dobie, Lee et al. 1996, Zhou, Zhang et al. 2014). Studies integrating genes into a single, specific locus have been successful in creating long-term stable integrants, for example the use of the Col1A1 locus in transgenic mouse experiments (Hochedlinger, Yamada et al. 2005, Beard, Hochedlinger et al. 2006, Wernig, Lengner et al. 2008, Carey, Markoulaki et al. 2010, Bersten, Sullivan et al. 2015).

Given the high degree of complexity driving transgene instability, a more targeted approach was required. Experimental silencing of endogenous gene expression is often more informative on the molecular, cellular and pathophysiological roles that gene plays as it overcomes the artefactual effects that can arise from genetic overexpression. The recently developed CRISPR technology takes into account the advantages of site-specific genetic modification, in combination with gene silencing through the targeted knock-out of genes using quick and efficient methods (Ran, Hsu et al. 2013). This strategy would also remove the need for lentiviral integration or doxycycline treatment that both place selective stress on cells. This technology however is not without its limitations. Primer design as well as screening of clones that successfully have HIFα knocked out in all alleles can be complicated, but are routinely used with considerable success. One alternative would be to knock-down HIFα using

RNA interference (RNAi), however in the case of 5TGM1 cells this would require lentiviral integration which reintroduces the potential for stability issues like those reported in this chapter. Additionally, the low success rate of obtaining clones with complete HIFα knock-down makes this process less efficient compared to the reported highly efficient knockout achieved using CRISPR technology (Housden and Perrimon 2016).

Complete loss of HIF-1α and HIF-2α gene expression will directly address the involvement and role of each of the HIFs in tumour progression *in vivo,* without the complexity of variable HIFα expression observed using overexpression or knock-down techniques. In conclusion, the rapid and complete knockout of HIFα within the cell's genome makes CRISPR an attractive tool in subsequent experiments to create stable cells lines for use in the 5TGM1/C57BL/KaLwRij animal model to identify the roles of HIF-1α compared to HIF-2α in MM.

Chapter 4
THE EFFECT OF CRISPR-CAS9-MEDIATED DELETION OF HIFα IN 5TGM1 CELLS ON MYELOMA DISEASE DEVELOPMENT IN VIVO

4.1 Introduction

The use of the 5TGM1 LVTETPT cells in the previous chapter identified an issue with dTomato expression both *in vitro* and *in vivo*, thereby preventing selection and stable transgene expression of HIFα. A new strategy was required to reliably modify HIFα expression in 5TGM1 cells for subsequent use in the 5TGM1/C57BL/KaLwRij MM mouse model, and to ultimately assess their roles in disease progression *in vivo*, with targeted gene disruption chosen. While this approach does not enable inducible and reversible modification of HIFα expression in 5TGM1 cells, this strategy will enable the role of HIFα in myeloma disease establishment and progression to be assessed.

Since its discovery, CRISPR-Cas9 technology has fast replaced other methods of genetic engineering owing to its simplicity and efficiency. The Cas9 endonuclease cleaves DNA at a specific site determined by a single guided RNA (sgRNA), resulting in a doubled stranded break (DSB) (Jinek, East et al. 2013, Mali, Yang et al. 2013, Ran, Hsu et al. 2013). Importantly, this gene editing approach is highly customisable through the use of a 20-nucleotide guide sequence within the sgRNA that directs Cas9 activity through base-pair recognition (Jinek, Chylinski et al. 2012). In its simplest form, the repair of the DSB by non-homologous end joining very frequently leads to small insertions or deletions of nucleotides, resulting in frame shifts or the introduction of nonsense mutations in the coding regions of the gene of interest. This method of generating gene knockouts using sgRNA-directed DSBs, is simpler than other targeted DNA cleavage techniques such as zinc finger nucleases (ZFNs) and Transcription Activator-Like Effector Nucleases (TALENs) that require new protein design, synthesis and validation for every DNA target (Kim, Cha et al. 1996, Christian, Cermak et al. 2010). Moreover, this method is more efficient than more traditional methods of gene editing that rely on homologous recombination.

An alternative to targeted gene deletion is to knock down expression using RNAi-based methods. RNAi has been widely used to knockdown gene expression through post transcriptional pathways, however, this technique does not result in the complete loss

of expression of the gene of interest. The cellular post transcriptional pathways employed to knockdown gene expression, such as Dicer and Argonaute, are also used by eukaryotic cells for endogenous gene silencing (Doudna and Charpentier 2014). The CRISPR-Cas9 system is used as part of a bacterial immune response, thus removing any endogenous competition that could generate complex side effects in mammalian cells. When compared to CRISPR-Cas9, RNAi is inefficient and often results in partial knockdown of gene expression (Shalem, Sanjana et al. 2014, Housden and Perrimon 2016).

The comparatively simple, effective and efficient CRISPR-Cas9 system was chosen as the best available method to knockout *Hifα* gene expression in 5TGM1 cells. The knock out lines could then be used in the 5TGM1/C57BL/KaLwRij animal model to determine the specific roles of the HIFα transcription factors in myeloma disease establishment and progression.

4.2 Results

4.2.1 Cloning and screening of HIFα CRISPR knockout 5TGM1 cell lines

Murine *Hif1α* and *Hif2α* genes were targeted for cleavage by a Cas9 endonuclease using tailored sgRNAs. This knockout strategy employed pairs of sgRNAs targeting intron regions either side of a key exon. The simultaneous cleavage of the introns either side of the exon should result in its deletion as the two introns are joined in the process of repair (Figure 4.1) (Cong, Ran et al. 2013, Mali, Yang et al. 2013). Given that successful clones will result in the loss of an entire exon, this experimental design allowed for efficient characterisation of successful knockout clones by PCR using screening primers adjacent to the sgRNA sites (Figure 4.1 A) (Canver, Bauer et al. 2014). This was advantageous over the use of a single guide RNA that produces small insertion/deletion mutations (indels) that require more rigorous sequencing approaches to detect and characterise successful knockouts (Ran, Hsu et al. 2013).

Exon 2 was specifically selected for deletion in both HIFα genes, as it encodes the N-terminal bHLH domain critical for DNA binding and dimerisation. Furthermore, the length of exon 2 for both HIF-1α and HIF-2α is 191 bp, so removal of the entire exon will result in both a loss of the essential bHLH domain, as well as a frameshift for the remaining coding region of the HIFα protein. The exon removal strategy used sgRNAs designed to function with the *Streptococcus pyogenes* Cas9 (SpCas9) endonuclease. As such, each sgRNA contained a *Hifα*-targeted sequence located directly upstream of the SpCas9-specific protospacer adjacent motif (PAM) sequence, 5'-NGG-3' (Table 4.1) (Jinek, Chylinski et al. 2012). Additionally, as insertion of the guide sequences into the Cas9-expressing pSpCas9 vector was performed using the BbsI restriction enzyme site, the sgRNA design included 5' and 3' complementary overhangs enabling it to be directly cloned into the digested vector (Table 4.1).

Although CRISPR-Cas9 technology is more efficient than other methods of targeted gene disruption, DSBs at undesired locations of the genome can occur, through tolerated mismatches between the sgRNA and target DNA (Cong, Ran et al. 2013, Fu,

Foden et al. 2013). These off-target effects can be minimised through specific sgRNA design. Genomic sequences from *Hif1α* or *Hif2α* were analysed using the Benchling online CRISPR design tool to generate sgRNAs with low mismatches (off-target) and high activity (on-target) scores as specified in Table 4.1 (Hsu, Scott et al. 2013, Ran, Hsu et al. 2013, Doench, Hartenian et al. 2014). These scores were represented numerically from 0-100, where a higher score corresponded to higher activity (on-target) and specificity (off-target) of the sgRNA-guided Cas9. Despite creating sgRNAs predicted to have high activity, some reports suggest that some variability between sgRNAs exists in relation to off-target effects and the genetic knockout produced (Fu, Foden et al. 2013, Jinek, East et al. 2013, Shalem, Sanjana et al. 2014). Therefore, to control for potential off-target effects, two independent sets of sgRNAs (A and B) targeting each *Hifα* gene were designed (Figure 4.1 A).

To generate the HIFα CRISPR knockout cell lines, the sgRNAs were first cloned into the pSpCas9 plasmids as described above and in section 2.1.7. These vectors encode and express the Cas9 endonuclease, the HIFα-targeting sgRNAs, and GFP. The GFP produced from the pSpCas9 vector could not be used to sort transfected cells due to the constitutive expression of GFP in the 5TGM1 cells, requiring the co-transfection of a LV410 plasmid that constitutively expresses dsRed (LV410-dsRed) (Figure 4.1 B). As such, 5TGM1 cells were transiently co-transfected with two sgRNA expressing plasmids, pSpCas9-HIFα-Int1 (either variant A or B) and pSpCas9-HIFα-Int2 (either variant A or B), together with LV410-dsRed (Figure 4.1 B). 48 hours after transient transfection, single cells expressing both GFP and dsRed were sorted into 96 well trays by FACS (Figure 4.1 B). Monoclonal control lines (Cas9 EV and Cas9 EV 2) were similarly created by transiently co-transfecting 5TGM1 cells with the empty pSpCas9 (without sgRNA targeting HIFα) and the LV410-dsRed plasmids, and using FACS, single cells expressing both GFP and dsRed were isolated. The generation of monoclonal cell lines was favoured as it would eliminate confounding results from a pool of heterogeneously modified cells. Following 2-3 weeks of clonal cell expansion *in vitro*, gDNA from each clone was extracted and assessed by PCR for the loss of exon 2.

Note that all of the sgRNA design and cloning , and the generation and screening of 5TGM1 HIFα knockout cell lines was performed by Yinan Ma, a Masters student in the laboratory. However, I created the EV Cas9 control lines independently, and also repeated the entire screening procedure independently with both sets of HIF-1α and HIF-2α sgRNAs.
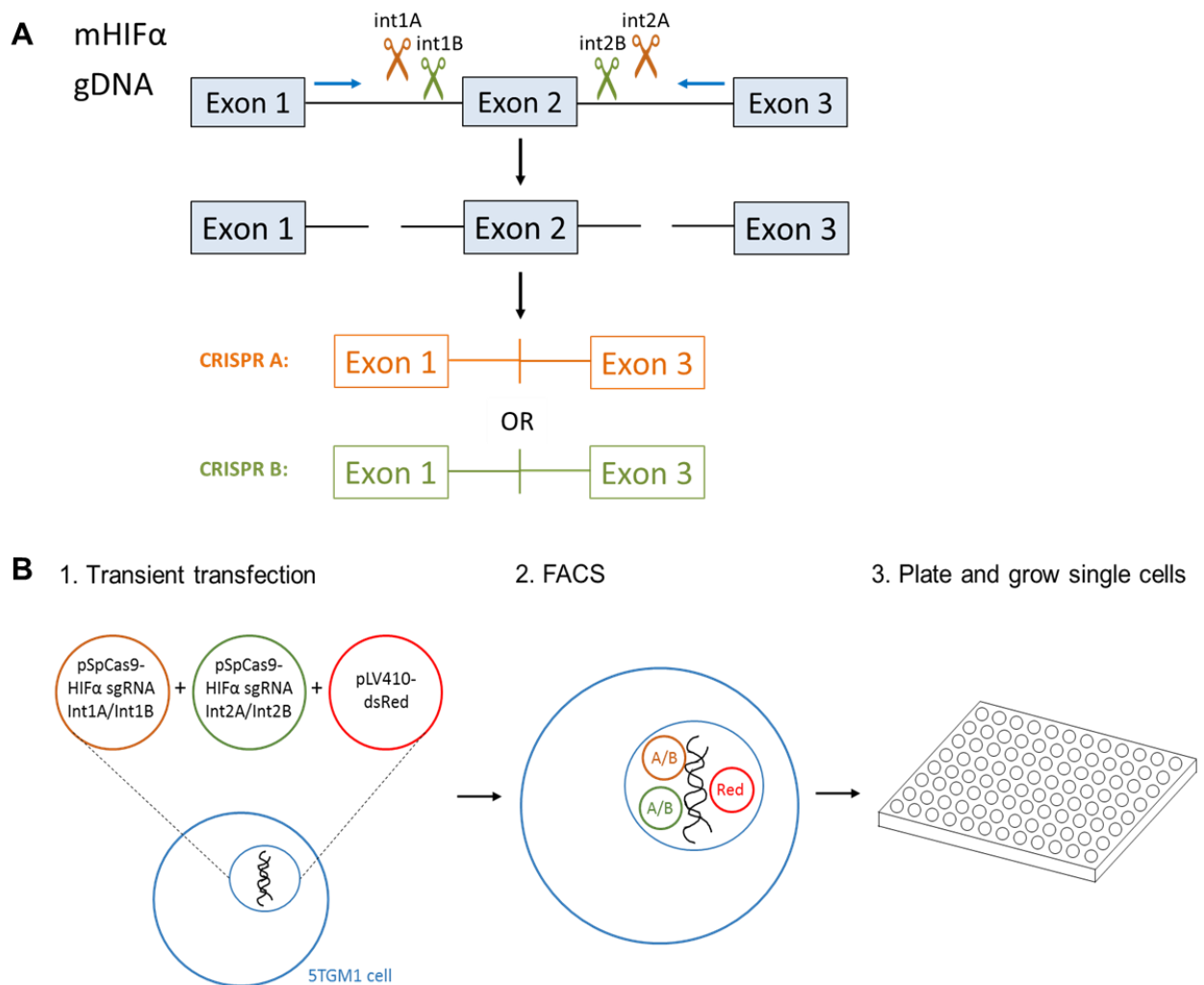
Figure 4.1: CRISPR design strategy to create 5TGM1 HIF-1α and HIF-2α knockout stable cell lines. CRISPR-Cas9 technology was used to generate clonal HIFα knockout 5TGM1 cell lines. A) sgRNA sequences were designed to specifically target sites located within introns (labelled 'int1' and 'int2') either side of exon 2 in *Hif1α* or *Hif2α* (Yinan Ma, University of Adelaide). Two sets of sgRNAs with adjacent targeting sequences were designed (labelled 'A' and 'B') to control for off target effects. Simultaneous activity of both sgRNAs should result in the loss of exon 2, shown as CRISPR A and CRISPR B. PCR primers (blue arrows) flanking the sgRNA targeted sequences were used for screening the loss of exon 2, allowing for the differentiation between wild type and knockout clones. B) Schematic representation of the methodology used to create the monoclonal knockout HIFα 5TGM1 cell lines. Cells were sorted by FACS for constitutive GFP expression of 5TGM1 cells and dsRed from transient transfection.

The aim of these experiments was to generate at least one knockout clone with each primer set (A and B) for *in vivo* experimentation. The expected PCR product sizes for gDNA extracted from successful HIF-1α (A and B) and HIF-2α (A and B) CRISPR clones are listed in Table 4.2. The first experiment by Yinan Ma generated 27 HIF-1α and 15 HIF-2α surviving monoclonal cell lines following FACS analysis, that were subsequently screened for deletion of exon 2 (Figure 4.3).

PCR amplification of the HIF-1α clones (performed by Yinan Ma) failed to identify any heterozygous or knockout cell lines, where all of the gDNA samples amplified a band of approximately 1400 bp corresponding to the wild type allele containing an intact exon 2, with no products corresponding to loss of exon 2 evident (Table 4.2).

The transient transfection and selection experiments were repeated by myself with the following modification; the alternative combinations of sgRNAs designed for targeted knockout of HIF-1α were used with 5TGM1 cells co-transfected with int1A and int2B, or int2A and int1B, to create HIF-1α AB and HIF-1α BA clones. Using this transfection approach, I generated a further 56 clones for HIF-1α monoclonal cell lines and analysed them by PCR for the loss of exon 2 (Table 4.3). Similar to the results obtained in the first experiment, all clones produced PCR products corresponding to the unmodified allele containing exon 2, indicating that all of the clones contained at least one functional allele of HIF-1α, with no HIF-1α knockout lines obtained.

In summary, for HIF-1α, a total of 83 clones were analysed over 2 rounds of transfection, sorting and screening using 4 combinations of sgRNAs to target exon 2, but all clones retained at least one allele containing exon 2, demonstrating that this strategy to knockout HIF-1α was clearly deficient. Given all of the previous issues with generating inducible systems of expression, the relative success in generating HIF-2α knockout cell lines (discussed below), and the greater interest in deciphering the role of HIF-2α in MM, it was decided that analysis of the role of HIF-1α loss in 5TGM1 cells would not be pursued further in the context of this thesis.

PCR analysis of the 15 HIF-2α monoclonal cell lines identified 13 clones representing either wild type or heterozygous genotypes with respect to the presence of exon 2 (Table 4.3). Wild type clones produced a single band of approximately 1830 bp, whilst heterozygous clones showed two bands of approximately 1830 bp and 550 bp for sgRNA pair A, or approximately 1830 bp and 560 bp for sgRNA pair B clones (Table 4.2). Most importantly, 2 clones were identified as potential knockouts via PCR, one from each pair of sgRNAs targeting HIF-2α (A and B). One of these clones, HIF-2α CRISPR B1-1, produced a single band of approximately 560 bp, whereas the second clone, HIF-2α CRISPR A3-7, did not produce any PCR products (Figure 4.2 A).

I repeated the transient transfection and selection experiments to create more monoclonal knockout HIF-2α (A and B) 5TGM1 cell lines. This second round of transfections produced an additional 44 HIF-2α clones that were subsequently analysed by PCR for the loss of exon 2 (Table 4.3). Unfortunately, all of these clones produced PCR products consistent with at least one wild type allele containing an intact exon 2. From these combined experiments, only 2 out of 59 HIF-2 CRISPR 5TGM1 cell lines were knockout lines and further demonstrated a poor knockout efficiency in 5TGM1 cells. As such, the HIF-2α CRISPR B1-1 and HIF-2α CRISPR A3-7 knockout cell lines were used for all subsequent experiments performed.

The 560 bp band corresponding to the predicted loss of exon 2 that was amplified from HIF-2α CRISPR B1-1 gDNA and subcloned into the pGEM-T easy plasmid. A total of 12 pGEM-Teasy clones containing the 560 bp HIF-2α CRISPR B1-1 PCR fragment were randomly selected and analysed by Sanger sequencing (Figure 4.2 B). The sequences from all 12 clones were identical, showing the deletion of a 1.284 kb fragment. This deletion included the region containing exon 2 and adjacent intron sequence from between the sgRNA int1B and int2B target sequences, as well as an additional 10 nucleotides. The loss of additional nucleotides is common in CRISPR-Cas9 mediated cleavage and repair, where cut sites are often associated with the randomised loss or gain of a few nucleotides known as "scars", although large deletions can also occur (Shin and Wang 2017). Given only one band was amplified

from all 12 clones, this was consistent with the second allele containing a larger deletion that prevented amplification by the PCR primers.

Table 4.1: Design of guide sequences targeting murine *Hif1α* and *Hif2α* intron regions to result in the deletion of exon 2 using CRISPR-Cas9 technology.

	Target	Oligo (sense strand)	PAM	On-target	Off-target
Group A	HIF-1α int1	CACCgatccgcaggtgggctagtaa	agg	49.7	92.6
	HIF-1α int2	CACCgtttttaaagagcggcgttat	ggg	38.5	91.2
	HIF-2α int1	CACCgacccgtgttagtacgtgata	tgg	43.2	93.3
	HIF-2α int2	CACCgtggagcgggactctcgccag	agg	62.7	90.1
Group B	HIF-1α int1	CACCggagtcagagtgctgatccgc	agg	53.7	84.8
	HIF-1α int2	CACCgttttttaaagagcggcgtta	tgg	36.7	90.4
	HIF-2α int1	CACCgtccatatcacgtactaacac	ggg	60.1	89.1
	HIF-2α int2	CACCggactctcgccagaggtccag	agg	60.9	76.5

PAM: 5'-NGG-3' specific for SpCas9, CACCg: specific for BbsI ligation into PX458

Table 4.2: Expected product size using PCR to differentiate between wildtype and HIFα knockout clones.

	PCR Product Sizes (bp)		
Primer Target	Wildtype	Knockout A	Knockout B
HIF-1α	1417	305	319
HIF-2α	1831	550	562

A

B
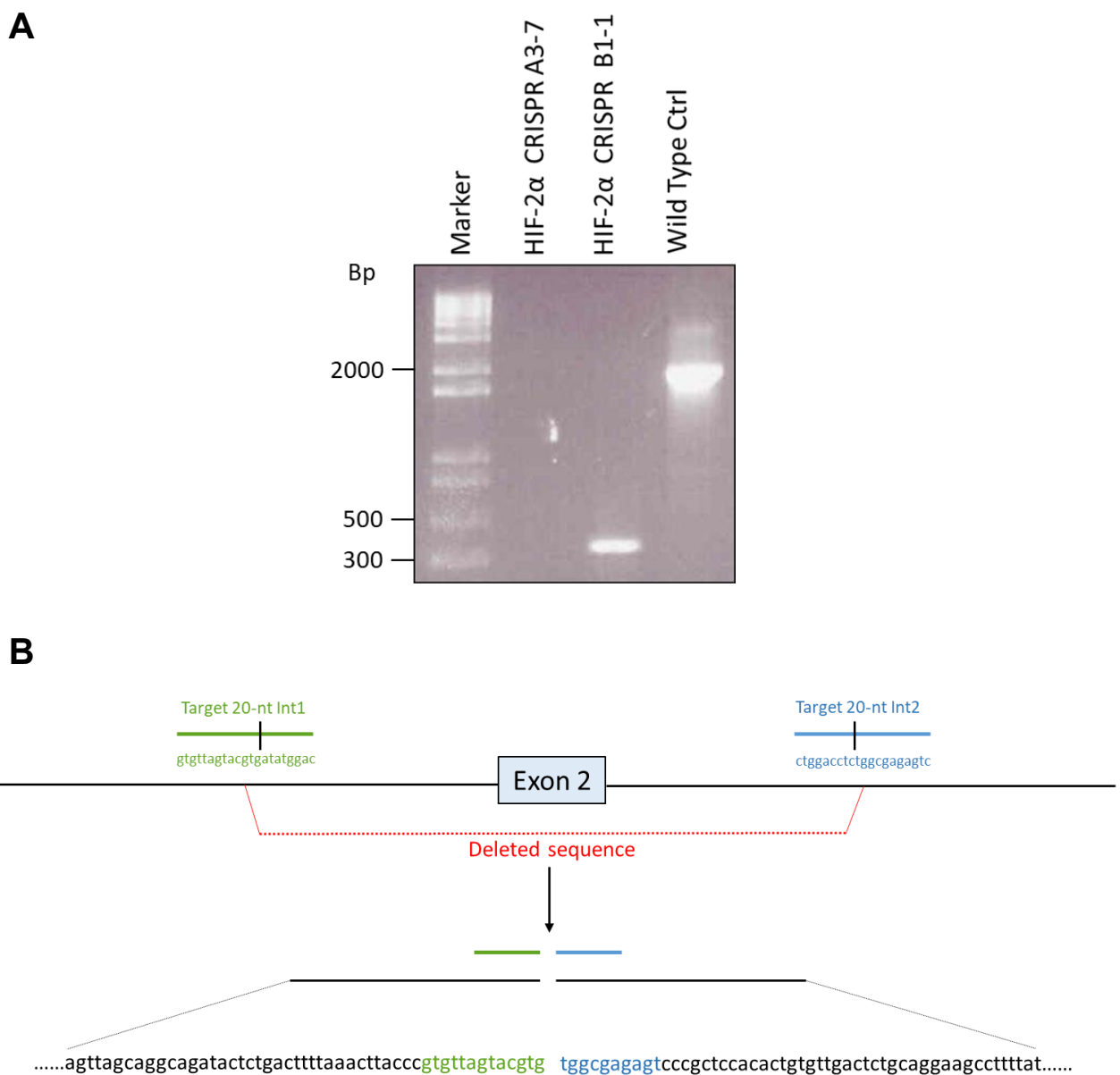
Figure 4.2: Analysis of 5TGM1 HIF-2α knockout cell lines. A) Characterisation of genomic DNA from 5TGM1 HIF-2α knockout cell lines by PCR using HIF-2α screening primers. Wildtype cells compared to HIF-2α CRISPR A3-7 and HIF-2α CRISPR B1-1 clones. Bp, base pair B) Sequencing results from the HIF-2α CRISPR B1-1 560 bp band subcloned into pGem-T easy, showing the loss of exon2 and adjacent intron sequence.

Table 4.3: Number of wild type, heterozygous, and homozygous knockout 5TGM1 HIFα clones following PCR screening.

		Number clones screened	Knockout	Wild type or Heterozygous
First experiment[1]	HIF-1α	27	0	27
	HIF-2α	15	2	13
Second experiment[2]	HIF-1α	56	0	56
	HIF-2α	47	0	47

[1.] Performed by Yinan Ma
[2.] Performed by Natalia Martin

The HIF-2α CRISPR A3-7 clone produced no products from the PCR with HIF-2α primers, indicating that it either contained modified HIF-2α alleles that could not be amplified by the primers, or the genomic DNA was of poor quality. To ascertain the quality of the genomic DNA for the HIF-2α CRISPR A3-7 clone, a PCR reaction was performed using the HIF-1α screening primers (Figure 4.3 A). A band corresponding to the expected size of 1417 bp was amplified from 5TGM1 wildtype, HIF-2α CRISPR B1-1 and HIF-2α CRISPR A3-7 gDNA samples verifying that gDNA quality was not a contributing factor.

These findings supported the presence of large deletions in both alleles of HIF-2α in the HIF-2α CRISPR A3-7 line, and previous results were consistent with a large deletion in one allele of the HIF-2α CRISPR B1-1 line. To further characterise the deletions in these lines, a series of primers targeting sequences upstream and downstream of the original screening primers (Figure 4.1 A) were designed (Figure 4.3 B). Four primer sets (2-5) were designed to amplify 238, 223, 299 and 233 bp PCR products respectively (Table 4.4). These primers were located in regions flanking exon 2 to map the predicted larger deletions produced by RNA-guided Cas9 activity. PCR reactions using the 4 primer sets were performed on gDNA extracted from 5TGM1 wildtype, Cas9 EV controls, HIF-2α CRISPR A3-7 and HIF-2α CRISPR B1-1 cell lines.

The results from the PCR reactions showed that all four cell lines, including the HIF-2α CRISPR A3-7 and HIF-2α CRISPR B1-1 cell lines, produced bands corresponding to the expected size for all primer sets (Figure 4.4 A). This demonstrated that the target intron regions surrounding exon 2 spanned by these primers was intact. This was not surprising for the control lines or the HIF-2α CRISPR B1-1 cell line as the characterisation of one allele showed a deletion between the two sgRNA sites leaving the regions spanned by these PCR primers intact (Figure 4.2). However, it demonstrated that each of the regions spanned by these primers were present in at least one allele of HIF-2α in the HIF-2α CRISPR A3-7 cell line.

These findings were extended by rearranging the forward and reverse primer sets to PCR amplify through the deleted exon 2 (Figure 4.4 B). Specifically, the forward primer from set 3 was used in combination with the reverse primer from set 4 (3F & 4R), and the forward primer from set 2 was used in combination with the reverse primer from set 5 (2F & 5R). It was expected that products of 2632 bp (3F & 4R) and 3502 bp (2F & 5R) would be produced from 5TGM1 wildtype and Cas9 EV control cells. For the characterised allele in HIF-2α CRISPR B1-1, products of 1313 bp (3F & 4R) and 2183 bp (2F & 5R) were expected. However, for the second uncharacterised allele in HIF-2α CRISPR B1-1, and the two uncharacterised alleles in HIF-2α CRISPR A3-7, it was expected that either no products, or products smaller than 1313 bp (3F & 4R) and 2183 bp (2F & 5R) would be produced, contingent upon the size of deletions (Table 4.5).

The results showed that the predicted bands were observed with both primer sets for wildtype and Cas9 EV controls, and the smaller predicted bands for the characterised allele of HIF-2α CRISPR B1-1. However, no band was amplified from HIF-2α CRISPR A3-7 with either 3F/4R or 2F/5R primer sets, and there were no smaller products observed with HIF-2α CRISPR B1-1 (Figure 4.4 B).

A

B

→ : Original screening primers flanking CRISPR cut sites

→ : Screening Primer Set 2

→ : Screening Primer Set 3

→ : Screening Primer Set 4

→ : Screening Primer Set 5

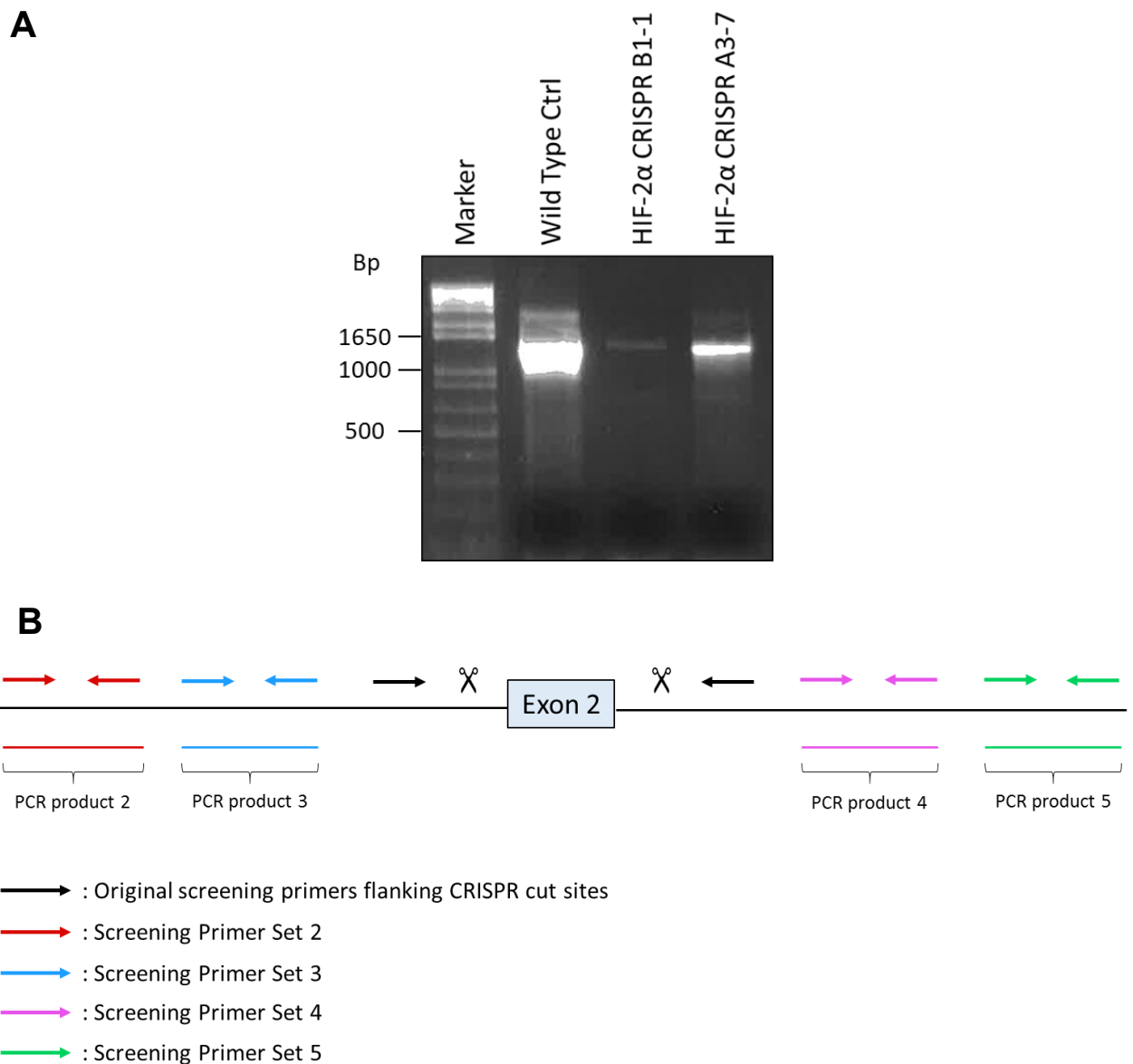**Figure 4.3: Characterisation by PCR of the HIF-2α CRISPR A3-7 monoclonal cell line.** A) PCR amplification of gDNA from 5TGM1 wildtype, HIF-2α CRISPR B1-1 and HIF-2α CRISPR A3-7 using HIF-1α screening primers. Expected band size was 1417 bp. B) Schematic of screening strategy using a series of primers flanking exon 2 of HIF-2α to characterise CRISPR deletion in the *HIF-2α* allele of HIF-2α CRISPR A3-7 cell line.

Table 4.4: PCR screening of 5TGM1 HIFα CRISPR A3-7 and B1-1 cell lines.

	PCR Product Sizes (bp)
Primer Set 2	238
Primer Set 3	223
Primer Set 4	299
Primer Set 5	233

Table 4.5: PCR screening of 5TGM1 HIFα CRISPR A3-7 and B1-1 cell lines using an alternative combination of screening primers.

	PCR Product Sizes (bp)		
	Wildtype	Known B1-1 modified allele	Other alleles containing deletions
Primers 3F & 4R	2632	1313	<1313
Primers 2F & 5R	3502	2183	<2183
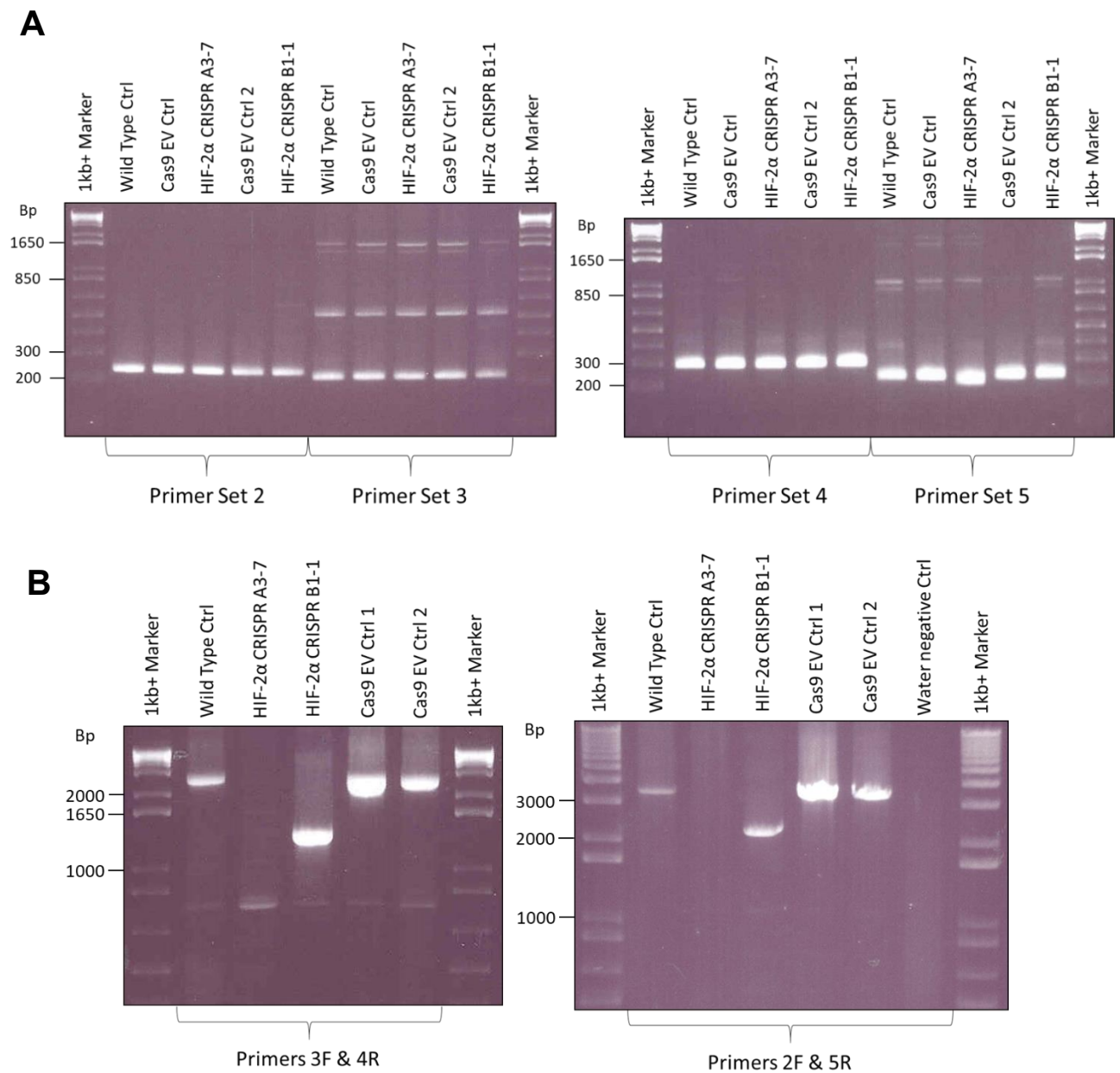
Figure 4.4: PCR using a series of primers positioned within intron 1 and intron 2 of HIF-2α to characterise deletions in HIF-2α CRISPR A3-7 and B1-1 cell lines. A) PCR amplification of gDNA extracts from 5TGM1 wildtype, Cas EV controls, HIF-2α CRISPR A3-7 and HIF-2α CRISPR B1-1 cell lines using screening primer sets described in Figure 4.3 B. The expected PCR products for sets 2, 3, 4 and 5 are 238, 223, 299 and 223 bp, respectively B) PCR amplification using an alternative combination of forward and reverse primers from primer sets 2, 3, 4 and 5. The expected products these PCR reactions are 2632 (3F & 4R) and 3502 (2F & 5R) bp.

From these data, it was surmised that distinct deletions on each allele of the HIF-2α CRISPR A3-7 cell line was responsible for the results observed. Specifically, cleavage of one allele by Cas9 in intron 1 resulted in a large deletion encompassing exon 2 and a large part of intron 2, including the sites for primer sets 4 and 5 (Figure 4.5). This would allow for amplification of this allele using primer sets 2 and 3. In addition, cleavage of the second allele by Cas9 in intron 2 resulted in the loss of exon 2 and a large portion of intron 1, including the sites for primer sets 2 and 3. This would allow for amplification of this allele using primer sets 4 and 5. Together, these larger deletions account for the successful PCR amplification of smaller fragments adjacent to exon 2 as shown in Figure 4.4 A, whilst PCR analysis of larger regions including exon 2 failed to amplify any products from HIF-2α CRISPR A3-7 gDNA (Figure 4.4 B). Similarly, a large deletion in intron 1 and/or intron 2 of the second allele in HIF-2α CRISPR B1-1 would prevent amplification using the 3F/4R and 2F/5R primer sets. Together these data are consistent with the loss of both copies of exon 2 in these two cell lines, and consequently would be predicted to result in the loss of HIF-2α expression.

To confirm that HIF-2α CRISPR A3-7 and HIF-2α CRISPR B1-1 were indeed HIF-2α knockout lines, *Hif2α* mRNA expression was assessed in cells cultured under normoxic or hypoxic conditions for 48 hours and compared with Cas9 EV control and wild type cell lines (Figure 4.6). Quantitative PCR analysis of *Hif2α* cDNA was performed using primers that span exon-exon junctions. Specifically, the forward primer spanned the exon 1/2 junction, whilst the reverse primer spanned exon 2/3.

A significant 15-30 fold hypoxia-dependent induction of *Hif2α* mRNA was observed in Cas9 EV control cells (p=0.03) and for Cas9 EV2 control cells (p=0.04), with almost undetectable levels of mRNA detectable in normoxia as observed previously (Figure 3.1). In contrast, both the HIF-2α CRISPR A3-7 and HIF-2α CRISPR B1-1 samples showed essentially no detectable *Hif2α* mRNA in normoxia or hypoxia, confirming the loss of *Hif2α* mRNA expression in both of these cell lines.

Next, numerous attempts were made to confirm the knockout of HIF-2α at the protein level in both the HIF-2α CRISPR A3-7 and HIF-2α CRISPR B1-1 cell lines. Firstly, total protein extracts were taken from 5TGM1 wildtype, Cas EV controls, HIF-2α CRISPR A3-7 and HIF-2α CRISPR B1-1 cell lines cultured in normoxic or hypoxic conditions for 48 hours. Western blot analysis of these extracts failed to detect HIF-2α protein, as previously observed in Chapter 3. A HIF-2α antibody was also used to immunoprecipitate HIF-2α from these total protein extracts, before analysing these immunoprecipitates by western blot. Once again, no HIF-2α was observed in the immunoprecipitates from any of the cell lines in hypoxia or normoxia.

In a final attempt to confirm loss of HIF-2α protein in these knockout lines, whole cell extracts were analysed proteomically. The 5TGM1 wildtype samples (both normoxic and hypoxic) were reduced, alkylated and tryptically digested prior to analysis by Nano liquid chromatography electrospray ionisation tandem mass spectrometry (Nano-LC-ESI-MS/MS), but peptides corresponding to HIF-2α were not detected under any conditions. As transcription factors are commonly expressed at low levels and can be difficult to detect by proteomic analysis in whole cell extracts, the relative levels of HIF-2α protein were concentrated by separating the samples by DSD-PAGE and excising the regions corresponding to an apparent molecular weight of 100 to 120 kD. These proteins were then tryptically digested, extracted and analysed by mass spectrometry, but once again peptides corresponding to HIF-2α were not consistently detected under any conditions.

These experiments are consistent with HIF-2α being expressed at relatively low levels in the 5TGM1 cell line, a not uncommon issue with the detection of HIF-2α protein in mouse cell lines (Dan Peet, personal communication). However, while the consistent detection of HIF-2α protein in these 5TGM1 cell lines was not possible using the currently available commercial antibodies, the more sensitive mRNA expression results confirm the loss of HIF-2α expression in both of the HIF-2α CRISPR A3-7 and HIF-2α CRISPR B1-1 cell lines.
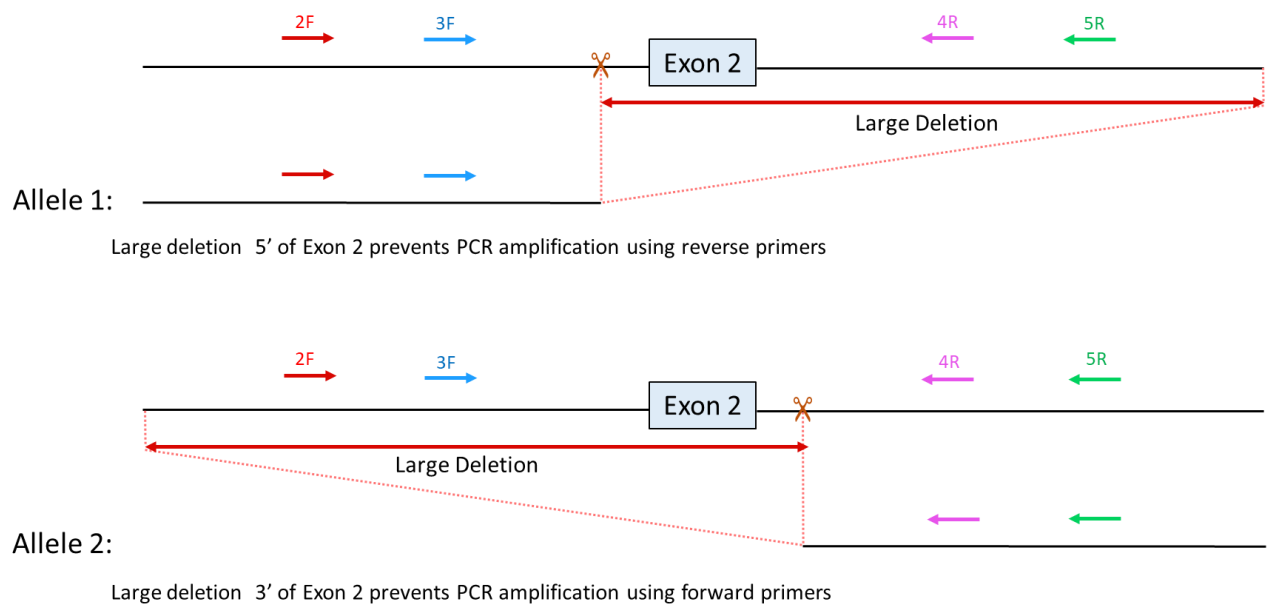
5TGM1 HIF-2α CRISPR A3-7 genotype:

Figure 4.5: Schematic showing the hypothesised knockout genotype for 5TGM1 HIF-2α CRISPR A3-7 cells. Diagram shows Cas9 cleavage sites and distinct large deletions on each allele that encompass exon 2 and 2 PCR primer sites.
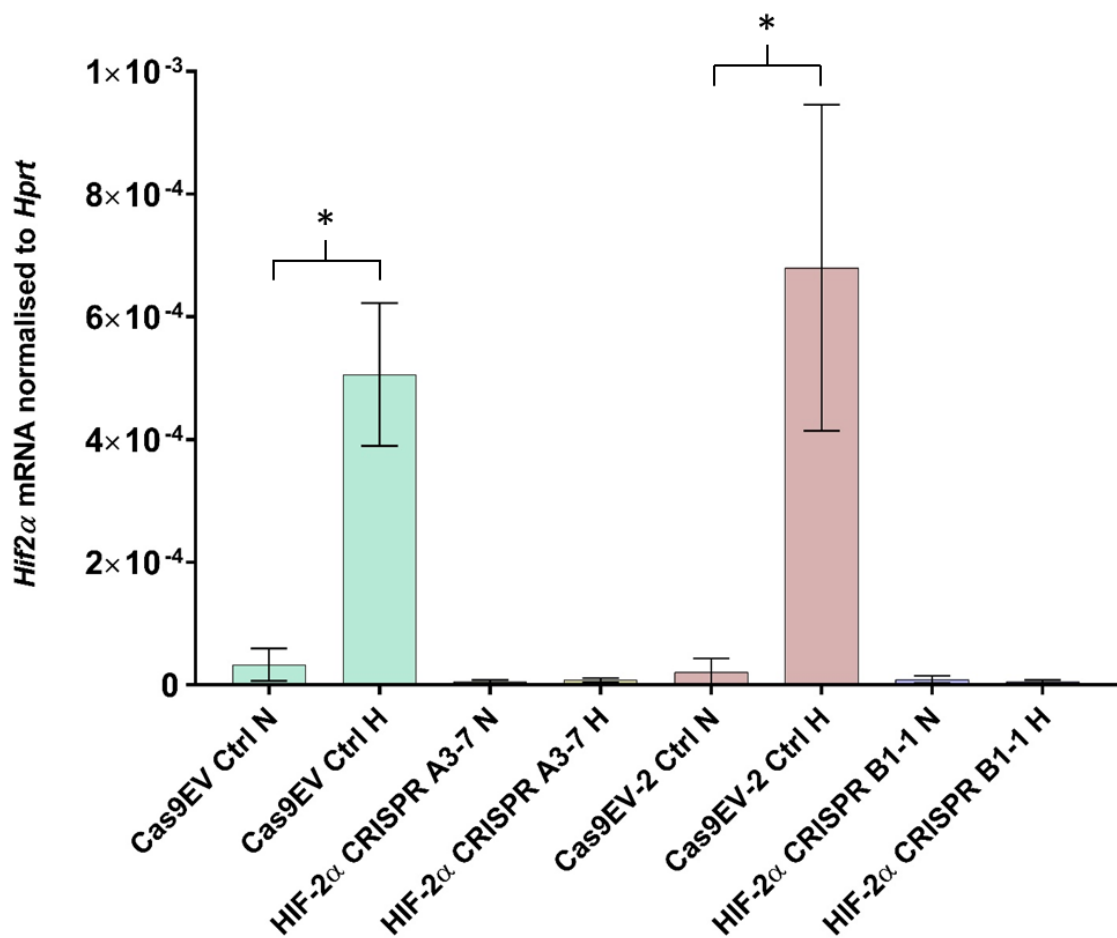
Figure 4.6: Characterisation of 5TGM1 HIF-2α CRISPR monoclonal cell lines in normoxia versus hypoxia. Cas EV control, Cas9 EV2 control, HIF-2α CRISPR A3-7 and HIF-2α CRISPR B1-1 cells were cultured for 48 hours in either normoxic or hypoxic conditions. RNA was extracted, reverse transcribed and quantitative PCR analysis performed using *Hif2α* primers. Relative expression of each gene was assessed by normalising to the housekeeping gene *Hprt*. Data is graphed as mean values of 3 independent experiments, each performed in triplicate, +/- standard error of the mean, where significance was determined using paired student t-test (* p-value <0.05).

4.2.2 Characterisation of 5TGM1 HIF-2α CRISPR knockout cell lines

4.2.2.3   Luciferase expression in 5TGM1 HIF-2α CRISPR knockout cells

The expression of luciferase from the stably integrated triple modality gene was critical for assessing homing and expansion of tumour in the 5TGM1/C57BL/KaLwRij mouse model. Prior to the use of the 5TGM1 HIF-2α CRISPR knockout cell lines *in vivo*, their luciferase activity was assessed using bioluminescence imaging. To this end, Cas9 EV controls, HIF-2α CRISPR A3-7 and HIF-2α CRISPR B1-1 cells were plated at densities of $1x10^6$, $2x10^5$, $4x10^4$, $8x10^3$ and $1.6x10^3$ cells per well in 96 well plates, D-luciferin was added and luminescence measured using the Xenogen IVIS imaging system. Whilst the HIF-2α CRISPR A3-7 and HIF-2α CRISPR B1-1 knockout lines showed significantly differing luciferase activity (approximately 2-fold, p=0.0008), two of the Cas9 EV control lines with activity that matched each of the knockout cells were identified (Figure 4.7). Specifically, the Cas9 EV control showed comparable luciferase activity to the HIF-2α CRISPR A3-7 cell line, whilst the Cas9 EV2 control matched the HIF-2α CRISPR B1-1 cell line.
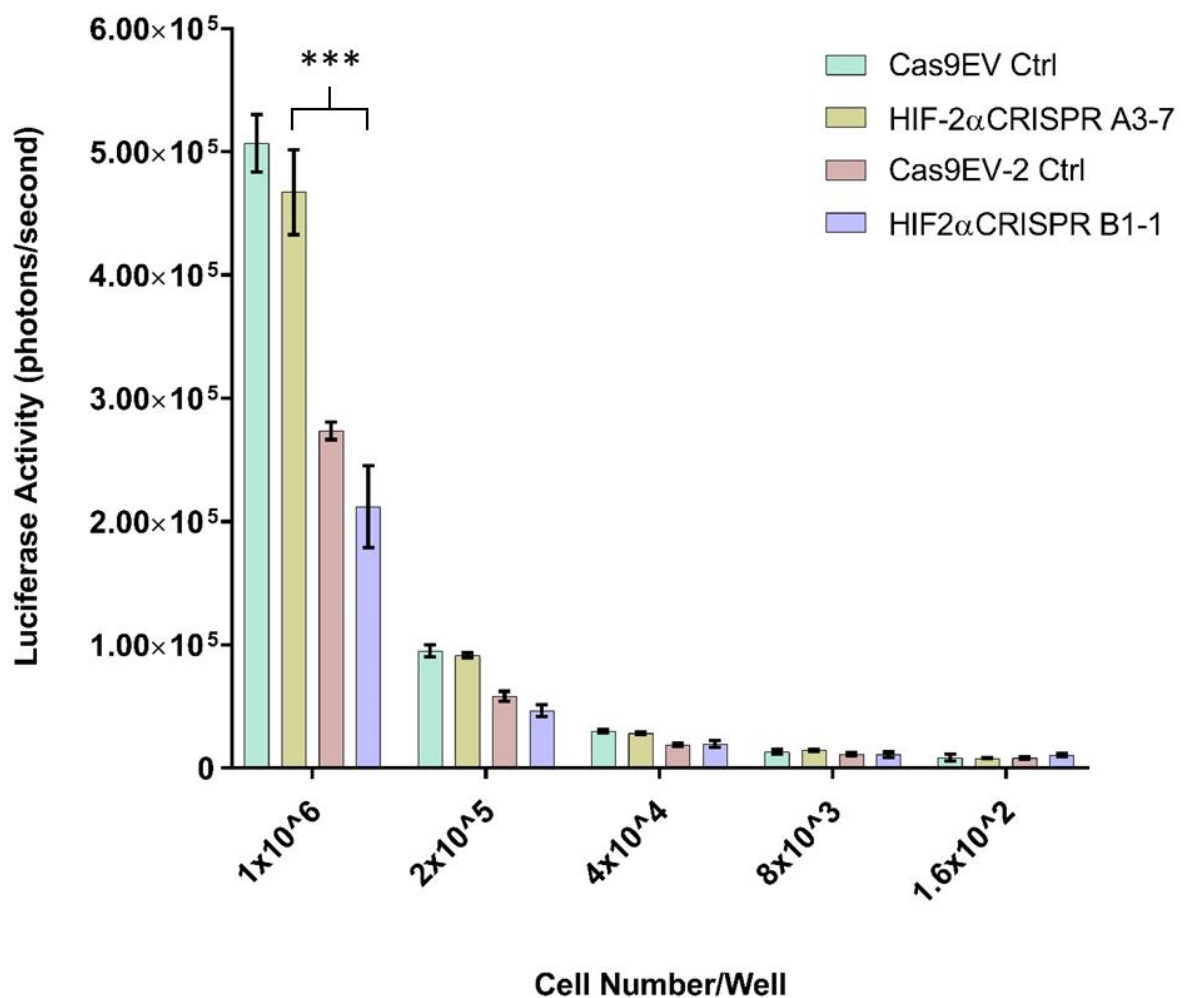
Figure 4.7: Analysis of luciferase activity of 5TGM1 Cas9 control and HIF-2α knockout cell lines. Constitutive luciferase expression was determined for Cas9 EV and EV-2 controls and HIF-2α CRISPR A3-7 and HIF-2α CRISPR B1-1 monoclonal cell lines. Cells were plated at 1/5 serial dilutions from $1x10^6$ to 320 cells/well in triplicate in a 96-well tray. D-luciferin was added to each well at a final concentration of 3 mg/mL and incubated at 37ºC for 30 minutes. Images were taken at an exposure time of 10 minutes, and light emission (photons/sec) measured using the IVIS Xenogen™. Data are mean values +/- standard error of the mean of 3 independent experiments, each with triplicate samples, where significance was determined using paired student t-test (*** p-value <0.001).

4.2.2.4   Proliferation of 5TGM1 HIF-2α CRISPR knockout cells

The HIF-2α transcription factor regulates a number of target genes, some of which lead to changes in downstream pathways critical to cellular behaviour and survival (Biswas, Troy et al. 2010, Lee and Simon 2015). Any possible changes to cellular proliferation as a result of HIF-2α deletion, or other possible changes to the 5TGM1 cells, could influence disease progression in MM, hence cell proliferation rates were determined prior to animal studies. 5TGM1 Cas9 EV control, Cas9 EV2 control, HIF-2α CRISPR A3-7 and HIF-2α CRISPR B1-1 cell lines were seeded at 5×10^3 cells/100 μL in a 96-well plate and cultured for 3 days in both normoxic and hypoxic conditions. Bioluminescence was measured and final cell number in each sample determined using a standard curve.

Comparative analyses of the Cas9 control and HIF-2α CRISPR knock out lines showed no difference in proliferation rate following 3 days growth (Figure 4.8). While the proliferation rates of all cells were approximately 4-fold lower in hypoxia compared to normoxia, the proliferation rates of the HIF-2α CRISPR knockout lines were not significantly different to the Cas9 control lines under each condition (Figure 4.8 A and B respectively). Consequently, any differences observed in disease progression in the 5TGM1/C57BL/KaLwRij MM model between mice injected with the Cas9 EV control cells and the HIF-2α knockout cells would be unlikely to be due to inherent differences in cellular proliferation.

A

B
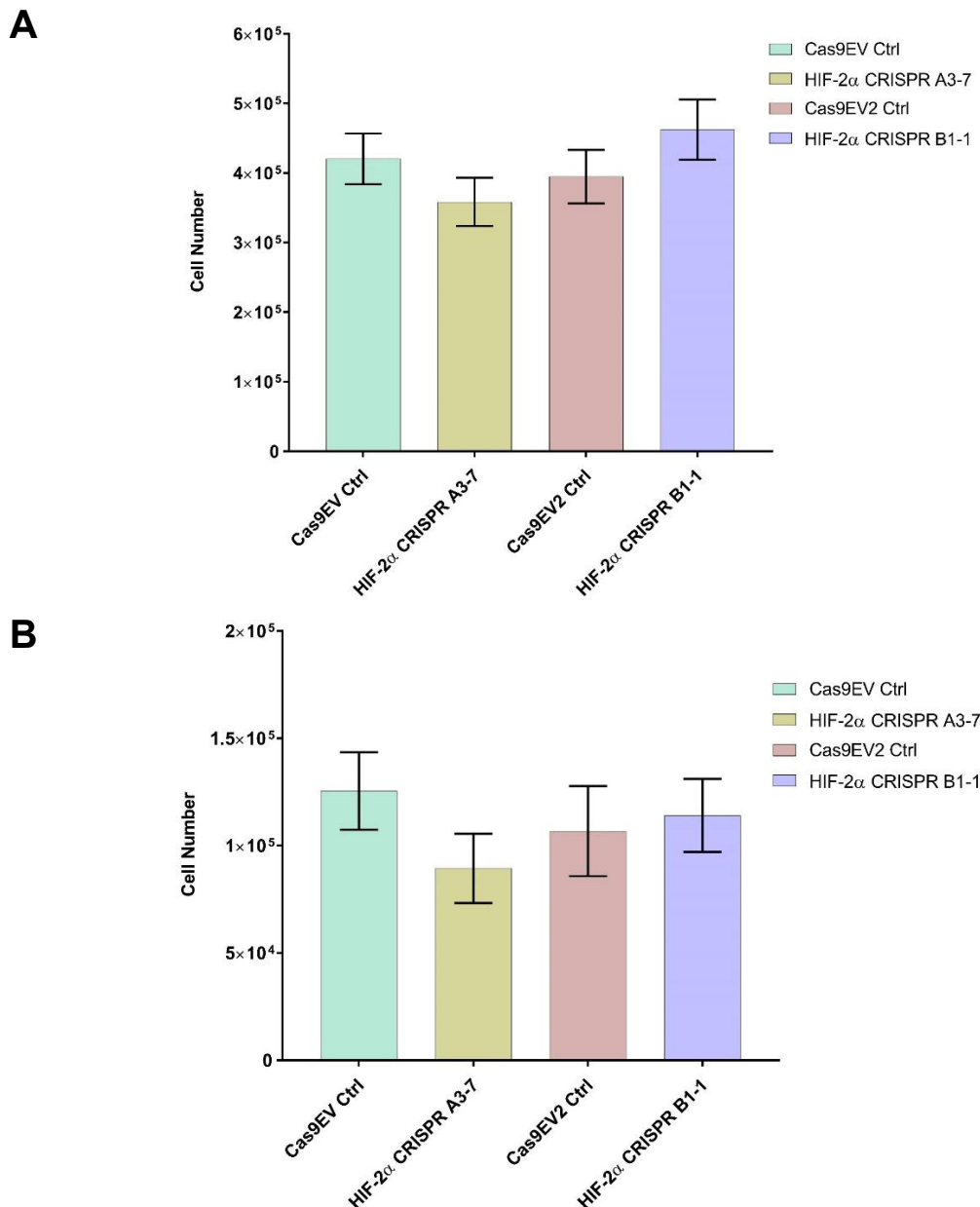
Figure 4.8: Comparative analysis of proliferation rates between 5TGM1 Cas9 EV control, HIF-2α CRISPR A3-7, Cas9 EV2 control and HIF-2α CRISPR B1-1 cell lines. Cellular proliferation rates were comparatively assessed between 5TGM1 Cas9 EV Ctrl, HIF-2α CRISPR A3-7, Cas9 EV2 Ctrl and HIF-2α CRISPR B1-1 monoclonal cell lines. Cells were plated at 5×10^3 cells/100 µL in triplicate in a 96-well plate, and cultured for 3 days in either normoxia (A) or hypoxia (B). Bioluminescence was assessed following 30 mg/mL D-luciferin treatment using the IVIS Lumina XRMS™. Final cell numbers in each sample were determined using a standard curve of 2×10^3 - 5×10^5 cells. Data are mean values +/- standard error of the mean for triplicate samples, and are representative of three independent experiments.

4.2.3   In vivo study of the role of HIF-2α in MM using 5TGM1 HIF-2α CRISPR knockout cell lines

Given the successful generation and characterisation of the two HIF-2α knockout 5TGM1 lines, and the generation and selection of appropriate matched control cell lines, the contribution of HIF-2α in the *in vivo* mouse model of MM was investigated. To this end, the Cas9 EV control, HIF-2α CRISPR A3-7, Cas9 EV2 control and HIF-2α CRISPR B1-1 5TGM1 cell lines were used in the well-established 4 week 5TGM1/C57BL/KaLwRij mouse model described previously (Dallas, Garrett et al. 1999). Frozen aliquots of each cell line, stored at the same passage, were thawed and grown for 3 days.

Each of these cell lines constituted an independent treatment group which contained 5 age and gender-matched C57BL/KaLwRij mice that were each inoculated with 5×10^5 of cells in 100 μL of PBS via tail vein injection, consistent with previous studies (Noll, Hewett et al. 2014). Cas9 EV and HIF-2α CRISPR A3-7 injected mice were between 7.5 and 8.5 weeks of age, and all female for direct comparative analyses. Injections for the HIF-2α CRISPR B1-1 and matched Cas9 EV2 control lines were performed on mice that were between 6.5 and 8 weeks of age, and all male for comparative analyses between these two treatment groups.

Tumour establishment and progression in the bone was monitored 2 weeks, 3 weeks and 4 weeks post tail vein injection using *in vivo* bioluminescence. Mice were administered with D-luciferin via intraperitoneal injection, and imaged with the IVIS Spectrum[TM]. Intra medullary tumour was first detected in 3/5 Cas9 EV and 3/5 Cas9 EV2 control mice by *in vivo* bioluminescence imaging at 3 weeks post injection (Figure 4.9), as typically observed with control 5TGM1 cells in the C57BL/KaLwRij MM model. In contrast, intramedullary tumour was only detected in one HIF-2α CRISPR B1-1 injected mouse, and not detected in any of the HIF-2α CRISPR A3-7 mice at 3 weeks post injection.

Bioluminescence analyses at the end of the experiment at 4 weeks post-injection demonstrated that mice injected with the Cas9 EV and Cas9 EV2 control cells developed disseminated tumour, most notably to the hind leg and spinal vertebrae, as observed in mouse 1, 2 and 4 in the Cas9 EV group and mouse 1, 3 and 4 in the Cas9 EV2 group (Figure 4.10 A-D). In these control groups, Cas9 EV (mouse 1) and Cas9 EV2 (mouse 2) did not develop any visible tumour at 4 weeks post injection using *in vivo* bioluminescence. At the same time point, mouse 1, 3, 4 and 5 from the HIF-2α CRISPR B1-1 group developed visible tumour. Whilst 4 out of 5 mice from the HIF-2α CRISPR B1-1 group developed tumour compared to 3 out of 5 in the matched Cas9 EV2 control, bioluminescent measurements showed that the tumour burden was higher in the Cas9 EV2 mice (Figure 4.10 E).

Whilst tumour was visible in the Cas9 EV controls and HIF-2α CRISPR B1-1 groups, none of the mice injected with the HIF-2α CRISPR A3-7 cells, developed any significant tumour (Figure 4.10 A-D). These observations were reflected in the quantification of tumour burden measured throughout the 4-week study and presented in Figure 4.10 E, where HIF-2α CRISPR A3-7 containing mice showed a significant lack of tumour development compared to the Cas9 EV control mice after 4 weeks post injection (p=0.0002) (Figure 4.10 E). Over the course of the experiment, HIF-2α CRISPR B1-1 injected mice showed a delayed increase in tumour burden over 4 weeks of tumour burden quantification compared to the Cas9 EV2 control mice (Figure 4.10 E). Although the differences in tumour burden between Cas9 EV2 and HIF-2α CRISPR B1-1 injected mice data did not reach statistical significance, the observed delay in tumour development was consistent with the data for the Cas9 EV and HIF-2α CRISPR A3-7 comparative experiment. Together, these data demonstrate that the loss of HIF-2α in 5TGM1 cells resulted in a delay or complete loss of tumour establishment and progression *in vivo* compared to matched control cell lines using the 5TGM1/C57BL/KaLwRij 4 week disease model.

A

Front View

B

Back View
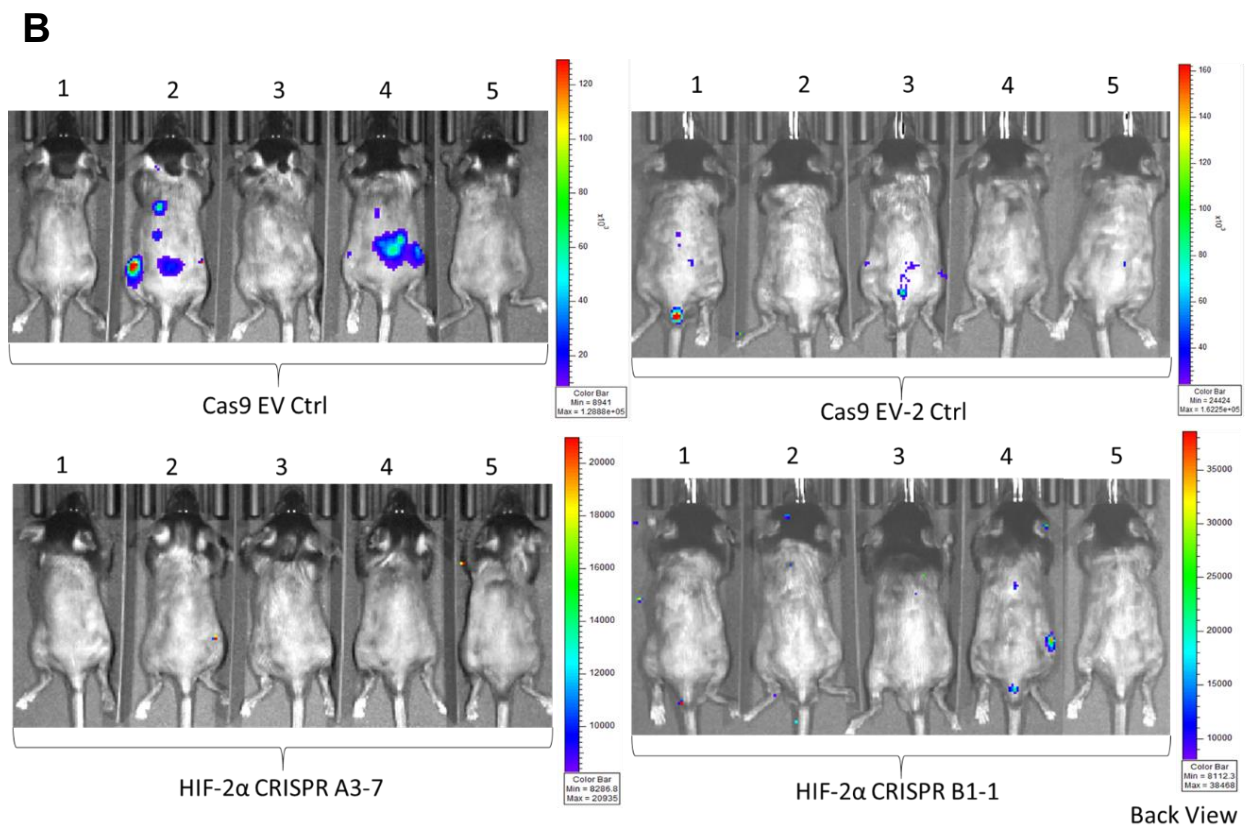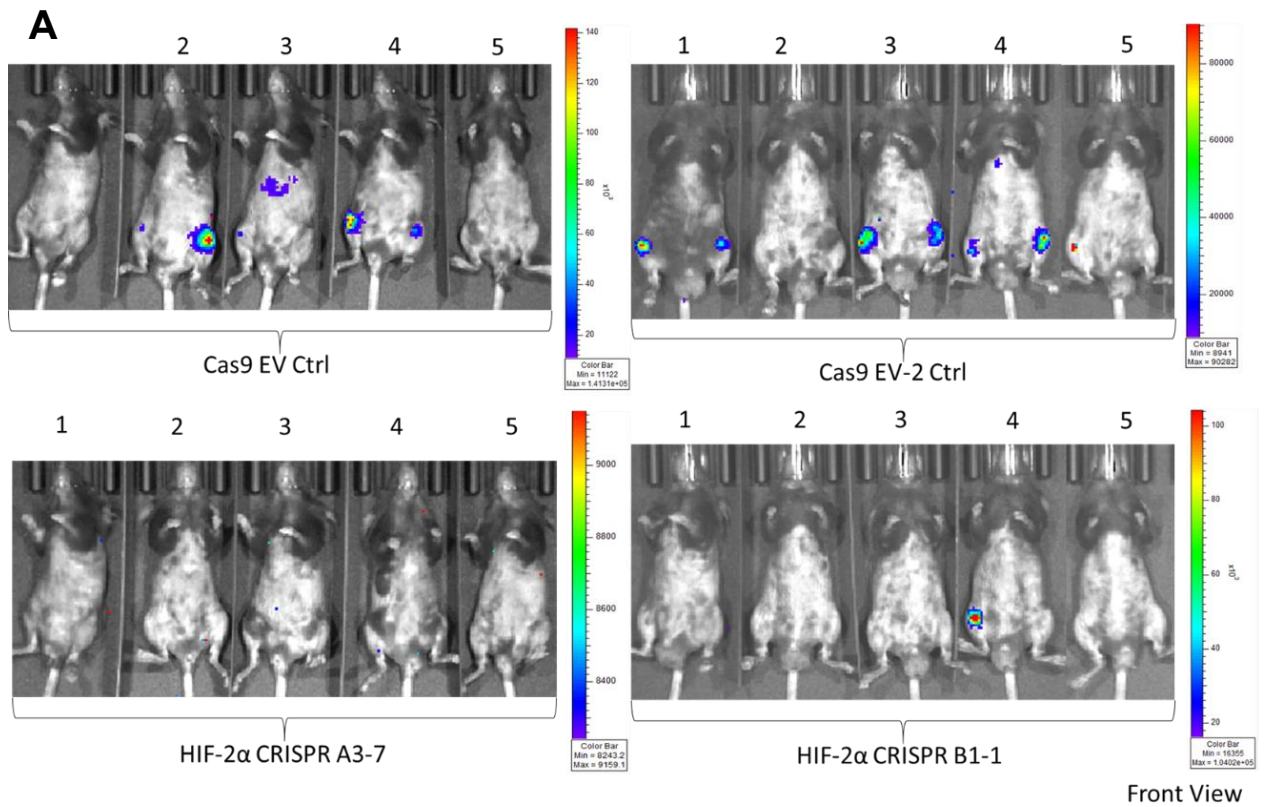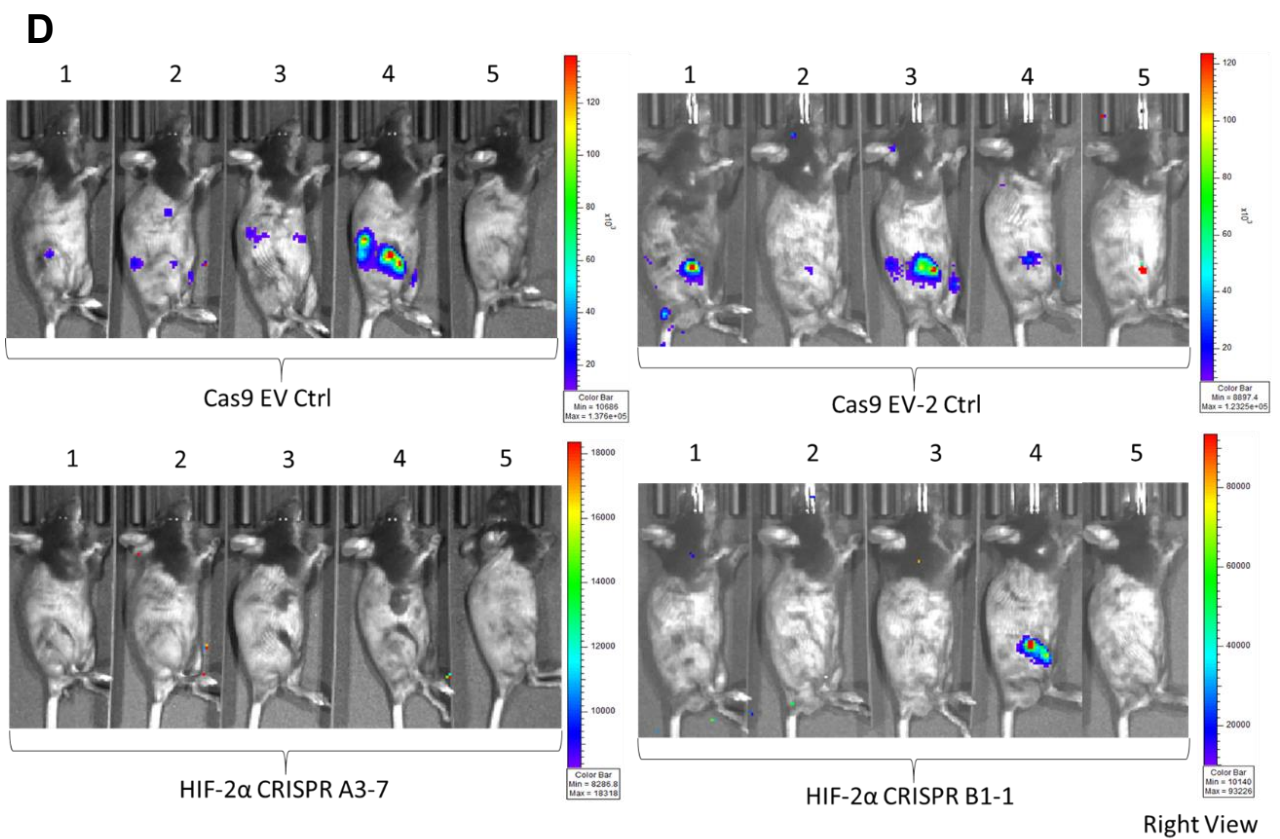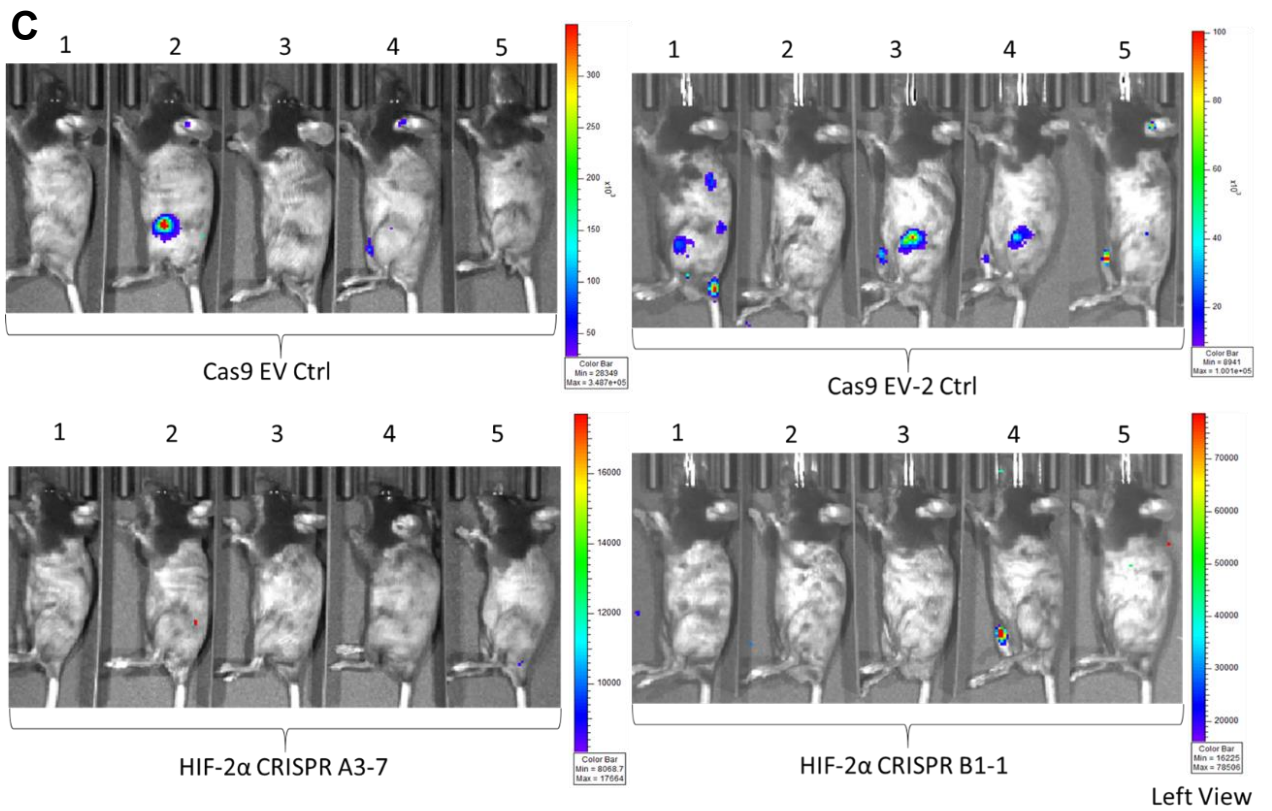
Figure 4.9: Analysis of early tumour development in mice injected with 5TGM1 Cas9 EV controls, HIF-2α CRISPR A3-7 and HIF-2α CRISPR B1-1 cells. Tail vein injections of 5TGM1 Cas9 EV, HIF-2α CRISPR A3-7, Cas9 EV2 and HIF-2α CRISPR B1-1 cells were performed on C57Bl/KaLwRij mice. Cellular growth and dissemination at 3 weeks post injection was assessed by intraperitoneal injection of D-luciferin and *in vivo* bioluminescence captured from the front (A), back (B), left (C) and right (D) viewpoints using the IVIS Lumina XRMS™.

A

Cas9 EV Ctrl

Cas9 EV-2 Ctrl

HIF-2α CRISPR A3-7

HIF-2α CRISPR B1-1

Front View

B

Cas9 EV Ctrl

Cas9 EV-2 Ctrl

HIF-2α CRISPR A3-7

HIF-2α CRISPR B1-1

Back View

C

Cas9 EV Ctrl

Cas9 EV-2 Ctrl

HIF-2α CRISPR A3-7

HIF-2α CRISPR B1-1

Left View

D

Cas9 EV Ctrl

Cas9 EV-2 Ctrl

HIF-2α CRISPR A3-7

HIF-2α CRISPR B1-1

Right View
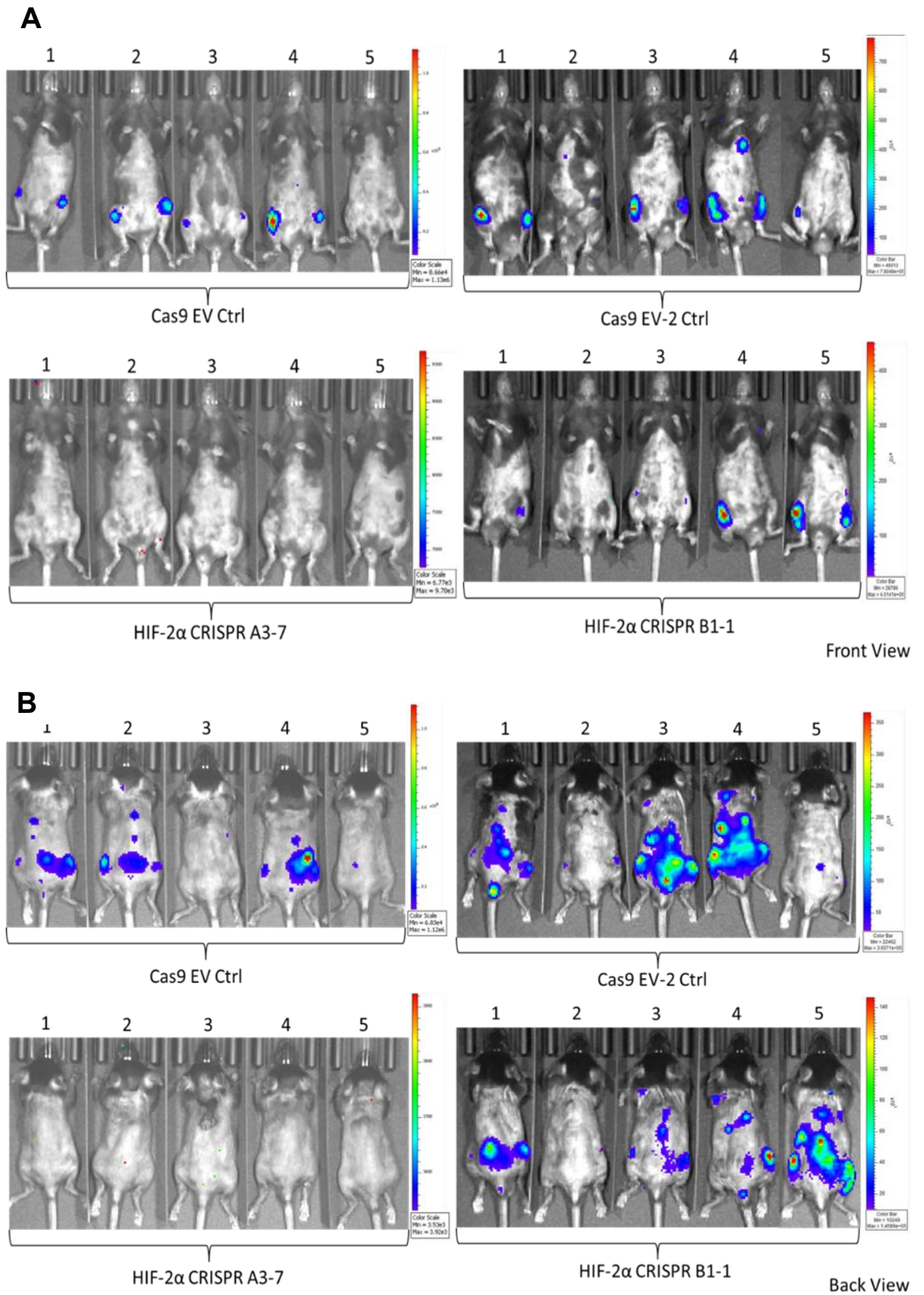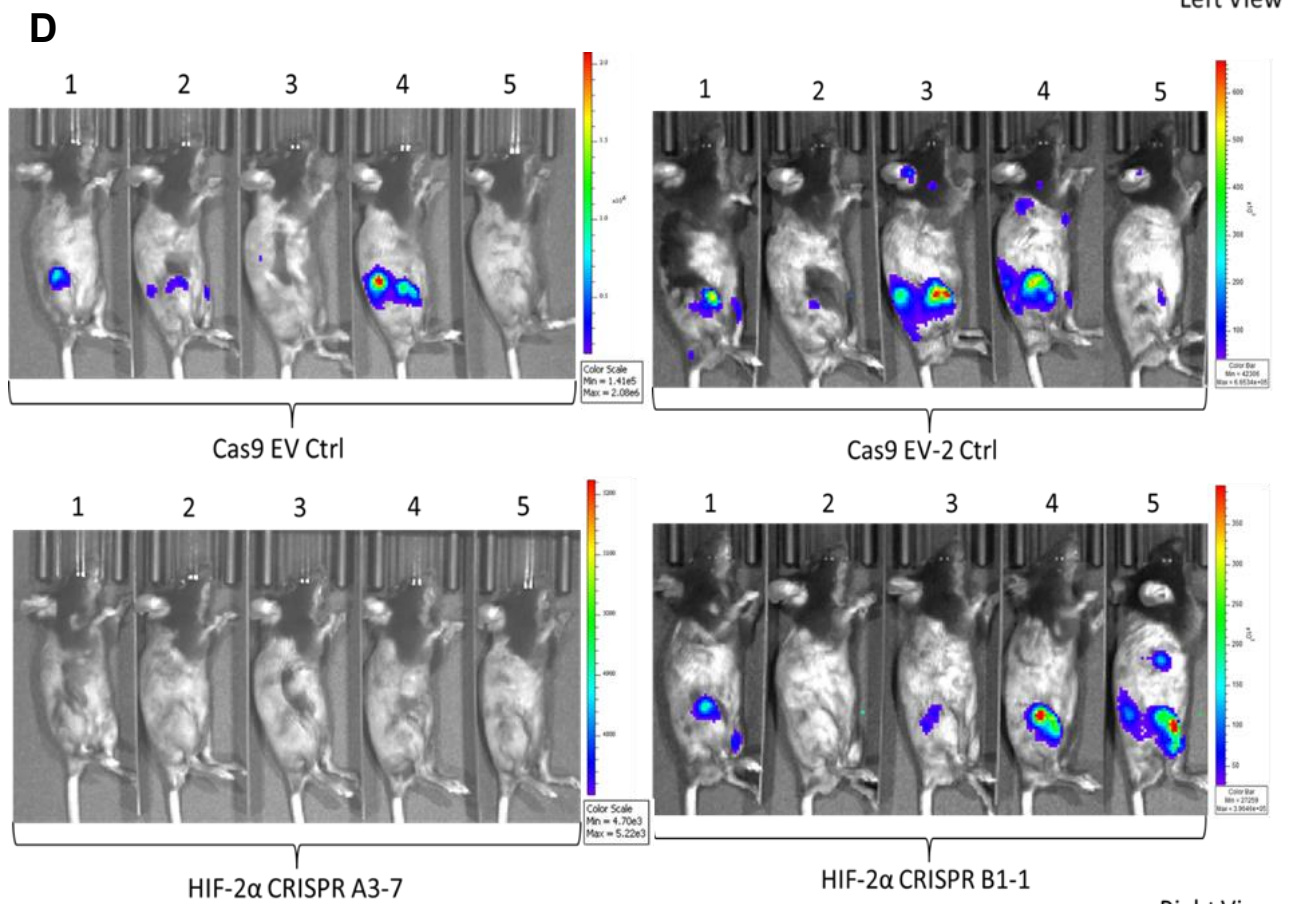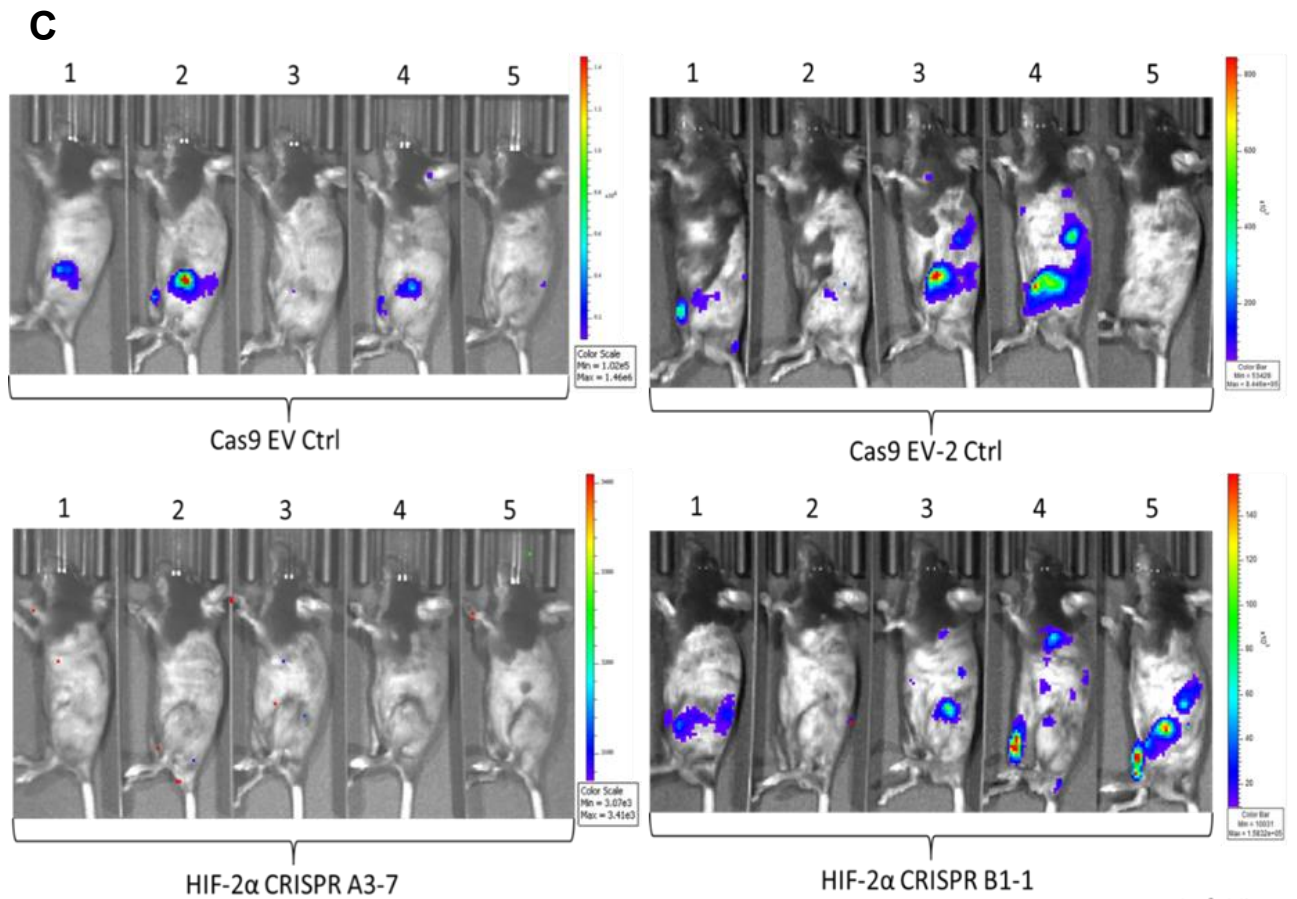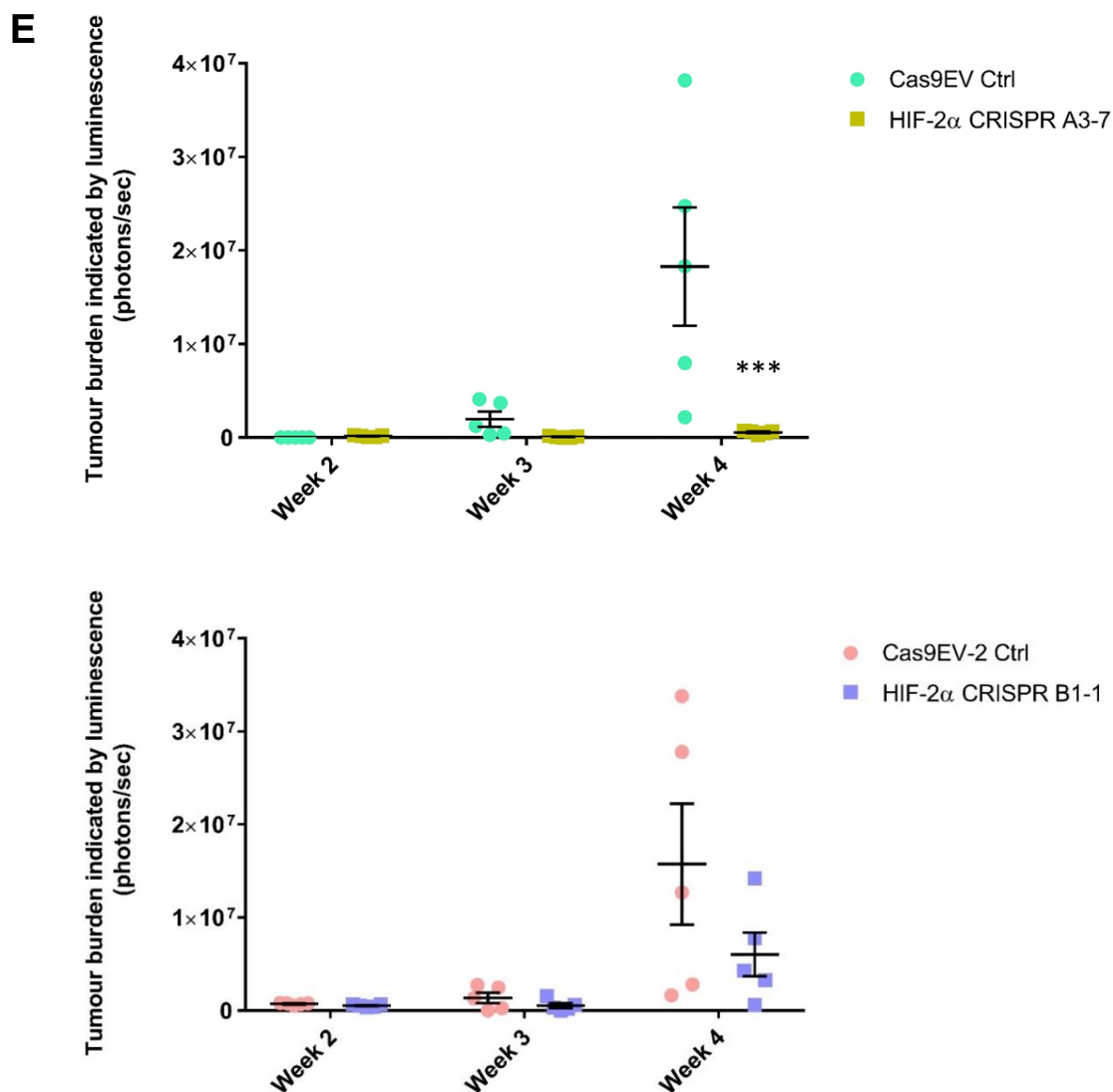
Figure 4.10: 5TGM1 HIF-2α CRISPR A3-7 and HIF-2α CRISPR B1-1 cells display delayed expansion and dissemination compared to Cas9 EV and Cas9 EV2 respectively in a 4 week mouse model of MM. Tail vein injections of 5TGM1 Cas9 EV, HIF-2α CRISPR A3-7, Cas9 EV2 and HIF-2α CRISPR B1-1 cells were performed on C57Bl/KaLwRij mice. Cellular growth and dissemination at 4 weeks post injection was assessed by intraperitoneal injection of D-luciferin and *in vivo* bioluminescence captured from the front (A), back (B), left (C) and right (D) viewpoints using the IVIS Lumina XRMS™. E) The luciferase activity of each mouse was quantified weekly (IVIS Spectrum™) and graphed as a measure of tumour burden. The mean for each mouse group (n=5) +/- standard error of the mean shown for each week post injection, where significance was determined using two-way ANOVA with Sidak's post-test (*** p-value <0.001)

Following 4 weeks of disease progression, all mice were humanely killed. As the spleen is a known site for disease involvement in animal models of MM (Asosingh, Radl et al. 2000), the spleens were removed, placed into fixative, embedded in wax and sections prepared for microscopic analysis. In addition, the hind legs of mice were fixed, decalcified and similarly processed in preparation for staining. Sections from both the hind leg and the spleen were stained with an antibody to GFP to identify BM infiltration of the modified 5TGM1 cells to support *in vivo* bioluminescence findings (Figure 4.11). 5TGM1 colonies (Figure 4.11 A and B) and dissemination (Figure 4.11 C) were observed within the femoral and tibial BM of mice displaying disease by *in vivo* bioluminescence, confirming establishment and expansion of MM.

In human patients, MM is clinically diagnosed by a number of factors including the secretion of excessive clonal antibodies, called paraprotein (Rajkumar, Dimopoulos et al. 2014). To further characterise MM progression, paraprotein production was measured in the mouse model. To do this, cardiac bleeds were performed from all Cas9 EV and HIF-2α CRISPR injected mice following 4 weeks of disease development and the serum was analysed by gel electrophoresis in combination with Amido Black staining to both separate and visualise the serum proteins (Figure 4.12). Serum paraprotein was detected in 9 out of 10 mice injected with Cas9 EV control cells, whereas all 10 mice injected with HIF-2α CRISPR knockout cells showed comparatively low to no detectable paraprotein (Figure 4.12).

The lack of detectable paraprotein in mice containing HIF-2α CRISPR A3-7 cells correlated with a complete lack of detectable tumour in the same mice using *in vivo* bioluminescence (Figure 4.10 A-D, 4.12 A). Plotting relative paraprotein levels against tumour burden, as measured by bioluminescence for both the Cas9EV control and HIF-2α CRISPR A3-7 mice, confirmed this correlation (R^2: 0.8213, Figure 4.13 A). The detection of paraprotein in the HIF-2α CRISPR B1-1 injected mice was more variable, but overall an absence or low level of paraprotein was detected compared to the Cas9 EV2 control mice (Figure 4.12 B). These paraprotein levels generally corresponded with the HIF-2α CRISPR B1-1 mouse *in vivo* bioluminescence data (Figure 4.10)

where, for example, mouse 2 showed almost no detectable tumour burden and the lowest paraprotein expression levels, whereas mouse 5 had the highest tumour burden and the highest level of paraprotein expression. However, due to the higher variability in these data the correlation between paraprotein and tumour burden in the Cas9 EV2 and HIF-2α CRISPR B1-1 mice was not as clear as that observed in the data with the HIF-2α CRISPR A3-7 cells (Figure 4.13).

Overall, these paraprotein data were consistent with the tumour burden observed via *in vivo* bioluminescence, and confirmed the delayed progression of MM as a result of HIF-2α knockout in 5TGM1 cells, supporting the original hypothesis that HIF-2α plays a critical role in MM disease progression *in vivo*.
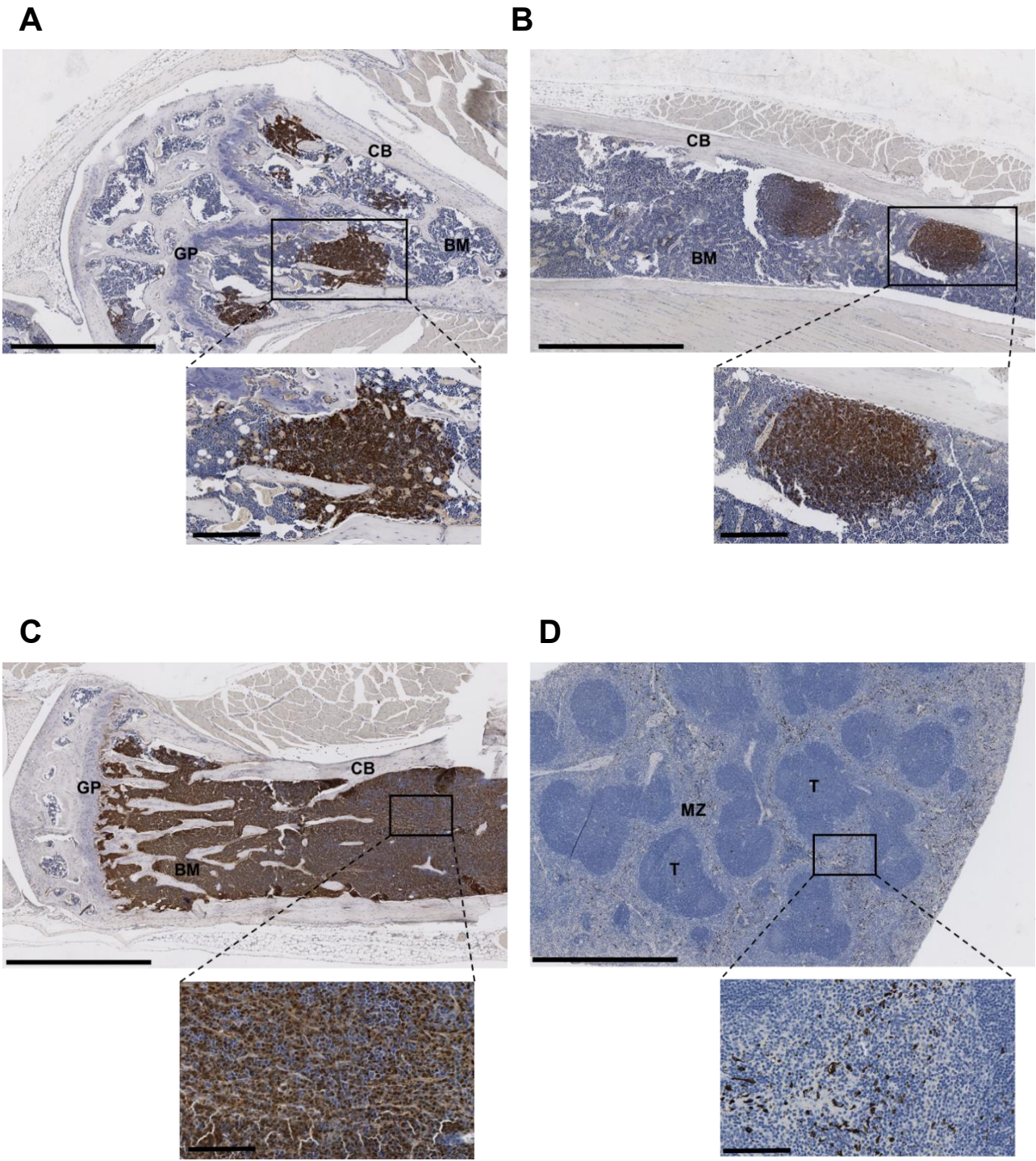
Figure 4.11: Immunohistochemical staining of 5TGM1 cells verified tumour dissemination and establishment in mice. GFP staining of 5TGM1 cells (brown) in femoral, tibial and splenic sections from 5TGM1/C57BL/KaLwRij mice 4 weeks post injection. A) Femur section showing 5TGM1 colonies within the BM of a Cas9 EV injected mouse (scale bar, 1 mm). Inset showing an individual colony (scale bar, 200 µm). GP, growth plate; BM, bone marrow; CB, cortical bone. B) Tibia section showing two 5TGM1 colonies in the BM of a Cas9 EV2 injected mouse (scale bar, 1 mm). Inset showing an individual colony (scale bar, 200 µm). C) Tibia section showing tumour expansion throughout the BM of a Cas9 EV2 injected mouse (top scale bar, 1 mm). Inset individual cells (scale bar, 100 µm). D) Splenic section of a Cas9 EV injected mouse showing single 5TGM1 (scale bar, 1 mm). Inset showing individual cells (scale bar, 100 µm). MZ, marginal zone (red pulp); T, T-cell parafollicular zone (white pulp).
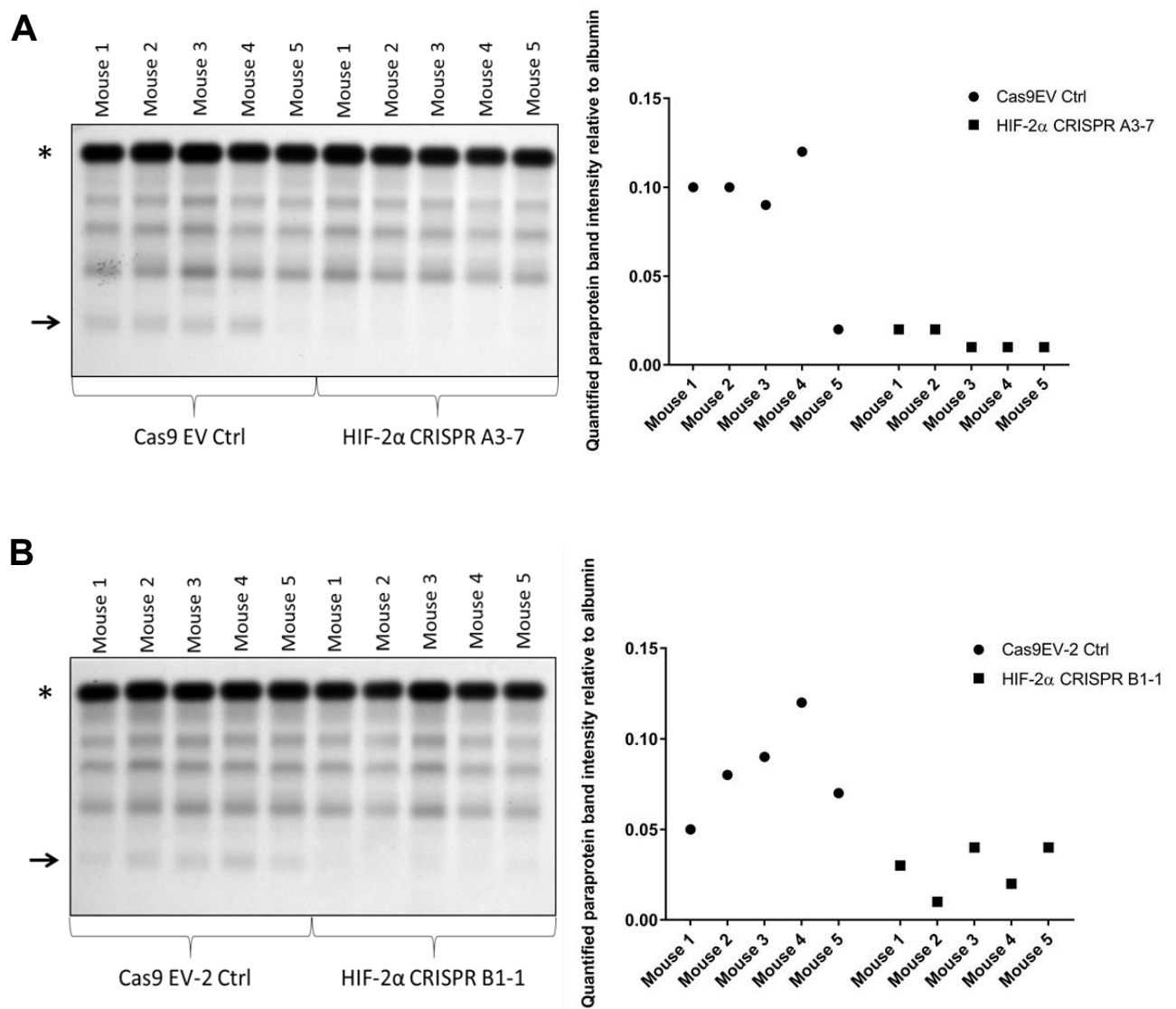
Figure 4.12: Paraprotein detection and quantification in mouse serum samples. Blood serum was collected from each mouse at the end of the study (4 weeks post injection). Serum proteins were separated using electrophoresis, and paraprotein measured for A) Cas9 EV ctrl compared to HIF-2α CRISPR A3-7 injected mice and B) Cas9 EV2 ctrl compared to HIF-2α CRISPR B1-1 mice. Quantified paraprotein levels (bands marked with arrow) were normalised to albumin (band marked with asterisks), and represented graphically for all mouse samples (A and B).
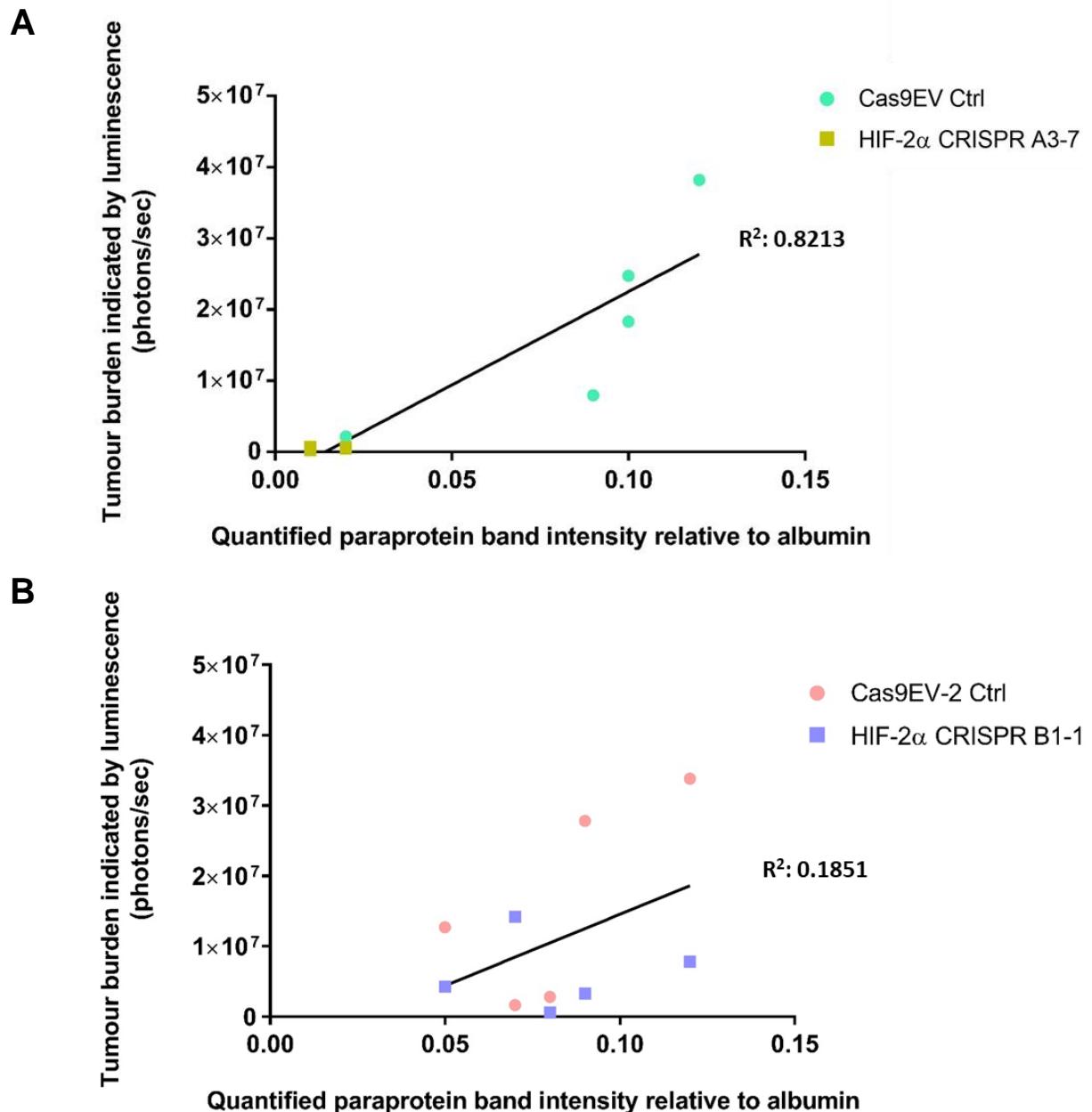
Figure 4.13: Correlation between tumour burden and paraprotein in mice injected with 5TGM1 Cas9 EV controls, HIF-2α CRISPR A3-7 and HIF-2α CRISPR B1-1 cells. Tail vein injections of A) 5TGM1 Cas9 EV, HIF-2α CRISPR A3-7, B) Cas9 EV2 and HIF-2α CRISPR B1-1 cells were performed on C57Bl/KaLwRij mice. The luciferase activity of each mouse was quantified as a measurement of tumour burden 4 weeks post-injection (Figure 4.10 E), and directly correlated with quantified paraprotein (Figure 4.12). Correlation significance was determined using linear regression analyses for data in A) (R^2 value of 0.8213) and B) (R^2 value of 0.1851).

4.3 Discussion

CRISPR-Cas9 gene editing, specifically targeting HIF-1α and HIF-2α, was used to modify HIFα expression in the murine 5TGM1 myeloma cell line, in order to ascertain their role in MM disease initiation and progression. In recent years, this technology has been commonly used for targeted gene disruption with considerable success (Hwang, Fu et al. 2013, Kim, Kim et al. 2014). As with many other technologies that alter gene expression, the success rate is dependent on the expression system used, specific targeting strategy and cell type targeted. The work within this chapter employed the use of two cut sites and subsequent DNA repair for the removal of a large fragment containing exon 2. This strategy had been employed to successfully delete large DNA fragments (between 0.35 and 1000 kb), with knockout frequencies of 1 – 15% in mammalian cells (Canver, Bauer et al. 2014, He, Proudfoot et al. 2015). Other studies using multiple sgRNAs to generate large deletions in animals have reported up to 25% disruption frequency (Zhang, Jia et al. 2015, Song, Yuan et al. 2016).

The efficiency of Cas9 cleavage and repair in the 5TGM1 cells was low, with a generation frequency of 2 out of 59 clones for HIF-2α knockout and 0 out of 83 for HIF-1α knockout lines (Table 4.3). Previous studies have significantly knocked-down HIF-1α expression in MM cells and have not resulted in cellular death, making this an unlikely explanation for the lack of HIF-1α knockout clones (Martin, Diamond et al. 2009, Storti, Bolzoni et al. 2013). The deletion of a large fragment using two sgRNAs, as opposed to generating small indels with a single sgRNA, is unlikely to be a contributing factor, given that large disruptions have been performed with great success and fragment size does not correlate with knockout frequency in cells (He, Proudfoot et al. 2015). Issues with the sgRNA design is also not likely to explain the low knockout frequency, as 8 different sets of guides were used in this chapter. Another possible contributing factor is the dose of Cas9 and sgRNA within the 5TGM1 cells. If the Cas9 and sgRNA expression were limited, this could be negatively effecting knockout efficiency as has been suggested previously (Canver, Bauer et al. 2014). Given the poor transfection efficiency of 5TGM1 cells, low cellular uptake of either or

both pSpCas9-HIFα-Int1A/B and pSpCas9-HIFα-Int2A/B plasmids could be limiting Cas9 nuclease and sgRNA expression.

5TGM1 cells are known to have poor transfection efficiency as discussed in the previous chapter, where lentiviral transduction has been successfully used to improve plasmid delivery. Lentiviral delivery of Cas9 and sgRNA has previously been shown to efficiently generate knockout cell lines (Shalem, Sanjana et al. 2014, Zhou, Zhu et al. 2014, Joung, Konermann et al. 2017). Future experiments using lentiviral transduction would increase the number of cells expressing the Cas9 nuclease and sgRNAs, providing more monoclonal lines to screen for successful HIF knockout from a single experiment. This method would also result in prolonged expression of Cas9 nuclease and the sgRNA from the integrated plasmid, and therefore improve knockout efficiency given the current transient transfection technique results in only sort term expression of Cas9 nuclease and sgRNAs. Hence this lentiviral-based CRISPR strategy should be used to generate HIF-1α and additional HIF-2α knockout 5TGM1 lines for subsequent experiments. It would, however, be important to assess the long-term effects of constitutive Cas9 expression from the stable cell lines both *in vitro* and *in vivo*.

The low efficiency rates resulted in the creation of only two HIF-2α knockout clones, one from each sgRNA design (HIF-2α CRISPR A3-7 and HIF-2α CRISPR B1-1), and no HIF-1α clones despite multiple experimental attempts. Whilst both HIF-1α and HIF-2α are important contributors to MM disease, HIF-2α has been implicated as a major contributor to MM disease severity (Martin, Diamond et al. 2009), but its specific role *in vivo* in MM remains poorly understudied. Hence, this project used the HIF-2α CRISPR A3-7 and HIF-2α CRISPR B1-1 cell lines to assess the specific contribution of HIF-2α to MM pathogenesis. Although these two cell lines show comparatively varied luciferase activity (Figure 4.7 and Figure 4.8), suitable luciferase-expression matched control lines were identified for each cell line.

Extensive PCR screening of the two HIF-2α CRISPR knockout lines identified the loss of exon 2 in both clones. Specifically, a 1269 bp loss was identified for at least one allele from the B1-1 clone (Figure 4.4). Subsequent sequencing analyses of 12 B1-1 clones indicated that either all alleles in the 5TGM1 HIF-2α CRISPR B1-1 cells contained the identical deletion, which is highly unlikely, or the more likely scenario that the second modified allele was not present in the single band amplified by PCR. Given that no other bands were amplified, this was consistent with the second allele containing a larger deletion that prevented amplification by the PCR primers. Comparatively, PCR screening identified a >3500 bp loss from the A3-7 clone for both alleles (Figure 4.4 and Figure 4.5). To further characterise the larger deletions in the HIF-2α CRISPR A3-7 alleles, primers amplifying from increasingly distal sites could be designed for PCR screening.

The loss of HIF-2α mRNA expression from both the HIF-2α CRISPR A3-7 and HIF-2α CRISPR B1-1 5TGM1 cell lines was confirmed via qPCR (Figure 4.6). However, attempts to detect the hypoxic upregulation of HIF-2α protein in 5TGM1 cells by western blotting and immunoprecipitation proved unsuccessful. Although this differed from the hypoxic induction of HIF-2α observed in human MM cell lines (Martin, Diamond et al. 2009), this was not completely unexpected. Functionally important factors, including transcription factors, are, in general, expressed at relatively low levels, often making them difficult to quantify or detect in cells (Ghaemmaghami, Huh et al. 2003, Vaquerizas, Kummerfeld et al. 2009). In addition, using the best available commercial antibodies, numerous other laboratories in this field have experienced considerable difficulty in detecting mouse HIF-2α protein in cell lines or *in vivo* compared to human HIF-2α (Dan Peet, personal communication). Efforts to optimise immunoprecipitation experiments in future should include screening other commercially available HIF-2α antibodies or creating a new antibody raised against murine HIF-2α. Immunoprecipitation could also be combined with subsequent mass spectrometry to improve detection of HIF-2α protein.

The 5TGM1 Cas9 EV, Cas9 EV2, HIF-2α CRISPR A3-7 and HIF-2α CRISPR B1-1 cell lines were injected into C57BL/KaLwRij mice and MM development assessed *in vivo*. Both Cas9 EV and Cas9 EV2 control lines disseminated throughout mice over 4 weeks (Figure 4.10), demonstrating that the modification of the 5TGM1 cells did not adversely affect their ability to generate MM disease *in vivo*. This was further confirmed by the presence of paraprotein in mouse blood serum (Figure 4.12) and by the establishment and dissemination of Cas9 EV control cells to the BM and spleen (Figure 4.11). MM cell dissemination to the spleen is not commonly seen in humans, but is often observed in animal models of the disease (Asosingh, Radl et al. 2000, Simmons, Hildreth et al. 2015).

Cellular colony formation within endosteal niches found within the BM has been observed previously with the 5TGM1 cell line (Lawson, McDonald et al. 2015). Furthermore, localised growth of 5TGM1 colonies in areas such as the distal femoral BM (Figure 4.11 A) is consistent with previous studies (Asosingh, De Raeve et al. 2005, Nombela-Arrieta, Pivarnik et al. 2013, Wang, Benedito et al. 2013). Singular MM cells were also located within the spleen but no colonies were evident, (Figure 4.11 D) consistent with previous findings demonstrating that single MM cells can lie dormant within tissue microenvironments for future relapse, rather than immediately proliferating to form colonies (Lawson, McDonald et al. 2015). Cellular dormancy has previously been proposed as a contributing aspect to MM disease progression and an important factor in MM therapy resistance and relapse (Kellner, Liu et al. 2013, Lawson, McDonald et al. 2015). As such, I propose that the single cells found within the spleen are dormant and could contribute to tumour growth in mice beyond the 4 week analysis time frame.

The HIF-2α CRISPR A3-7 and HIF-2α CRISPR B1-1 cell lines showed reduced to no tumour dissemination and disease development following 4 weeks of *in vivo* growth compared to the Cas9 EV and Cas9 EV2 controls, respectively (Figure 4.10 and 4.12). Specifically, analysis of tumour burden in individual mice at week 2, week 3 and week 4 post-injection with HIF-2α CRISPR B1-1 cells did not show a complete loss of tumour

compared to Cas9 EV2 mice, but rather a slower development of tumour expansion compared to Cas9 EV2 control injected mice (Figure 4.10 E). Despite this promising result, the comparative difference in tumour burden between Cas9 EV2 and HIF-2α CRISPR B1-1 injected mice did not reach significance. As only 3 out of 5 Cas9 EV2 injected mice developed tumour, future animal experiments should incorporate more mice per treatment group to reach significance.

Data for HIF-2α CRISPR A3-7 injected mice were more dramatic, showing no detectable tumour dissemination *in vivo*, even after 4 weeks (Figure 4.10). The complete lack of tumour growth was unlikely to be due to a general reduction in cellular proliferation, as these cells proliferated at a similar rate to the control cells when cultured Figure 4.8.

The difference observed between the significant lack of tumour burden in the HIF-2 CRISPR A3-7 mouse group and only a trend towards decreased tumour burden in the HIF-2α CRISPR B1-1 mouse group (Figure 4.10) could be due to a number of factors. The most likely contributing factors are experimental, specifically the gender differences between both groups, where the Cas9 EV and HIF-2α CRISPR A3-7 mice were female and the Cas9 EV2 and HIF-2α CRISPR B1-1 mice were male. It is known that there are gender-related differences in disease outcome in mouse studies (Trani, Moon et al. 2013, Amos-Landgraf, Heijmans et al. 2014). Furthermore, the staggered timing of animal injections between the HIF-2α CRISPR A3-7 and HIF-2α CRISPR B1-1 groups could have introduced variability, making direct comparisons between the two groups impossible. These factors can be addressed in future experiments by repeating the animal experiments in both genders for both knockout cell lines.

Additional factors, aside from those related to the animal experiment, include genetic variations between the two HIF-2α knockout cell lines, which is supported by the differential luciferase activity observed between the two cell lines (Figure 4.7). Further genetic characterisation of the cell lines, particularly the HIF-2α CRISPR A3-7 line, using PCR and sequencing would help clarify differences in *Hif2α* disruption between

the two lines that may be contributing to the *in vivo* data. Although there is considerable variation in tumour burden between the HIF-2α CRISPR A3-7 and HIF-2α CRISPR B1-1 cell lines, the Cas9 EV control lines that had been through the same transfection and selection process do not show any major differences in tumour development despite their difference in luciferase activity (Figure 4.7 and Figure 4.10 E). This strongly supported the dependence on the loss of HIF-2α expression for the observed decrease in tumour burden in 5TGM1 HIF-2α CRISPR A3-7 and HIF-2α CRISPR B1-1 injected C57BL/KaLwRij mice.

In conclusion, the work in this chapter showed that a loss of HIF-2α transcription factor expression in MM cells had a significant effect on MM disease, dramatically delaying progression. Furthermore, the loss of HIF-2α alone was sufficient to affect disease development, meaning that HIF-1α cannot compensate to maintain the normal rate of MM progression *in vivo*, confirming a non-redundant role for HIF-2α. These data demonstrate that HIF-2α is a critical contributing factor to MM disease and worthy of further investigation in terms of not only the spatial, temporal and mechanism of its function, but also as a potential therapeutic target for MM patients.

Chapter 5
FINAL DISCUSSION AND FUTURE DIRECTIONS

5.1 HIF-2α plays a critical role in MM disease progression

The work in this thesis tested multiple vector systems for use in the 5TGM1 MM cell line, with the aim of altering HIFα gene expression to assessing their role in MM disease progression. HIF-2α expression was successfully knocked out using CRISPR-Cas9 technology, therefore creating cell lines that were used to further characterise the role of HIF-2α in MM disease progression *in vivo*. Specifically, CRISPR-Cas9 knock out of HIF-2α in the 5TGM1 MM mouse model resulted in a delay in disease progression and an overall decrease in disease development.

5.1.1 Immediate future experiments: refining and expanding HIF-2α knockout in 5TGM1/C57BL/KaLwRij mice

Following the difficulties encountered in creating 5TGM1 cell lines stably overexpressing HIFα in Chapter 3, CRISPR-Cas9 technology was used to successfully generate HIF-2α knockout 5TGM1 lines suitable for the functional assessment of the role of HIF-2α in MM using the 5TGM1/C57BL/KaLwRij mouse model. Although the use of dual sgRNAs to generate HIF-1α knockout 5TGM1 cell lines was unsuccessful, alternative experimental techniques, such as those discussed in section 4.3, could be used to generate these cell lines. To this end, current studies in the laboratory are focused on generating HIF-1α knockout 5TGM1 lines that will enable head-to-head evaluation of the relative role of HIF-1α and HIF-2α in MM disease initiation and progression.

Initial studies used the HIF-2 CRISPR A3-7 and HIF-2 CRISPR B1-1 5TGM1 cells *in vivo*, where mice injected with HIF-2 CRISPR A3-7 displayed a significantly reduced tumour burden compared to control mice, whilst HIF-2 CRISPR B1-1 injected mice displayed a trend towards delayed disease progression compared to control mice. As proposed in section 4.3, in future experiments, both female and male mice should be used to eliminate potential gender-bias that may contribute to the difference in overall disease progression observed between HIF-2 CRISPR A3-7 and HIF-2 CRISPR B1-1 5TGM1 mouse groups compared to their Cas9 EV controls. Furthermore, repeating

the experiment in both genders would demonstrate that these data are reproducible and improve statistical significance.

To confirm the significance of HIF-2α in MM disease progression, complementary experiments could be performed using known HIF-2α inhibitors. The novel HIF-2α antagonist, PT2399, functions by disrupting the dimerisation of human HIF-2α and HIFβ. PT2399 has been successfully used to reduce tumour burden in preclinical xenograft mouse models of clear cell renal cell carcinoma (Chen, Hill et al. 2016, Cho, Du et al. 2016). Based on previous studies (Martin, Diamond et al. 2009), similar experiments could be performed in a MM Matrigel-graft model experiment. Specifically, 5TGM1 control or 5TGM1 HIF-2α knockout cells (generated as described in Chapter 4) could be mixed with Matrigel and subcutaneously injected into nude mice and the PT2399 administered at doses similar to those previously described (Chen, Hill et al. 2016, Cho, Du et al. 2016). Tumour development in response to PT2399 treatment could be assessed using bioluminescence imaging and tumour diameter measurements (Martin, Diamond et al. 2009). The inclusion of the 5TGM1 HIF-2α knockout cells would enable the anti-MM effects to be differentiated from any off-target effects the drug may have.

5.2   HIF-2α and MM PC homing and dissemination

The loss of HIF-2α expression in 5TGM1 cells did not result in the complete elimination of disease, but resulted in a delay in the establishment and progression of disease *in vivo* (Figure 4.10). The data presented here, showed that the 5TGM1 HIF-2α knockout cells could home to the BM and disseminate, but at a much slower rate than control cells. This significant reduction in tumour burden could not be attributed to the marginally slower proliferation rate of the knockout cells (Figure 4.8). A possible explanation, as described above, is that HIF-2α may play a critical role in MM PC migration, specifically, through processes involved in egress from the BM, dissemination and homing to other skeletal and splenic sites.

The homing of both non-malignant PCs and MM PCs is dependent on a number of ligand-cell surface receptor interactions including CD44 and HA (hyaluronan), CCR2 and MCP-1, uPAR and MMP9, CXCR4 and CXCL12 (Cyster 2003, Menu, Asosingh et al. 2004, Menu, Asosingh et al. 2006). Comparatively, less is known about the molecular processes that drive MM PC dissemination. A study by Azab *et al* (Azab, Hu et al. 2012), identified a correlation between BM hypoxia and MM PC egress, re-circulation and homing, with data suggesting a role for HIFα-regulated pathways. More recently, HIF-2α has been implicated as a potential regulator of MM PC dissemination through the CXCL12 and CCR1 pathways (Vandyke, Zeissig et al. 2017). MM PC homing and dissemination is critically important in MGUS to MM disease progression, and the re-population and growth of MM PCs in relapsed patients following treatment (Ghobrial 2012).

Further characterisation is required to ascertain the role of HIF-2α in either MM PC homing or dissemination or both, where *in vitro* and *in vivo* experiments using HIF-2α knockout MM cells could help identify HIF-2α-dependent molecular and biological pathways involved in these processes. Specifically, these experiments would be performed using 5TGM1 HIF-2α knockout cell lines (generated in Chapter 4), HIF-1α knockout and Cas9 EV control 5TGM1 cells. MM PC surface receptors such as

186

CXCR4, CD44, CCR2 and uPAR could be assessed using qPCR and flow cytometry to identify if HIF-2α directly regulates pathways associated with BM homing (CXCR4, CD44, CCR2 and uPAR) and dissemination (CXCR4 and CCR1). This could be supported by *in vitro* adhesion experiments, where HIF-2α knockout, HIF-1α knockout and Cas9 EV control 5TGM1 cells are plated onto BM stromal cells isolated from the femora of C57BL/KaLwRij mice (as described by Menu *et al* and Azab *et al* (Menu, Asosingh et al. 2006, Azab, Runnels et al. 2009)) to assess the effects of HIFα expression on cellular adhesion. In parallel to the adhesion assays, *in vitro* trans-well migration assays could be performed, as described previously (Menu, Asosingh et al. 2004, Menu, Asosingh et al. 2006, Azab, Hu et al. 2012, Vandyke, Zeissig et al. 2017), using MMP9 (MMP9 localises MM PCs to the extravascular compartment of the BM), MCP-1 (promotes migration to the BM endothelium) and CXCL12 as chemoattractants to assess the functional role of HIF-2α on these pathways.

Previous studies have shown that HIF-1α regulates MMP9 (Storti, Bolzoni et al. 2013) and that both HIF-1α and HIF-2α upregulate CXCL12 (Martin, Diamond et al. 2009). Combined with the observed delay in MM PC homing and dissemination *in vivo* (Figure 4.10), it is possible that functional HIF-1α could contribute to the delayed residual disease progression. As such, in the experiments proposed above, it would be expected that both 5TGM1 HIF-1α and HIF-2α knockout lines would display decreased adhesion and migration, with a greater decrease observed in the HIF-2α knockout cell lines. Furthermore, the assessment of cell surface receptors in HIF-1α and HIF-2α knockout cell lines may detect changes in some of the same factors, as previously demonstrated for the CXCL12/CXCR4 axis (Martin, Diamond et al. 2009, Azab, Hu et al. 2012). However, based on the data in chapter 4 and findings by Martin *et al* (Martin, Diamond et al. 2009), HIF-2α would be expected to have a greater effect on expression levels of some receptors such as CXCR4. Furthermore, as the knockout of HIF-2α appears to be non-redundant, it is also possible that unique factors displaying differential expression in HIF-2α and HIF-1α knockout cells may be identified.

To further characterise the potential contribution of HIF-2α to MM dissemination, the number of circulating MM cells in mice injected with HIF-2α knockout cells could be compared with mice injected with HIF-1α knockout and Cas9 EV control 5TGM1 cells using FACS. Whilst the *in vivo* bioluminescence imaging used in this dissertation allowed for the assessment of MM PC dissemination and tumour burden, recent developments in this methodology should be considered for future analyses of MM PC dissemination *in vivo*. A recent study by Iwano *et al* described the use of an evolved version of the luciferase/D-luciferin system called the AkaBLI system (Iwano, Sugiyama et al. 2018). These experiments utilised a composition of AkaLumine-HCL (substrate) and Akaluc (luciferase) and subsequent analysis in mice, allowing for the visualisation of single cells in deep tissues, in real time. The 5TGM1 HIF-2α CRISPR knockout lines, Cas9 EV control lines and HIF-1α knockout cell lines could be modified to express Akaluc, injected into C57BL/KaLwRij mice and used to analyse 5TGM1 dissemination over the 4-week disease model with higher sensitivity and accuracy then shown previously.

In addition to the experiments proposed above, detailed *in vivo* assessment of the effect of HIF-2α knockout in MM cells over time would be valuable to further characterise the role of HIF-2α in MM PC dissemination. Given the success of using CRISPR-Cas9 technology to knockout HIF-2α in the 5TGM1/C57BL/KaLwRij MM mouse model, an inducible CRISPR-Cas9 system could be advantageous. It is important to note that unlike the overexpression system generated in Chapter 3, which became unstable over time, the CRISPR-Cas9 knockout is permanent. Since the creation of the HIF-2α knockout lines and subsequent *in vivo* analyses described in this dissertation, inducible CRISPR-Cas9 experiments have been successfully performed on embryonic stem cell (ESC)-derived mice (Dow, Fisher et al. 2015). Specifically, this system would contain a plasmid encoding the sgRNA targeting HIF-2α and the Cas9 endonuclease under the control of a TRE3G promoter. Similar to the system used in Chapter 3, the TRE3G promoter would allow for the temporal knockout of HIF-2α following exposure to doxycycline treatment. Doxycycline treatment would be administered to HIF-2α knockout 5TGM1/C57BL/KaLwRij at various time points post-injection and the effect on tumour growth and dissemination assessed using *in*

vivo bioluminescence and, MM PC dissemination, could be evaluated using the Akaluc *in vivo* approaches. However, it should be noted that the inducible knockout *in vivo* would invariably result in a mixture of homozygous and heterozygous HIF-2α knockout cells and could complicate data interpretation.

5.3 The role of HIF-2α-regulated pathways in MM homing and dissemination

5.3.1 Candidate HIF-2α target genes potentially contributing to MM homing and dissemination

CXCL12 is a known disease marker for MM due to its elevated expression in patients, and its role in mediating MM PC migration, angiogenesis and bone resorption (Zannettino, Farrugia et al. 2005, Menu, Asosingh et al. 2006, Diamond, Labrinidis et al. 2009). Importantly, CXCL12 is known to be directly upregulated by HIF-2α, and to a lesser extent HIF-1α, in hypoxia, resulting in the promotion of tumour growth and angiogenesis in a MM disease context (Martin, Diamond et al. 2009). A recent publication by Vandyke *et al* (Vandyke, Zeissig et al. 2017) further explored these findings by assessing the role of the HIF-2α-CXCL12 regulation pathway on disease dissemination.

Homing of MM PCs to the BM is driven by a chemotactic response to CXCL12 expression from BM stromal cells (Menu, Asosingh et al. 2006, Alsayed, Ngo et al. 2007). The persistent expression of CXCL12 helps retain and expand the MM PCs within the BM, through CXCL12 and CXCR4 interactions. In order for cells to egress the BM and enter the circulation, a change in CXCL12-CXCR4 signalling between MM PCs and BM stromal cells is required, specifically through decreased expression of CXCR4 on MM PCs (Azab, Runnels et al. 2009, Bao, Lai et al. 2013, Stessman, Mansoor et al. 2013). Consistent with these findings, analyses of HIF-2α and CXCL12 expression in MM PCs suggest that both play a crucial role in regulating MM dissemination by overcoming the cellular response to exogenous CXCL12 stimuli (Vandyke, Zeissig et al. 2017). Specifically, overexpression of either HIF-2α or CXCL12 in RPMI-8226 MM cells resulted in a decrease of CXCR4 expression, migration towards CXCL12 and adhesion to BM mesenchymal stromal cells. The observed correlation between HIF-2α and MM PC migration is consistent with previous findings showing that hypoxic conditions within the BM promote MM PC circulation and tumour progression (Azab, Hu et al. 2012). These data directly implicate HIF-2α in MM

PC migration through its target gene CXCL12, therefore linking the HIF-2α-CXCL12 pathway with MM dissemination *in vitro*.

Analyses of CXCL12 expression from 5TGM1 HIF-2α CRISPR knockout cells *in vitro* and isolated *ex vivo*, as described in section 5.2, would help characterise the role of the HIF-2α-CXCL12 axis in MM disease progression. Based on data in section 5.2 and the known role of HIF-1α in CXCL12 regulation, it would be expected that CXCL12 expression will be reduced in HIF-1α knockout cells compared to the Cas9 EV controls. Importantly, CXCL12 expression would be further reduced in 5TGM1 HIF-2α knockout cells compared to 5TGM1 HIF-1α knockout and Cas9 EV control cells, but not completely abolished due to active HIF-1α.

In addition to CXCL12, the chemokine receptor CCR1 was also identified as a new potential HIF-2α-regulated target gene in MM dissemination (Vandyke, Zeissig et al. 2017). Whilst CCR1 has been previously identified as a HIF-1α target in hypoxia (Dong, Khalil et al. 2010, Copple, Bai et al. 2011), this was the first study to identify this chemokine as a HIF-2α target gene. CCR1 expression was upregulated following either hypoxia treatment or HIF-2α overexpression in the human LP-1 MM cell line. Additionally, the CCR1/CCL3 axis was found to promote MM PC migration independently of the CXCL12/CXCR4 axis, potentially nullifying the MM PC response to elevated BM CXCL12 expression. Furthermore, CCR1 upregulation was associated with elevated circulating MM PCs in patients that correlated with a poorer disease outcome. While this was the first study to correlate CCR1 expression with MM dissemination, the associated ligand CCL3 has been shown to be elevated in circulating MM cells and linked to migration *in vitro* (Moller, Stromberg et al. 2003, Terpos, Politou et al. 2003). Outside of the MM disease context, CCR1 has been linked with cellular migration and cancer metastasis (Kitamura, Fujishita et al. 2010, Hirai, Fujishita et al. 2014, Schanz, Red-Horse et al. 2014).

The role of CCR1 in MM dissemination as a HIF-2α-dependent target remains to be confirmed *in vivo*, and as such I propose analysing CCR1 expression in HIF-2α CRISPR knockout cells *in vitro* and isolated *ex vivo* from the 5TGM1 MM mouse model. It is important to note that like CXCL12, CCR1 is a confirmed HIF-1α target gene and would still be regulated by HIF-1α in MM, although to a lesser extent than that observed with HIF-2α, which is consistent with the lowered tumour burden still observed by *in vivo* bioluminescence (Figure 4.10).

5.3.2   Identification of novel HIF-2α target genes contributing to MM disease progression and confirmation of known targets

While emerging evidence highlight a role for HIF-2α in MM disease progression, very few HIF-2α-specific targets have been identified. As discussed in Chapter 1, it is known that the HIFs regulate hundreds of target genes that are cell type and context dependent. As such, it is critical to profile which target genes are significantly regulated by HIF-2α in MM PCs, to both confirm the target genes characterised in section 5.2 and 5.3.1, and to more broadly characterise the role of HIF-2α in MM PC disease progression. This could be achieved by performing RNAseq on 5TGM1 Cas9 EV control, HIF-1α and HIF-2α CRISPR knockout cell lines (section 5.1). Specifically, the Cas9 EV control, HIF-2α knockout and HIF-1α knockout cell lines would be cultured in normoxia and hypoxia for 48 hours to allow for the hypoxia-dependent upregulation of HIF-2α and HIF-1α-specific target genes.

While the data from these *in vitro* experiments would provide a general map of the pathways regulated by HIF-2α in 5TGM1 cells, these studies would be limited by the use of static hypoxic conditions without reference to the stimuli provided by a BM microenvironment *in vivo*. As such, it would be beneficial to complement these experiments with *in vivo* analyses using the 5TGM1/C57BL/KaLwRij mouse model. Specifically, the 5TGM1 Cas9 EV control, HIF-1α and HIF-2α knockout cell lines could be injected into C57BL/KaLwRij mice as previously described, and the GFP-expressing 5TGM1 cells isolated at various stages of disease progression using FACS. RNAseq could then be performed to assess the HIF-2α-dependent changes in gene

expression compared to control and 5TGM1 HIF-1α knockout injected mice. The genes identified from cell lines treated in hypoxia *in vitro* will be compared to the cells isolated *ex vivo*, providing valuable comparative analyses between an artificial hypoxic environment and the BM microenvironment. Furthermore, these data would characterise changes in gene expression at early versus late stages of disease that are directly affected by HIF-2α, providing novel insight with regard to the role of HIF-2α-regulated pathways at different stages of MM disease progression *in vivo*. Importantly, the RNAseq data from both the *in vitro* and *in vivo* experiments will confirm HIF-2α dependent regulation of genes known to be critical to MM, as well as potentially identify unknown targets for future studies.

5.4   Significance in other blood diseases

The findings detailed in this dissertation, showing that HIF-2α is critical for disease progression in MM, are in keeping with previous studies highlighting an association between HIFα expression and disease prognosis in other cancers (Lofstedt, Fredlund et al. 2007). HIFα activation has been explored in other blood diseases including acute myeloid leukemia (AML), acute promyelocytic leukemia (APL), acute lymphoblastic leukemia (ALL), chronic myeloblastic leukemia (CML) and chronic lymphoblastic leukemia (CLL) (Schito, Rey et al. 2017). In these cancers, upregulation of HIFα has been associated with malignant growth through a number of biological pathways including angiogenesis, metabolism, proliferation, homing, migration and metastasis. As has been observed in other diseases, the majority of data is centred around the role of HIF-1α, with a paucity of data on HIF-2α. Despite this, HIF-2α has still been implicated in a number of haematological diseases.

One such haematological disease, is AML, where comparative analyses of HIF-1α and HIF-2α function have been performed in hematopoietic stem cells (HSCs) and AML (Rouault-Pierre, Lopez-Onieva et al. 2013). Knock down of HIF-2α and HIF-1α resulted in HSC apoptosis and decreased engraftment of human AML cells in mice. Similarly, using mouse models of AML, overexpression of HIF-2α was found to result in accelerated disease development *in vivo* (Forristal, Brown et al. 2015).

Similarly, a comparative assessment of the role of HIF-1α and HIF-2α has been performed in the haematological disease APL. Genetic mutations are critical in APL pathogenesis, where *in vitro* and *in vivo* xenograft experiments demonstrated that HIF-1α, and to a lesser extent, HIF-2α, regulated pathways were activated to promote disease through cellular migration and angiogenesis (Coltella, Percio et al. 2014). Consistent with these findings, HIF-1α has recently been shown to regulate CLL cell migration, preventing expansion within the BM and spleen in mouse xenograft models, ultimately prolonging survival (Valsecchi, Coltella et al. 2016). Specifically, loss of HIF-

1α expression resulted in decreased chemotaxis and adhesion between CLL cells and BM stromal cells through the CXCL12/CXCR4 axis.

These data highlight the importance of HIFα and its regulated genes in other haematological diseases, and demonstrate both similarities and differences in the roles of HIF-1α and HIF-2α, as has been observed in MM. However, there is a general paucity of comparative HIF-1α and HIF-2α analyses and, more importantly, of HIF-2α-specific data in blood cancers. As such, the characterisation of HIF-2α in MM disease progression would provide significant findings that could inform other haematological diseases found to have abrogated HIF-2α expression in future.
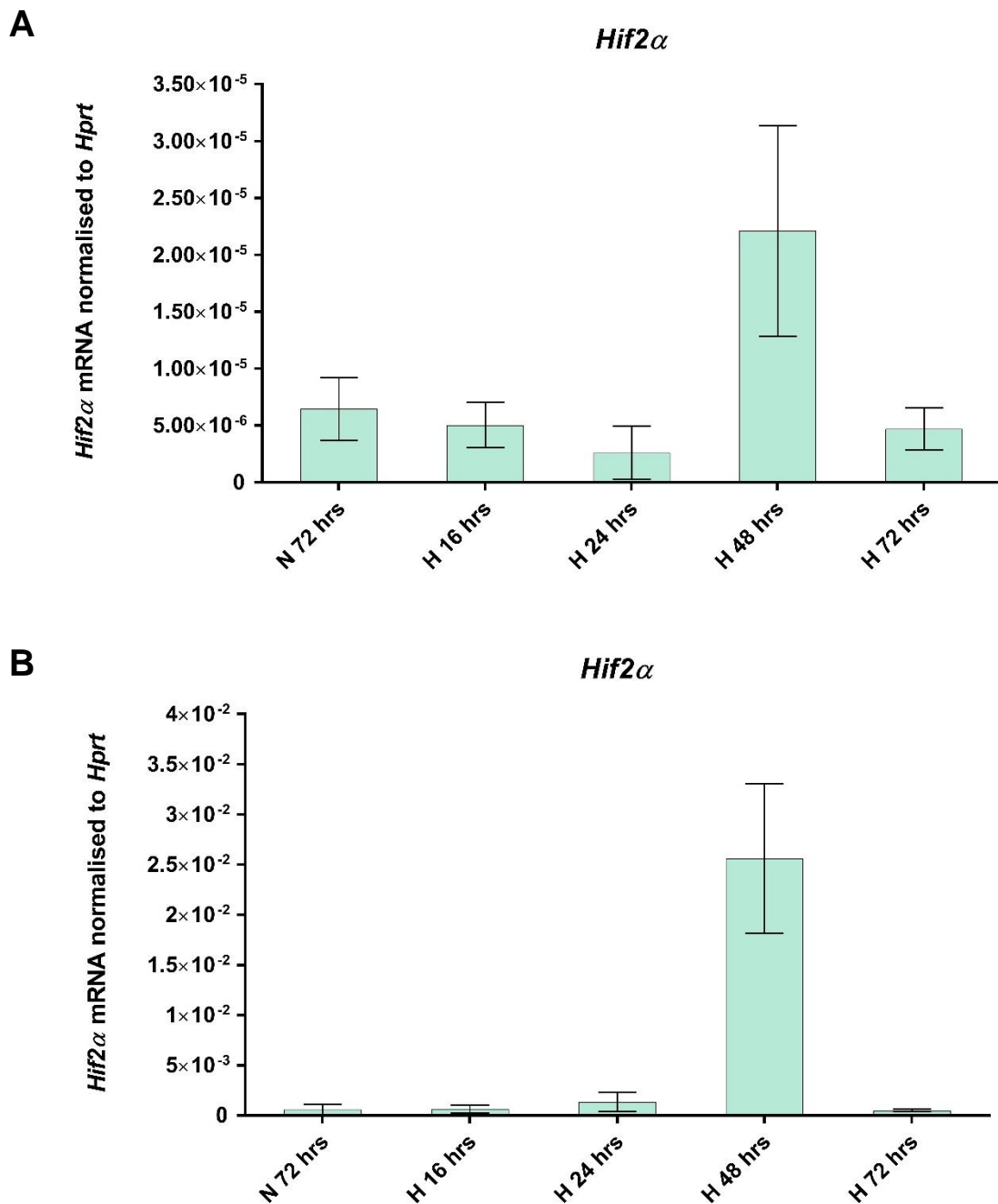
5.5 HIF-2α as a therapeutic target

Although MM is an incurable disease, current therapies including the proteasome inhibitor bortezomib (Richardson, Barlogie et al. 2003) and the immunomodulatory drugs thalidomide (Singhal, Mehta et al. 1999) and lenalidomide (Rajkumar, Hayman et al. 2005) have been used successfully to treat new and relapsed patients. Similarly, targeted drug treatment against specific oncogenes has shown to be effective for MM patients in clinical trials (Manier, Salem et al. 2016). Whilst complex combinations of mutations are acquired during the progression of MGUS to MM, many symptoms are common between patients. Identification and direct targeting of key contributors of disease would aid in the generation of new targeted treatments for MM.

MM PC migration and dissemination is crucial to disease progression, and importantly, for MM PCs to migrate and establish in new BM sites (Ghobrial 2012). As such, the number of circulating cells in the peripheral blood of newly diagnosed patients is used as an indicator for survival prognosis (Witzig, Gertz et al. 1996, Nowakowski, Witzig et al. 2005). Consistent with this finding, MM cells treated with a CXCR4 inhibitor displayed sensitivity to treatment, consistent with the role of CXCL12/CXCR4 axis in cellular migration (Azab, Runnels et al. 2009). Given the promising role of HIF-2α in regulating MM dissemination (Vandyke, Zeissig et al. 2017), HIF-2α could be an effective therapeutic target in both newly diagnosed and relapsed patients. To this end, a phase I clinical trial using the HIF-2α antagonist PT2385 is currently underway on patients with various forms of RCC and kidney cancer in the U.S.A (Identifier: NCT02293980). The trial is due for completion by the end of 2018 and will be informative on the potential use of PT2385 in other clinical trials, including future MM patient studies. Furthermore, the characterisation of homing and dissemination pathways proposed in this chapter, will identify known and potentially novel genes directly regulated by HIF-2α in MM *in vivo*, thereby identifying new target genes for future treatment development.

5.6   Concluding remarks

The research in this thesis has generated tools for the functional analysis of HIF-2α in a mouse model of MM. Preliminary experiments using CRISPR-Cas9 technology show that HIF-2α plays an important role in MM disease. The proposed future experiments will provide new insights into MM PC homing and dissemination and shed light on how HIF-2α regulates these crucial processes. The use of the HIF-2α knockout lines, alongside HIF-1α knockout lines generated in the future, will allow us to decipher the importance of HIF-2α and how it governs MM disease progression. As HIF-2α overexpression is likely to contribute to poor prognosis and relapse, therapies targeting HIF-2α may prove useful in the treatment in MM patients. Furthermore, by defining the contribution of HIF-2α-regulated pathways in MM, the cell lines created could also be used to help identify novel downstream therapeutic targets.

APPENDICES

A

B

Appendix 1: *Hif2α* gene expression in response to hypoxia in 5TGM1 cells. 5TGM1 cells were cultured in normoxia (N) for 72 hours or hypoxia (H) for 16, 24, 48 and 72 hours. RNA was extracted and equivalent amounts were reverse transcribed and used for quantitative PCR analysis performed using *Hif2α* primers. Relative expression of each gene was normalised to the housekeeping gene *Hprt*. Data are graphed as the mean of triplicate samples +/- standard error of the mean from a single experiment (A and B), and are 2 representatives of 3 independent experiments.

A

B
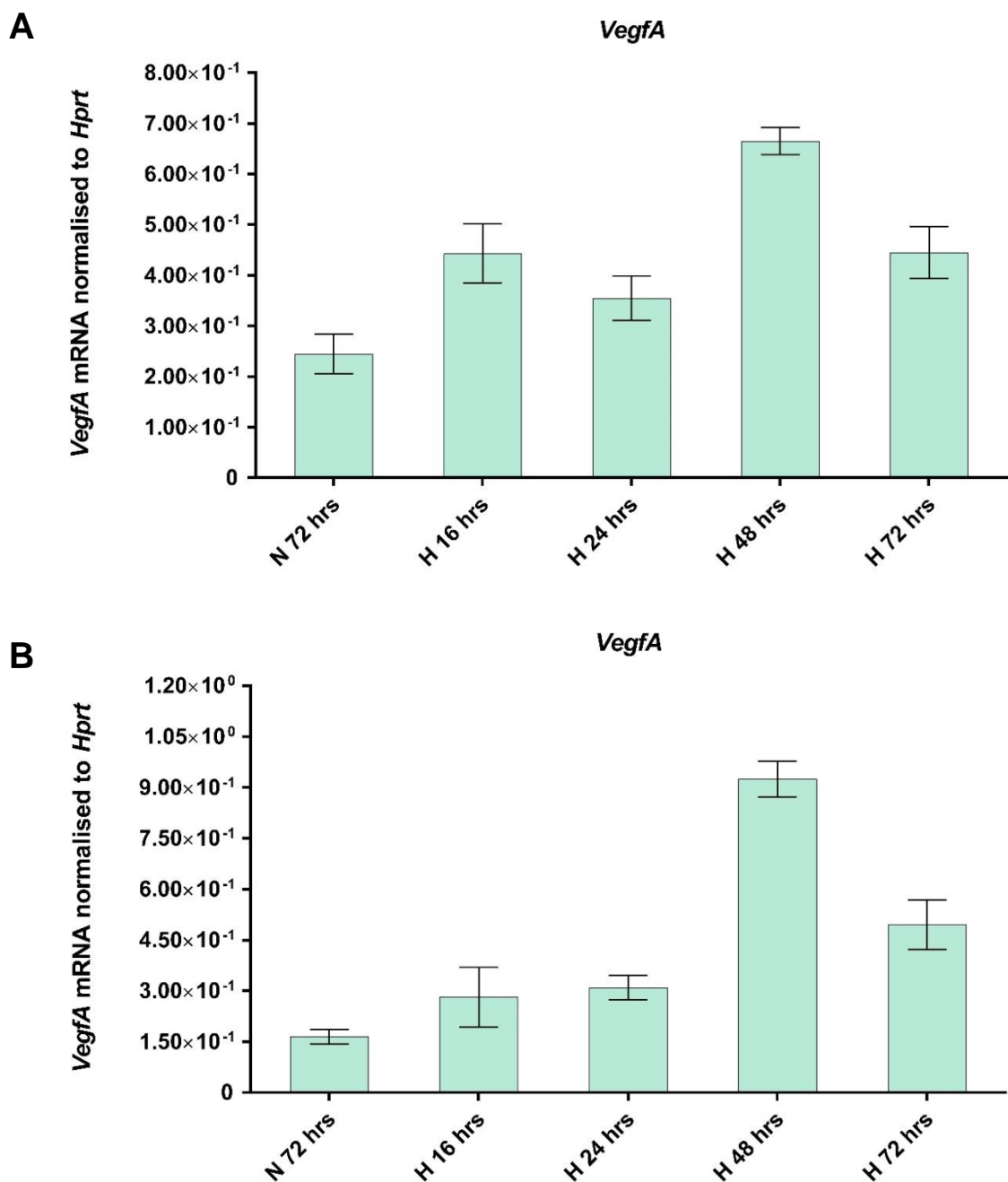
Appendix 2: *VegfA* gene expression in response to hypoxia in 5TGM1 cells. 5TGM1 cells were cultured in normoxia (N) for 72 hours or hypoxia (H) for 16, 24, 48 and 72 hours. RNA was extracted and equivalent amounts were reverse transcribed and used for quantitative PCR analysis performed using *VegfA* primers. Relative expression of each gene was normalised to the housekeeping gene *Hprt*. Data are graphed as the mean of triplicate samples +/- standard error of the mean from a single experiment (A and B), and are 2 representatives of 3 independent experiments.

A

B

Appendix 3: *Bnip3* gene expression in response to hypoxia in 5TGM1 cells. 5TGM1 cells were cultured in normoxia (N) for 72 hours or hypoxia (H) for 16, 24, 48 and 72 hours. RNA was extracted and equivalent amounts were reverse transcribed and used for quantitative PCR analysis performed using *Bnip3* primers. Relative expression of each gene was normalised to the housekeeping gene *Hprt*. Data are graphed as the mean of triplicate samples +/- standard error of the mean from a single experiment (A and B), and are 2 representatives of 3 independent experiments.
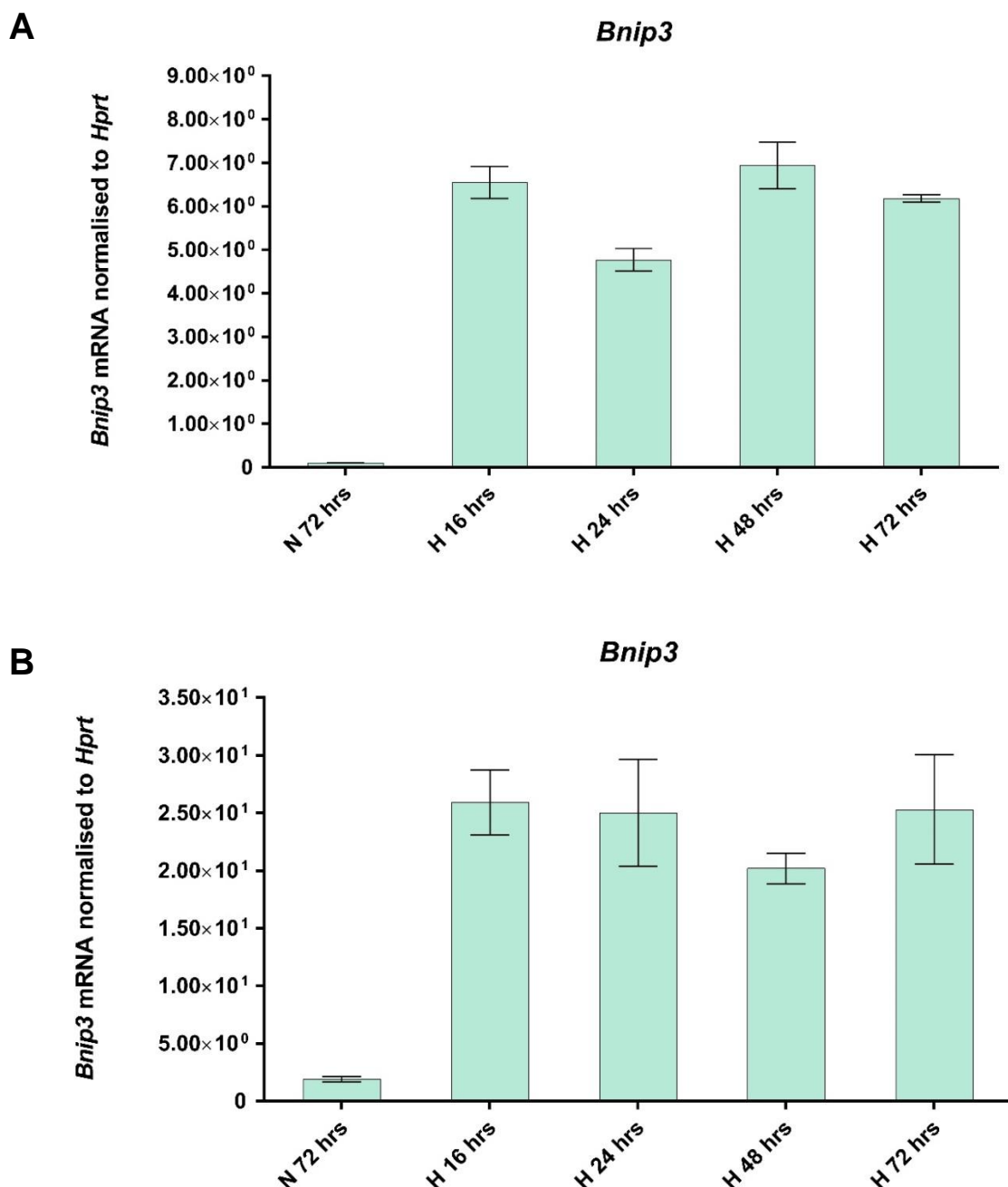
A

B
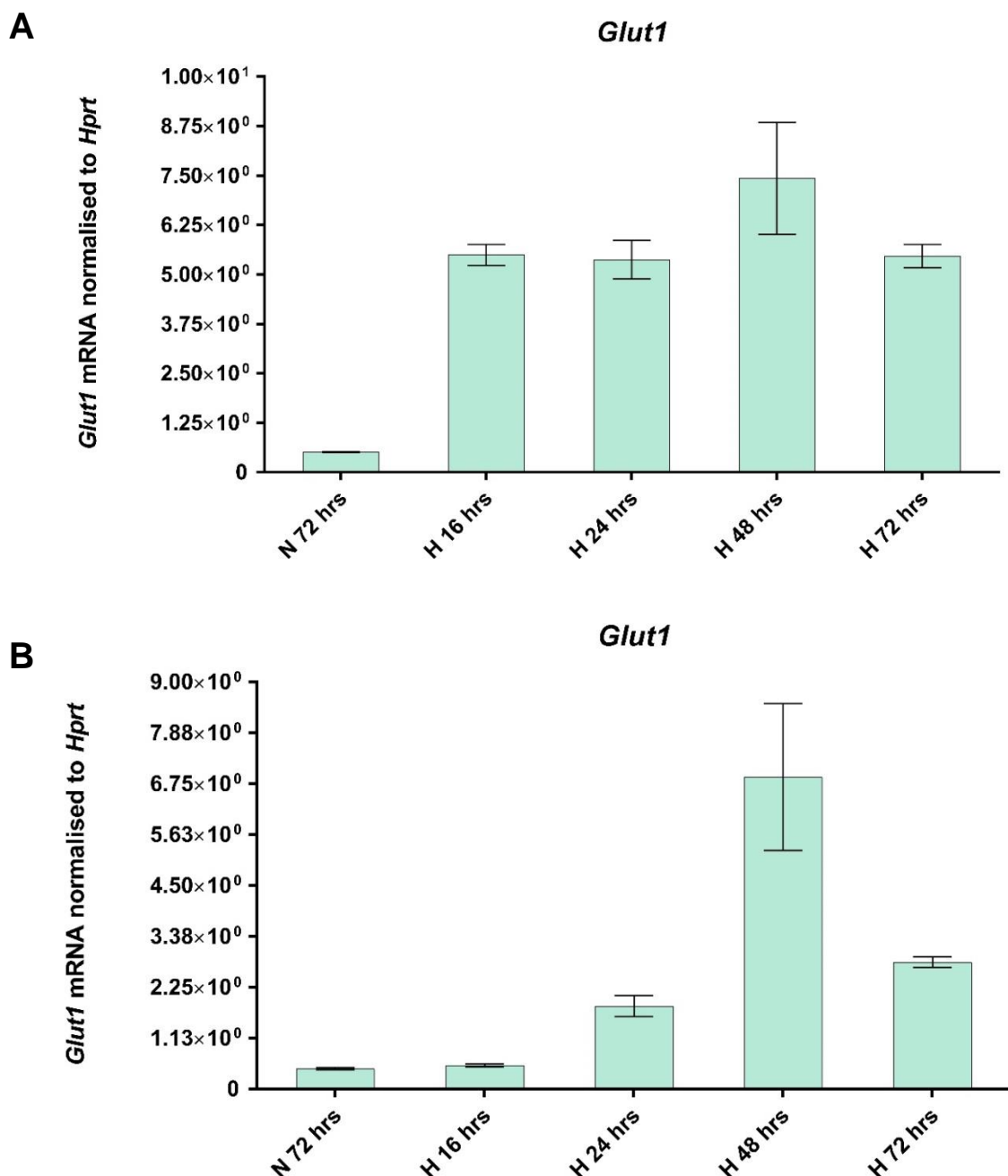
Appendix 4: *Glut1* gene expression in response to hypoxia in 5TGM1 cells. 5TGM1 cells were cultured in normoxia (N) for 72 hours or hypoxia (H) for 16, 24, 48 and 72 hours. RNA was extracted and equivalent amounts were reverse transcribed and used for quantitative PCR analysis performed using *Glut1* primers. Relative expression of each gene was normalised to the housekeeping gene *Hprt*. Data are graphed as the mean of triplicate samples +/- standard error of the mean from a single experiment (A and B), and are 2 representatives of 3 independent experiments.
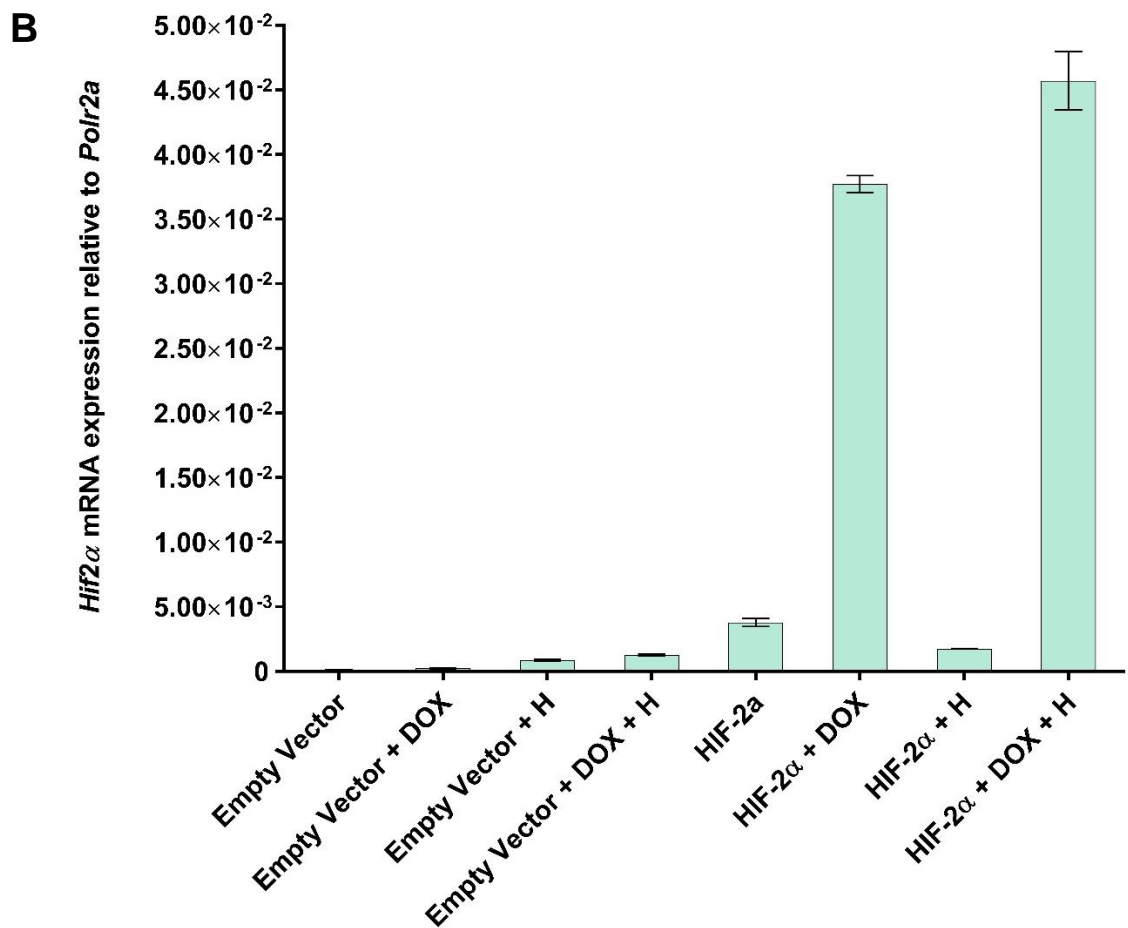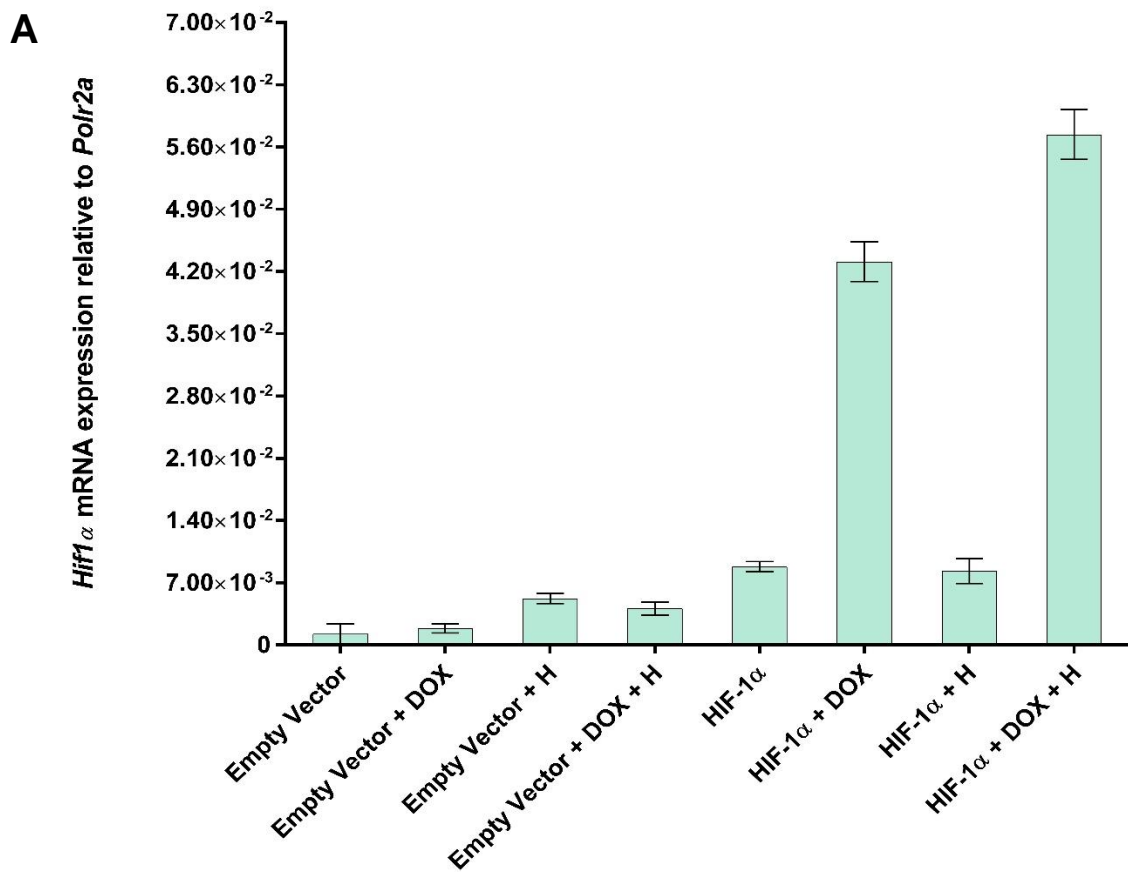
Appendix 5: Assessment of *Hif1α* and *Hif2α* mRNA induction in 5TGM1 cells integrated with the LVT-HIFα-ETPT vector. 5TGM1 cell lines were infected with lentivirus particles containing either the LVTETPT, LVT-HIF-1α-EPTP, or LVT-HIF-2α-EPTP vectors and where specified, cultured for 16 hours with no treatment, in hypoxia (+H), with doxycycline at a final concentration of 2 μg/mL (+DOX) or both (+DOX+H). Cellular mRNA was extracted and cDNA produced for quantitative PCR analysis. Samples were then assessed for either *Hif1α* (A) or *Hif2α* (B) mRNA expression normalised to the housekeeping gene *Polr2a*. Data are representative of three independent experiments.

A

B

Appendix 6: Assessment of *Hif1α* and *Hif2α* mRNA induction in 5TGM1 cells integrated with the LVT-HIFα-ETPT vector. 5TGM1 cell lines were infected with lentivirus particles containing either the LVTETPT, LVT-HIF-1α-EPTP, or LVT-HIF-2α-EPTP vectors and where specified, cultured for 16 hours with no treatment, in hypoxia (+H), with doxycycline at a final concentration of 2 µg/mL (+DOX) or both (+DOX+H). Cellular mRNA was extracted and cDNA produced for quantitative PCR analysis. Samples were then assessed for either *Hif1α* (A) or *Hif2α* (B) mRNA expression normalised to the housekeeping gene *Polr2a*. Data are representative of three independent experiments.

REFERENCES

Alici, E., K. V. Konstantinidis, A. Aints, M. S. Dilber and M. Abedi-Valugerdi (2004). "Visualization of 5T33 myeloma cells in the C57BL/KaLwRij mouse: establishment of a new syngeneic murine model of multiple myeloma." Exp Hematol **32**(11): 1064-1072.

Alsayed, Y., H. Ngo, J. Runnels, X. Leleu, U. K. Singha, C. M. Pitsillides, J. A. Spencer, T. Kimlinger, J. M. Ghobrial, X. Jia, G. Lu, M. Timm, A. Kumar, D. Cote, I. Veilleux, K. E. Hedin, G. D. Roodman, T. E. Witzig, A. L. Kung, T. Hideshima, K. C. Anderson, C. P. Lin and I. M. Ghobrial (2007). "Mechanisms of regulation of CXCR4/SDF-1 (CXCL12)-dependent migration and homing in multiple myeloma." Blood **109**(7): 2708-2717.

Amos-Landgraf, J. M., J. Heijmans, M. C. Wielenga, E. Dunkin, K. J. Krentz, L. Clipson, A. G. Ederveen, P. G. Groothuis, S. Mosselman, V. Muncan, D. W. Hommes, A. Shedlovsky, W. F. Dove and G. R. van den Brink (2014). "Sex disparity in colonic adenomagenesis involves promotion by male hormones, not protection by female hormones." Proc Natl Acad Sci U S A **111**(46): 16514-16519.

Ansel, K. M., R. B. Harris and J. G. Cyster (2002). "CXCL13 is required for B1 cell homing, natural antibody production, and body cavity immunity." Immunity **16**(1): 67-76.

Appelhoff, R. J., Y. M. Tian, R. R. Raval, H. Turley, A. L. Harris, C. W. Pugh, P. J. Ratcliffe and J. M. Gleadle (2004). "Differential function of the prolyl hydroxylases PHD1, PHD2, and PHD3 in the regulation of hypoxia-inducible factor." J Biol Chem **279**(37): 38458-38465.

Aragones, J., P. Fraisl, M. Baes and P. Carmeliet (2009). "Oxygen sensors at the crossroad of metabolism." Cell Metab **9**(1): 11-22.

Arpin, C., J. Dechanet, C. Van Kooten, P. Merville, G. Grouard, F. Briere, J. Banchereau and Y. J. Liu (1995). "Generation of memory B cells and plasma cells in vitro." Science **268**(5211): 720-722.

Asosingh, K., H. De Raeve, M. de Ridder, G. A. Storme, A. Willems, I. Van Riet, B. Van Camp and K. Vanderkerken (2005). "Role of the hypoxic bone marrow microenvironment in 5T2MM murine myeloma tumor progression." Haematologica **90**(6): 810-817.

Asosingh, K., H. De Raeve, E. Menu, I. Van Riet, E. Van Marck, B. Van Camp and K. Vanderkerken (2004). "Angiogenic switch during 5T2MM murine myeloma tumorigenesis: role of CD45 heterogeneity." Blood **103**(8): 3131-3137.

Asosingh, K., H. De Raeve, I. Van Riet, B. Van Camp and K. Vanderkerken (2003). "Multiple myeloma tumor progression in the 5T2MM murine model is a multistage and dynamic process of differentiation, proliferation, invasion, and apoptosis." Blood **101**(8): 3136-3141.

Asosingh, K., J. Radl, I. Van Riet, B. Van Camp and K. Vanderkerken (2000). "The 5TMM series: a useful in vivo mouse model of human multiple myeloma." Hematol J **1**(5): 351-356.

Azab, A. K., J. Hu, P. Quang, F. Azab, C. Pitsillides, R. Awwad, B. Thompson, P. Maiso, J. D. Sun, C. P. Hart, A. M. Roccaro, A. Sacco, H. T. Ngo, C. P. Lin, A. L. Kung, R. D. Carrasco, K. Vanderkerken and I. M. Ghobrial (2012). "Hypoxia promotes dissemination of multiple myeloma through acquisition of epithelial to mesenchymal transition-like features." Blood **119**(24): 5782-5794.

Azab, A. K., J. M. Runnels, C. Pitsillides, A. S. Moreau, F. Azab, X. Leleu, X. Jia, R. Wright, B. Ospina, A. L. Carlson, C. Alt, N. Burwick, A. M. Roccaro, H. T. Ngo, M. Farag, M. R. Melhem, A. Sacco, N. C. Munshi, T. Hideshima, B. J. Rollins, K. C. Anderson, A. L. Kung, C. P. Lin and I. M. Ghobrial (2009). "CXCR4 inhibitor AMD3100 disrupts the interaction of multiple myeloma cells with the bone marrow microenvironment and enhances their sensitivity to therapy." Blood **113**(18): 4341-4351.

Bakhashab, S., S. Lary, F. Ahmed, H. J. Schulten, A. Bashir, F. W. Ahmed, A. L. Al-Malki, H. S. Jamal, M. A. Gari and J. U. Weaver (2014). "Reference genes for expression studies in hypoxia and hyperglycemia models in human umbilical vein endothelial cells." G3 (Bethesda) **4**(11): 2159-2165.

Bao, L., Y. Lai, Y. Liu, Y. Qin, X. Zhao, X. Lu, Q. Jiang, J. Lu and X. Huang (2013). "CXCR4 is a good survival prognostic indicator in multiple myeloma patients." Leuk Res **37**(9): 1083-1088.

Barrett, J. M., K. A. Parham, J. B. Pippal, M. P. Cockshell, P. A. Moretti, S. L. Brice, S. M. Pitson and C. S. Bonder (2011). "Over-expression of sphingosine kinase-1 enhances a progenitor phenotype in human endothelial cells." Microcirculation **18**(7): 583-597.

Beard, C., K. Hochedlinger, K. Plath, A. Wutz and R. Jaenisch (2006). "Efficient method to generate single-copy transgenic mice by site-specific integration in embryonic stem cells." Genesis **44**(1): 23-28.

Benita, Y., H. Kikuchi, A. D. Smith, M. Q. Zhang, D. C. Chung and R. J. Xavier (2009). "An integrative genomics approach identifies Hypoxia Inducible Factor-1 (HIF-1)-target genes that form the core response to hypoxia." Nucleic Acids Res **37**(14): 4587-4602.

Berenson, J. R. (2005). "Myeloma bone disease." Best Pract Res Clin Haematol **18**(4): 653-672.

Berra, E., E. Benizri, A. Ginouves, V. Volmat, D. Roux and J. Pouyssegur (2003). "HIF prolyl-hydroxylase 2 is the key oxygen sensor setting low steady-state levels of HIF-1alpha in normoxia." Embo j **22**(16): 4082-4090.

Bersten, D. C., A. E. Sullivan, D. Li, V. Bhakti, S. J. Bent and M. L. Whitelaw (2015). "Inducible and reversible lentiviral and Recombination Mediated Cassette Exchange (RMCE) systems for controlling gene expression." PLoS One **10**(3): e0116373.

Bianchi, G. and K. C. Anderson (2014). "Understanding biology to tackle the disease: Multiple myeloma from bench to bedside, and back." CA Cancer J Clin **64**(6): 422-444.

Birgegard, G., P. Gascon and H. Ludwig (2006). "Evaluation of anaemia in patients with multiple myeloma and lymphoma: findings of the European CANCER ANAEMIA SURVEY." Eur J Haematol **77**(5): 378-386.

Biswas, S., H. Troy, R. Leek, Y. L. Chung, J. L. Li, R. R. Raval, H. Turley, K. Gatter, F. Pezzella, J. R. Griffiths, M. Stubbs and A. L. Harris (2010). "Effects of HIF-1alpha and HIF2alpha on Growth and Metabolism of Clear-Cell Renal Cell Carcinoma 786-0 Xenografts." J Oncol **2010**: 757908.

Borsi, E., G. Perrone, C. Terragna, M. Martello, A. F. Dico, G. Solaini, A. Baracca, G. Sgarbi, G. Pasquinelli, S. Valente, E. Zamagni, P. Tacchetti, G. Martinelli and M. Cavo (2014). "Hypoxia inducible factor-1 alpha as a therapeutic target in multiple myeloma." Oncotarget **5**(7): 1779-1792.

Borsi, E., G. Perrone, C. Terragna, M. Martello, E. Zamagni, P. Tacchetti, L. Pantani, A. Brioli, A. F. Dico, B. A. Zannetti, S. Rocchi and M. Cavo (2014). "HIF-1alpha inhibition blocks the cross talk between multiple myeloma plasma cells and tumor microenvironment." Exp Cell Res **328**(2): 444-455.

Boutin, A. T., A. Weidemann, Z. Fu, L. Mesropian, K. Gradin, C. Jamora, M. Wiesener, K. U. Eckardt, C. J. Koch, L. G. Ellies, G. Haddad, V. H. Haase, M. C. Simon, L. Poellinger, F. L. Powell and R. S. Johnson (2008). "Epidermal sensing of oxygen is essential for systemic hypoxic response." Cell **133**(2): 223-234.

Bracken, C. P., A. O. Fedele, S. Linke, W. Balrak, K. Lisy, M. L. Whitelaw and D. J. Peet (2006). "Cell-specific regulation of hypoxia-inducible factor (HIF)-1alpha and HIF-2alpha stabilization and transactivation in a graded oxygen environment." J Biol Chem **281**(32): 22575-22585.

Bruick, R. K. and S. L. McKnight (2001). "A conserved family of prolyl-4-hydroxylases that modify HIF." Science **294**(5545): 1337-1340.

Campo, E., S. H. Swerdlow, N. L. Harris, S. Pileri, H. Stein and E. S. Jaffe (2011). "The 2008 WHO classification of lymphoid neoplasms and beyond: evolving concepts and practical applications." Blood **117**(19): 5019-5032.

Canver, M. C., D. E. Bauer, A. Dass, Y. Y. Yien, J. Chung, T. Masuda, T. Maeda, B. H. Paw and S. H. Orkin (2014). "Characterization of genomic deletion efficiency

mediated by clustered regularly interspaced palindromic repeats (CRISPR)/Cas9 nuclease system in mammalian cells." J Biol Chem **289**(31): 21312-21324.

Carey, B. W., S. Markoulaki, C. Beard, J. Hanna and R. Jaenisch (2010). "Single-gene transgenic mouse strains for reprogramming adult somatic cells." Nat Methods **7**(1): 56-59.

Chen, W., H. Hill, A. Christie, M. S. Kim, E. Holloman, A. Pavia-Jimenez, F. Homayoun, Y. Ma, N. Patel, P. Yell, G. Hao, Q. Yousuf, A. Joyce, I. Pedrosa, H. Geiger, H. Zhang, J. Chang, K. H. Gardner, R. K. Bruick, C. Reeves, T. H. Hwang, K. Courtney, E. Frenkel, X. Sun, N. Zojwalla, T. Wong, J. P. Rizzi, E. M. Wallace, J. A. Josey, Y. Xie, X. J. Xie, P. Kapur, R. M. McKay and J. Brugarolas (2016). "Targeting renal cell carcinoma with a HIF-2 antagonist." Nature **539**(7627): 112-117.

Cheong, C. M., A. W. Chow, S. Fitter, D. R. Hewett, S. K. Martin, S. A. Williams, L. B. To, A. C. Zannettino and K. Vandyke (2015). "Tetraspanin 7 (TSPAN7) expression is upregulated in multiple myeloma patients and inhibits myeloma tumour development in vivo." Exp Cell Res **332**(1): 24-38.

Chng, W. J., S. Kumar, S. Vanwier, G. Ahmann, T. Price-Troska, K. Henderson, T. H. Chung, S. Kim, G. Mulligan, B. Bryant, J. Carpten, M. Gertz, S. V. Rajkumar, M. Lacy, A. Dispenzieri, R. Kyle, P. Greipp, P. L. Bergsagel and R. Fonseca (2007). "Molecular dissection of hyperdiploid multiple myeloma by gene expression profiling." Cancer Res **67**(7): 2982-2989.

Cho, H., X. Du, J. P. Rizzi, E. Liberzon, A. A. Chakraborty, W. Gao, I. Carvo, S. Signoretti, R. K. Bruick, J. A. Josey, E. M. Wallace and W. G. Kaelin (2016). "On-target efficacy of a HIF-2alpha antagonist in preclinical kidney cancer models." Nature **539**(7627): 107-111.

Choi, S. M., H. Oh and H. Park (2008). "Microarray analyses of hypoxia-regulated genes in an aryl hydrocarbon receptor nuclear translocator (Arnt)-dependent manner." Febs j **275**(22): 5618-5634.

Christian, M., T. Cermak, E. L. Doyle, C. Schmidt, F. Zhang, A. Hummel, A. J. Bogdanove and D. F. Voytas (2010). "Targeting DNA double-strand breaks with TAL effector nucleases." Genetics **186**(2): 757-761.

Coltella, N., S. Percio, R. Valsecchi, R. Cuttano, J. Guarnerio, M. Ponzoni, P. P. Pandolfi, G. Melillo, L. Pattini and R. Bernardi (2014). "HIF factors cooperate with PML-RARalpha to promote acute promyelocytic leukemia progression and relapse." EMBO Mol Med **6**(5): 640-650.

Compernolle, V., K. Brusselmans, T. Acker, P. Hoet, M. Tjwa, H. Beck, S. Plaisance, Y. Dor, E. Keshet, F. Lupu, B. Nemery, M. Dewerchin, P. Van Veldhoven, K. Plate, L. Moons, D. Collen and P. Carmeliet (2002). "Loss of HIF-2alpha and inhibition of VEGF

impair fetal lung maturation, whereas treatment with VEGF prevents fatal respiratory distress in premature mice." Nat Med **8**(7): 702-710.

Cong, L., F. A. Ran, D. Cox, S. Lin, R. Barretto, N. Habib, P. D. Hsu, X. Wu, W. Jiang, L. A. Marraffini and F. Zhang (2013). "Multiplex genome engineering using CRISPR/Cas systems." Science **339**(6121): 819-823.

Copple, B. L., S. Bai, L. D. Burgoon and J. O. Moon (2011). "Hypoxia-inducible factor-1alpha regulates the expression of genes in hypoxic hepatic stellate cells important for collagen deposition and angiogenesis." Liver Int **31**(2): 230-244.

Cramer, T., Y. Yamanishi, B. E. Clausen, I. Forster, R. Pawlinski, N. Mackman, V. H. Haase, R. Jaenisch, M. Corr, V. Nizet, G. S. Firestein, H. P. Gerber, N. Ferrara and R. S. Johnson (2003). "HIF-1alpha is essential for myeloid cell-mediated inflammation." Cell **112**(5): 645-657.

Cyster, J. G. (2003). "Homing of antibody secreting cells." Immunol Rev **194**: 48-60.

Dallas, S. L., I. R. Garrett, B. O. Oyajobi, M. R. Dallas, B. F. Boyce, F. Bauss, J. Radl and G. R. Mundy (1999). "Ibandronate reduces osteolytic lesions but not tumor burden in a murine model of myeloma bone disease." Blood **93**(5): 1697-1706.

Degrassi, A., D. M. Hilbert, S. Rudikoff, A. O. Anderson, M. Potter and H. G. Coon (1993). "In vitro culture of primary plasmacytomas requires stromal cell feeder layers." Proc Natl Acad Sci U S A **90**(5): 2060-2064.

Dengler, V. L., M. D. Galbraith and J. M. Espinosa (2014). "Transcriptional regulation by hypoxia inducible factors." Crit Rev Biochem Mol Biol **49**(1): 1-15.

Diamond, P., A. Labrinidis, S. K. Martin, A. N. Farrugia, S. Gronthos, L. B. To, N. Fujii, P. D. O'Loughlin, A. Evdokiou and A. C. Zannettino (2009). "Targeted disruption of the CXCL12/CXCR4 axis inhibits osteolysis in a murine model of myeloma-associated bone loss." J Bone Miner Res **24**(7): 1150-1161.

Dimopoulos, M. A., E. Kastritis, L. Rosinol, J. Blade and H. Ludwig (2008). "Pathogenesis and treatment of renal failure in multiple myeloma." Leukemia **22**(8): 1485-1493.

Dobie, K. W., M. Lee, J. A. Fantes, E. Graham, A. J. Clark, A. Springbett, R. Lathe and M. McClenaghan (1996). "Variegated transgene expression in mouse mammary gland is determined by the transgene integration locus." Proc Natl Acad Sci U S A **93**(13): 6659-6664.

Doench, J. G., E. Hartenian, D. B. Graham, Z. Tothova, M. Hegde, I. Smith, M. Sullender, B. L. Ebert, R. J. Xavier and D. E. Root (2014). "Rational design of highly

active sgRNAs for CRISPR-Cas9-mediated gene inactivation." Nat Biotechnol **32**(12): 1262-1267.

Dong, F., M. Khalil, M. Kiedrowski, C. O'Connor, E. Petrovic, X. Zhou and M. S. Penn (2010). "Critical role for leukocyte hypoxia inducible factor-1alpha expression in post-myocardial infarction left ventricular remodeling." Circ Res **106**(3): 601-610.

Doudna, J. A. and E. Charpentier (2014). "Genome editing. The new frontier of genome engineering with CRISPR-Cas9." Science **346**(6213): 1258096.

Dow, L. E., J. Fisher, K. P. O'Rourke, A. Muley, E. R. Kastenhuber, G. Livshits, D. F. Tschaharganeh, N. D. Socci and S. W. Lowe (2015). "Inducible in vivo genome editing with CRISPR-Cas9." Nat Biotechnol **33**(4): 390-394.

Edwards, C. M., J. R. Edwards, S. T. Lwin, J. Esparza, B. O. Oyajobi, B. McCluskey, S. Munoz, B. Grubbs and G. R. Mundy (2008). "Increasing Wnt signaling in the bone marrow microenvironment inhibits the development of myeloma bone disease and reduces tumor burden in bone in vivo." Blood **111**(5): 2833-2842.

Edwards, C. M., J. Zhuang and G. R. Mundy (2008). "The pathogenesis of the bone disease of multiple myeloma." Bone **42**(6): 1007-1013.

Eleutherakis-Papaiakovou, V., A. Bamias, D. Gika, A. Simeonidis, A. Pouli, A. Anagnostopoulos, E. Michali, T. Economopoulos, K. Zervas and M. A. Dimopoulos (2007). "Renal failure in multiple myeloma: incidence, correlations, and prognostic significance." Leuk Lymphoma **48**(2): 337-341.

Eliasson, P. and J. I. Jonsson (2010). "The hematopoietic stem cell niche: low in oxygen but a nice place to be." J Cell Physiol **222**(1): 17-22.

Ellis, J. (2005). "Silencing and variegation of gammaretrovirus and lentivirus vectors." Hum Gene Ther **16**(11): 1241-1246.

Ellis, J. and S. Yao (2005). "Retrovirus silencing and vector design: relevance to normal and cancer stem cells?" Curr Gene Ther **5**(4): 367-373.

Elvidge, G. P., L. Glenny, R. J. Appelhoff, P. J. Ratcliffe, J. Ragoussis and J. M. Gleadle (2006). "Concordant regulation of gene expression by hypoxia and 2-oxoglutarate-dependent dioxygenase inhibition: the role of HIF-1alpha, HIF-2alpha, and other pathways." J Biol Chem **281**(22): 15215-15226.

Epstein, A. C., J. M. Gleadle, L. A. McNeill, K. S. Hewitson, J. O'Rourke, D. R. Mole, M. Mukherji, E. Metzen, M. I. Wilson, A. Dhanda, Y. M. Tian, N. Masson, D. L. Hamilton, P. Jaakkola, R. Barstead, J. Hodgkin, P. H. Maxwell, C. W. Pugh, C. J. Schofield and P. J. Ratcliffe (2001). "C. elegans EGL-9 and mammalian homologs define a family of dioxygenases that regulate HIF by prolyl hydroxylation." Cell **107**(1): 43-54.

Ferlay, J., I. Soerjomataram, R. Dikshit, S. Eser, C. Mathers, M. Rebelo, D. M. Parkin, D. Forman and F. Bray (2015). "Cancer incidence and mortality worldwide: sources, methods and major patterns in GLOBOCAN 2012." Int J Cancer **136**(5): E359-386.

Forristal, C. E., A. L. Brown, F. M. Helwani, I. G. Winkler, B. Nowlan, V. Barbier, R. J. Powell, G. A. Engler, S. M. Diakiw, A. C. Zannettino, S. Martin, D. Pattabiraman, R. J. D'Andrea, I. D. Lewis and J. P. Levesque (2015). "Hypoxia inducible factor (HIF)-2alpha accelerates disease progression in mouse models of leukemia and lymphoma but is not a poor prognosis factor in human AML." Leukemia **29**(10): 2075-2085.

Fu, Y., J. A. Foden, C. Khayter, M. L. Maeder, D. Reyon, J. K. Joung and J. D. Sander (2013). "High-frequency off-target mutagenesis induced by CRISPR-Cas nucleases in human cells." Nat Biotechnol **31**(9): 822-826.

Gado, K., S. Silva, K. Paloczi, G. Domjan and A. Falus (2001). "Mouse plasmacytoma: an experimental model of human multiple myeloma." Haematologica **86**(3): 227-236.

Garrett, I. R., S. Dallas, J. Radl and G. R. Mundy (1997). "A murine model of human myeloma bone disease." Bone **20**(6): 515-520.

Ghaemmaghami, S., W. K. Huh, K. Bower, R. W. Howson, A. Belle, N. Dephoure, E. K. O'Shea and J. S. Weissman (2003). "Global analysis of protein expression in yeast." Nature **425**(6959): 737-741.

Ghobrial, I. M. (2012). "Myeloma as a model for the process of metastasis: implications for therapy." Blood **120**(1): 20-30.

Giatromanolaki, A., M. Bai, D. Margaritis, K. L. Bourantas, M. I. Koukourakis, E. Sivridis and K. C. Gatter (2010). "Hypoxia and activated VEGF/receptor pathway in multiple myeloma." Anticancer Res **30**(7): 2831-2836.

Gibson, D. G., L. Young, R. Y. Chuang, J. C. Venter, C. A. Hutchison, 3rd and H. O. Smith (2009). "Enzymatic assembly of DNA molecules up to several hundred kilobases." Nat Methods **6**(5): 343-345.

Gruber, M., C. J. Hu, R. S. Johnson, E. J. Brown, B. Keith and M. C. Simon (2007). "Acute postnatal ablation of Hif-2alpha results in anemia." Proc Natl Acad Sci U S A **104**(7): 2301-2306.

Gu, Y. Z., S. M. Moran, J. B. Hogenesch, L. Wartman and C. A. Bradfield (1998). "Molecular characterization and chromosomal localization of a third alpha-class hypoxia inducible factor subunit, HIF3alpha." Gene Expr **7**(3): 205-213.

Harris, A. L. (2002). "Hypoxia--a key regulatory factor in tumour growth." Nat Rev Cancer **2**(1): 38-47.

Hauser, A. E., G. F. Debes, S. Arce, G. Cassese, A. Hamann, A. Radbruch and R. A. Manz (2002). "Chemotactic responsiveness toward ligands for CXCR3 and CXCR4 is regulated on plasma blasts during the time course of a memory immune response." J Immunol **169**(3): 1277-1282.

He, Z., C. Proudfoot, A. J. Mileham, D. G. McLaren, C. B. Whitelaw and S. G. Lillico (2015). "Highly efficient targeted chromosome deletions using CRISPR/Cas9." Biotechnol Bioeng **112**(5): 1060-1064.

Heikkila, M., A. Pasanen, K. I. Kivirikko and J. Myllyharju (2011). "Roles of the human hypoxia-inducible factor (HIF)-3alpha variants in the hypoxia response." Cell Mol Life Sci **68**(23): 3885-3901.

Hewitson, K. S., L. A. McNeill, M. V. Riordan, Y. M. Tian, A. N. Bullock, R. W. Welford, J. M. Elkins, N. J. Oldham, S. Bhattacharya, J. M. Gleadle, P. J. Ratcliffe, C. W. Pugh and C. J. Schofield (2002). "Hypoxia-inducible factor (HIF) asparagine hydroxylase is identical to factor inhibiting HIF (FIH) and is related to the cupin structural family." J Biol Chem **277**(29): 26351-26355.

Hirai, H., T. Fujishita, K. Kurimoto, H. Miyachi, S. Kitano, S. Inamoto, Y. Itatani, M. Saitou, T. Maekawa and M. M. Taketo (2014). "CCR1-mediated accumulation of myeloid cells in the liver microenvironment promoting mouse colon cancer metastasis." Clin Exp Metastasis **31**(8): 977-989.

Hochedlinger, K., Y. Yamada, C. Beard and R. Jaenisch (2005). "Ectopic expression of Oct-4 blocks progenitor-cell differentiation and causes dysplasia in epithelial tissues." Cell **121**(3): 465-477.

Hoffman, E. C., H. Reyes, F. F. Chu, F. Sander, L. H. Conley, B. A. Brooks and O. Hankinson (1991). "Cloning of a factor required for activity of the Ah (dioxin) receptor." Science **252**(5008): 954-958.

Holmquist-Mengelbier, L., E. Fredlund, T. Lofstedt, R. Noguera, S. Navarro, H. Nilsson, A. Pietras, J. Vallon-Christersson, A. Borg, K. Gradin, L. Poellinger and S. Pahlman (2006). "Recruitment of HIF-1alpha and HIF-2alpha to common target genes is differentially regulated in neuroblastoma: HIF-2alpha promotes an aggressive phenotype." Cancer Cell **10**(5): 413-423.

Housden, B. E. and N. Perrimon (2016). "Comparing CRISPR and RNAi-based screening technologies." Nat Biotechnol **34**(6): 621-623.

Hsu, P. D., D. A. Scott, J. A. Weinstein, F. A. Ran, S. Konermann, V. Agarwala, Y. Li, E. J. Fine, X. Wu, O. Shalem, T. J. Cradick, L. A. Marraffini, G. Bao and F. Zhang (2013). "DNA targeting specificity of RNA-guided Cas9 nucleases." Nat Biotechnol **31**(9): 827-832.

Hu, C. J., S. Iyer, A. Sataur, K. L. Covello, L. A. Chodosh and M. C. Simon (2006). "Differential regulation of the transcriptional activities of hypoxia-inducible factor 1 alpha (HIF-1alpha) and HIF-2alpha in stem cells." Mol Cell Biol **26**(9): 3514-3526.

Hu, C. J., L. Y. Wang, L. A. Chodosh, B. Keith and M. C. Simon (2003). "Differential roles of hypoxia-inducible factor 1alpha (HIF-1alpha) and HIF-2alpha in hypoxic gene regulation." Mol Cell Biol **23**(24): 9361-9374.

Huang, L. E., Z. Arany, D. M. Livingston and H. F. Bunn (1996). "Activation of hypoxia-inducible transcription factor depends primarily upon redox-sensitive stabilization of its alpha subunit." J Biol Chem **271**(50): 32253-32259.

Huang, L. E., J. Gu, M. Schau and H. F. Bunn (1998). "Regulation of hypoxia-inducible factor 1alpha is mediated by an O2-dependent degradation domain via the ubiquitin-proteasome pathway." Proc Natl Acad Sci U S A **95**(14): 7987-7992.

Huang, Y., R. P. Hickey, J. L. Yeh, D. Liu, A. Dadak, L. H. Young, R. S. Johnson and F. J. Giordano (2004). "Cardiac myocyte-specific HIF-1alpha deletion alters vascularization, energy availability, calcium flux, and contractility in the normoxic heart." Faseb j **18**(10): 1138-1140.

Hwang, W. Y., Y. Fu, D. Reyon, M. L. Maeder, S. Q. Tsai, J. D. Sander, R. T. Peterson, J. R. Yeh and J. K. Joung (2013). "Efficient genome editing in zebrafish using a CRISPR-Cas system." Nat Biotechnol **31**(3): 227-229.

Iba, H., T. Mizutani and T. Ito (2003). "SWI/SNF chromatin remodelling complex and retroviral gene silencing." Rev Med Virol **13**(2): 99-110.

Ivan, M., K. Kondo, H. Yang, W. Kim, J. Valiando, M. Ohh, A. Salic, J. M. Asara, W. S. Lane and W. G. Kaelin, Jr. (2001). "HIFalpha targeted for VHL-mediated destruction by proline hydroxylation: implications for O2 sensing." Science **292**(5516): 464-468.

Iwano, S., M. Sugiyama and H. Hama (2018). "Single-cell bioluminescence imaging of deep tissue in freely moving animals." **359**(6378): 935-939.

Iyer, N. V., L. E. Kotch, F. Agani, S. W. Leung, E. Laughner, R. H. Wenger, M. Gassmann, J. D. Gearhart, A. M. Lawler, A. Y. Yu and G. L. Semenza (1998). "Cellular and developmental control of O2 homeostasis by hypoxia-inducible factor 1 alpha." Genes Dev **12**(2): 149-162.

Jaakkola, P., D. R. Mole, Y. M. Tian, M. I. Wilson, J. Gielbert, S. J. Gaskell, A. Kriegsheim, H. F. Hebestreit, M. Mukherji, C. J. Schofield, P. H. Maxwell, C. W. Pugh and P. J. Ratcliffe (2001). "Targeting of HIF-alpha to the von Hippel-Lindau ubiquitylation complex by O2-regulated prolyl hydroxylation." Science **292**(5516): 468-472.

Jewell, U. R., I. Kvietikova, A. Scheid, C. Bauer, R. H. Wenger and M. Gassmann (2001). "Induction of HIF-1alpha in response to hypoxia is instantaneous." Faseb j **15**(7): 1312-1314.

Jiang, B. H., E. Rue, G. L. Wang, R. Roe and G. L. Semenza (1996). "Dimerization, DNA binding, and transactivation properties of hypoxia-inducible factor 1." J Biol Chem **271**(30): 17771-17778.

Jiang, B. H., J. Z. Zheng, S. W. Leung, R. Roe and G. L. Semenza (1997). "Transactivation and inhibitory domains of hypoxia-inducible factor 1alpha. Modulation of transcriptional activity by oxygen tension." J Biol Chem **272**(31): 19253-19260.

Jinek, M., K. Chylinski, I. Fonfara, M. Hauer, J. A. Doudna and E. Charpentier (2012). "A programmable dual-RNA-guided DNA endonuclease in adaptive bacterial immunity." Science **337**(6096): 816-821.

Jinek, M., A. East, A. Cheng, S. Lin, E. Ma and J. Doudna (2013). "RNA-programmed genome editing in human cells." Elife **2**: e00471.

Joung, J., S. Konermann and J. S. Gootenberg (2017). "Genome-scale CRISPR-Cas9 knockout and transcriptional activation screening." **12**(4): 828-863.

Kellner, J., B. Liu, Y. Kang and Z. Li (2013). "Fact or fiction--identifying the elusive multiple myeloma stem cell." J Hematol Oncol **6**: 91.

Kim, J. H., S. R. Lee, L. H. Li, H. J. Park, J. H. Park, K. Y. Lee, M. K. Kim, B. A. Shin and S. Y. Choi (2011). "High cleavage efficiency of a 2A peptide derived from porcine teschovirus-1 in human cell lines, zebrafish and mice." PLoS One **6**(4): e18556.

Kim, S., D. Kim, S. W. Cho, J. Kim and J. S. Kim (2014). "Highly efficient RNA-guided genome editing in human cells via delivery of purified Cas9 ribonucleoproteins." Genome Res **24**(6): 1012-1019.

Kim, Y. G., J. Cha and S. Chandrasegaran (1996). "Hybrid restriction enzymes: zinc finger fusions to Fok I cleavage domain." Proc Natl Acad Sci U S A **93**(3): 1156-1160.

Kitamura, T., T. Fujishita, P. Loetscher, L. Revesz, H. Hashida, S. Kizaka-Kondoh, M. Aoki and M. M. Taketo (2010). "Inactivation of chemokine (C-C motif) receptor 1 (CCR1) suppresses colon cancer liver metastasis by blocking accumulation of immature myeloid cells in a mouse model." Proc Natl Acad Sci U S A **107**(29): 13063-13068.

Klein, S., M. Roghani and D. B. Rifkin (1997). "Fibroblast growth factors as angiogenesis factors: new insights into their mechanism of action." Exs **79**: 159-192.

Koivunen, P., M. Hirsila, V. Gunzler, K. I. Kivirikko and J. Myllyharju (2004). "Catalytic properties of the asparaginyl hydroxylase (FIH) in the oxygen sensing pathway are distinct from those of its prolyl 4-hydroxylases." <u>J Biol Chem</u> **279**(11): 9899-9904.

Kyle, R. A., M. A. Gertz, T. E. Witzig, J. A. Lust, M. Q. Lacy, A. Dispenzieri, R. Fonseca, S. V. Rajkumar, J. R. Offord, D. R. Larson, M. E. Plevak, T. M. Therneau and P. R. Greipp (2003). "Review of 1027 patients with newly diagnosed multiple myeloma." <u>Mayo Clin Proc</u> **78**(1): 21-33.

Kyle, R. A. and S. V. Rajkumar (2004). "Multiple myeloma." <u>N Engl J Med</u> **351**(18): 1860-1873.

Kyle, R. A., E. D. Remstein, T. M. Therneau, A. Dispenzieri, P. J. Kurtin, J. M. Hodnefield, D. R. Larson, M. F. Plevak, D. F. Jelinek, R. Fonseca, L. J. Melton, 3rd and S. V. Rajkumar (2007). "Clinical course and prognosis of smoldering (asymptomatic) multiple myeloma." <u>N Engl J Med</u> **356**(25): 2582-2590.

Labrinidis, A., P. Diamond, S. Martin, S. Hay, V. Liapis, I. Zinonos, N. A. Sims, G. J. Atkins, C. Vincent, V. Ponomarev, D. M. Findlay, A. C. Zannettino and A. Evdokiou (2009). "Apo2L/TRAIL inhibits tumor growth and bone destruction in a murine model of multiple myeloma." <u>Clin Cancer Res</u> **15**(6): 1998-2009.

Laker, C., J. Meyer, A. Schopen, J. Friel, C. Heberlein, W. Ostertag and C. Stocking (1998). "Host cis-mediated extinction of a retrovirus permissive for expression in embryonal stem cells during differentiation." <u>J Virol</u> **72**(1): 339-348.

Lando, D., D. J. Peet, J. J. Gorman, D. A. Whelan, M. L. Whitelaw and R. K. Bruick (2002). "FIH-1 is an asparaginyl hydroxylase enzyme that regulates the transcriptional activity of hypoxia-inducible factor." <u>Genes Dev</u> **16**(12): 1466-1471.

Lando, D., D. J. Peet, D. A. Whelan, J. J. Gorman and M. L. Whitelaw (2002). "Asparagine hydroxylation of the HIF transactivation domain a hypoxic switch." <u>Science</u> **295**(5556): 858-861.

Lawson, M. A., M. M. McDonald, N. Kovacic, W. Hua Khoo, R. L. Terry, J. Down, W. Kaplan, J. Paton-Hough, C. Fellows, J. A. Pettitt, T. Neil Dear, E. Van Valckenborgh, P. A. Baldock, M. J. Rogers, C. L. Eaton, K. Vanderkerken, A. R. Pettit, J. M. Quinn, A. C. Zannettino, T. G. Phan and P. I. Croucher (2015). "Osteoclasts control reactivation of dormant myeloma cells by remodelling the endosteal niche." <u>Nat Commun</u> **6**: 8983.

LeBien, T. W. and T. F. Tedder (2008). "B lymphocytes: how they develop and function." <u>Blood</u> **112**(5): 1570-1580.

Lee, K. E. and M. C. Simon (2015). "SnapShot: Hypoxia-Inducible Factors." <u>Cell</u> **163**(5): 1288-1288.e1281.

Liao, D., C. Corle, T. N. Seagroves and R. S. Johnson (2007). "Hypoxia-inducible factor-1alpha is a key regulator of metastasis in a transgenic model of cancer initiation and progression." Cancer Res **67**(2): 563-572.

Libouban, H. (2015). "The use of animal models in multiple myeloma." Morphologie **99**(325): 63-72.

Lin, Q., X. Cong and Z. Yun (2011). "Differential hypoxic regulation of hypoxia-inducible factors 1alpha and 2alpha." Mol Cancer Res **9**(6): 757-765.

Lofstedt, T., E. Fredlund, L. Holmquist-Mengelbier, A. Pietras, M. Ovenberger, L. Poellinger and S. Pahlman (2007). "Hypoxia inducible factor-2alpha in cancer." Cell Cycle **6**(8): 919-926.

Luther, S. A., A. Bidgol, D. C. Hargreaves, A. Schmidt, Y. Xu, J. Paniyadi, M. Matloubian and J. G. Cyster (2002). "Differing activities of homeostatic chemokines CCL19, CCL21, and CXCL12 in lymphocyte and dendritic cell recruitment and lymphoid neogenesis." J Immunol **169**(1): 424-433.

Mali, P., L. Yang, K. M. Esvelt, J. Aach, M. Guell, J. E. DiCarlo, J. E. Norville and G. M. Church (2013). "RNA-guided human genome engineering via Cas9." Science **339**(6121): 823-826.

Manier, S., K. Z. Salem, J. Park, D. A. Landau, G. Getz and I. M. Ghobrial (2016). "Genomic complexity of multiple myeloma and its clinical implications." Nat Rev Clin Oncol.

Manning, L. S., N. L. Chamberlain, M. F. Leahy and F. T. Cordingley (1995). "Assessment of the therapeutic potential of cytokines, cytotoxic drugs and effector cell populations for the treatment of multiple myeloma using the 5T33 murine myeloma model." Immunol Cell Biol **73**(4): 326-332.

Martin, S. (2008). Molecular and cellular mechanisms of increased angiogenesis in Multiple Myeloma: a role for CXCL12. PhD Thesis, University of Adelaide.

Martin, S. K., A. L. Dewar, A. N. Farrugia, N. Horvath, S. Gronthos, L. B. To and A. C. Zannettino (2006). "Tumor angiogenesis is associated with plasma levels of stromal-derived factor-1alpha in patients with multiple myeloma." Clin Cancer Res **12**(23): 6973-6977.

Martin, S. K., P. Diamond, S. A. Williams, L. B. To, D. J. Peet, N. Fujii, S. Gronthos, A. L. Harris and A. C. Zannettino (2009). "The HIF-2 transcription factor is a novel regulator of aberrant CXCL12 expression in multiple myeloma plasma cells." Haematologica.

Mason, S. D., R. A. Howlett, M. J. Kim, I. M. Olfert, M. C. Hogan, W. McNulty, R. P. Hickey, P. D. Wagner, C. R. Kahn, F. J. Giordano and R. S. Johnson (2004). "Loss of skeletal muscle HIF-1alpha results in altered exercise endurance." PLoS Biol **2**(10): e288.

Mastrogiannaki, M., P. Matak, B. Keith, M. C. Simon, S. Vaulont and C. Peyssonnaux (2009). "HIF-2alpha, but not HIF-1alpha, promotes iron absorption in mice." J Clin Invest **119**(5): 1159-1166.

Maxwell, P. H., G. U. Dachs, J. M. Gleadle, L. G. Nicholls, A. L. Harris, I. J. Stratford, O. Hankinson, C. W. Pugh and P. J. Ratcliffe (1997). "Hypoxia-inducible factor-1 modulates gene expression in solid tumors and influences both angiogenesis and tumor growth." Proc Natl Acad Sci U S A **94**(15): 8104-8109.

Maxwell, P. H., M. S. Wiesener, G. W. Chang, S. C. Clifford, E. C. Vaux, M. E. Cockman, C. C. Wykoff, C. W. Pugh, E. R. Maher and P. J. Ratcliffe (1999). "The tumour suppressor protein VHL targets hypoxia-inducible factors for oxygen-dependent proteolysis." Nature **399**(6733): 271-275.

Menu, E., K. Asosingh, S. Indraccolo, H. De Raeve, I. Van Riet, E. Van Valckenborgh, I. Vande Broek, N. Fujii, H. Tamamura, B. Van Camp and K. Vanderkerken (2006). "The involvement of stromal derived factor 1alpha in homing and progression of multiple myeloma in the 5TMM model." Haematologica **91**(5): 605-612.

Menu, E., K. Asosingh, I. Van Riet, P. Croucher, B. Van Camp and K. Vanderkerken (2004). "Myeloma cells (5TMM) and their interactions with the marrow microenvironment." Blood Cells Mol Dis **33**(2): 111-119.

Milosevic, J., M. Maisel, F. Wegner, J. Leuchtenberger, R. H. Wenger, M. Gerlach, A. Storch and J. Schwarz (2007). "Lack of hypoxia-inducible factor-1 alpha impairs midbrain neural precursor cells involving vascular endothelial growth factor signaling." J Neurosci **27**(2): 412-421.

Mole, D. R., C. Blancher, R. R. Copley, P. J. Pollard, J. M. Gleadle, J. Ragoussis and P. J. Ratcliffe (2009). "Genome-wide association of hypoxia-inducible factor (HIF)-1alpha and HIF-2alpha DNA binding with expression profiling of hypoxia-inducible transcripts." J Biol Chem **284**(25): 16767-16775.

Moller, C., T. Stromberg, M. Juremalm, K. Nilsson and G. Nilsson (2003). "Expression and function of chemokine receptors in human multiple myeloma." Leukemia **17**(1): 203-210.

Morgan, G. J., B. A. Walker and F. E. Davies (2012). "The genetic architecture of multiple myeloma." Nat Rev Cancer **12**(5): 335-348.

Mori, Y., N. Shimizu, M. Dallas, M. Niewolna, B. Story, P. J. Williams, G. R. Mundy and T. Yoneda (2004). "Anti-alpha4 integrin antibody suppresses the development of multiple myeloma and associated osteoclastic osteolysis." Blood **104**(7): 2149-2154.

Muller, P. Y., H. Janovjak, A. R. Miserez and Z. Dobbie (2002). "Processing of gene expression data generated by quantitative real-time RT-PCR." Biotechniques **32**(6): 1372-1374, 1376, 1378-1379.

Mundy, G. R. (1998). "Myeloma bone disease." Eur J Cancer **34**(2): 246-251.

Niwa, O., Y. Yokota, H. Ishida and T. Sugahara (1983). "Independent mechanisms involved in suppression of the Moloney leukemia virus genome during differentiation of murine teratocarcinoma cells." Cell **32**(4): 1105-1113.

Noll, J. E., D. R. Hewett, S. A. Williams, K. Vandyke, C. Kok, L. B. To and A. C. Zannettino (2014). "SAMSN1 is a tumor suppressor gene in multiple myeloma." Neoplasia **16**(7): 572-585.

Noll, J. E., S. A. Williams, L. E. Purton and A. C. Zannettino (2012). "Tug of war in the haematopoietic stem cell niche: do myeloma plasma cells compete for the HSC niche?" Blood Cancer J **2**: e91.

Nombela-Arrieta, C., G. Pivarnik, B. Winkel, K. J. Canty, B. Harley, J. E. Mahoney, S. Y. Park, J. Lu, A. Protopopov and L. E. Silberstein (2013). "Quantitative imaging of haematopoietic stem and progenitor cell localization and hypoxic status in the bone marrow microenvironment." Nat Cell Biol **15**(5): 533-543.

Nowakowski, G. S., T. E. Witzig, D. Dingli, M. J. Tracz, M. A. Gertz, M. Q. Lacy, J. A. Lust, A. Dispenzieri, P. R. Greipp, R. A. Kyle and S. V. Rajkumar (2005). "Circulating plasma cells detected by flow cytometry as a predictor of survival in 302 patients with newly diagnosed multiple myeloma." Blood **106**(7): 2276-2279.

Ortiz-Barahona, A., D. Villar, N. Pescador, J. Amigo and L. del Peso (2010). "Genome-wide identification of hypoxia-inducible factor binding sites and target genes by a probabilistic model integrating transcription-profiling data and in silico binding site prediction." Nucleic Acids Res **38**(7): 2332-2345.

Oyajobi, B. O., S. Munoz, R. Kakonen, P. J. Williams, A. Gupta, C. L. Wideman, B. Story, B. Grubbs, A. Armstrong, W. C. Dougall, I. R. Garrett and G. R. Mundy (2007). "Detection of myeloma in skeleton of mice by whole-body optical fluorescence imaging." Mol Cancer Ther **6**(6): 1701-1708.

Palumbo, A. and K. Anderson (2011). "Multiple myeloma." N Engl J Med **364**(11): 1046-1060.

Papetti, M. and I. M. Herman (2002). "Mechanisms of normal and tumor-derived angiogenesis." Am J Physiol Cell Physiol **282**(5): C947-970.

Pawlyn, C., L. Melchor, A. Murison, C. P. Wardell, A. Brioli, E. M. Boyle, M. F. Kaiser, B. A. Walker, D. B. Begum, N. B. Dahir, P. Proszek, W. M. Gregory, M. T. Drayson, G. H. Jackson, F. M. Ross, F. E. Davies and G. J. Morgan (2015). "Coexistent hyperdiploidy does not abrogate poor prognosis in myeloma with adverse cytogenetics and may precede IGH translocations." Blood **125**(5): 831-840.

Peng, J., L. Zhang, L. Drysdale and G. H. Fong (2000). "The transcription factor EPAS-1/hypoxia-inducible factor 2alpha plays an important role in vascular remodeling." Proc Natl Acad Sci U S A **97**(15): 8386-8391.

Peyssonnaux, C., V. Datta, T. Cramer, A. Doedens, E. A. Theodorakis, R. L. Gallo, N. Hurtado-Ziola, V. Nizet and R. S. Johnson (2005). "HIF-1alpha expression regulates the bactericidal capacity of phagocytes." J Clin Invest **115**(7): 1806-1815.

Podar, K., P. G. Richardson, T. Hideshima, D. Chauhan and K. C. Anderson (2007). "The malignant clone and the bone-marrow environment." Best Pract Res Clin Haematol **20**(4): 597-612.

Ponomarev, V., M. Doubrovin, I. Serganova, J. Vider, A. Shavrin, T. Beresten, A. Ivanova, L. Ageyeva, V. Tourkova, J. Balatoni, W. Bornmann, R. Blasberg and J. Gelovani Tjuvajev (2004). "A novel triple-modality reporter gene for whole-body fluorescent, bioluminescent, and nuclear noninvasive imaging." Eur J Nucl Med Mol Imaging **31**(5): 740-751.

Potter, M. (1986). "Plasmacytomas in mice." Semin Oncol **13**(3): 275-281.

Pugh, C. W., J. F. O'Rourke, M. Nagao, J. M. Gleadle and P. J. Ratcliffe (1997). "Activation of hypoxia-inducible factor-1; definition of regulatory domains within the alpha subunit." J Biol Chem **272**(17): 11205-11214.

Pulte, D., A. Gondos and H. Brenner (2011). "Improvement in survival of older adults with multiple myeloma: results of an updated period analysis of SEER data." Oncologist **16**(11): 1600-1603.

Qin, J. Y., L. Zhang, K. L. Clift, I. Hulur, A. P. Xiang, B. Z. Ren and B. T. Lahn (2010). "Systematic comparison of constitutive promoters and the doxycycline-inducible promoter." PLoS One **5**(5): e10611.

Radl, J. (1990). "Age-related monoclonal gammapathies: clinical lessons from the aging C57BL mouse." Immunol Today **11**(7): 234-236.

Radl, J. (1999). "Multiple myeloma and related disorders. Lessons from an animal model." Pathol Biol (Paris) **47**(2): 109-114.

Radl, J., J. W. Croese, C. Zurcher, M. H. van den Enden-Vieveen, R. J. Brondijk, M. Kazil, J. J. Haaijman, P. H. Reitsma and O. L. Bijvoet (1985). "Influence of treatment with APD-bisphosphonate on the bone lesions in the mouse 5T2 multiple myeloma." Cancer **55**(5): 1030-1040.

Radl, J., J. W. Croese, C. Zurcher, M. H. Van den Enden-Vieveen and A. M. de Leeuw (1988). "Animal model of human disease. Multiple myeloma." Am J Pathol **132**(3): 593-597.

Radl, J., E. D. De Glopper, H. R. Schuit and C. Zurcher (1979). "Idiopathic paraproteinemia. II. Transplantation of the paraprotein-producing clone from old to young C57BL/KaLwRij mice." J Immunol **122**(2): 609-613.

Rajkumar, S. V., M. A. Dimopoulos, A. Palumbo, J. Blade, G. Merlini, M. V. Mateos, S. Kumar, J. Hillengass, E. Kastritis, P. Richardson, O. Landgren, B. Paiva, A. Dispenzieri, B. Weiss, X. LeLeu, S. Zweegman, S. Lonial, L. Rosinol, E. Zamagni, S. Jagannath, O. Sezer, S. Y. Kristinsson, J. Caers, S. Z. Usmani, J. J. Lahuerta, H. E. Johnsen, M. Beksac, M. Cavo, H. Goldschmidt, E. Terpos, R. A. Kyle, K. C. Anderson, B. G. Durie and J. F. Miguel (2014). "International Myeloma Working Group updated criteria for the diagnosis of multiple myeloma." Lancet Oncol **15**(12): e538-548.

Rajkumar, S. V., S. R. Hayman, M. Q. Lacy, A. Dispenzieri, S. M. Geyer, B. Kabat, S. R. Zeldenrust, S. Kumar, P. R. Greipp, R. Fonseca, J. A. Lust, S. J. Russell, R. A. Kyle, T. E. Witzig and M. A. Gertz (2005). "Combination therapy with lenalidomide plus dexamethasone (Rev/Dex) for newly diagnosed myeloma." Blood **106**(13): 4050-4053.

Ran, F. A., P. D. Hsu, J. Wright, V. Agarwala, D. A. Scott and F. Zhang (2013). "Genome engineering using the CRISPR-Cas9 system." Nat Protoc **8**(11): 2281-2308.

Rankin, E. B., M. P. Biju, Q. Liu, T. L. Unger, J. Rha, R. S. Johnson, M. C. Simon, B. Keith and V. H. Haase (2007). "Hypoxia-inducible factor-2 (HIF-2) regulates hepatic erythropoietin in vivo." J Clin Invest **117**(4): 1068-1077.

Raval, R. R., K. W. Lau, M. G. Tran, H. M. Sowter, S. J. Mandriota, J. L. Li, C. W. Pugh, P. H. Maxwell, A. L. Harris and P. J. Ratcliffe (2005). "Contrasting properties of hypoxia-inducible factor 1 (HIF-1) and HIF-2 in von Hippel-Lindau-associated renal cell carcinoma." Mol Cell Biol **25**(13): 5675-5686.

Reijmers, R. M., M. Spaargaren and S. T. Pals (2013). "Heparan sulfate proteoglycans in the control of B cell development and the pathogenesis of multiple myeloma." FEBS J **280**(10): 2180-2193.

Ria, R., I. Catacchio, S. Berardi, A. De Luisi, A. Caivano, C. Piccoli, V. Ruggieri, M. A. Frassanito, D. Ribatti, B. Nico, T. Annese, S. Ruggieri, A. Guarini, C. Minoia, P. Ditonno, E. Angelucci, D. Derudas, M. Moschetta, F. Dammacco and A. Vacca (2014). "HIF-1alpha of bone marrow endothelial cells implies relapse and drug resistance in

patients with multiple myeloma and may act as a therapeutic target." Clin Cancer Res **20**(4): 847-858.

Ria, R., K. Todoerti, S. Berardi, A. M. Coluccia, A. De Luisi, M. Mattioli, D. Ronchetti, F. Morabito, A. Guarini, M. T. Petrucci, F. Dammacco, D. Ribatti, A. Neri and A. Vacca (2009). "Gene expression profiling of bone marrow endothelial cells in patients with multiple myeloma." Clin Cancer Res **15**(17): 5369-5378.

Richardson, P. G., B. Barlogie, J. Berenson, S. Singhal, S. Jagannath, D. Irwin, S. V. Rajkumar, G. Srkalovic, M. Alsina, R. Alexanian, D. Siegel, R. Z. Orlowski, D. Kuter, S. A. Limentani, S. Lee, T. Hideshima, D. L. Esseltine, M. Kauffman, J. Adams, D. P. Schenkein and K. C. Anderson (2003). "A phase 2 study of bortezomib in relapsed, refractory myeloma." N Engl J Med **348**(26): 2609-2617.

Rouault-Pierre, K., L. Lopez-Onieva, K. Foster, F. Anjos-Afonso, I. Lamrissi-Garcia, M. Serrano-Sanchez, R. Mitter, Z. Ivanovic, H. de Verneuil, J. Gribben, D. Taussig, H. R. Rezvani, F. Mazurier and D. Bonnet (2013). "HIF-2alpha protects human hematopoietic stem/progenitors and acute myeloid leukemic cells from apoptosis induced by endoplasmic reticulum stress." Cell Stem Cell **13**(5): 549-563.

Ryan, H. E., J. Lo and R. S. Johnson (1998). "HIF-1 alpha is required for solid tumor formation and embryonic vascularization." EMBO J **17**(11): 3005-3015.

Salceda, S. and J. Caro (1997). "Hypoxia-inducible factor 1alpha (HIF-1alpha) protein is rapidly degraded by the ubiquitin-proteasome system under normoxic conditions. Its stabilization by hypoxia depends on redox-induced changes." J Biol Chem **272**(36): 22642-22647.

Sastry, L., T. Johnson, M. J. Hobson, B. Smucker and K. Cornetta (2002). "Titering lentiviral vectors: comparison of DNA, RNA and marker expression methods." Gene Ther **9**(17): 1155-1162.

Schanz, A., K. Red-Horse, A. P. Hess, D. M. Baston-Bust, C. Heiss and J. S. Krussel (2014). "Oxygen regulates human cytotrophoblast migration by controlling chemokine and receptor expression." Placenta **35**(12): 1089-1094.

Schito, L., S. Rey and M. Konopleva (2017). "Integration of hypoxic HIF-alpha signaling in blood cancers." Oncogene **36**(38): 5331-5340.

Schodel, J., D. R. Mole and P. J. Ratcliffe (2013). "Pan-genomic binding of hypoxia-inducible transcription factors." Biol Chem **394**(4): 507-517.

Scortegagna, M., K. Ding, Y. Oktay, A. Gaur, F. Thurmond, L. J. Yan, B. T. Marck, A. M. Matsumoto, J. M. Shelton, J. A. Richardson, M. J. Bennett and J. A. Garcia (2003). "Multiple organ pathology, metabolic abnormalities and impaired homeostasis of reactive oxygen species in Epas1-/- mice." Nat Genet **35**(4): 331-340.

Scortegagna, M., K. Ding, Q. Zhang, Y. Oktay, M. J. Bennett, M. Bennett, J. M. Shelton, J. A. Richardson, O. Moe and J. A. Garcia (2005). "HIF-2alpha regulates murine hematopoietic development in an erythropoietin-dependent manner." Blood **105**(8): 3133-3140.

Scortegagna, M., M. A. Morris, Y. Oktay, M. Bennett and J. A. Garcia (2003). "The HIF family member EPAS1/HIF-2alpha is required for normal hematopoiesis in mice." Blood **102**(5): 1634-1640.

Semenza, G. L. (2003). "Angiogenesis in ischemic and neoplastic disorders." Annu Rev Med **54**: 17-28.

Semenza, G. L. (2011). "Oxygen sensing, homeostasis, and disease." N Engl J Med **365**(6): 537-547.

Semenza, G. L. (2014). "Oxygen sensing, hypoxia-inducible factors, and disease pathophysiology." Annu Rev Pathol **9**: 47-71.

Semenza, G. L. and G. L. Wang (1992). "A nuclear factor induced by hypoxia via de novo protein synthesis binds to the human erythropoietin gene enhancer at a site required for transcriptional activation." Mol Cell Biol **12**(12): 5447-5454.

Shalem, O., N. E. Sanjana, E. Hartenian, X. Shi, D. A. Scott, T. Mikkelson, D. Heckl, B. L. Ebert, D. E. Root, J. G. Doench and F. Zhang (2014). "Genome-scale CRISPR-Cas9 knockout screening in human cells." Science **343**(6166): 84-87.

Shapiro-Shelef, M. and K. Calame (2004). "Plasma cell differentiation and multiple myeloma." Curr Opin Immunol **16**(2): 226-234.

Shin, H. Y. and C. Wang (2017). "CRISPR/Cas9 targeting events cause complex deletions and insertions at 17 sites in the mouse genome." **8**: 15464.

Shweiki, D., A. Itin, D. Soffer and E. Keshet (1992). "Vascular endothelial growth factor induced by hypoxia may mediate hypoxia-initiated angiogenesis." Nature **359**(6398): 843-845.

Simmons, J. K., B. E. Hildreth, 3rd, W. Supsavhad, S. M. Elshafae, B. B. Hassan, W. P. Dirksen, R. E. Toribio and T. J. Rosol (2015). "Animal Models of Bone Metastasis." Vet Pathol **52**(5): 827-841.

Singhal, S., J. Mehta, R. Desikan, D. Ayers, P. Roberson, P. Eddlemon, N. Munshi, E. Anaissie, C. Wilson, M. Dhodapkar, J. Zeddis and B. Barlogie (1999). "Antitumor activity of thalidomide in refractory multiple myeloma." N Engl J Med **341**(21): 1565-1571.

Skuli, N., L. Liu, A. Runge, T. Wang, L. Yuan, S. Patel, L. Iruela-Arispe, M. C. Simon and B. Keith (2009). "Endothelial deletion of hypoxia-inducible factor-2alpha (HIF-2alpha) alters vascular function and tumor angiogenesis." <u>Blood</u> **114**(2): 469-477.

Song, Y., L. Yuan, Y. Wang, M. Chen, J. Deng, Q. Lv, T. Sui, Z. Li and L. Lai (2016). "Efficient dual sgRNA-directed large gene deletion in rabbit with CRISPR/Cas9 system." <u>Cell Mol Life Sci</u> **73**(15): 2959-2968.

Sowter, H. M., R. R. Raval, J. W. Moore, P. J. Ratcliffe and A. L. Harris (2003). "Predominant role of hypoxia-inducible transcription factor (Hif)-1alpha versus Hif-2alpha in regulation of the transcriptional response to hypoxia." <u>Cancer Res</u> **63**(19): 6130-6134.

Stessman, H. A., A. Mansoor, F. Zhan, S. Janz, M. A. Linden, L. B. Baughn and B. Van Ness (2013). "Reduced CXCR4 expression is associated with extramedullary disease in a mouse model of myeloma and predicts poor survival in multiple myeloma patients treated with bortezomib." <u>Leukemia</u> **27**(10): 2075-2077.

Storti, P., M. Bolzoni, G. Donofrio, I. Airoldi, D. Guasco, D. Toscani, E. Martella, M. Lazzaretti, C. Mancini, L. Agnelli, K. Patrene, S. Maiga, V. Franceschi, S. Colla, J. Anderson, A. Neri, M. Amiot, F. Aversa, G. D. Roodman and N. Giuliani (2013). "Hypoxia-inducible factor (HIF)-1alpha suppression in myeloma cells blocks tumoral growth in vivo inhibiting angiogenesis and bone destruction." <u>Leukemia</u> **27**(8): 1697-1706.

Subarsky, P. and R. P. Hill (2003). "The hypoxic tumour microenvironment and metastatic progression." <u>Clin Exp Metastasis</u> **20**(3): 237-250.

Swindle, C. S. and C. A. Klug (2002). "Mechanisms that regulate silencing of gene expression from retroviral vectors." <u>J Hematother Stem Cell Res</u> **11**(3): 449-456.

Szymczak, A. L., C. J. Workman, Y. Wang, K. M. Vignali, S. Dilioglou, E. F. Vanin and D. A. Vignali (2004). "Correction of multi-gene deficiency in vivo using a single 'self-cleaving' 2A peptide-based retroviral vector." <u>Nat Biotechnol</u> **22**(5): 589-594.

Takeda, K., H. L. Aguila, N. S. Parikh, X. Li, K. Lamothe, L. J. Duan, H. Takeda, F. S. Lee and G. H. Fong (2008). "Regulation of adult erythropoiesis by prolyl hydroxylase domain proteins." <u>Blood</u> **111**(6): 3229-3235.

Talarico, D., A. F. Peverali, E. Ginelli, R. Meneveri, C. Mondello and G. Della Valle (1988). "Satellite DNA induces unstable expression of the adjacent herpes simplex virus tk gene cotransfected in mouse cells." <u>Mol Cell Biol</u> **8**(3): 1336-1344.

Talks, K. L., H. Turley, K. C. Gatter, P. H. Maxwell, C. W. Pugh, P. J. Ratcliffe and A. L. Harris (2000). "The expression and distribution of the hypoxia-inducible factors HIF-

1alpha and HIF-2alpha in normal human tissues, cancers, and tumor-associated macrophages." Am J Pathol **157**(2): 411-421.

Terpos, E., M. Politou, R. Szydlo, J. M. Goldman, J. F. Apperley and A. Rahemtulla (2003). "Serum levels of macrophage inflammatory protein-1 alpha (MIP-1alpha) correlate with the extent of bone disease and survival in patients with multiple myeloma." Br J Haematol **123**(1): 106-109.

Tian, H., R. E. Hammer, A. M. Matsumoto, D. W. Russell and S. L. McKnight (1998). "The hypoxia-responsive transcription factor EPAS1 is essential for catecholamine homeostasis and protection against heart failure during embryonic development." Genes Dev **12**(21): 3320-3324.

Tomita, S., M. Ueno, M. Sakamoto, Y. Kitahama, M. Ueki, N. Maekawa, H. Sakamoto, M. Gassmann, R. Kageyama, N. Ueda, F. J. Gonzalez and Y. Takahama (2003). "Defective brain development in mice lacking the Hif-1alpha gene in neural cells." Mol Cell Biol **23**(19): 6739-6749.

Trani, D., B. H. Moon, B. Kallakury, D. P. Hartmann, K. Datta and A. J. Fornace, Jr. (2013). "Sex-dependent differences in intestinal tumorigenesis induced in Apc1638N/+ mice by exposure to gamma rays." Int J Radiat Oncol Biol Phys **85**(1): 223-229.

Urashima, M., B. P. Chen, S. Chen, G. S. Pinkus, R. T. Bronson, D. A. Dedera, Y. Hoshi, G. Teoh, A. Ogata, S. P. Treon, D. Chauhan and K. C. Anderson (1997). "The development of a model for the homing of multiple myeloma cells to human bone marrow." Blood **90**(2): 754-765.

Vacca, A., D. Ribatti, L. Roncali, G. Ranieri, G. Serio, F. Silvestris and F. Dammacco (1994). "Bone marrow angiogenesis and progression in multiple myeloma." Br J Haematol **87**(3): 503-508.

Valsecchi, R., N. Coltella, D. Belloni, M. Ponente, E. Ten Hacken, C. Scielzo, L. Scarfo, M. T. Bertilaccio, P. Brambilla, E. Lenti, F. Martinelli Boneschi, A. Brendolan, E. Ferrero, M. Ferrarini, P. Ghia, G. Tonon, M. Ponzoni, F. Caligaris-Cappio and R. Bernardi (2016). "HIF-1alpha regulates the interaction of chronic lymphocytic leukemia cells with the tumor microenvironment." Blood **127**(16): 1987-1997.

van den Akker, T. W., J. Radl, E. Franken-Postma and A. Hagemeijer (1996). "Cytogenetic findings in mouse multiple myeloma and Waldenstrom's macroglobulinemia." Cancer Genet Cytogenet **86**(2): 156-161.

Vanderkerken, K., H. De Raeve, E. Goes, S. Van Meirvenne, J. Radl, I. Van Riet, K. Thielemans and B. Van Camp (1997). "Organ involvement and phenotypic adhesion profile of 5T2 and 5T33 myeloma cells in the C57BL/KaLwRij mouse." Br J Cancer **76**(4): 451-460.

Vandyke, K., M. N. Zeissig, D. R. Hewett, S. K. Martin, K. M. Mrozik, C. M. Cheong, P. Diamond, L. B. To, S. Gronthos, D. J. Peet, P. I. Croucher and A. C. W. Zannettino (2017). "HIF-2alpha Promotes Dissemination of Plasma Cells in Multiple Myeloma by Regulating CXCL12/CXCR4 and CCR1." Cancer Res **77**(20): 5452-5463.

Vaquerizas, J. M., S. K. Kummerfeld, S. A. Teichmann and N. M. Luscombe (2009). "A census of human transcription factors: function, expression and evolution." Nat Rev Genet **10**(4): 252-263.

Vroemen, M., N. Weidner and A. Blesch (2005). "Loss of gene expression in lentivirus- and retrovirus-transduced neural progenitor cells is correlated to migration and differentiation in the adult spinal cord." Exp Neurol **195**(1): 127-139.

Wang, G. L., B. H. Jiang, E. A. Rue and G. L. Semenza (1995). "Hypoxia-inducible factor 1 is a basic-helix-loop-helix-PAS heterodimer regulated by cellular O2 tension." Proc Natl Acad Sci U S A **92**(12): 5510-5514.

Wang, G. L. and G. L. Semenza (1993). "Characterization of hypoxia-inducible factor 1 and regulation of DNA binding activity by hypoxia." J Biol Chem **268**(29): 21513-21518.

Wang, G. L. and G. L. Semenza (1995). "Purification and characterization of hypoxia-inducible factor 1." J Biol Chem **270**(3): 1230-1237.

Wang, L., R. Benedito, M. G. Bixel, D. Zeuschner, M. Stehling, L. Savendahl, J. J. Haigh, H. Snippert, H. Clevers, G. Breier, F. Kiefer and R. H. Adams (2013). "Identification of a clonally expanding haematopoietic compartment in bone marrow." Embo j **32**(2): 219-230.

Wehrli, N., D. F. Legler, D. Finke, K. M. Toellner, P. Loetscher, M. Baggiolini, I. C. MacLennan and H. Acha-Orbea (2001). "Changing responsiveness to chemokines allows medullary plasmablasts to leave lymph nodes." Eur J Immunol **31**(2): 609-616.

Weidemann, A., Y. M. Kerdiles, K. X. Knaup, C. A. Rafie, A. T. Boutin, C. Stockmann, N. Takeda, M. Scadeng, A. Y. Shih, V. H. Haase, M. C. Simon, D. Kleinfeld and R. S. Johnson (2009). "The glial cell response is an essential component of hypoxia-induced erythropoiesis in mice." J Clin Invest **119**(11): 3373-3383.

Wenger, R. H., D. P. Stiehl and G. Camenisch (2005). "Integration of oxygen signaling at the consensus HRE." Sci STKE **2005**(306): re12.

Wernig, M., C. J. Lengner, J. Hanna, M. A. Lodato, E. Steine, R. Foreman, J. Staerk, S. Markoulaki and R. Jaenisch (2008). "A drug-inducible transgenic system for direct reprogramming of multiple somatic cell types." Nat Biotechnol **26**(8): 916-924.

White, S. M., M. Renda, N. Y. Nam, E. Klimatcheva, Y. Zhu, J. Fisk, M. Halterman, B. J. Rimel, H. Federoff, S. Pandya, J. D. Rosenblatt and V. Planelles (1999). "Lentivirus vectors using human and simian immunodeficiency virus elements." J Virol **73**(4): 2832-2840.

Wiesener, M. S., J. S. Jurgensen, C. Rosenberger, C. K. Scholze, J. H. Horstrup, C. Warnecke, S. Mandriota, I. Bechmann, U. A. Frei, C. W. Pugh, P. J. Ratcliffe, S. Bachmann, P. H. Maxwell and K. U. Eckardt (2003). "Widespread hypoxia-inducible expression of HIF-2alpha in distinct cell populations of different organs." Faseb J **17**(2): 271-273.

Witzig, T. E., M. A. Gertz, J. A. Lust, R. A. Kyle, W. M. O'Fallon and P. R. Greipp (1996). "Peripheral blood monoclonal plasma cells as a predictor of survival in patients with multiple myeloma." Blood **88**(5): 1780-1787.

Xia, X., M. E. Lemieux, W. Li, J. S. Carroll, M. Brown, X. S. Liu and A. L. Kung (2009). "Integrative analysis of HIF binding and transactivation reveals its role in maintaining histone methylation homeostasis." Proc Natl Acad Sci U S A **106**(11): 4260-4265.

Yaccoby, S., B. Barlogie and J. Epstein (1998). "Primary myeloma cells growing in SCID-hu mice: a model for studying the biology and treatment of myeloma and its manifestations." Blood **92**(8): 2908-2913.

Yao, S., T. Sukonnik, T. Kean, R. R. Bharadwaj, P. Pasceri and J. Ellis (2004). "Retrovirus silencing, variegation, extinction, and memory are controlled by a dynamic interplay of multiple epigenetic modifications." Mol Ther **10**(1): 27-36.

Zannettino, A. C., A. N. Farrugia, A. Kortesidis, J. Manavis, L. B. To, S. K. Martin, P. Diamond, H. Tamamura, T. Lapidot, N. Fujii and S. Gronthos (2005). "Elevated serum levels of stromal-derived factor-1alpha are associated with increased osteoclast activity and osteolytic bone disease in multiple myeloma patients." Cancer Res **65**(5): 1700-1709.

Zhan, F., E. Tian, K. Bumm, R. Smith, B. Barlogie and J. Shaughnessy, Jr. (2003). "Gene expression profiling of human plasma cell differentiation and classification of multiple myeloma based on similarities to distinct stages of late-stage B-cell development." Blood **101**(3): 1128-1140.

Zhang, J., C. Wang, N. Ke, J. Bliesath, J. Chionis, Q. S. He, Q. X. Li, J. E. Chatterton, F. Wong-Staal and D. Zhou (2007). "A more efficient RNAi inducible system for tight regulation of gene expression in mammalian cells and xenograft animals." RNA **13**(8): 1375-1383.

Zhang, L., R. Jia, N. J. Palange, A. C. Satheka, J. Togo, Y. An, M. Humphrey, L. Ban, Y. Ji, H. Jin, X. Feng and Y. Zheng (2015). "Large genomic fragment deletions and insertions in mouse using CRISPR/Cas9." PLoS One **10**(3): e0120396.

Zhong, H., A. M. De Marzo, E. Laughner, M. Lim, D. A. Hilton, D. Zagzag, P. Buechler, W. B. Isaacs, G. L. Semenza and J. W. Simons (1999). "Overexpression of hypoxia-inducible factor 1alpha in common human cancers and their metastases." Cancer Res **59**(22): 5830-5835.

Zhou, Y., T. Zhang, Q. K. Zhang, Y. Jiang, D. G. Xu, M. Zhang, W. Shen and Q. J. Pan (2014). "Unstable expression of transgene is associated with the methylation of CAG promoter in the offspring from the same litter of homozygous transgenic mice." Mol Biol Rep **41**(8): 5177-5186.

Zhou, Y., S. Zhu, C. Cai, P. Yuan, C. Li, Y. Huang and W. Wei (2014). "High-throughput screening of a CRISPR/Cas9 library for functional genomics in human cells." Nature **509**(7501): 487-491.